High pressure synthesis and investigations of properties of boron allotropes and boron carbide

DISSERTATION

zur Erlangung des akademischen Grades eines
Doktors der Naturwissenschaften (Dr. rer. nat.)
an der Bayreuther Graduiertenschule für Mathematik und
Naturwissenschaften (BayNAT) der Universität Bayreuth

vorgelegt von

Irina Chuvashova
aus Obninsk (Russland)

Bayreuth, 2017

This doctoral thesis was prepared at the Bavarian Research Institute of Experimental Geochemistry and Geophysics and the Laboratory of Crystallography of the University of Bayreuth from 10/2014 until 03/2017 and was supervised by Prof. Dr. Leonid Dubrovinsky and Prof. Dr. Natalia Dubrovinskaia.

This is a full reprint of the dissertation submitted to obtain academic degree of Doctor of Natural Sciences (Dr. rer. nat.) and approved by the Bayreuth Graduate School of Mathematical and Natural Sciences (BayNAT) of the University of Bayreuth.

Date of submission: 01.03.2017

Date of defense: 12.06.2017

Doctoral committee:

Prof. Dr. Natalia Dubrovinskaia   (1st reviewer)

Prof. Dr. Jürgen Senker   (2nd reviewer)

Dr. Hauke Marquardt   (chairman)

Prof. Dr. Leonid Dubrovinky

Summary

Boron, the 5th element of the Periodic Table, is nonmetallic, hard material with high melting point and boiling temperature. Despite decades of extensive investigations, boron and boron-rich solids remain in focus of modern research, because there are many long-standing fundamental questions related to boron chemistry, crystal-chemistry, bonding, polymorphism, and physical properties of boron allotropes and compounds, which have not been resolved yet. There are also a number of theoretical predictions, which require experimental verification. New knowledge is gained due to contemporary progress in materials synthesis and methods of their investigations.

My work aimed at the development of the high-pressure high-temperature (HPHT) synthesis of single crystals of boron allotropes and boron-rich compounds, which could be used further for precise investigations of their structures, properties, and behavior at extreme conditions. The HPHT synthesis using the large-volume-press technique yields single crystals of especially high purity and quality. I performed the synthesis of single crystals of β-B using the large-volume press with toroidal anvils (toroidal press) recently installed in the Laboratory of Crystallography. I contributed to the development of the toroidal cell assembly and conducted pressure and temperature calibrations of this new press that I describe in the thesis in detail.

Knowledge about the HPHT behavior of elemental materials and compounds is important for fundamental understanding of bonding evolution, phase transformations, and establishing of P,T-phase diagrams, which are of high significance for materials' synthesis and applications. In my project I focused on high-pressure investigations of α-B, β-B and stoichiometric boron carbide, $B_{13}C_2$. Diamond anvil cell (DAC) technique was used for *in situ* studies of single crystals at high pressures and room temperature, as well as at extreme HPHT conditions with double-sided laser heating of samples in DACs. Various analytical techniques I used include synchrotron and in-house X-ray diffraction (XRD), Raman and infra-red (IR) spectroscopy, and scanning electron microscopy (SEM).

The structure of α-B was studied at pressures up to 60 GPa by single-crystal XRD in a diamond anvil cell. The bulk modulus of α-B was found to be $K_{300} = 224(7)$ GPa, while the bulk modulus of individual B_{12} icosahedra K_{ico} appeared to be as high as 273(12) GPa. Thus, the compressibility of icosahedra is considerably lower than that of the bulk material. Measurements of interatomic distances as a function of pressure revealed that the intericosahedral two-electron-two-center (2e2c) bonds are almost as stiff as intraicosahedral ones, in accordance with the previous experimental data. The 2e3c intericosahedral bond shows much higher compliance compared to other bonds in α-B. The vibrational properties of α-B under pressure were investigated by Raman spectroscopy up to 160 GPa and synchrotron IR spectroscopy up to 53 GPa for the first time and gave evidence of the structural stability of this boron allotrope in the broad pressure interval, in agreement with X-

ray diffraction data. Metallization of α-B was not observed up to 160 GPa. A comparison of theoretical calculations of the behavior of Raman modes of α-B under stress conditions with experimental data led to conclusion that stress in certain directions results in the splitting of some of the Raman modes.

Structures of all hitherto known boron allotropes (α-B, β-B, γ-B, δ-B, and ε-B) are based on various arrangements of B_{12} icosahedra, since three valence electrons of boron are insufficient to form a simple covalent structure. However, theoretical calculations suggest a possibility of the existence of a non-icosahedral boron allotrope with the α-Ga type structure. Verifying this prediction was one of the tasks of my research. I conducted a series of high-pressure high-temperature experiments in diamond anvil cells (DACs) and demonstrated that the predicted boron allotrope (we denoted it as ζ-B) could be synthesized by laser-heating of single crystals of β-B to over 2100 K at pressures above 115 GPa. Synchrotron *in situ* single-crystal X-ray diffraction revealed the α-Ga-type orthorhombic structure (space group *Cmce*) with the unit cell parameters *a* = 2.7039(10) Å, *b* = 4.8703(32) Å, *c* = 2.9697(6) Å (Z=8). It may be described as a stacking along the (010) direction of distorted and corrugated hexagonal nets with the 3^6 topology. Measured precisely interatomic distances and linear compressibilities along the major crystallographic directions do not allow interpreting the structure as layered, as earlier proposed. The newly synthesized ζ-B studied in the pressure range from 115 to 132 GPa was found to be less compressible than any other of previously known boron allotropes.

The single crystals of β-B used as precursors for synthesis of ζ-B were X-rayed upon compression up to 102 GPa that allowed me to get the equation of state of β-B in the Mbar pressure range: the bulk modulus was found to be K=183(3) GPa (K′=3.4(1)). No phase changes were observed.

Additionally to boron allotropes, I investigated compressional behavior of stoichiometric boron carbide $B_{13}C_2$ up to 68 GPa using HP XRD. This study was motivated not only by availability of unique single crystals of the boron carbide synthesized in our group by the HPHT technique, but also by its practical importance. Boron carbide is used for manufacturing shielding powders and coatings applied as energy absorbers for dynamic protection and its mechanical properties and limits of stability under loading are of both scientific and practical interest for ballistic applications. Our single-crystal synchrotron X-ray diffraction investigations revealed structural stability of stoichiometric boron carbide $B_{13}C_2$ in the studied pressure range. A comparison of the unit cell volume reduction with the reduction of the volume of the B_{12} icosahedron upon compression of $B_{13}C_2$ from ambient pressure to 60 GPa revealed their similarity. This confirms that the stoichiometric boron carbide $B_{13}C_2$ is a true covalent compound and does show neither 'molecular-like' nor 'inversed molecular-like' solid behavior upon compression, as previously disputed. Our

analysis has shown that, in agreement with the modern understanding of bonding in α–B, γ–B, and $B_{13}C_2$ based on the experimental electron-density studies, the compressional behavior of these boron allotropes and boron carbide depends on the types of bonding involved in the course of compression, so that the 'effective compressibility' of B_{12} icosahedra may vary in a broad range, from ca. 14% in α–B to ca. 18% in $B_{13}C_2$, as compared to ca. 18% of compression of the corresponding crystals.

To summarize, the present work resulted in the HPHT synthesis of the first previously unknown non-icosahedral boron allotrope ζ-B. This finding confirmed earlier theoretical predictions, which stayed unproven for decades because of experimental challenges which couldn't be overcome until recently. Structural stability of α-B and β-B in the Mbar pressure range and $B_{13}C_2$ up to 68 GPa was experimentally proven. Accurate measurements of the unit cell and B_{12} icosahedra volumes of the stoichiometric boron carbide $B_{13}C_2$ as a function of pressure led to conclusion that they undergo a similar reduction upon compression that is typical for covalently bonded solids. Neither 'molecular-like' nor 'inversed molecular-like' solid behavior upon compression was detected that has closed a long-standing scientific dispute. A comparison of the compressional behavior of $B_{13}C_2$ with that of α–B and γ–B allotropes and B_4C showed that it is determined by the types of bonding involved in the course of compression.

Zusammenfassung

Bor, das fünfte Element im Periodensystem der Elemente, ist ein nichtmetallisches hartes Material mit hohem Schmelzpunkt und hoher Siedetemperatur. Trotz jahrzehntelanger umfassender Untersuchungen stehen Bor und Bor-reiche Feststoffe weiterhin im Blickfeld der modernen Forschung; es gibt immer noch viele grundlegende Fragen in Bezug auf die Chemie von Bor, auf seine Kristallchemie und seine Bindungen, seinen Polymorphismus und die physikalischen Eigenschaften der Bor-Allotrope und Bor-Verbindungen, die nicht zufriedenstellend geklärt sind. Auch eine Reihe an theoretischen Vorhersagen bedarf einer experimentellen Bestätigung. Neues Wissen kann aufgrund des aktuellen Fortschritts bei der Materialsynthese und bei Untersuchungsmethoden gewonnen werden.

Ziel meiner Arbeit war die Entwicklung einer Hochdruck-Hochtemperatur (high-pressure high-temperature, HPHT) Synthese für Einkristalle von Bor-Allotropen und Bor-reichen Verbindungen, die für weitere genaue Untersuchungen ihrer Struktur, ihrer Eigenschaften und ihres Verhaltens bei extremen Bedingungen verwendet werden können. Die HPHT Synthese liefert unter Verwendung der sogenannten „Großvolumen-Presstechnik" Einkristalle von besonders hoher Reinheit und Qualität. Ich führte unter Verwendung einer Großvolumen-Presse mit ringförmigen Stempeln (toroidale Presse) die Synthese von β-Bor Einkristallen durch; diese Presse ist vor kurzem am Lehrstuhl für Kristallographie installiert worden. Dabei trug ich zur Entwicklung der Ringzellenanordnung bei und führte die Druck- und Temperaturkalibrierungen dieser neuen Presse durch, was in der Doktorarbeit im Detail beschrieben wird.

Das Wissen um das HPHT Verhalten elementarer Materialien und Verbindungen ist wichtig für das grundlegende Verständnis von Bindungsverhalten, Phasenumwandlungen und das Erstellen von P,T Phasendiagrammen, welche sowohl für die Materialsynthese als auch für Anwendungen von großer Bedeutung sind. Meine Arbeiten beschäftigten sich mit den Hochdruck-Untersuchungen an α-B und β-B und an stöchiometrischem Borcarbid, $B_{13}C_2$. Unter Verwendung von Diamantstempelzellen (diamond anvil cell, DAC) wurden in situ Untersuchungen an Einkristallen bei hohen Drücken und Zimmertemperatur durchgeführt, sowie unter extremen HPHT Bedingungen mittels doppelseitiger Laserheizung von Proben in DACs. Die verschiedenen von mir verwendeten analytischen Techniken beinhalten Synchrotron und in-house Röntgenstrahlbeugung (X-ray diffraction, XRD), Raman- und Infrarot- (IR) Spektroskopie und Rasterelektronenmikroskopie (scanning electron microscopy, SEM).

Die Struktur von α-B wurde bei Drücken bis 60 GPa mittels Einkristall-Röntgenstrahlbeugung in einer Diamantstempelzelle untersucht. Der Kompressionsmodul von α-B wurde zu $K_{300} = 224(7)$ GPa bestimmt, während der Kompressionsmodul der einzelnen B_{12}-Ikosaeder K_{ico} mit 273(12) GPa deutlich höher liegt. Die Komprimierbarkeit der Ikosaeder ist also wesentlich kleiner

als die des Vollmaterials. Die Bestimmung der interatomaren Abstände als Funktion des Drucks zeigte, dass die interikosaedrischen zwei-Elektronen-zwei-Zentren (2e2c) Bindungen fast genauso stark sind wie die intraikosaedrischen Bindungen, in Übereinstimmung mit früheren experimentellen Daten. Die 2e3c interikosaedrische Bindung zeigt eine höhere Nachgiebigkeit im Vergleich zu den anderen Bindungen in α-B. Die Vibrationseigenschaften von α-B unter Druck wurden zum ersten Mal untersucht, mittels Raman-Spektroskopie bis 160 GPa und mittels Synchrotron IR-Spektroskopie bis 53 GPa. In Übereinstimmung mit Röntgenbeugungsdaten zeigen sie eine strukturelle Stabilität dieses Bor-Allotropes über einen großen Druckbereich. Eine Metallisierung von α-B wurde bis 160 GPa nicht beobachtet. Ein Vergleich von theoretischen Berechnungen des Verhaltens von Raman-Modalwerten von α-B unter Spannungsbedingungen mit experimentellen Ergebnissen führt zur Schlussfolgerung, dass Spannung in bestimmten Richtungen eine Aufspaltung einiger Raman-Modalwerte bewirkt.

Die Strukturen aller bisher bekannten Bor-Allotrope (α-B, β-B, γ-B, δ-B, und ε-B) basieren auf unterschiedlichen Anordnungen von B_{12}-Ikosaedern, da die drei Valenzelektronen des Bors nicht ausreichen, um einfache kovalente Strukturen auszubilden. Theoretische Berechnungen weisen allerdings auf die Möglichkeit hin, dass ein nichtikosaedrisches Bor-Allotrop im α-Ga Strukturtyp existieren kann. Die Bestätigung dieser Vorhersage war ein Ziel meiner Arbeiten. Dazu führte ich eine Reihe an HPHT Versuchen in DACs durch und konnte zeigen, dass das vorhergesagte Bor-Allotrop (wir bezeichneten es als ζ-B) mittels Laser-Heizung von β-B Einkristallen bei Temperaturen über 2100 K und Drücken über 115 GPa synthetisiert werden kann. Synchrotron in situ Einkristall-Röntgenbeugung bestätigte die orthorhombische α-Ga Struktur in der Raumgruppe *Cmce* mit den Gitterparametern a = 2.7039(10) Å, b = 4.8703(32) Å und c = 2.9697(6) Å (Z = 8). Die Struktur kann als Stapelung entlang der (010) Richtung von verzerrten und gewellten hexagonalen Netzen mit der 3^6 Topologie beschrieben werden. Genau gemessene interatomare Abstände und die linearen Komprimierbarkeiten entlang der kristallographischen Hauptrichtungen erlauben es aber nicht, die Struktur als Schichtstruktur zu beschreiben, wie zuvor vorgeschlagen. Das neu hergestellte ζ-B wurde im Druckbereich 115 bis 132 GPa untersucht und zeigt eine niedrigere Komprimierbarkeit als die der anderen und bereits vorher bekannten Bor-Allotrope.

Die Einkristalle des β-B, die als Ausgangsstoff für die Synthese des ζ-B dienten, wurden mittels Röntgenstrahlen bis zu einer Verdichtung von 102 GPa untersucht, was mir erlaubte, die Zustandsgleichung von β-B im Mbar-Druckbereich zu erstellen: der Kompressionsmodul ist K = 183(3) GPa (K′ = 3.4(1)). Eine Phasenumwandlung wurde nicht beobachtet.

In Ergänzung zu den Bor-Allotropen habe ich das Kompressionsverhalten des stöchiometrischen Borcarbids $B_{13}C_2$ mittels Hochdruck-Röntgenstrahlbeugung (HP XRD) bis

68 GPa untersucht. Diese Analyse wurde nicht nur durch die Verfügbarkeit der Einkristalle von Borcarbid veranlasst, die in unserer Arbeitsgruppe mittels der HPHT Technik hergestellt wurden, sondern auch aufgrund der Wichtigkeit für Anwendungen. Borcarbid wird zur Herstellung von Schutzpulvern und Beschichtungen benötigt, die als Energiedämpfer für dynamischen Schutz angewendet werden. Seine mechanischen Eigenschaften und Stabilitätsgrenzen unter Belastung sind für ballistische Anwendungen sowohl von wissenschaftlichem als auch von praktischem Interesse. Unsere Untersuchungen an Einkristallen mittels Synchrotron-Röntgenstrahlbeugung bestätigten die strukturelle Stabilität des stöchiometrischen Borcarbids $B_{13}C_2$ im untersuchten Druckbereich. Ein Vergleich der Verringerung des Volumens der Elementarzelle mit der Verringerung des Volumens eines B_{12}-Ikosaeders von Normaldruck bis 60 GPa zeigt ihre Ähnlichkeit auf. Dies bestätigt, dass das stöchiometrische Borcarbid $B_{13}C_2$ tatsächlich eine kovalente Verbindung ist und unter Druck weder ein ‚Molekül-ähnliches' noch ein ‚entgegengesetzt Molekül-ähnliches' Festkörperverhalten zeigt, wie es vorher diskutiert worden war. Unsere Analyse zeigte, in Übereinstimmung mit dem auf experimentellen Elektronendichteuntersuchungen basierenden modernen Verständnis der Bindungsverhältnisse in α–B, γ–B und $B_{13}C_2$, dass das Kompressionsverhalten dieser Bor-Allotrope und des Borcarbid von den Bindungstypen abhängt, die am Kompressionsverlauf beteiligt sind, so dass die ‚effektive Komprimierbarkeit' des B_{12}-Ikosaeders über einen großen Bereich variieren kann, von etwa 14% in α–B bis etwa 18% in $B_{13}C_2$, verglichen mit den etwa 18% Komprimierbarkeit der dazugehörigen Kristalle.

Zusammenfassend führte die hier vorgestellte Arbeit zur HPHT Synthese des ersten nichtikosaedrischen und bisher unbekannten Bor-Allotropes ζ-B. Das bestätigte frühere theoretische Vorhersagen, die jahrzehntelang ungeprüft und unbewiesen bleiben, da bis jetzt die nötigen experimentellen Herausforderungen nicht gemeistert werden konnten. Die strukturelle Stabilität von α-B und β-B im Mbar-Druckbereich und von $B_{13}C_2$ bis 68 GPa wurde experimentell bewiesen. Sorgfältige Messungen der Volumina der Elementarzellen und des B_{12} Ikosaeders des stöchiometrischen Borcarbids $B_{13}C_2$ als Funktion des Drucks führten zu der Schlussfolgerung, dass sie ähnliche Verringerungen unter Kompression durchlaufen, welche charakteristisch für kovalente Verbindungen sind. Weder ein ‚Molekül-ähnliches' noch ein ‚entgegengesetzt Molekül-ähnliches' Festkörperverhalten unter Kompression wurde beobachtet, wodurch eine langanhaltende wissenschaftliche Kontroverse beendet werden konnte. Ein Vergleich des Kompressionsverhaltens von $B_{13}C_2$ mit dem der α–B und γ–B Allotrope und von B_4C zeigte, dass dieses Verhalten von den Bindungstypen bestimmt wird, die am Kompressionsverlauf beteiligt sind.

Acknowledgments

Contents

Contents

I.   INTRODUCTION

I.1. Application of boron and boron-rich compounds

Boron, the 5th element of the Periodic table, is nonmetallic, hard material with high melting point (2076°C) and boiling temperature (3927 °C). Its powder has black-greyish or dark-brown color. At ambient conditions boron is known as a poor semiconductor and its electric conductivity rapidly increases with temperature, so that at 600 °C it is 100 times higher than at room temperature [1]. Boron has two naturally occurring and stable isotopes, ^{11}B (80.1%) and ^{10}B (19.9%) [2]. ^{10}B has high neutron capture cross-section, high heat-resistance and nontoxicity so it is used as a material for the control rods of nuclear reactors [3], for a radiation shield [4,5], and for a neutron counting detector as well as for medicine (boron neutron capture therapy [6-8]). For producing distinctive green color, amorphous boron is used in pyrotechnic flares as well as rocket fuel igniter [9]. Use of amorphous boron as a gasket material in high pressure experiments [10] improves hydrostatic conditions, and quality of X-ray diffraction patterns. High hardness, exceptional chemical stability in crystalline form, formation of electron-deficient bonds [11-13], pressure-induced metallization and superconductivity [14] and partially unknown phase diagram [15-17] still make elemental boron very attractive to scientific community despite its wide application in pure form and in compounds.

Boron is not found in nature as an elemental material, but it forms compounds, which due to variety of their physical and chemical properties play an important role in human activities since antiquity [18]. Nowadays they are widely used as superhard materials, superconductors, dielectrics and B-doped semiconductors as well as reinforcing chemical additives. Composites on the base of boron are characterized by extreme strength and lightweight used as filaments for advanced aerospace structures and in personal security (bullet-proof vest) [19].

Boron forms several commercially important compounds. One of them is boron oxide. It is used as a fluxing agent in ceramics and glassmaking. It makes glass tough and heat-resistant. In the production of borosilicate glasses and glass fibers boron oxide plays an important role alongside with borax ($Na_2B_4O_7 \cdot 10\ H_2O$). The borosilicate glass is non-conducting and used as insulator layers in semiconductor industry. The chemical stability of borosilicate glasses allows their use as materials for chemical tools. Borax is also used as a cleansing fluid, a water softener, insecticide, herbicide and disinfectant.

Metal borides are also hard and durable materials [20,21] and are employed as mechanical parts exposed to high strain (turbine and rotor blades, sports equipment). Moreover, due to their high electrical conductivity metal borides serve as electrode materials [22], for example, as high energy batteries [23]. MgB_2 is a superconductor at 39 K and used in form of wires for tomographs [14]. LaB_6 along with being a superconductor with relatively low transition temperature of 0.45 K

[24] has a low work function what allows to use it in transmission electron microscopy and electron beam lithography. Hafnium boride has high melting point (3543 K) and low thermal expansion coefficient that leads to its successful use in thermal shock experiments [25,26]. TaB_2 is not corrosive even in boiling aqua Regis.

The most interesting of boron compounds are boron nitride and boron carbide. Boron nitride is the second hardest material suppressed only by diamond (Vickers hardness is 49-54 GPa [27]). Its remarkable chemical and thermal stability allows its use in high-temperature equipment. Boron nitride nanotubes are similar to carbon nanotubes, but more thermally and chemically stable. Unlike carbon nanotubes, boron nitride nanotubes are electrical insulators.

Boron carbide is one of the most widely used hard materials, surpassed only by diamond and boron nitride. Due to its high melting point and thermal stability, high abrasion resistance, extreme hardness and low density, boron carbide is used for manufacturing shielding powders and coatings, applied as energy absorbers for dynamic protection. Mechanical properties of boron carbide and limits of its stability under loading are thus of both scientific and practical interest for ballistic applications. Theoreticians [28] predicted a phase transition in boron carbide at 25 GPa, which may explain, why it is destroyed upon dynamic tests at about this pressure. Experimental investigations of the behavior of boron carbide under pressure gave, however, controversial results, which require verification.

I.2. Boron allotropes and its PT phase diagram

Boron has five currently established allotropes (α-B, β-B, γ-B, δ-B (T-50), and ε-B [15,16,29]), and all of them have a common structural feature, B_{12} icosahedron as major building block. Each allotrope possesses a unique Raman spectrum [15,16,29].

I.2.1. α-boron

Since first crystallization of pure boron in 1909 [30] and some successful synthesis in 1950s and 1960s [15,31-34] there was a long time of the absence of any references of synthesis of α-boron single crystals. However, recently [35] a methodology of reproducible synthesis was developed using high pressure and high temperature as main force of transformations.

Rhombohedral α-B (space group $R\bar{3}m$) has the simplest structure [35-40] among all of boron phases: it consists of B_{12} icosahedra located at the corners of its rhombohedral unit cell. Unit cell parameters are refined from single crystal X-ray diffraction: $a = 4.9179(5)$ Å, $c = 12.5805(16)$ Å in hexagonal settings [35]. Although its structure was established long ago (Fig. I.2-1), the bonding

situation in α-B at ambient pressure was clarified only recently [12] due to the analysis of the electron-density in α-B based on experimental single-crystal X-ray diffraction data. It was found that icosahedra form "close-packed" layers and between them there are 2e2c (two-electron two-center) B1-B1 intercluster bonds of the similar nature as the 2e2c bonds in γ-B [13] (Fig. I.2-1A), while within the same layer (Fig. I.2-1B) icosahedra are held together by electron deficient 2e3c (two-electron three-center) B2-B2-B2 bonds which are different from the 2e3c bond in γ-B [12].

| A | B |
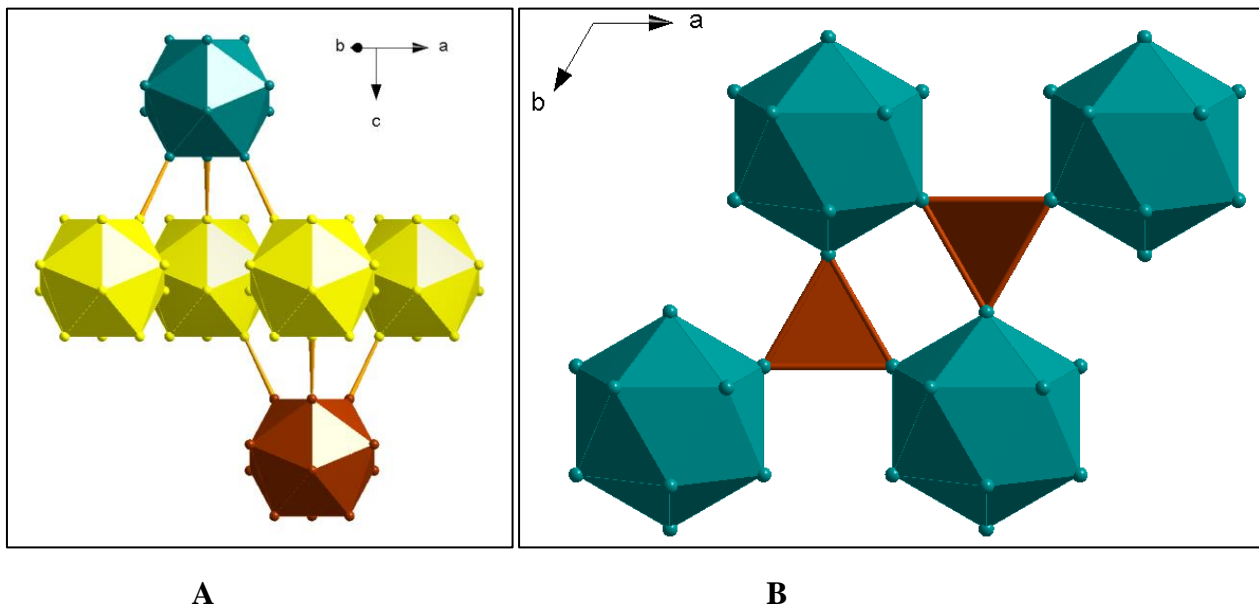
Figure I.2-1. Structure of α-B **A.** along the *y* direction, **B.** along the *c* axis.

α-B is extremely hard (Vickers hardness on polycrystalline aggregates 38(2) GPa [41]), dense (2.46 g/cm^3), thermally and chemically inert. It is a direct band gap semiconductor (2.0 eV [32], 2.4 eV [42], or 2.15(2) eV [41]).

Raman spectroscopy investigations of α-B were started by Richter and Ploog [43] in 1964. Since that time, alongside with theoretical calculations and assignment of the Raman modes [44-47] at ambient conditions (Figure I.2-2), a number of high-pressure experiments have been performed [36,44,48,49]. Raman spectroscopy measurements at room temperature to 80 GPa on polycrystalline samples [49] and on single crystals up to 30 GPa [36] and 71 GPa [48] did not show any phase transitions in α-B in according with powder X-ray diffraction experiments up to 106 GPa [49] and 200 GPa [50].
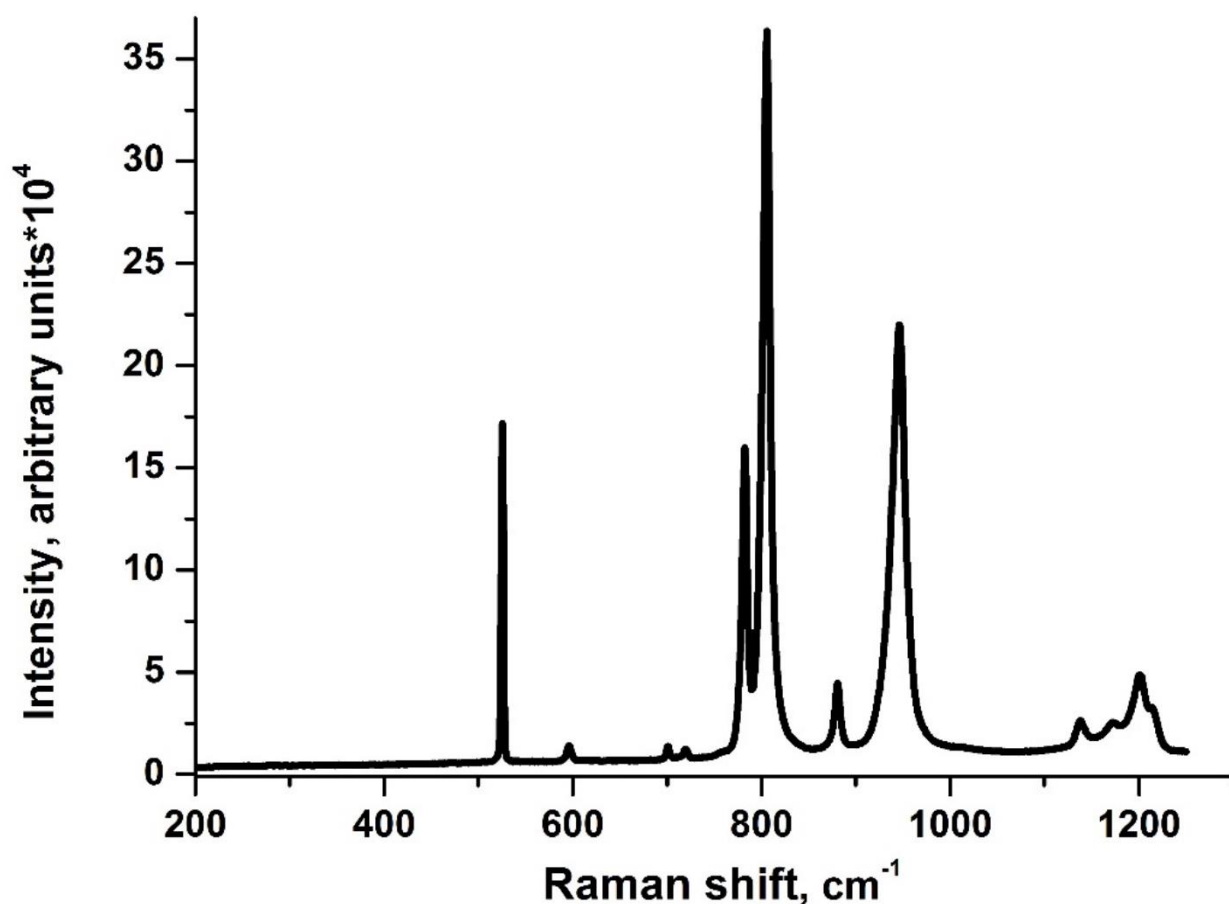
Figure I.2-2. Raman spectrum of α-B.

IR spectroscopy studies were performed experimentally on powder samples at ambient conditions [51-53] and theoretically in numerous works [46,47,51,54-56]. The bands were identified in the transmission spectrum in the range from 400 to 1300 cm^{-1}.

It is already 100 years passed since α-boron was obtained in a crystalline form for the first time, but several problems still remain. Accurate determination of atomic coordinates and thermal parameters of α-B is required. High pressure IR spectroscopy can recognize metallization of α-B theoretically predicted at about 50 GPa, however, no reference was found so far. Structural stability at pressures higher than 100 GPa is needed to be verified.

I.2.2. β-boron

Under heating up to 1473 K at ambient pressure, α-B transforms into β-B [36]. β-B is the most common phase and the one commercially available. It can be crystallized from melt at ambient pressure as well as produced by chemical vapor deposition method [57].

β-B was the first pure boron phase discovered [58]. The structure was solved several years later [59-61]. β-boron crystallizes in form of crystals with a rhombohedral structure (space group $R\bar{3}m$) with the unit cell parameters $a = 10.932(1)$ Å, $c = 23.818(3)$ Å in a hexagonal settings [62]. Modern view on the structure is based on single-crystal X-ray diffraction experiment suggesting 320.1 atoms per a hexagonal unit cell distributed over 20 crystallographically independent positions [62]. The crystal structure contains B_{12} icosahedra, B_{28}–B–B_{28} fragments and interstitial B atoms (Figure I.2-3). B_{28} fragments consist of 3 B_{12} icosahedra sharing their faces. B_{12} icosahedra form 3-dimensional framework with B_{28}–B–B_{28} fragments inside the voids. The main feature of β-B that makes its structure the most complex among all known boron allotropes is presence of voids and partially occupied positions [45]. According to [62], the occupancies of B13 and B16–B20 vary from 3.7(4) % to 74.5(6) %.

A.	**B.**
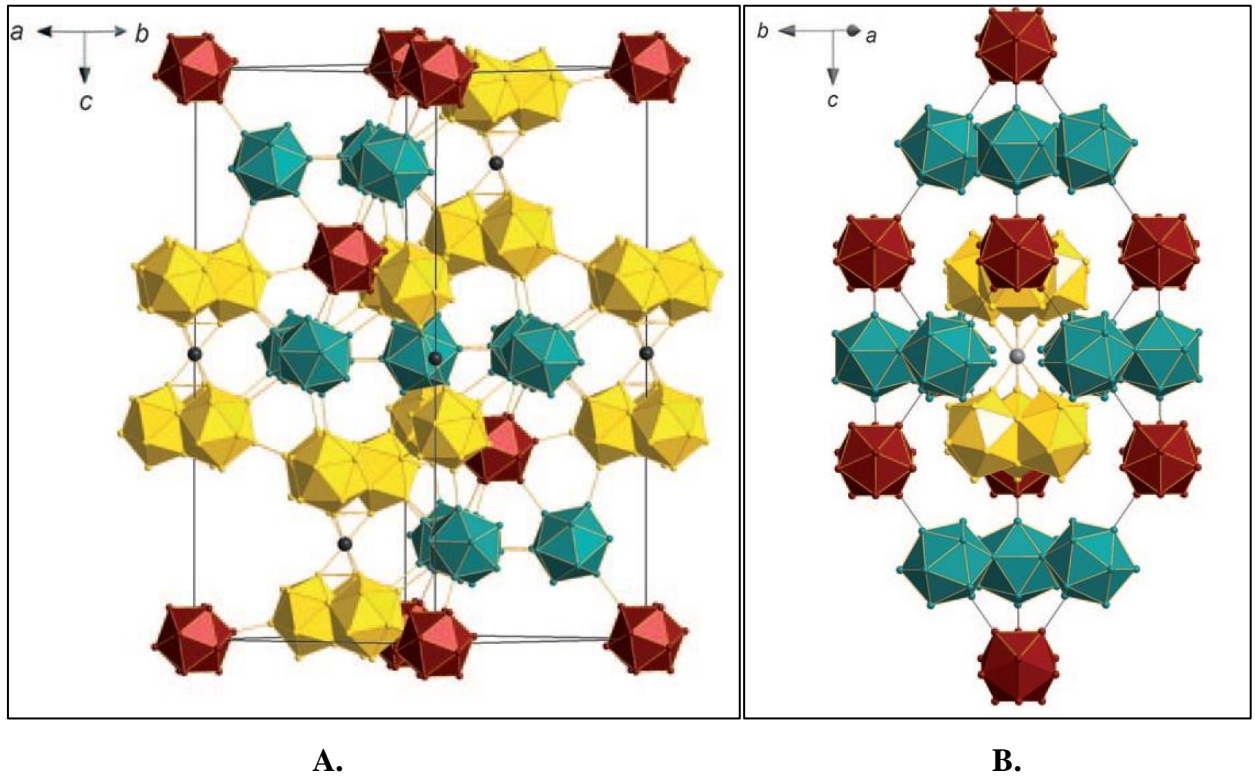
Figure I.2-3. Structure of β-B, picture is taken from [15] **A.** in hexagonal settings, **B.** in rhombohedral settings.

Availability of β-boron leads to a lot of studies on optical [63], electrical [64] and mechanical [65] properties. In a conductivity measurement a transformation of β-B from a wide band gap semiconductor to a superconductor at 160 GPa was found [14] what is in agreement with previous theoretical predictions [66].

However, due to its complexity, the structure of β-B is poorly understood. The determination of equation of state (EoS) is certainly an important tool to progress in the understanding of boron. For β-B the EoS were measured in the ranges of $0 - 10$ GPa [67] by means of neutron powder diffraction, in the ranges of $0 - 30$ GPa [68] as well as at different temperatures by powder X-ray diffraction and in the ranges of $2 - 97$ GPa [69] using powder and single-crystal X-ray diffraction. The β-B is found to be more compressible (bulk modulus K = 185–210 GPa [67-69]) in comparison with α-B (K = 213–224 GPa [48,67]). In [68] there was a transition to T-192 (known as tetragonal-II phase, it wasn't reproduced) detected upon double-sided laser heating of the sample at pressures above 10 GPa. However, this transition wasn't observed in [69] where the pressure-induced amorphization at about 100 GPa was observed. So, further investigations of β-B at high pressures are required.

I.2.3. γ-boron

First obtained in 1965 [70] as a powder, γ-B is a reddish-colored high-pressure phase of boron [71]. Its orthorhombic structure has a *Pnnm* space group. Unit cell parameters (a = 5.0563(4) Å, b = 5.6126(5) Å and c = 6.9710(7) Å) were refined from single crystal X-ray diffraction data [72]. The structure of γ-B consists of B_{12} icosahedra and B_2 dumbbells covalently bonded with each other [13,72-74] (Figure I.2-4).
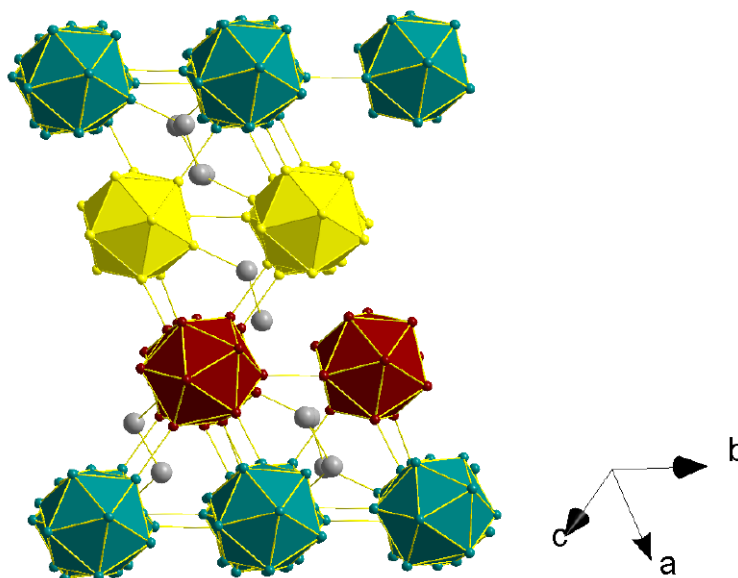
Figure I.2-4. Structure of γ-B [72].

Raman spectrum is unique for the high pressure high temperature modification of boron (Figure I.2-5).
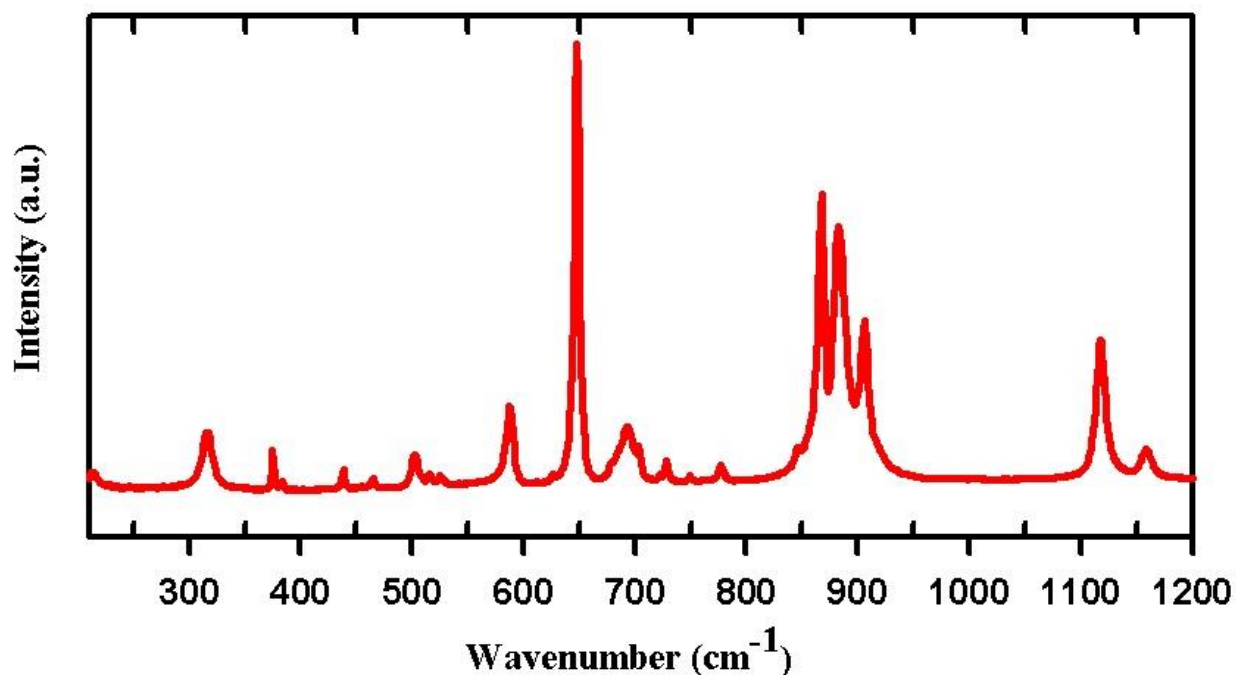
Figure I.2-5. Raman spectrum of single crystal of γ -boron (from [75]).

γ-B was experimentally demonstrated to be stable up to 30 GPa and 2000 K [72] and theoretically predicted to be stable in the pressure range from 19 GPa to 78 GPa [76], to 89 GPa [73] or to 93 GPa [77].

Experimental charge density study [13] revealed covalent polycenter bonds in B_{12} icosahedron, electron-deficient 1e2c bond between two neighboring polyhedra and a unique polar-covalent 2e3c bond between a pair of atoms of one B_{12} group and one atom of the dumbbell. This unique bond explains the observed charge separation in γ-B [13].

γ-B is extremely hard (Vickers microhardness is 58 GPa) [72,78] and very dense (X-ray density 2.54(1) g/cm^3). It is optically transparent with an optical absorption edge of 2.1 eV, a poor electrical conductor with a resistivity on the order of 106 Ω·cm at ambient conditions. Resistivity decreases with increasing temperature, indicating semiconductor behavior of γ-boron [75]. At about 40 GPa γ-B undergoes an isostructural phase transformation, probably due to reducing of the polarity of covalent bonds visualized by discontinuous behavior in the mode Grueneisen parameter and splitting of several Raman peaks [79].

I.2.4. δ-boron

Tetragonal phase of boron, T-50 or δ-B, was a matter of serious discussion since its discovery in 1943 by [80]. Theoretical calculations [81,82] predicted instability of B_{50} due to its electronic configuration and that it can be stabilized by small amounts of foreign atoms such as carbon, nitrogen or transition elements. Only recently this phase was synthesized in the presence of other boron allotropes [29].

δ-B crystallizes as needle-shaped grey-reddish semitransparent crystals. The structure refined by means of single crystal X-ray diffraction is tetragonal (*P4₂/nnm* space group) with the unit cell parameters $a = 8.708(9)$ Å, $c = 5.0750(8)$ Å [29]. The unit cell of δ-B consists of 50 boron atoms. They form four icosahedra, and two atoms localize in the intericosahedral space [41] (Figure I.2-6).
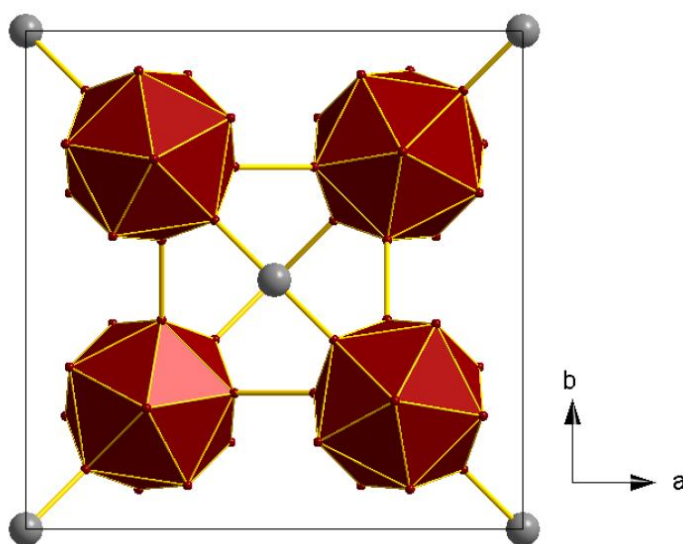
Figure I.2-6. Structure of T-50 (δ-B), the picture is taken from [29].

Raman spectrum of δ-B is drastically distinct from those of other boron polymorphs. It has one dominating intense Raman peak at 491 cm^{-1} (Figure I.2-7).
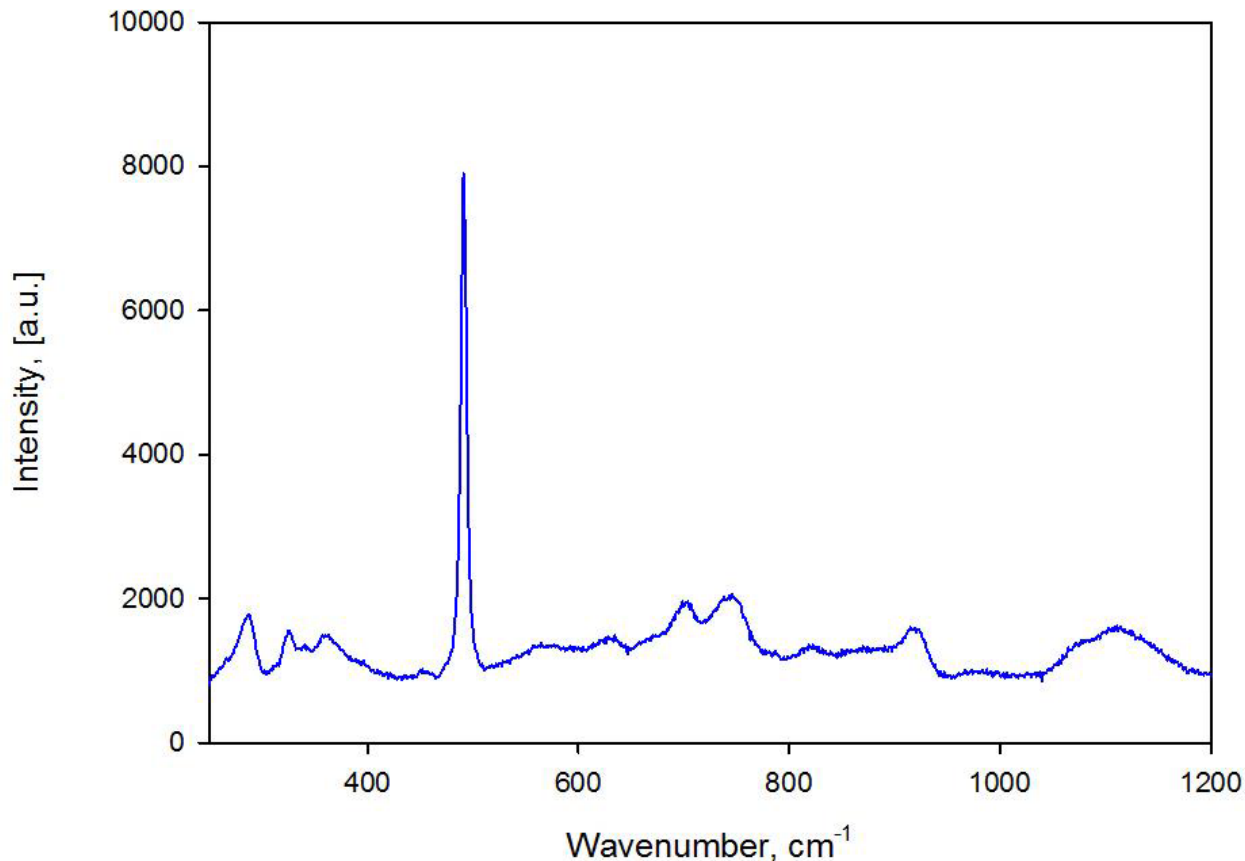
Figure I.2-7. Raman spectrum of single crystal of δ-boron from [29].

According to the experimental studies [29], δ-B crystals appeared at pressures above 9 GPa in the field of stability of γ-B and always in the presence of other boron polymorphs, what points towards metastability of this boron phase.

I.2.5. ε-boron

In a relatively narrow pressure-temperature field, at pressures of 8–9 GPa and temperatures of 1873 – 2073 K, yellow-reddish-orange, transparent, plate-shaped crystals of ε-B were found [29]. This boron phase has rhombohedral structure (space group $R\bar{3}m$) with unit cell parameters $a = 5.5940(7)$ Å, $c = 12.0756(16)$ Å (hexagonal setting). The arrangement of B_{12} icosahedra is similar to that in the α-B structure. In the intericosahedral space there are tree-atomic linear groups consisting of boron atoms oriented along the main body-diagonal of the unit cell. (Figure I.2-8.) The structure resembles the stoichiometric $B_{13}C_2$ [11] with C-B-C linear groups instead of B-B-B groups of ε-B [29].
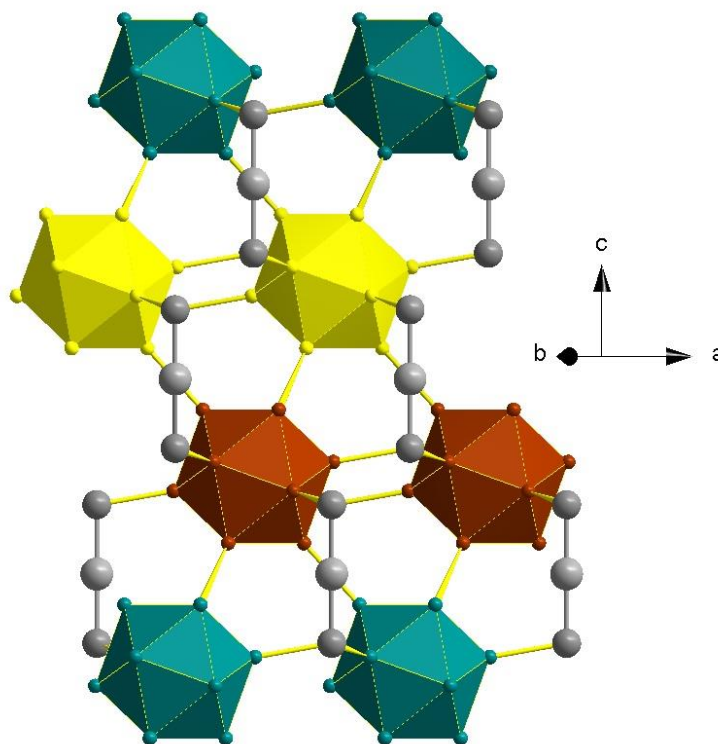
Figure I.2-8. Structure of ε-B in hexagonal settings [29].

The Raman spectrum of ε-B is different from the spectra of any other boron polymorphs [29], but alike to that of boron carbide $B_{13}C_2$ with a small shift of about 5 cm^{-1} (Figure I.2-9). Taking into account that the crystals appeared only in the presence of the other boron phases and upon heating at high pressure they transformed to β-B or γ-B (depending on the stability fields), this phase is considered to be metastable.
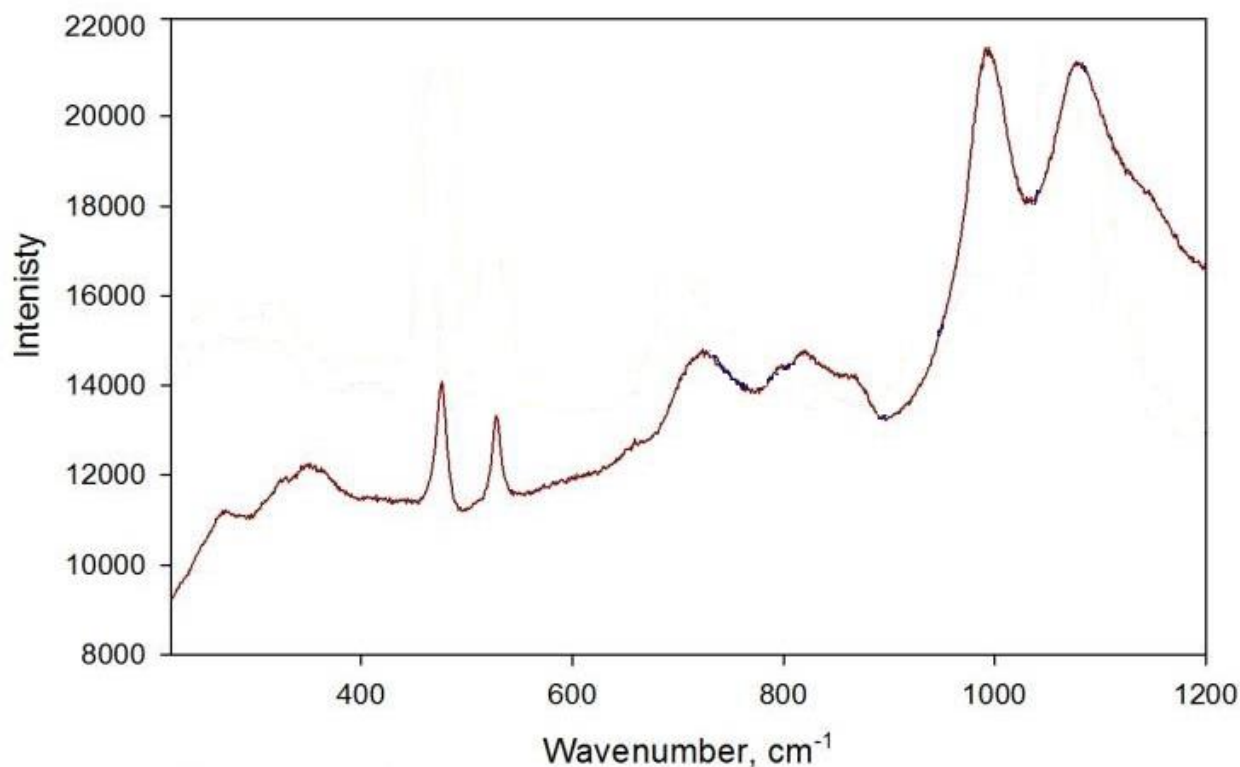
Figure I.2-9. Raman spectrum of single crystal of ε-boron from [29].

Microhardness of ε-boron (55-60 GPa) [29] is higher compared to boron carbide (38 GPa) despite the similarities in the structure. ε-B is as hard as γ-B (60 GPa) [71] but harder than other boron allotropes [41].

I.2.6. PT phase diagram of boron.

Boron has been widely studied due to its complex polymorphism. Boron's three valence electrons are too localized to make metallic bonding and insufficient in number to form a simple covalent structure. Thus, as a solution boron atoms form B_{12} icosahedron, a major building block for all known allotropes, linked together in a variety of ways [15,16].

Phase diagrams are established for the majority of elements and compounds, but for elemental boron phase diagram is still under discussion. The phase boundary separating the β-B and γ-B phases was experimentally found by [83]. The phase boundaries between α-B and β-B were established experimentally by [16]. The resulting phase diagram (Figure I.2-10) is quite different from the one recently proposed in [84] (Figure I.2-11A). In particular, in the diagram of [84] the field of stability of α-B is absolutely absent and the phase boundaries do not agree with [16]. As their studies were based on solid-solid phase transitions in boron under pressure, so the phase boundaries [84] do not correspond to equilibrium ones. Applied temperature might not be enough to overcome the energy barrier for a phase transition. That means the equilibrium phase boundaries may be shifted to lower

pressures and temperatures [41]. The phase diagram drawn by [85] (Figure I.2-11B) is based only on a few experimental points related to the HPHT synthesis conditions of β-B and mostly on theoretical predictions by [73,86].
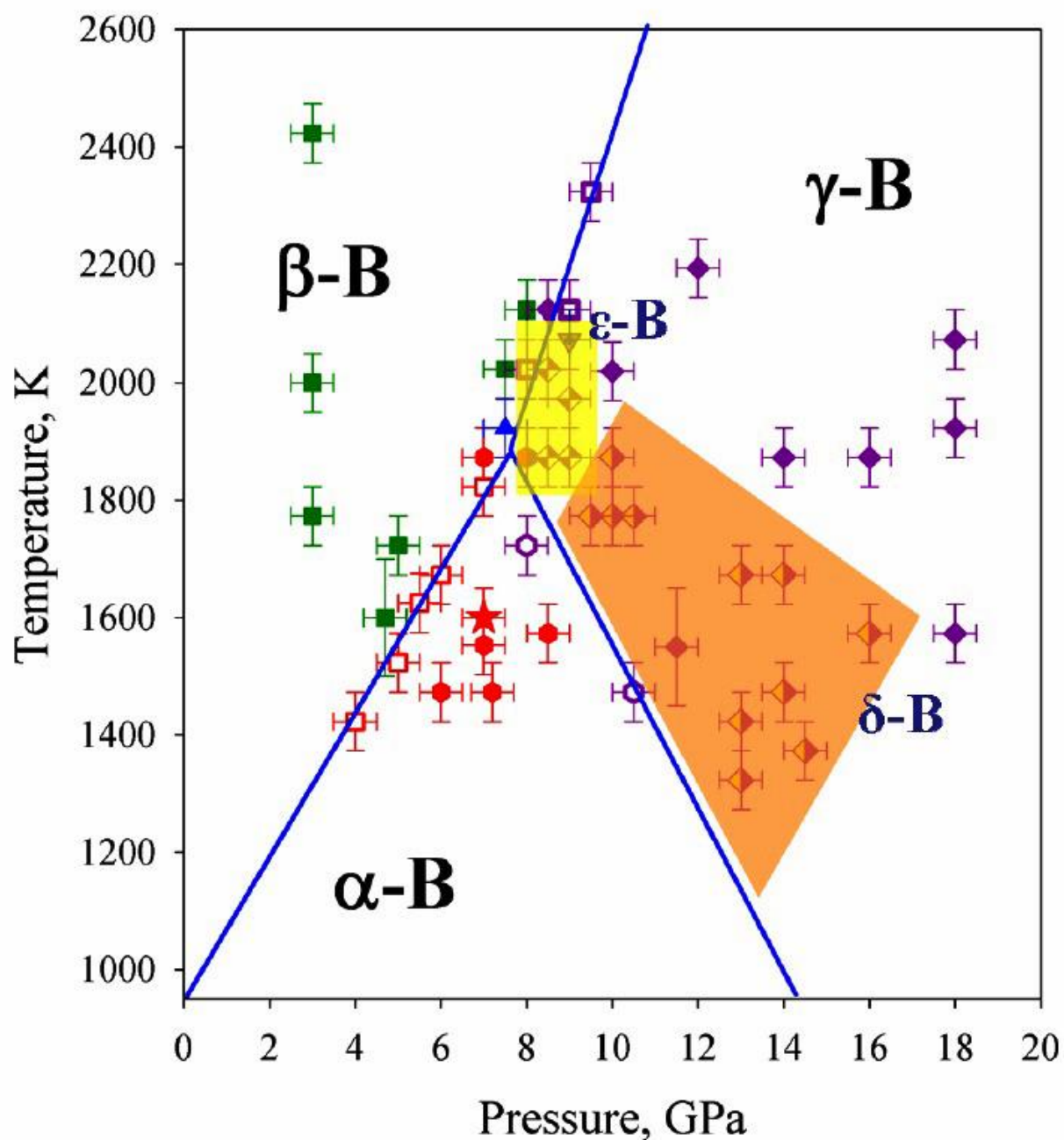
Figure I.2-10. Phase diagram of boron based on experiments by [29].
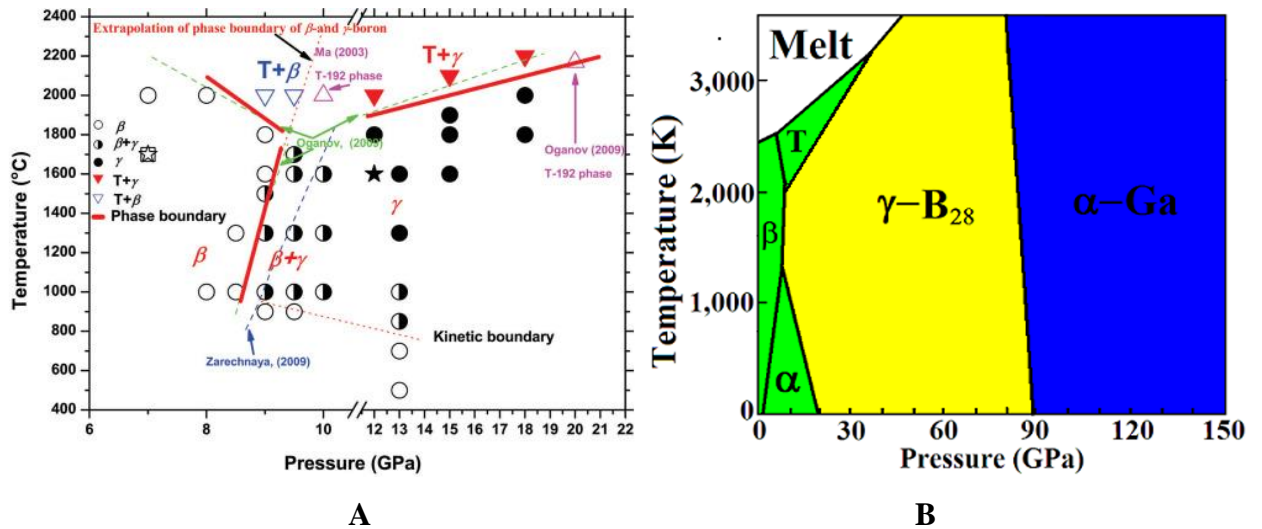
Figure I.2-11. A. Phase diagram of boron based on experiments by [84]. **B.** Theoretical phase diagram of boron by [73].

The ground state of the elemental boron has been long-standing controversy for decades and it is open question that requires clarification. Extrapolation of the α-/β-B boundary reported by [16] to ambient pressure suggests α-B to be thermodynamically stable low-temperature boron phase below 1000 K what agrees well with previously reported experiments [32,71] and theoretical calculations [87-89]. However, in these predictions the ideal structure of β-B was used without taking in account partially occupied sites and defects. Adding zero point energies[86] and ab initio Ising model describing the partial occupancy of β-B [90] makes the β-B more stable than α-B at ambient conditions. Moreover, the calculations [91] by means of electronic density functional theory methods result in lower energy of β-B at ambient conditions in comparison with α-B. However, the structure of β-B has a broken symmetry and uses only subsets of the fully symmetric Wyckoff positions [91]. Use of the DFT with pseudopotential method [17] suggested that α-B is mechanically stable and β-B is thermodynamically stable. Nevertheless, experimentally there is no evidence of stability of β-B over α-B.

Recent experimental phase diagram of boron including five allotropes, described above (α-B, β-B, γ-B, δ-B ("T-50"), and ε-B) is presented in Figure I.2-10 [29]. The invariant (triple) point between α-B, β-B, γ-B is at 7.6(5) GPa and 1880(50) K. Currently the experimental phase diagram is limited to 20 GPa and 2400 K, but there are a lot of theoretical predictions about behavior of boron at higher pressures and temperatures ([73,76,77,92-95]).

The possibility that boron could crystallize in 'α-Ga structural type' was first reported about 25 years ago [96]. Häusserman et al. were the first [97] who predicted the phase transition from α-B to α-Ga structure accompanied by nonmetal-metal transition happening at 74 GPa using *ab initio* calculations employing pseudopotentials and a plane wave basis set in the framework of the

density functional theory (DFT). The stability of α-Ga structured boron phase was found up to 790 GPa where a transition to *fcc* structure should take place. Simultaneously, Segal and Arias [98] performed calculations using method based on perturbation theory and all-electron calculations with plane-wave-basis in DFT. α-Ga-structured B phase was shown to be the lowest in energy phase under high pressure and energetically favorable between 71 GPa and around 500 GPa. Later investigations [73,76,77] reported higher stability of γ-B and moved its phase boundary with α-Ga-type B to 78 GPa [76], then to 89 GPa [73] and 93 GPa [77]. Calculations predict α-Ga-structured boron to be an incompressible (K_{300} = 263 GPa) [94] superconducting material with strong anisotropy due to its layered crystal structure [98,99]. Experimental findings on resistivity performed by [14] demonstrate that compression of β-B leads to metallization at pressure above 160 GPa and ambient temperature, and to formation of superconducting phase above 175 GPa and 6 K. The structural model of metallic superconducting boron is unknown. [97] proposed the α-Ga structure as a structural model for a metallic high-pressure modification of B after a phase transition of either semiconducting icosahedral α-B or β-B. We did not observe any transformations in β-B up to 115 GPa, and the transition to the α-Ga-structured phase required heating to very high temperatures. Thus, it is very improbable that B phase with the α-Ga structure may be associated with the metallic high-pressure modification of B discussed in [14,97]. Therefore, the behavior of boron at high pressure requires further investigations.

I.3. Boron carbide B$_{13}$C$_2$

Boron carbide B$_4$C was discovered in 1858 [100], and its crystal structure was first established in 1934 [101]. The structure of boron consists of B$_{12}$ icosahedra located in the corners of the rhombohedral unit cell and three-atom linear chains oriented along its body diagonal (Figure I.3-1). The unit cell parameters of B$_{13}$C$_2$ in hexagonal settings are a = 5.5962(3) Å, c = 12.0661(7) Å, (space group R$\bar{3}$m), as determined in [11]. The structure of B$_4$C is similar to the structure of metastable ε-B where B-B-B linear groups replaces C-B-C ones [29].
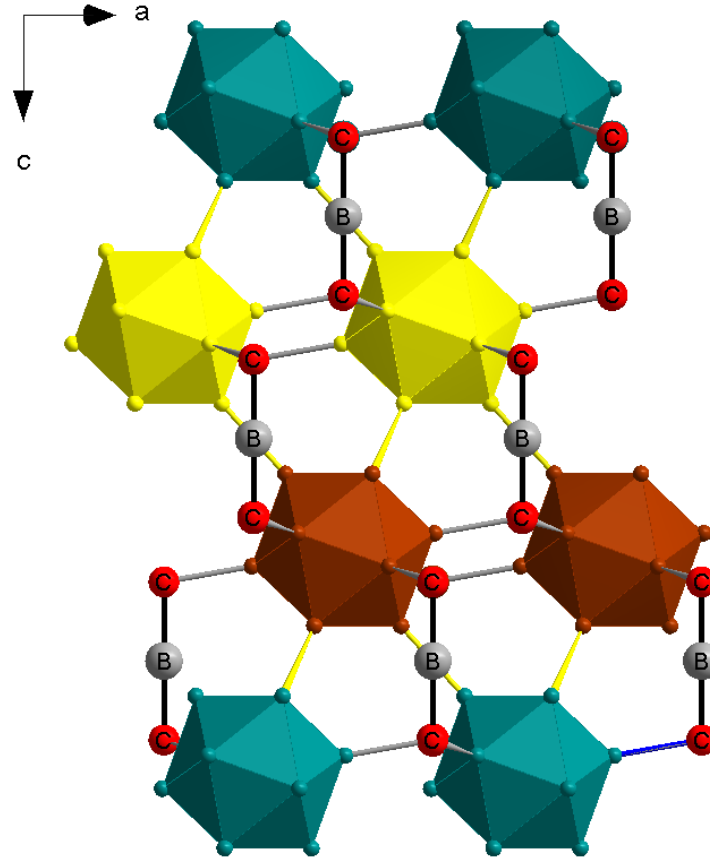
Figure I.3-1. Structure of $B_{13}C_2$ along the *b* direction in hexagonal settings [11].

Boron carbide exists as a single-phase material with a wide homogeneity range, from ~7 at. % ($B_{14}C$) to ~20 at. % ($B_{4.3}C$) of carbon [102-104]. This range of carbon concentrations is made possible by the substitution of boron and carbon atoms for one another within both the icosahedra and intericosahedral chains [105]. Along the whole homogeneity range, boron carbides were found to be degenerate, p-type semiconductors with potential applications as high temperature thermoelectric materials [105,106]. A critical issue, which is hotly debated, is the locations of C atoms in the crystal structure [102,103,105,107-115], which is under question due to the similarity in both electronic and nuclear scattering cross-sections for boron and carbon. Proposed stoichiometry is based on two extreme models, $B_{12}(CBB)$ on the boron-rich and $B_{11}C(CCC)$ on carbon-rich ends. Single crystals of boron carbide were synthesized in the form of $B_{4.3}C$ [116] and $B_{13}C_2$ [11,102]. The first one, $B_{4.3}C$, has $B_{11}C$ icosahedra, C-B-C chains, C-B-B chains and ~10% of vacancies in the linear chain [116]. The $B_{13}C_2$ contains only B_{12} icosahedra and C-B-C linear chains, as reported in [11].

Pressure-induced phase transition in boron carbide was reported for $B_{12}(CBC)$ at pressures of about 20-30 GPa [117] based on ballistic impact experiments. A small-volume-change phase transition at a shock stress of about 40 GPa was detected during dynamic compression [118,119].

Static compression experiments in a diamond anvil cell (DAC) [120] revealed a change in the unit cell parameters ratio at about 22 GPa. Recent single-crystal high pressure study indicated a phase transition near 40 GPa [116]. However, powder diffraction experiments on the high pressure behavior of boron carbide carried out up to 11 GPa [121], to ~50 GPa [122], and to 126 GPa [123] showed no phase transitions or amorphization in according with single-crystal XRD up to 74 GPa [108].

There were numerous IR spectroscopic theoretical [107,111,114,124-126] and experimental studies [107,114,122,124] of different compositions of boron carbide in its entire homogeneity range at ambient conditions. Vibrational frequencies of boron carbide are found in the interval from 400 to 1700 cm^{-1} (Figure I.3-2). The series of bands can be assigned to two types of motions: either of icosahedra, between 650 and 1100 cm^{-1}, or of the three-atom chains, in the spectral range of 1100 – 1600 cm^{-1}. However, there is still an intense discussion of assignment of the modes. The only high pressure IR spectroscopic experiments carried out up to 23 GPa in non-hydrostatic conditions [122] provided no evidences of phase transitions or weakening of IR modes.
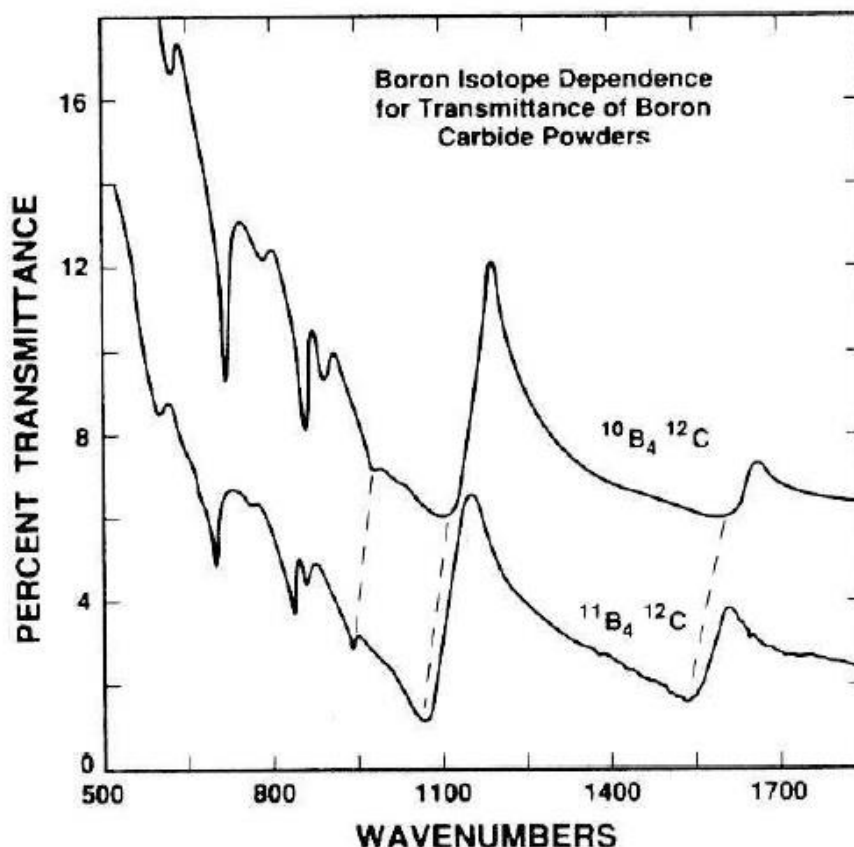
Figure I.3-2. Example of IR spectra of [10]B substituted boron carbide powder pressed into KBr pellets at ambient conditions. For details, see [114].

Raman spectroscopy investigations were performed in a number of works [106,107,116,122,127] supported by theoretical calculations [44,46,126,128]. At ambient

conditions, the frequencies of intraicosahedral vibrations fall into the range from 250 to 1060 cm^{-1} [112,129] (Figure I.3-3). The lines between 300 and 500 cm^{-1} are mainly attributed to the bending and stretching chain vibrations [112,128-130], while vibrations around 250-300 cm^{-1} refer to the icosahedral breathing modes, according to [107,122].
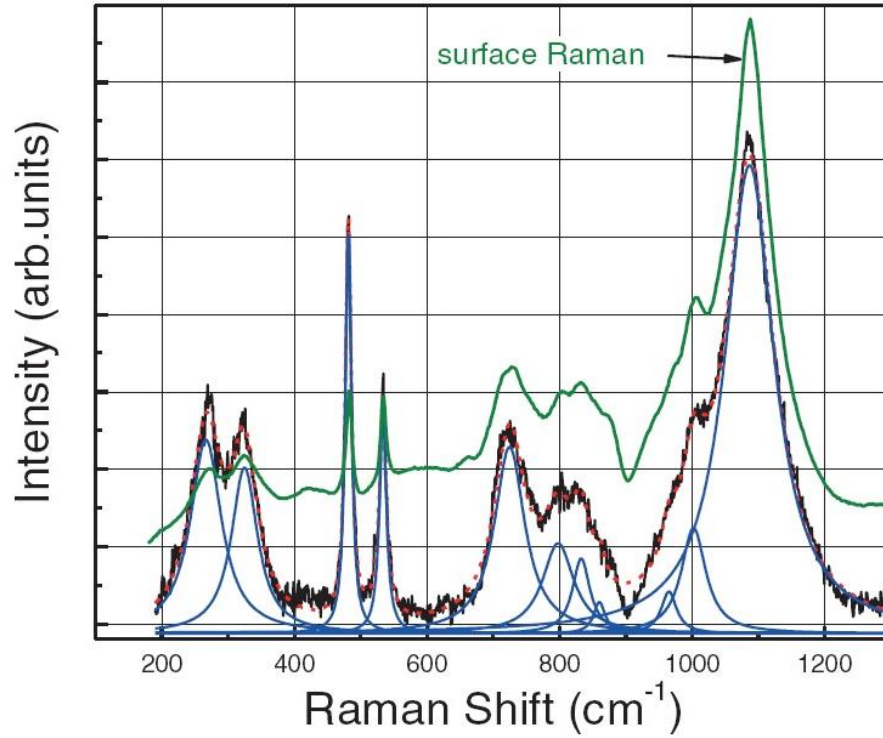
Figure I.3-3. Example of Raman spectra of B$_{4.3}$C at ambient conditions. For details, see [116].

Raman spectroscopy at high pressure was performed up to 50 GPa in quasi-hydrostatic conditions and up to 23 GPa in non-hydrostatic conditions [122]. Investigations of polycrystalline (powder) samples showed softening of two Raman modes (those at 268 cm^{-1} and 328 cm^{-1} at ambient conditions) that was attributed to the subtle distortion of the boron carbide structure. At the same time, Raman spectroscopy measurements on single crystals of boron carbides up to 36 GPa at room temperature [107,127] did not show any phase transitions. However, recent investigations up to 70 GPa [116] reveal a pressure-induced phase transition of B$_{4.3}$C near 40 GPa, attributed mainly to the changes in the structure of the C-B-C chain [116].

To resolve apparent contradictions described above, new high-pressure structural investigations, involving both spectroscopic and diffraction measurements, are highly necessary. Structural stability at around 40 GPa is needed to be verified.

Summarizing, the goals of the present work were to examine structural stability of boron and boron-rich compounds up to at least 100 GPa and to investigate the experimental boron phase diagram at pressure higher 20 GPa.

II.   METHODS AND INSTRUMENTS

In this work for high-pressure synthesis large volume press (LVP) with toroidal anvils was used. Chemical compositions of all the synthesized samples were verified by scanning electron microscopy. The studies of synthesized samples were carried out using spectroscopic (Raman and IR) techniques and X-ray diffraction performed "in house" as well as using synchrotron facilities. The *in-situ* experiments of high pressure behavior of the synthesized samples were conducted by means of the diamond anvil cell technique (DAC).

II.1. Synthesis techniques

II.1.1. Toroidal large volume press

A toroidal large volume press (or simply toroidal press) is a hydraulic press equipped with toroidal anvils, which comprise the HP device that is a descendant of Bridgman anvils apparatus. The toroidal-anvil apparatus was developed in Russia in 1970s and protected by the patents of the USA, Japan, Germany, France, and Great Britain [131]. It consists of two identical coaxial dies. Each die has a central section and a circular groove located concentrically (Figure II.1-1) [132]. When dies are forced together, the grooves form a central chamber and a secondary cavity of a toroidal shape, which enclose a gasket of a corresponding form (Figure II.1-1). The gasket contains a sample and its material serves as a pressure transmitting medium.
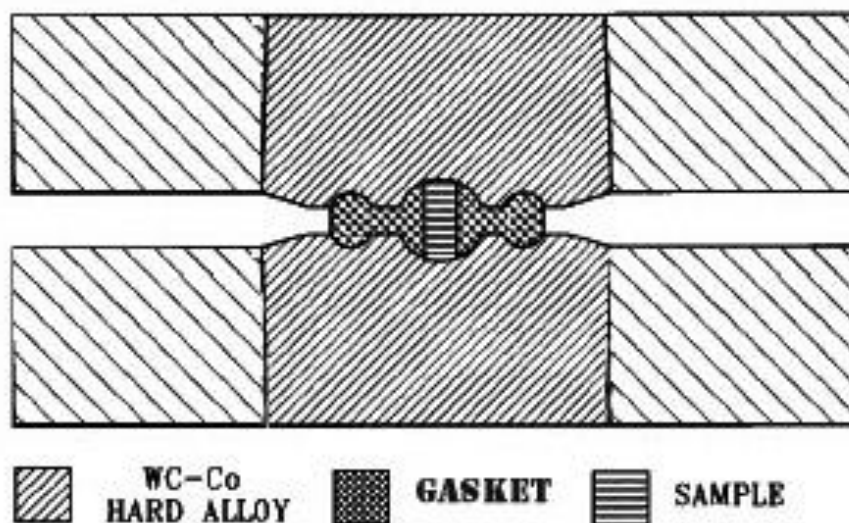
Figure II.1-1. Toroid type high pressure device with recessed central part [132].

'Toroid' sounds in keeping with 'Thor', in Scandinavian Mythology the god of thunder. Curiously, the Eyrarland Statue (from about AD 1000) found in Iceland (Figure II.1-2) depicts Thor with a hammer, whose shape resembles the profile of the toroidal anvil [133].

Figure II.1-2. The bronze statue from the Icelandic national museum which probably points Thor [133]. Red rectangular points the profile of the hammer, which this ancient god of a thunder, storm and fertility wielded in myths of ancient Germans and Scandinavians.

Toroidal device was not fully recognized in the world community because of unconventional geometry and the possibility of appreciable pressure gradients in the working zone. However, the presence of a toroidal recess around the central part on the working surfaces of the anvils reduces the extrusion of the central portion of a gasket and decreases the magnitude of shear stress in anvil what increases service life of the device and the maximum attainable pressure for the large sample volume ($\sim$10 cm^3 – $\sim$ 0.1 mm^3) [131]. Maximum pressure depends on the recess diameter (Toroid-10 – 14 GPa, Toroid-14 – 10 GPa, Toroid-50 – 7 GPa) and the material of the central part (WC – 15 GPa, artificial polycrystalline diamonds – 35 GPa in $\sim$0.1 mm^3) [131]. Recent developments for optimization of the LVP with toroidal anvils enhanced the pressure maximum to 25 GPa in volumes of $\sim$10 mm^3 using two stage device and double-toroidal anvils [131,134]. Extremely simple and reliable in operation, the device consists of two anvils that can be installed in a conventional hydraulic press. The preparation of an experimental cell with a gasket and sample assembly doesn't take as much time as for a multi-anvil experiment. Even at maximum pressures, the gap between the anvils remains sufficiently large for leading-in a number of measuring wires, what allows for

electrical measurements even during multiple cycles of increasing and decreasing pressure. Due to large clearance between the anvils, structural investigations are possible using X-ray and neutron scattering [135,136]. The geometry of the toroid cell allows introduction of a liquid-filled ampoule in the high pressure zone [132].

Nowadays, the Toroidal type high-pressure devices are used for synthesis of new materials as well as structural investigations [137-139] and measurements of different physical properties of substances (for example, electron transport properties, thermodynamic characteristics, viscosity, thermal conductivity, elastic characteristics, superconductivity under pressure) [131].

II.1.1.1. Description of the Orange Mammoth

The Large Volume Press installed in the Laboratory of Crystallography in the University of Bayreuth in 2014 (called Orange Mammoth, Figure II.1-3) is the 12MN Laboratory press of frame construction *MavoPress LPRU 1200 – 555/50* with toroidal anvils, manufactured by the Max Voggenreiter GmbH. It was designed in collaboration with Prof. Dubrovinskaia and Prof. Dubrovinsky of the University of Bayreuth and sponsored by the Deutsche Forschungsgemeinschaft.

In the image of the press system (Figure II.1-3A), its major parts are designated: the control block (1), the hydraulic aggregate (2), the working space with protecting windows (3) (Figure II.1-3B), the hydraulic cylinder (4), the water cooling system (5), the tilt crane (6). The anvils holder for cleaning of anvils and toroidal anvils (sets of different sizes are available) are shown in Figure II.1-3C. The press can be operated both manually and automatically, through the control system from the controlling laptop using the software installed. A program is written allowing to set the desirable parameters of an experiment, such as attained pressure, speed of compression and decompression as well as the duration of the experiment. If necessary, cycling experiments can also be programmed. The samples are heated using resistive heaters and temperature is monitored using calibration curves described below.
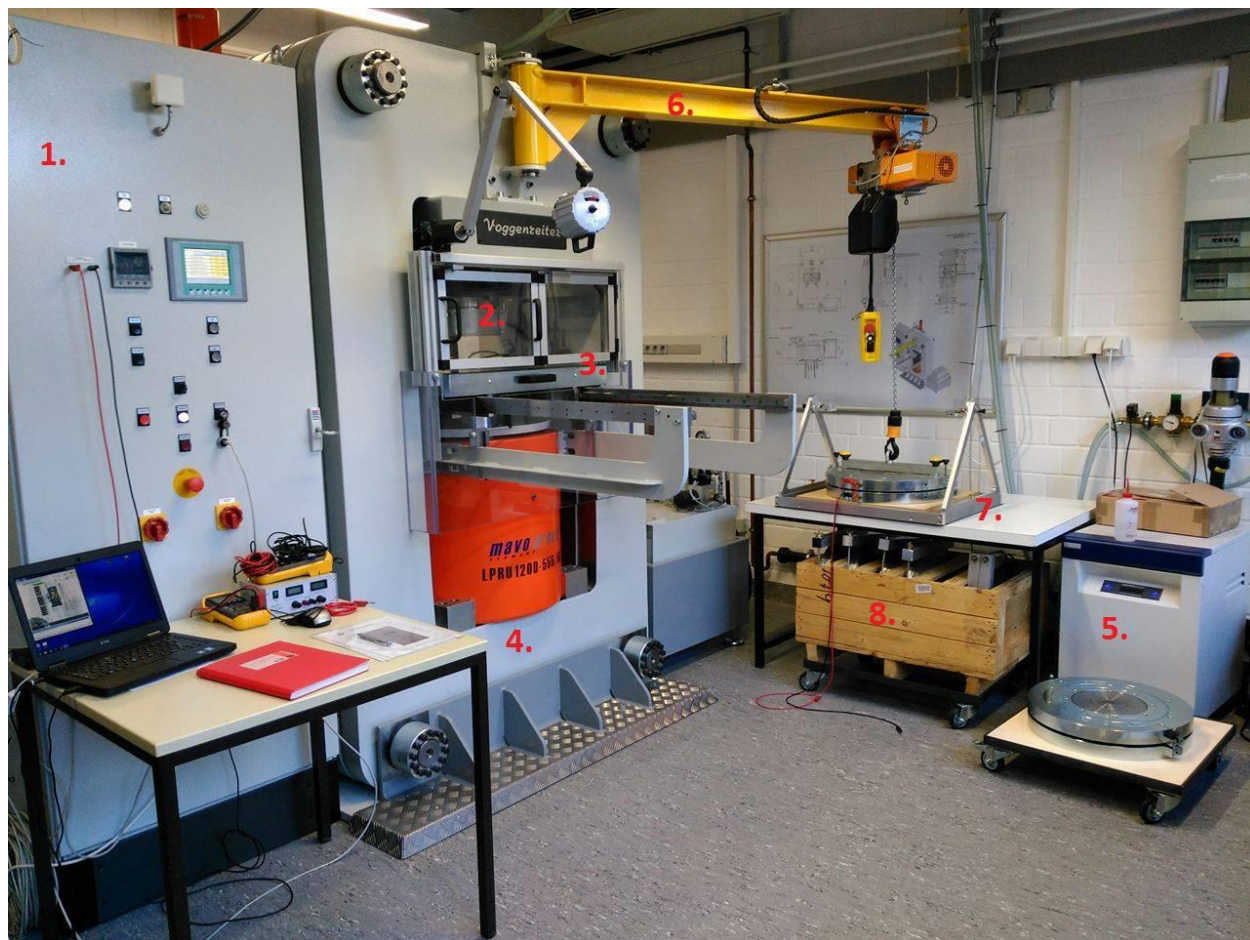
A.
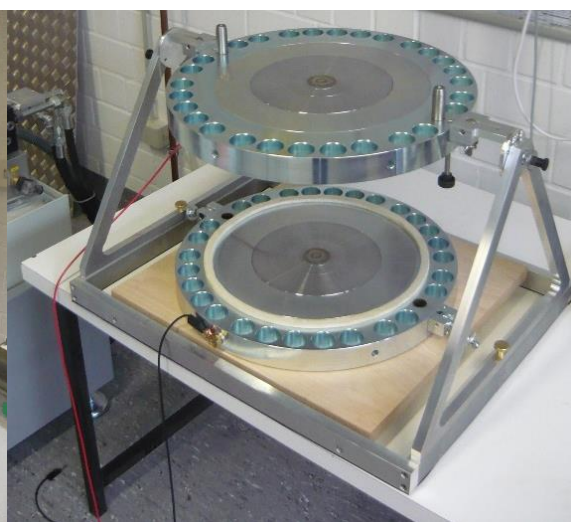
B. **C.**

Figure II.1-3. A. 12MN Laboratory press of frame construction MavoPress LPRU 1200 – 555/50. It is equipped with toroidal anvils. The system consists of the control box (1), the hydraulic aggregate (2), the working space with protecting windows (3), the hydraulic cylinder (4), the water cooling system (5), the tilt crane (6), cleaning holder (7), holder for spare sets of anvils (8). **B.** Enlarged photo of the working space with open protecting window (2). **C.** Enlarged photo of anvils in the cleaning holder (7).

Working space includes tool slides with the tool carriage used to transfer the anvils with the sample into the press. To the tool carriage the assembled anvils are transported with the help of the

tilt crane. The table of the holder for cleaning is the place where the anvils are stored between the experiments. Under the table there is a container with sets of changeable toroidal anvils with different sizes: Toroid-14, Toroid-25 and Toroid-40 (14, 25 and 40 mm is the central recess diameter, respectively). Toroid-40 can be used for the synthesis of large single crystals of diamond. For the current work, Toroid-14/6 and Toroid-14/8 were used (6 mm and 8 mm are the height of the gasket, respectively).

Toroidal anvil is made of WC with weight of 4400 g. The steel binding ring supports the anvil die around its outer diameter. All together a pair of anvils' weight is around 50 kg (Figure II.1-4.).
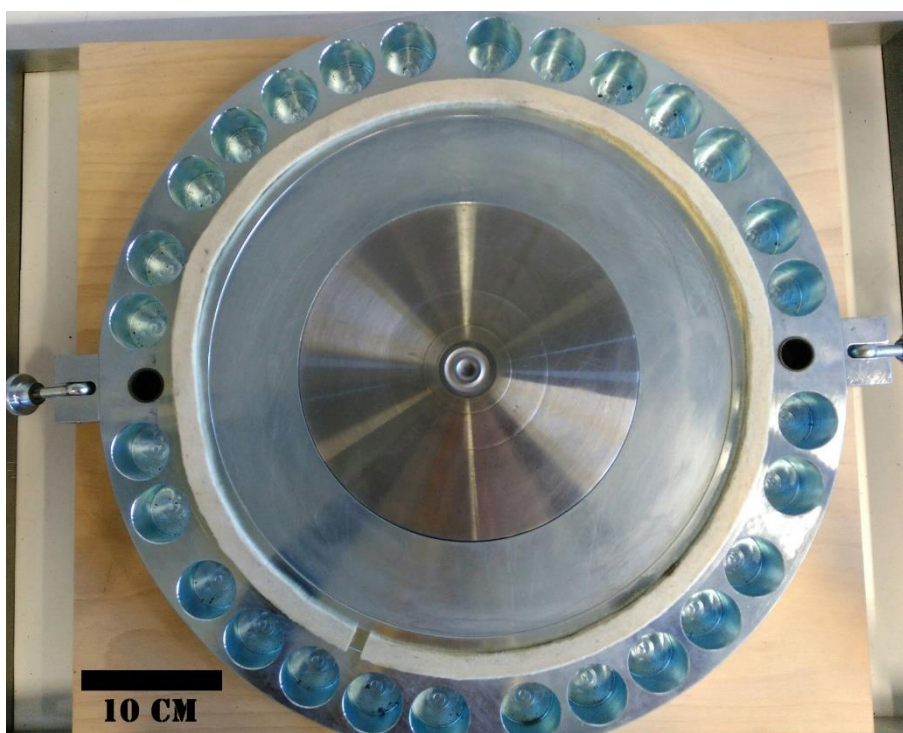
Figure II.1-4. Photo of toroidal anvil used for synthesis experiment in the present work. The inner core is made of WC. The steel binding ring supports the anvil die.

Between the anvils the sample assembly is placed. The assembly consists of (Figure II.1-5.):

1. a gasket made of either pyrophyllite annealed at 700°C for 24 h or sintered chromium doped magnesium oxide Cr:MgO produced by Ceramic Substrates & Components Ltd using 95% high purity MgO;

2. ZrO_2 insulator;

3. graphite heater;

4. h-BN capsule with sample volume of ~6.5 mm^3 for 6 mm thin gasket and ~10 mm^3 for 8 mm thick gasket.
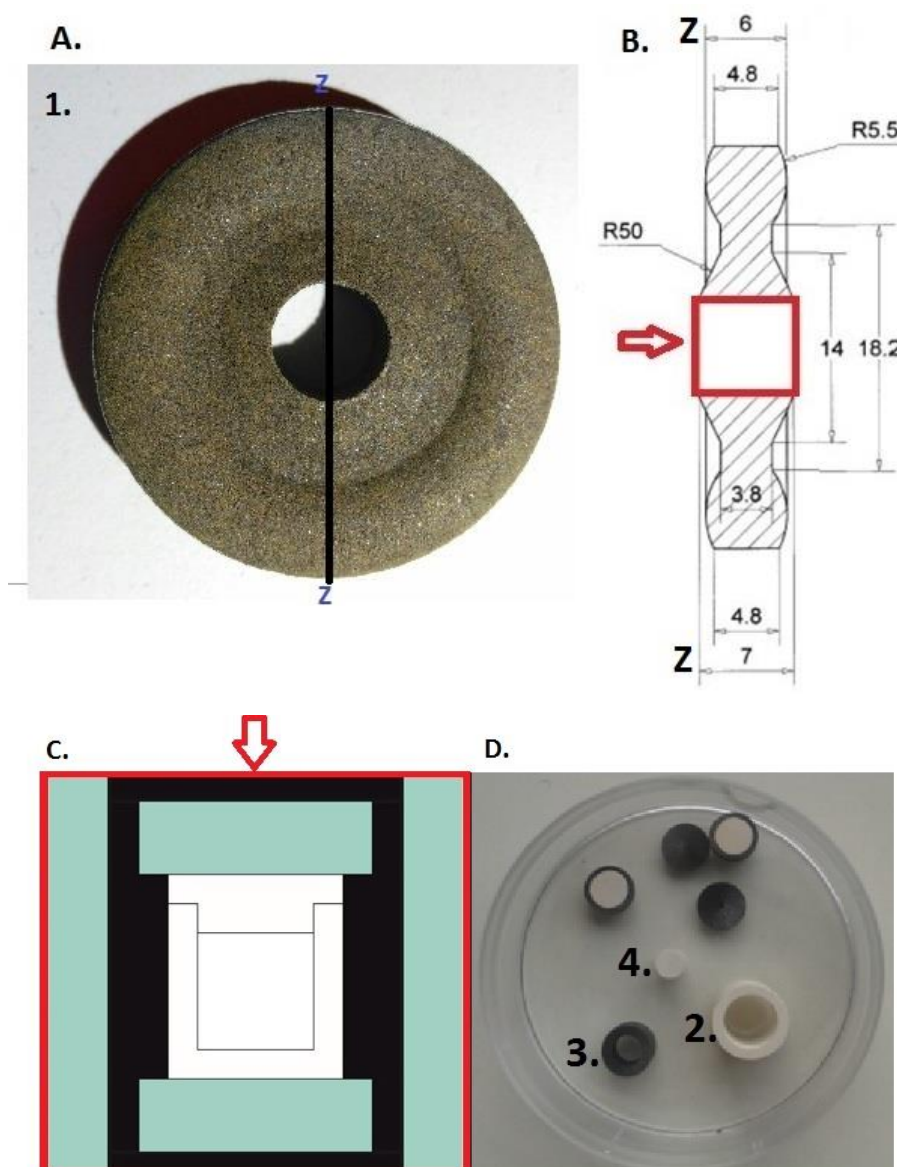
Figure II.1-5. The sample assembly for the laboratory toroidal LVP Orange Mammoth. The assembly consists of: 1. a gasket; 2. ZrO$_2$ insulator; 3. graphite heater; 4. h-BN capsule. **A.** Photo of a gasket made of sintered chromium doped magnesium oxide Cr:MgO produced by Ceramic Substrates & Components Ltd using 95% high purity MgO. **B.** Schematic representation of cross-section of gasket. **C.** Schematic representation of sample chamber. **D.** Photo of parts of assembly (2. ZrO$_2$ insulator; 3. graphite heater; 4. h-BN capsule).

II.1.1.2. Pressure calibration

For performing experiments on new LVP, dependence of pressure in the sample on the oil pressure, i.e. pressure calibration should be known. In this work pressure calibration experiments were performed at room temperature for all types of gaskets: made of pyrophyllite and Cr:MgO as well as for both thicknesses.

According to the International Practical Pressure Scale (IPPS) established in 1970s–1980s [140,141] by the International Association for the Advancement of High Pressure Science and

Technology (AIRAPT), in the pressure range above 1.4 GPa presses are calibrated using phase transitions and recommended values were published in [141]. Phase transitions in solids can be detected by numerous methods. The electrical resistance is one of the most useful and accurate determinations of the transition points.

In the current work, Bi and Yb were used as metals with pressure-induced fixed-point phase transitions. Thin, sequentially connected strips of Bi and Yb were placed between two cylinders of pyrophyllite, which were enclosed into the sample chamber of a toroidal cell (instead of a sample assembly) (Figure II.1-6). Copper strips connected calibrants (strips of Bi and Yb) with the upper and lower anvils, so that the electrical current could pass through the metals between the anvils when the cell is mounted between them for a calibration experiment (Figure II.1-6). In order to provide a better electrical contact a piece of Cu foil was placed additionally on both sides of the cell.
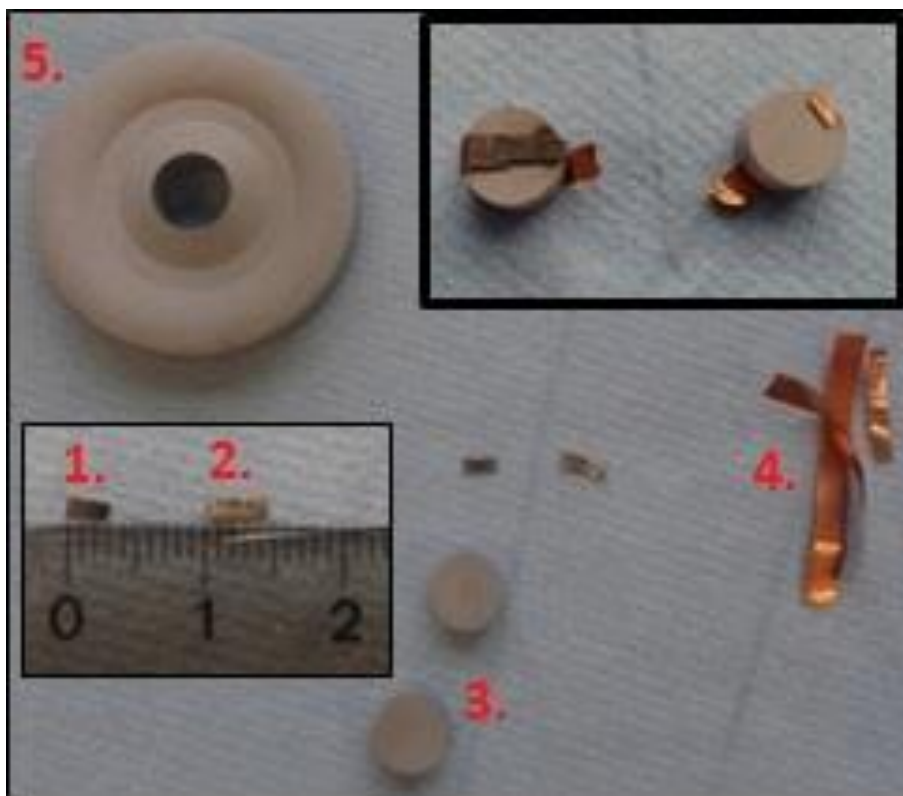
Figure II.1-6. Photos of sample assembly for pressure calibration experiments. 1. Bi strip, 2. Yb strip, 3. Pyrophilite cylinders, 4. Cu strips, 5. A gasket made of pyrophyllite annealed at 700°C for 24 h.

The anvils were placed in the working space and connected to the current source (4) and multimeter (5) (Figure II.1-7). The value of the current was 400 mA in every experiment. In order to obtain the values of pressure, the control box (1) was also connected to multimeter (2). Both multimeters were connected to the laptop (6), where the specially developed software read the values of the electrical resistance of the sample depending on the supplied pressure.

Figure II.1-7. Photo of toroidal press during pressure calibration experiments. The control box (1) is connected to multimeter (2). The toroidal anvils (3) are connected to the current source (4) and the electrical resistance of the sample is measured on the multimeter (5). Both multimeters are connected to the laptop (6), where the specially developed software read the values.

The assembly was compressed up to 180 bar of oil pressure with a speed of 6 bar/minute. Electrical resistance of the assembly was measured depending on the oil pressure during both compression and decompression. However, because of hysteresis in solid pressure transmitting substances, calibration of pressure apparatuses is usually made on the basis of ascending pressure (Figure II.1-8). Using the pressure of phase transitions at absolute scale (Table II.1-1), pressure calibration curves were plotted (Figure II.1-9). The maximum pressure achieved with Toroid-14/6 anvils is 10 GPa.
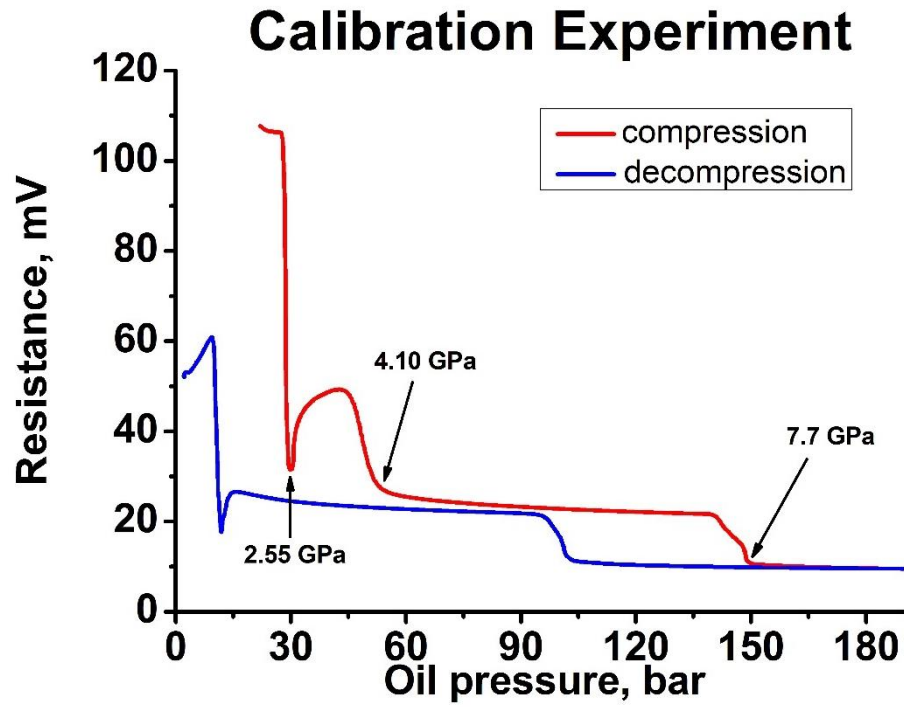
Figure II.1-8. Calibration curves for pyrophyllite toroidal cell with the Toroid-14/6 anvils. Dependence of the electrical resistance of the assembly on oil pressure during compression (red line) and decompression (blue line). Arrows points out the transitions taken for pressure calibration curves.

Table II.1-1. Values for pressure fixed points at room temperature taken from [141,142].

Transition	Pressure, GPa
Bi I-II	2.550(6)
Yb (fcc → bcc)	4.1(2)
Bi III-V (upper)	7.7(2)

Pressure calibration lines
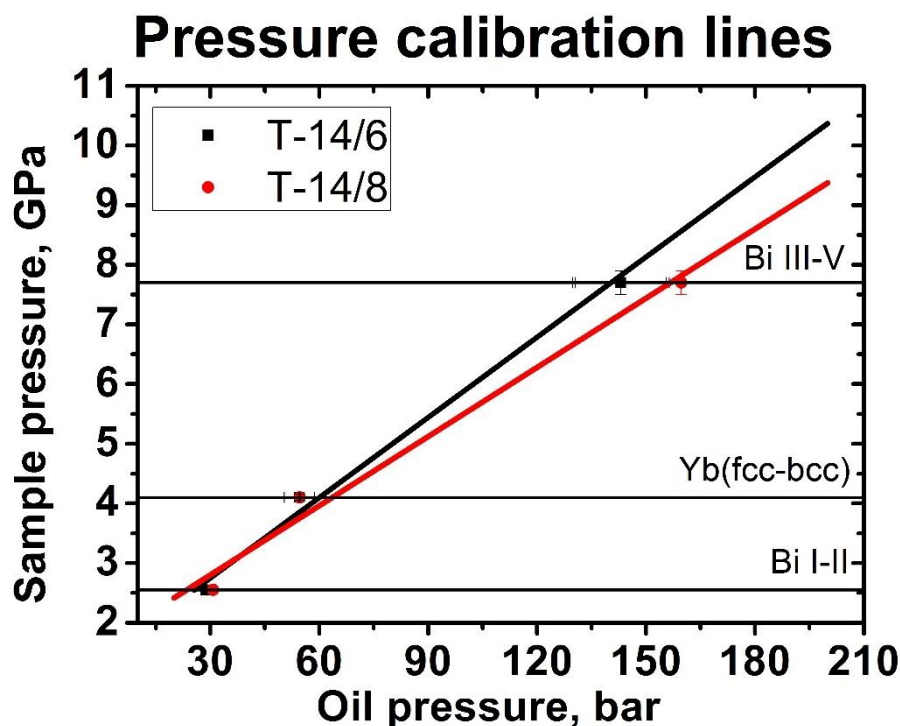
Figure II.1-9. Pressure calibration lines. Black line represents Toroid-14/6 (thickness of the gasket is 6 mm). Red line corresponds to Toroid-14/8 (thickness is 8 mm). Transition values are shown as horizontal lines as a guide for eyes.

II.1.1.3. Temperature calibration

For synthesis at extreme conditions, both pressure and temperature are needed. The fundamental worldwide used temperature scale is based on the second law of thermodynamics [140]. The International Temperature Scale updated in 1990s is based on 6 fixed points: ice, steam, boiling points of oxygen and sulfur, freezing points of silver and gold [143]. However, all of them are difficult to detect during high pressure experiment in LVP. There are several possibilities to calibrate temperature in HPHT experiments, for example, one can use a thermocouple (e.g., Pt-PtRh up to 1873 K), or determine melting points of some materials, or detect phase transitions in certain compounds under pressure. Although, use of a thermocouple is associated with some uncertainties in temperature determination (e.g., we can never insert it directly to the pressure chamber, or a correction of its emf under pressure is not always possible to introduce), it would be the most straightforward way to calibrate the electrical power *versus* temperature for the resistive graphite heaters we use. Unfortunately, it turned to be not the easiest way: all our attempts failed because during compression the thermocouples were broken.

Next possibility is the use of melting points of some compounds. In this work, metallic foils or wires of a number of metals (silver, aluminum, gold, platinum, and iron) were chosen. Pieces of metals (except for Al) were put into the capsule filled with NaCl used as a pressure transmitting medium (PTM) (as an example, Pt pieces in NaCl before the experiment are shown in Figure II.1-

41

10A). As Al reacts with NaCl, pieces of Al wire were put in the capsule without any PTM. The sample was compressed up to 3 GPa (the minimal pressure available on Orange Mammoth). The temperature was increased and the sample was kept under this temperature for 30 minutes. Temperature quenching was done by switching off the power. Afterwards, the decompression was done in 3 minutes.

After each experiment, the sample was analyzed by means of optical microscopy. Example of Pt pieces after the experiment is shown in Figure II.1-10B. For experiments with Al, SEM analysis was performed in order to find out if grains recrystallized or not.

A   **B**
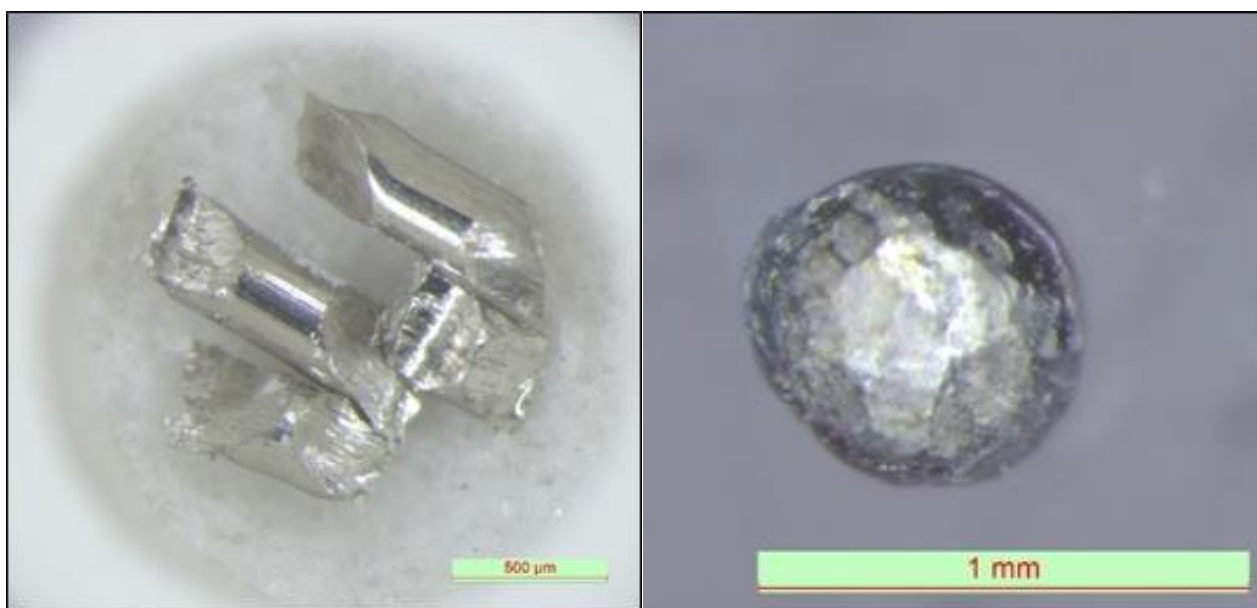
Figure II.1-10. A. Pt pieces in the capsule filled with NaCl before the experiment. **B.** Ingot of Pt after the experiment.

After carrying out several experiments for each metal, the dependence of temperature on applied power, i.e. temperature calibration curve was plotted as presented in Figure II.1-11. All synthesis experiments in the present work were carried out at pressure of 3 GPa.
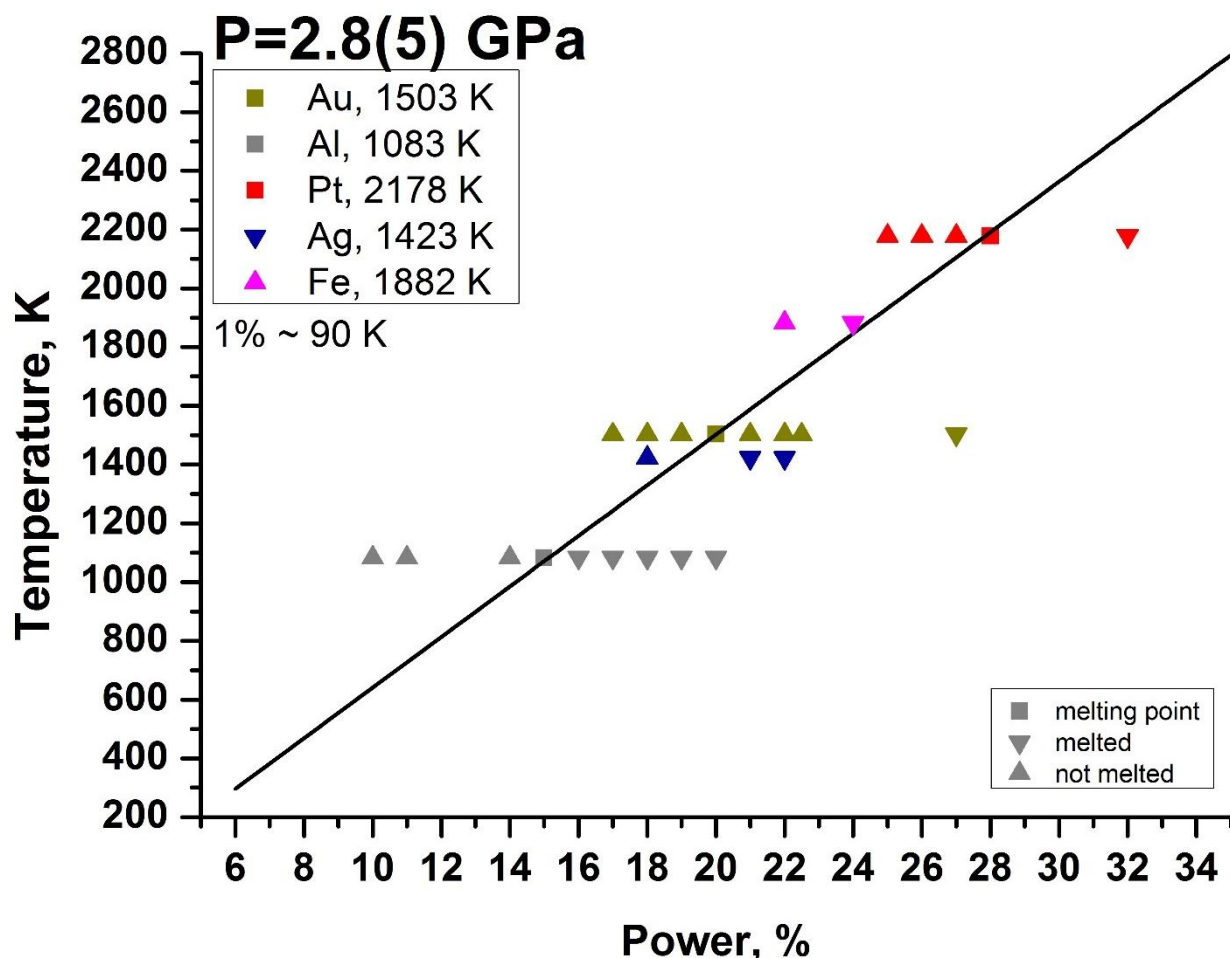
Figure II.1-11. Temperature calibration lines for Toroid-14/6. Metals used in experiments are Au (dark yellow), Al (grey), Pt (red), Ag (dark blue) and Fe (magenta). Up-triangle means not melted metal, down-triangle means melted metal, square represents the melting point. Black line is a linear fit of experimental values of melting temperature of metals *vs* electric power.

II.1.2. Diamond anvil cell

Diamond anvil cell is a universal device for matter research at extreme conditions. The technique was introduced in the late 1950s. Since then the range of attainable static pressure extends to 1 TPa [144], much higher than the estimated pressures at the Earth's center (~360 GPa). Small volume of the sample makes DAC ideal for high pressure single-crystal XRD measurements. Transparency in the wide range of radiation, from infrared (IR) to γ-ray regions allows *in situ* spectroscopic studies. DAC consists of a pair of polished diamonds, mounted on tungsten carbide seats placed in the metallic cell (Figure II.1-12). For current project, the BX90-type DACs [145] made at Bayerisches Geoinstitut (Bayreuth, Germany) and Boehler-Almax type [146] beveled diamonds with the culet diameters of 120 and 250 μm were used in high pressure experiments.

<div align="center">A   B</div>
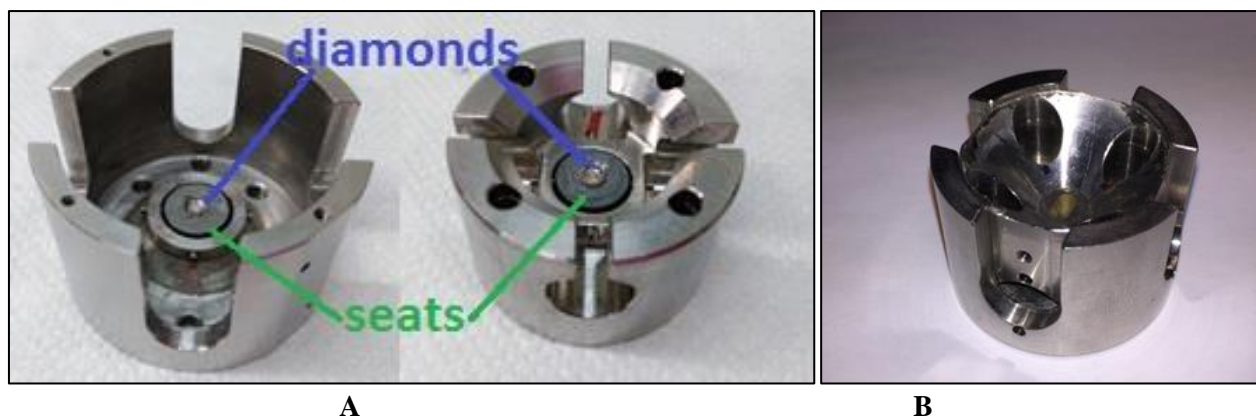
Figure II.1-12. A. Two (piston and cylinder) parts of the metallic body of a DAC with a pair of polished diamonds mounted on WC-seats. **B.** Photograph of a loaded cell.

Between the two opposing diamond culets a Re gasket is squeezed to 20-50-micron thickness. A sample together with a pressure transmitting medium and ruby as a pressure calibrant are loaded in the hole in the gasket forming a pressure chamber (Figure II.1-13).

<div align="center">A   B</div>
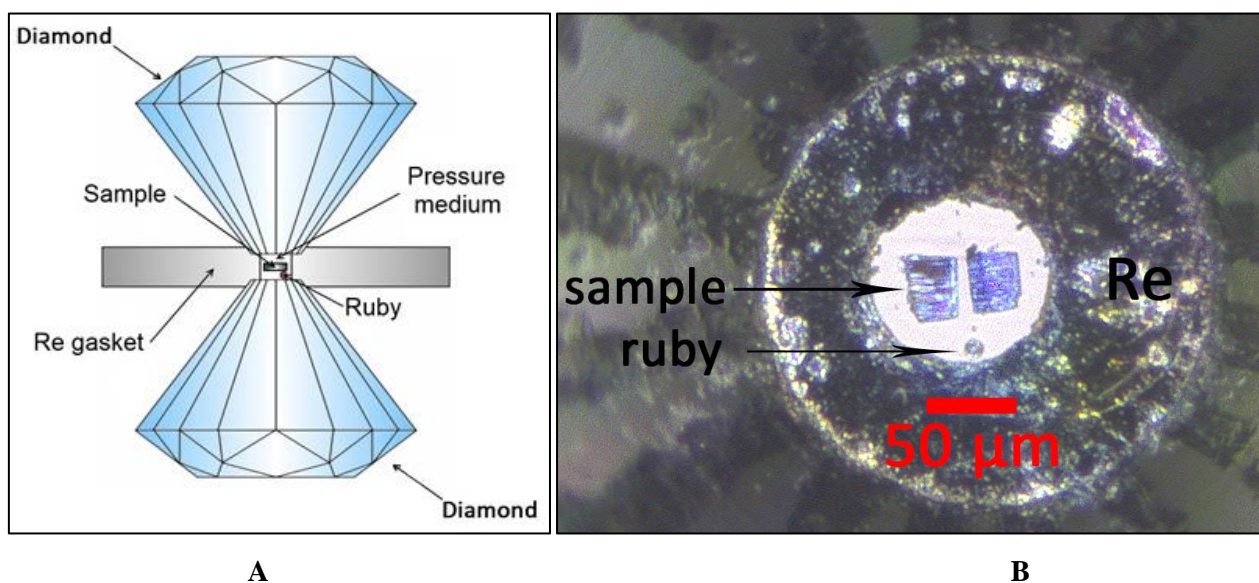
Figure II.1-13. A. The scheme of diamond anvil cell without metallic body and seats. **B.** Photograph of the pressure chamber taken under an optical microscope through the diamond anvil.

Pressure transmitting medium is used to transmit the pressure from diamonds to the sample. Inert gases are the best candidates as they create quasi-hydrostatic environment to at least 150 GPa. In the current work Ne was used as a pressure transmitting medium.

The pressure determination was done by ruby laser-induced fluorescence method [147,148] for preliminary P estimations as well as by powder X-ray diffraction obtaining the unit cell parameters of pressure calibrant Ne [149-151] (Figure II.1-14.).

A **B**
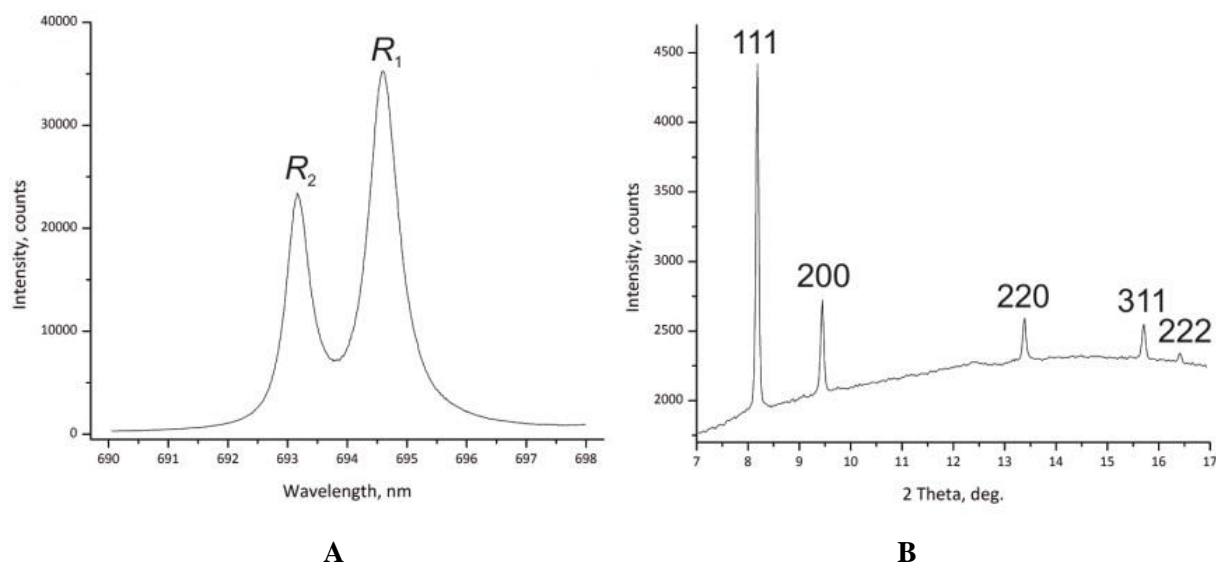
Figure II.1-14. A. Fluorescence spectra of ruby. For pressure estimation one measures a position of the lines *R*1. **B.** Powder XRD pattern of solid Ne at 12.3 GPa with indexed reflections used for calculation of the unit cell volume. The pressure is determined from Ne equation of state.

For generation of high temperatures in DACs there are two possibilities: external electrical resistive heating and laser heating [152,153]. In the current work double-side laser heating technique was used. It covers higher temperature range (1300-5000 K), allows to avoid large thermal gradients (compared with one side laser heating), and provides an opportunity to collect XRD simultaneously with heating [154].

II.2. Analytical techniques

II.2.1. X-ray diffraction

X-ray diffraction is a powerful non-destructive analytical technique used for determination of crystal structure and phase composition. Experiments at various pressures and temperatures allow measurements of compressibility and thermal expansion of materials. X-rays are a form of electromagnetic radiation with wavelength from 0.01 to 100 nm corresponding to energies in the range 100 eV to 100 keV.

There are two common ways to produce X-rays: X-ray tubes and synchrotrons. In X-ray tubes, X-rays are produced by bombarding a target of a suitable material with a focused electron beam. The focused beam size is about ~50 μm in diameter. In synchrotrons, electrons with high energy are deflected by electromagnetic fields, yielding X-ray emission. Synchrotrons provide by about billion times higher brilliance (the measure of photons that can be concentrated on a spot) of an X-ray beam than laboratory X-ray sources. A small focused X-ray beam is required for ultrahigh-pressure (100+ GPa) and laser heating experiments, when sample area is very tiny.

X-ray impinging on regular arrangement of the atoms in solid matter are scattered in various directions by the atomic electrons. The diffracted beams produce constructive interference when conditions satisfy Bragg's law, which gives the geometrical conditions under which a diffraction maximum can be observed:

$$n\lambda = 2d \sin\theta$$

where d is the interplanar spacing, θ is the Bragg angle, n is the order of interference, λ is the wavelength (Figure II.2-1.) [155-157].
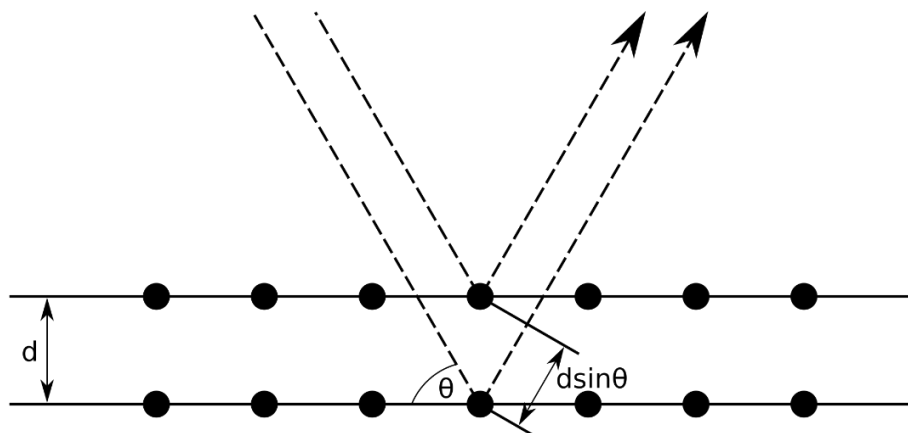
Figure II.2-1. Illustration of Bragg's law. Constructive interference conditions for a family of *hkl*-planes. Coherent waves meeting the family of *hkl* plains interfere with each other if the phase difference is equal to integer number of wavelengths. Figure is taken from [158].

Every *d* has corresponding indexes in the reciprocal space *h*, *k*, *l* (the Miller indices). They define families of lattice planes formed by atoms in a crystal. Measuring array of intensities with corresponding *hkl* makes possible to determine the structure parameters, the unit cell and solve the structure.

The directions of possible diffractions depend on the size and shape of the unit cell of the material. The intensities of the diffracted waves depend on the kind and arrangement of atoms on the crystal structure. As most materials are composed of many tiny crystallites, planes of differently oriented crystals, for which Bragg condition is met, reflect. Projection of three-dimensional reciprocal space onto one-dimensional *2θ* axis cause accidental and systematic peak overlap. Rietveld method creates a virtual separation of these overlapping peaks thereby allowing determination of atomic positions and lattice parameters as well as crystal structure solution.

Powder diffraction at high pressure is much more difficult task than at ambient conditions. Such experiments require long time of data collection due to a small amount of the material. Diamonds, solidified pressure transmitting medium, and sometimes a gasket exposed to the X-ray give rise to the diffraction rings that may overlap with the sample. Principles of powder X-ray diffraction (XRD) in DACs are presented in numerous reviews (see for instance, [159,160]).

In the present work, powder XRD measurements of the samples in DACs were carried out at room temperature in angle-dispersive mode with a wavelength of 0.2952 Å at the 13-IDD beamline at APS, Argonne. Diffraction images were collected at each pressure using a MAR CCD detector in the omega scanning range of −20° to +20° with an exposure time of 40 s. The images were integrated using the DIOPTAS software [161] and the resulting diffraction patterns were processed using biased model in the EXPGUI software [162] in the GSAS Software package [163].

Powder diffraction is a powerful and important tool, however, when there is a possibility of growing a single crystal of about 10 μm size, structure solution becomes easier task using advantages of single crystal X-ray diffraction: presence of each reflection individually; measurement of the intensity of each spot as a function of the Miller indices, etc.

Single crystal X-ray diffraction experiments at extreme conditions require very good quality single crystals as at high pressure the crystal is affected by stresses that cause strains propagating through the sample and deteriorating it. Therefore, a careful selection of the single crystal is necessary either on the in-house diffractometer or on the synchrotron facilities.

X-ray data collected in DAC have worse quality than at ambient conditions because the opening angle of the DAC doesn't exceed 80°. The available part of the reciprocal space is significantly small and the number of available reflections is limited what creates problem for the solution of low-symmetry structures and refinement of anisotropic thermal parameters. The high-pressure data suffer from the overlapping with peaks by diamond and rings of crystallized pressure

medium and gasket. Despite all these difficulties, single crystal X-ray diffraction is more powerful tool for obtaining atom positions in the structure at any conditions than powder diffraction.

Data collection is followed by data reduction performed using CrysAlisPro software [164,165]. The quality of the data is indicated by R_{int}, R_σ and $F_{obs}^2/\sigma_{int}(F_{obs}^2)$ values derived as follows:

$$R_{int} = \frac{\Sigma|F_{obs}^2 - \langle F_{obs}^2 \rangle|}{\Sigma|F_{obs}^2|},$$

$$R_\sigma = \frac{\Sigma[\sigma_{int}(F_{obs}^2)]}{\Sigma[F_{obs}^2]},$$

$$\sigma_{int}(F_{obs}^2) = \sqrt{\frac{\Sigma(F_{obs}^2 - \langle F_{obs}^2 \rangle)^2}{n}},$$

where the summations are taken over all input reflections; F_{obs}^2 is intensity corrected for Lorentz-polarization, $\langle F_{obs}^2 \rangle$ is its mean value over all measured equivalents; n – is the number of redundant reflections. Poor $F_{obs}^2/\sigma_{int}(F_{obs}^2)$, high R_σ values (< 3 for and $> 20\%$, respectively) and high R_{int} values mean that a dataset has insufficient intensities, whereas the opposite situation indicates more complicated case. When the number of the saturated intensities is too high, and the R_{int} value is low and does not anymore indicate the data quality. $F_{obs}^2/\sigma_{int}(F_{obs}^2)$ values are high and R_σ values are low in this case [155-157].

Next step of X-ray diffraction process is structure solution followed by structure refinement. The structure solution is a process using intensities of collected reflections for calculation of atomic positions and thermal parameters. Reflection intensities are equivalent to squared experimental structural amplitudes F_{hkl}^2 after applying special corrections:

$$I_{hkl} = c \cdot A \cdot L_p \cdot e \cdot T \dots \cdot |F_{hkl}^2|,$$

where c is the scale factor depending on the crystal volume, intensity of the primary beam and exposure time; A is the transmission factor; L_p is the Lorentz-polarization correction; e is the extinction correction; T is the Debye-Waller factor. F_{hkl} is the structural amplitude of the wave diffracted from a family of crystal lattice planes in units of scattering amplitude of a single electron. The wave diffracted from crystal lattice planes is described by the structure factor:

$$\mathbb{F}_{hkl} = F_{hkl} \exp(i\alpha_{hkl}) = \sum_{j=1}^{N} f_j exp[2\pi i(hx_j + ky_j + lz_j)] =$$

$$= \sum_{j=1}^{N} f_j cos[2\pi(hx_j + ky_j + lz_j)] + i \sum_{j=1}^{N} f_j sin[2\pi(hx_j + ky_j + lz_j)]$$

where N is number of all atoms in the unit cell, x_j, y_j, z_j are the coordinates of the jth atom, f_j is the scattering factor of the jth atom, and α_{hkl} is the phase of the diffracted beam. Structure factor is a complex number and its amplitude is derived from the diffraction experiment. There is a so-called phase problem as phases are unknown. There are several techniques in different structure solution

software for phase determination: direct methods, Patterson method, heavy-atom method, charge flipping, etc. However, incomplete high-pressure datasets can decrease chances of the structure solution especially for low-symmetry structures. As soon as the phases are derived, atomic coordinates can be calculated using dependence of electron density ρ_{xyz} on the structure factor $\mathbb{F}_{hkl}$ through inverse Fourier transformation:

$$\rho_{xyz} = \frac{1}{V} \sum_{hkl} \mathbb{F}_{hkl} \, exp[-2\pi i(hx + ky + lz)]$$

where V is the volume of the unit cell. Once initial structural model is obtained, the atomic positions, occupancies and anisotropic displacement parameters are refined [155].

Agreement between the model and experimental data is defined by so-called residual R-factors, which represent the quality of the structural model:

$$R_1 = \frac{\sum||F_{obs}| - |F_{calc}||}{\sum|F_{obs}|},$$

$$wR_2 = \left[\frac{\sum w|F_{obs}^2 - F_{calc}^2|}{\sum wF_{obs}^2}\right]^{0.5}$$

where F_{obs} − is the observed structure factor amplitude, F_{calc} − is the calculated structure factor amplitude from the model; and w − is the weighting factor individually derived for each measured reflection based on its standard uncertainty [155-157].

For current work the structures were solved and refined in the anisotropic approximation for all atoms (when not possible, in isotropic) by full matrix least-squares using SHELXL software [166] in the WinGX software package [165].

In the present work X-ray diffraction techniques were used for the phase identification and the structure solution. Boron is a light element, which makes it to be a weak X-rays scatterer. Therefore, acquiring data of acceptable quality requires using synchrotron radiation. Experiments on single-crystal X-ray diffraction were carried out on two synchrotron XRD beamlines: ID27 at the European Synchrotron Radiation Facility (ESRF) and P02.2 Extreme Conditions beamline at PETRA III, DESY.

At ID27 diffraction data were collected at 293 K using the Perkin Elmer XRD1621 flat panel detector. The monochromatic radiation had the wavelength of 0.37380 Å and the crystal-to-detector distance was 383 mm. A portable double-sided laser heating [154] system was used for experiments on ID27 (ESRF) to collect *in situ* single-crystal X-ray diffraction. Crystals were completely 'surrounded' by laser light and there were no measurable temperature gradients within the samples. The temperature variation during the heating did not exceed ±100 K.

At P02.2 diffraction data were collected at 293 K using the Perkin Elmer XRD1621 detector. The monochromatic radiation had the wavelength of 0.29464 Å and the crystal-to-detector distance was 439 mm.

II.2.2. Vibrational spectroscopy

Vibrational spectroscopy is a non–destructive, non–invasive energy sensitive method that is used for identification, characterization, structure elucidation, reaction monitoring, quality control, and quality assurance. Infrared (IR) and Raman spectroscopy are two forms of vibrational spectroscopy. These techniques measure changes in the vibrational state of molecules.

II.2.2.1. Raman spectroscopy

Raman spectroscopy is the powerful non-destructive tool for analyzing phonon spectra of crystalline solids. Material is exposed to the laser irradiation in a near ultraviolet – near infrared range. When a beam of light is impinged upon a molecule, photons are absorbed by the material and then scattered elastically or inelastically. Elastic scattering means that the scattered photon has exactly the same wavelength ν as the incident photon and is known as Rayleigh scatter. Most of the photons are scattered elastically. However, a small fraction of light is scattered inelastically, i.e. the molecule emits a photon of a slightly different energy ν_1, which gives a rise to a Raman scattering. This difference in energies $h(\nu \pm \nu_1)$ provides information about frequency of the oscillation modes (Figure II.2-2.) [167,168].
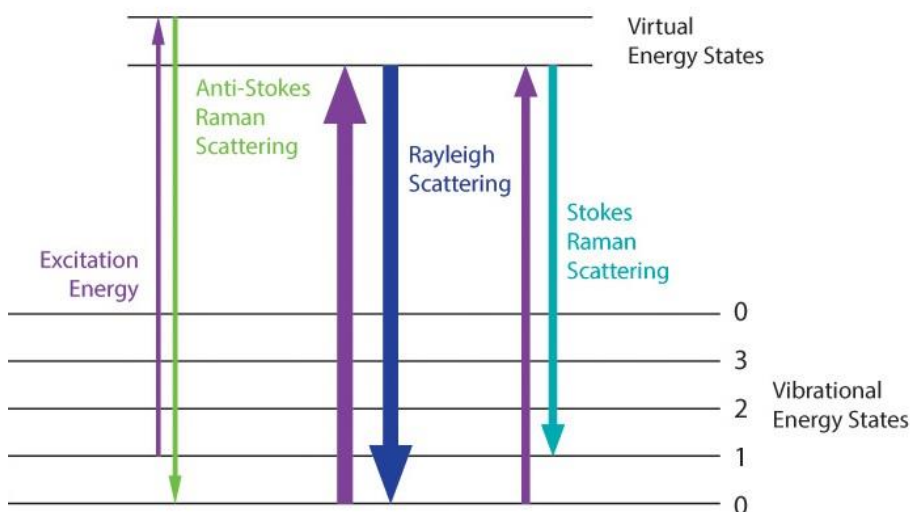
Figure II.2-2. Diagram of photon transitions in molecules under laser excitation. Figure taken from [169].

The peaks observed at higher frequency $(\nu + \nu_1)$ than the incident radiation (anti-Stokes lines) are less intense. In practice, due to the Stokes lines are more intense, the Raman shifts of those lines with respect to the Rayleigh line is measured (Figure II.2-3).
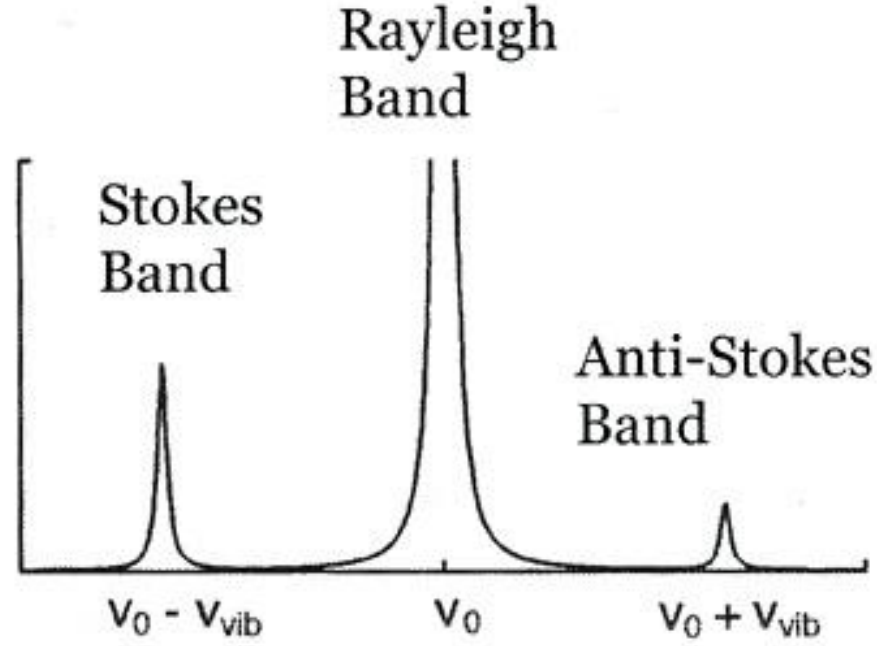
Figure II.2-3. Scheme of vibrational spectrum. Figure is taken from [170].

The Raman shifts, i.e. bands in a Raman spectrum represent the interaction of the incident light with a certain vibration of the nuclei. The vibrations of the nuclei depend on their sizes and masses, valences, and the forces between atoms, and the symmetry of a crystal structure. These factors affect the number of Raman bands, their relative intensities, their widths and polarizations.

The Raman effect is based on molecular deformations in electric field E ($E = E_0 \cos(2\pi v t)$, where v is frequency of induced electric field) determined by molecular polarizability α. The laser beam can be considered as an oscillating electromagnetic wave with electrical vector E. Upon interaction with the sample it induces electric dipole moment:

$$P = \alpha \cdot E.$$

If we consider q as a shift of a nuclei, and v_1 is an oscillation frequency of the molecule, then

$$q = q_0 \cos(2\pi v_1 t)$$

When the molecule vibrates, α is not a constant but depends on distance between atoms r:

$$\alpha = \alpha_0 + \left(\frac{\partial \alpha}{\partial q}\right)_0 q + \ldots, \text{ with } q = \Delta r.$$

Combining all above-mentioned equations:

$$P = \left(\alpha_0 + \left(\frac{\partial \alpha}{\partial q}\right)_0 q_0 \cos(2\pi v_1 t)\right) E_0 \cos(2\pi v t) =$$

$$= \alpha_0 E_0 \cos(2\pi v t) + \frac{1}{2}\left(\frac{\partial \alpha}{\partial q}\right)_0 q_0 E_0 (\cos(2\pi t(v + v_1)) + \cos(2\pi t(v - v_1)))$$

where the first term describes Rayleigh scattering on the frequency v and the second term describes Raman scattering on the Stokes (v–v_1) and anti-Stokes (v+v_1) frequencies [167,168].

Complex molecules or crystals have several types of vibrations. The classification of vibrations is based on group theory. To determine whether the vibration is active in Raman spectra, the selection rule must be applied to each normal vibration. From the last equation, it is clearly seem that vibration is Raman-active if the polarizability has changed with oscillations: $\left|\frac{\partial \alpha}{\partial q}\right| > 0$ [167].

Raman spectra can be obtained in situ in DACs as diamonds are transparent in this region of the electromagnetic radiation. Changes in Raman spectra at various pressures may mean structural changes of the sample.

In this work, high pressure behavior of the Raman modes of boron-rich samples was investigated on single crystals in DACs. The spectra were collected using DilorXY and LabRam systems equipped with the Ar (the excitation wavelength 514.5 nm) and He-Ne (632 nm) laser sources. The laser power in the range of 15–50 mW was applied. Raman spectra were collected in the region $200 - 1300 \, \text{cm}^{-1}$ by means of 5 accumulations for 120 seconds each on the Raman system with the green laser. The frequency resolution was $2 \, \text{cm}^{-1}$. The positions of Raman peaks and their maxima were determined by processing experimental data using PEAKFIT© v4.12 and Origin software.

II.2.2.2. Infrared spectroscopy

Infrared spectroscopy is a widespread spectroscopic technique to determine functional groups, to identify organic compounds, to study the progress of the reaction or to detect impurities of a sample. IR spectroscopy measures the vibrational energies of molecules and its intensity is much lower than during Raman scattering (Figure II.2-4.).
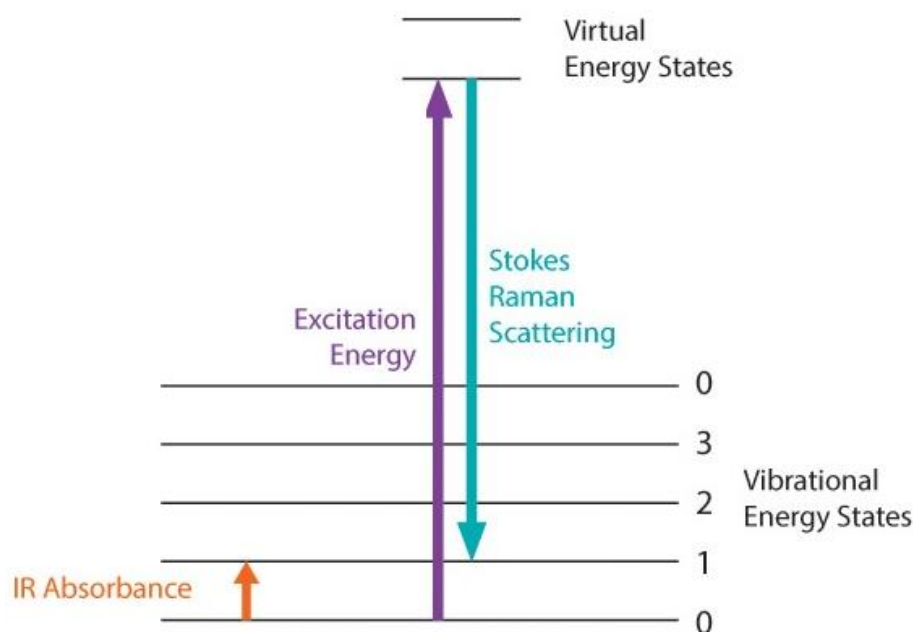
Figure II.2-4. Comparison diagram of intensity of photon transitions in molecules during Raman scattering and IR absorbance. Figure taken from [169].

The absorption of light in the infrared region of the electromagnetic spectrum gives a spectrum that corresponds to specific vibrational modes and is unique to each molecular structure examined. Contrary to Raman spectroscopy, for an IR detectable transition the molecule must undergo dipole moment change during vibration. The wavelength of monochromatic beam changes over time or Fourier transformation (FT) should be applied, in order to observe all the absorption lines within a specific range of the infrared region. FTIR is a fast IR method with higher spectral resolution and a decrease in noise [168].

In current thesis, the IR spectroscopy studies were performed on single crystals in DACs at ANKA Synchrotron Facility, Karlsruhe, Germany. The IR spectra were collected using a Vertex80v FTIR spectrometer coupled to an IRscopeII microscope (Bruker Optics, Ettlingen, Germany): at first, 32 accumulations for 300 seconds for each spectrum and after update 8 accumulations for 30 seconds for each spectrum, spectral resolution was 2 cm^{-1}. The positions of IR peaks were determined by processing experimental data using OPUS v7.2.139.1294 software.

II.2.3. Electron microscopy

Scanning electron microscopy (SEM) can be performed for verifying morphology of the synthesized samples and for qualitative determination of chemical composition of the samples. The samples were preliminary polished and coated by carbon with a thickness about 10 nm. A focused electron beam with energy range of 20 keV scans the surface of the sample. Different types of signals can be generated due to the interaction between electron beam and a sample. In this

investigation backscattered (BSE) and secondary (SE) electrons and photons of characteristic X-rays were used [171].

Backscattered electrons are electrons which are scattered on atoms inside the sample elastically. The intensity of the electron energy strongly depends on average atomic number (Z) of a certain phase and crystal orientation. Thus, the BSE images are useful for visualization of contrast from different chemical phases present in the sample [171].

Secondary electrons are electrons of primary beam hat are ejected from the K-shell of the sample atoms by inelastic scattering interactions with beam electrons. Due to their low energy, the electrons originate almost on a sample surface. Thus, SE are suitable for imaging of a surface morphology determining the contrast [171].

Characteristic X-rays are emitted when the electron beam ejects an inner shell electron from the sample, causing a higher-energy electron to fill the shell and release energy. These characteristic X-rays are used to identify the composition and measure the abundance of elements in the sample. This method is called energy-dispersive X-ray spectroscopy (EDX).

In this work, SEM analysis was done by SEM LEO Gemini 1530 equipped with Schottky emitter and use of EBSD technique and energy dispersive X-ray (EDX) analysis.

III. SCOPE OF THESIS

This chapter overviews the results presented in chapter IV. In the framework of my PhD project one paper was published, two manuscripts were submitted and one is prepared for submission to a peer-reviewed journal. Subchapter III.1 summarizes the results of the investigation of high pressure behavior of α-B. In subchapter III.2 the behavior under pressure of a more complex structure, containing B_{12} icosahedron − boron carbide is presented. Subchapter III.3. describes the results of the study of the most complex boron allotrope, β-B, which is used as a precursor material for high-pressure high-temperature synthesis. Particularly, the subchapter III.4 is devoted to a new non-icosahedral phase of boron, synthesized at very high pressures and temperatures in a DAC.

III.1. Investigation of single crystals of α-boron at high pressure

Single crystals of α-B were synthesized using the high-pressure high-temperature technique described in detail in [35]. Their structure and purity were carefully characterized [16] to assure the reliability of the obtained experimental results. The unit cell parameters of α-B in hexagonal settings are a = 4.9065(4) Å, c = 12.5658(5) Å [16] (the crystals used in the present study are from the same synthesis batch as in [16]).

Previously selected single crystals of α-B were placed in DACs and analyzed upon compression using single-crystal X-ray diffraction, Raman spectroscopy and synchrotron infra-red spectroscopy.

The DAC with α-B single crystals was compressed up to ~60 GPa. Up to the highest pressure reached in this study, all observed reflections perfectly match the α-B (space group $R\overline{3}m$) structure. No phase transition was observed. Measurements of compressibility revealed the value of bulk modulus K_{300} = 224(7) GPa (V_0 =261.94(3) Å^3, and K´ = 3.0(3), fitted with the third-order Birch-Murnaghan equation of state (3BM)), while the bulk modulus of individual B_{12} icosahedra K_{ico} appeared to be as high as 303(12) GPa (V_{ico0} = 12.47(5) Å^3, and K´ = 3.0(fixed), fitted with 3BM). Thus, the compressibility of icosahedra is considerably lower than that of the bulk material. The compressibility of the structure is almost the same along the a- and c-directions (Figure III.1-1).
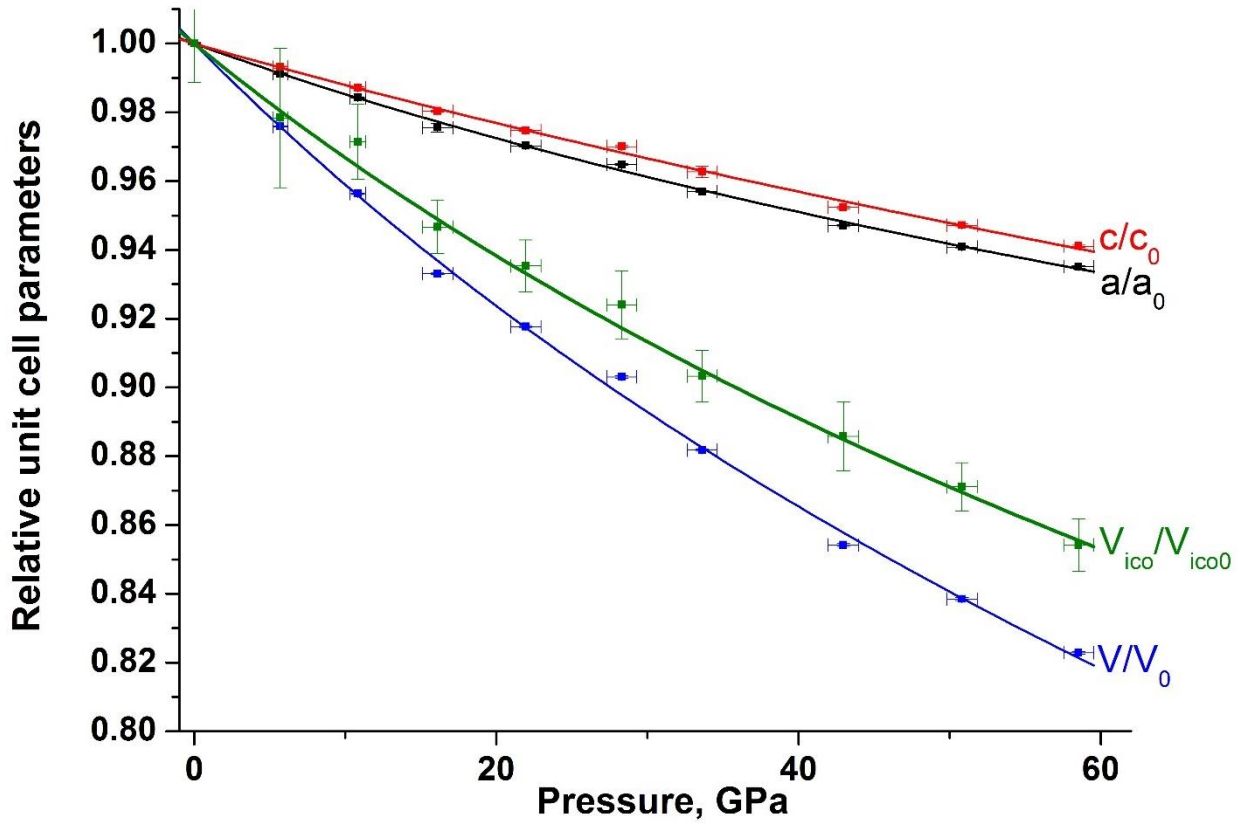
Figure III.1-1. Pressure-dependent evolution of the unit cell and B_{12} polyhedron volume and lattice parameter of α-B based on high-pressure single-crystal XRD data. Experimental data are dots with error bars. The margins of errors for the unit cell parameters are within the dots. Solid lines show the fit of the pressure-volume data with the third-order Birch-Murnaghan equation of state.

Measurements of interatomic distances as a function of pressure revealed that the intericosahedral 2e2c bonds are almost as stiff as intraicosahedral ones. This is in accordance with the previous experimental data [12], which showed that the intericosahedral 2e2c bond is the strongest one among all bonds in α-B. The 2e3c intericosahedral bond shows much higher compliance compared to other bonds in α-B.

Experimental results obtained by Raman spectroscopy of α-boron at ambient conditions agree well with those previously reported in [36,43-47]. During isothermal compression up to 160 GPa, we traced the most intense modes and a monotonous shift of the Raman peaks positions towards higher wavenumbers is observed (Figure III.1-2).
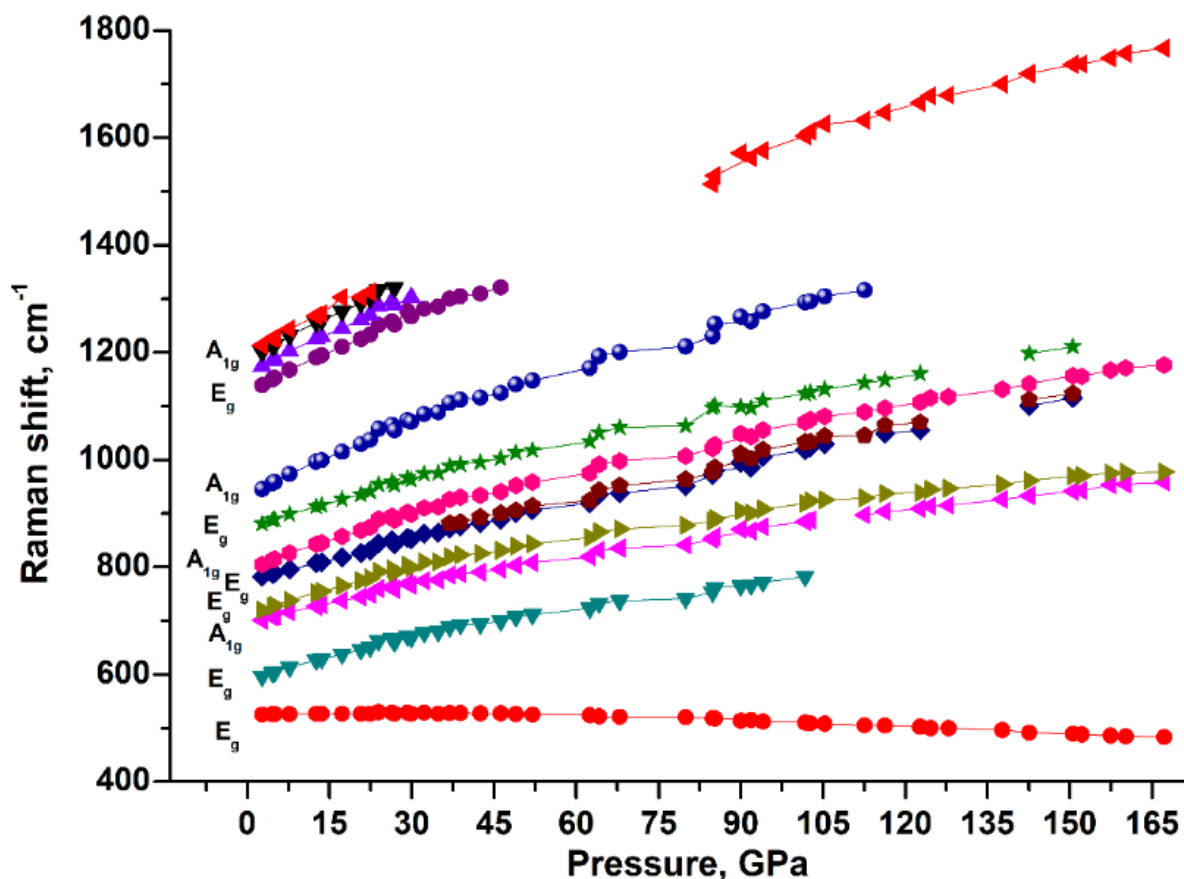
Figure III.1-2. The pressure-dependent evolution of the Raman modes of α-B measured in the pressure range from 3 to 167 GPa.

Between ~30 and 40 GPa a new mode at ca. 883 cm^{-1} appears. The splitting of modes may be an evidence not only of structural changes, but of a crystal strain under compression. Owing to specially designed experiment, the origin of the observed splitting of the E_g mode at ~865 cm^{-1} (774 cm^{-1} at ambient conditions) was explained as a result of stress imposed upon crystals due to the consequent bridging of the crystals between the anvils. Our conclusion is supported by theoretical calculations of the influence of strain on the behavior of Raman modes of α-B. Therefore, the structure was found to be stable up to the highest pressure reached.

This observation is confirmed by IR spectroscopy measurement. The IR spectra of α-B were obtained in the range from 600 to 1100 cm^{-1} up to ca. 53 GPa. The observed modes were assigned according to literature [51,52] at ambient pressure. No metallization or phase transitions were revealed by means of high-pressure IR spectroscopy.

III.2. Investigation of single crystals of $B_{13}C_2$ at high pressure

Single crystals of stoichiometric $B_{13}C_2$ obtained at high pressures (8.5–9 GPa) and high temperatures (1873–2073 K) using the large-volume-press technique were taken from the same synthesis batch as described in [11]. Previously selected single crystals of boron carbide were placed in DACs and analyzed upon compression using single-crystal X-ray diffraction.

Boron carbide crystallizes in rhombohedral structure (space group $R\bar{3}m$) with unit cell parameters a = 5.5962(3) Å, c = 12.0661(7) Å [11] (hexagonal settings). In the structure B_{12} icosahedra are located in the corners of the rhombohedral cell, and intericosahedral three-atom C-B-C linear chains are oriented along its body diagonal. The structure of $B_{13}C_2$ is very similar to those of α-B and γ-B, which can be described in terms of a cubic closest packing (*ccp*) of spheres, where B_{12} icosahedra play the role of "spheres".

The DAC with $B_{13}C_2$ single crystals was compressed up to ~70 GPa. All observed reflections perfectly match the $B_{13}C_2$ structure up to the highest pressure reached. Figure III.2-1 represents the dependence of the relative unit cell parameters (a/a_0 and c/c_0) and the relative unit cell (V/V_0) and icosahedron (V_{ico}/V_{ico0}) volumes on pressure up to 68 GPa. The structure of $B_{13}C_2$ is more compressible along the c direction, and the relative volume of the unit cell changes more rapidly compared to that of an icosahedron. Information on the compressibility obtained on the whole volume-pressure dataset showed that bulk moduli of the bulk material (K_{300} = 239(7) GPa, V_0 = 327.25(4) Å^3, K' = 3.2(3)) have very similar value to the bulk moduli of icosahedron (K_{300} = 239(23) GPa, V_0 = 12.50(3) Å^3, K' = 3.8(8)), what means that the bulk $B_{13}C_2$ and the icosahedron have the similar rigidity.
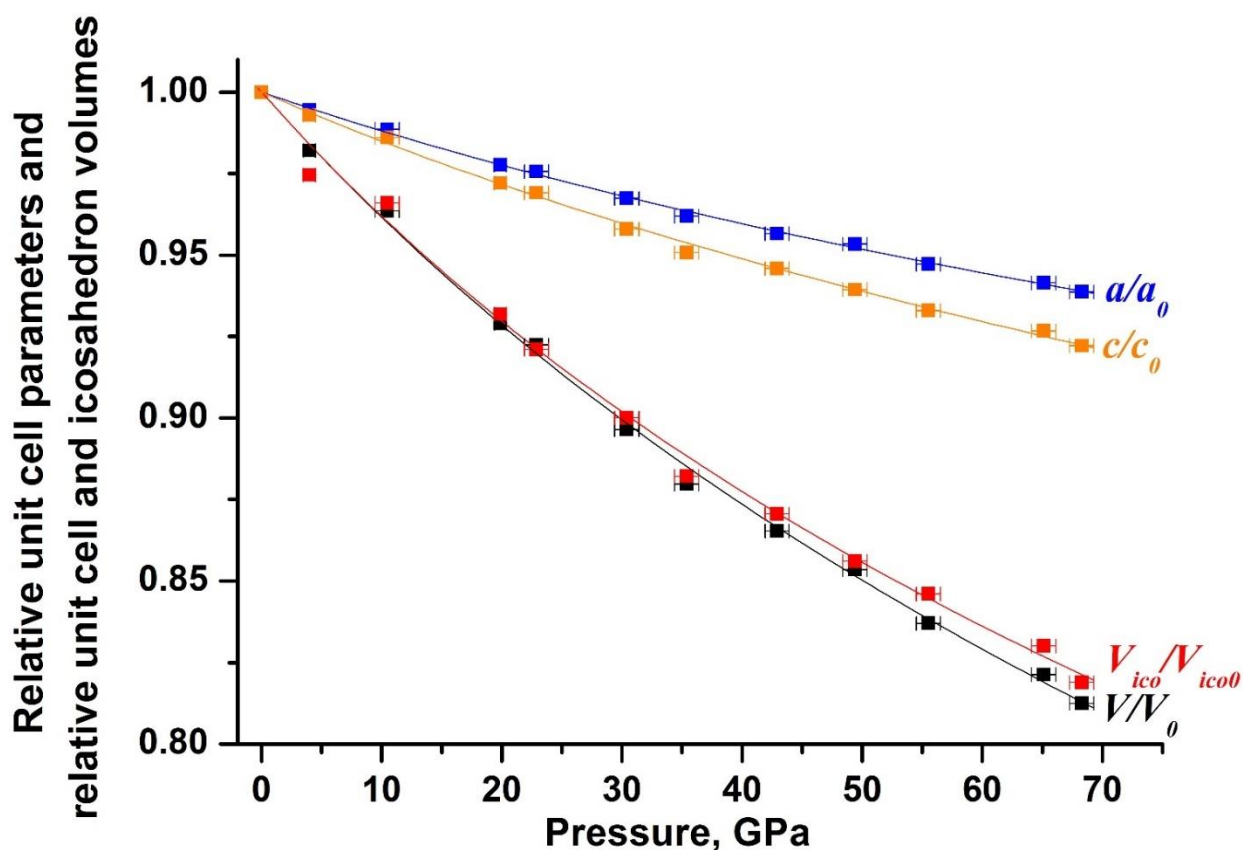
Figure III.2-1. Pressure-dependent evolution of unit cell volume, lattice parameters and volume of B_{12} icosahedra of $B_{13}C_2$ single crystals based on high-pressure single-crystal XRD data. Continuous lines show the fit of the pressure-volume data with the third-order Birch-Murnaghan equation of state.

Recent experimental electron-density study using low-temperature high-resolution single-crystal synchrotron X-ray diffraction data [11] clarified the bonding situation in the stoichiometric boron carbide $B_{13}C_2$. Its combination with our single-crystal X-ray diffraction data, collected at eleven pressure points in the interval from 4 GPa to 68 GPa, allowed us to follow changes in the length of each of the seven bonds in the structure of boron carbide $B_{13}C_2$. All bonds smoothly shorten under compression; their pressure-dependent evolution does not show any anomalies.

Bulk compressibility of boron carbide compared to compressibility of icosahedra has been a matter of debate. Nelmes et al. [121] reported the crystal structure to be more rigid than the icosahedron cluster, whereas Dera et al. [108] observed an opposite relation.

Our results have shown that the rigidity of the crystal structure of stoichiometric boron carbide $B_{13}C_2$ is similar to that of the B_{12} icosahedron. Within the standard uncertainty, the bulk moduli of the bulk material and the icosahedra we found to be similar. The volume reduction of the unit cell of $B_{13}C_2$ and the volume reduction of the icosahedron in the pressure interval between ambient and 60 GPa were calculated to be also similar (18.7% *versus* 18%, respectively); the difference is less than 1% and within the uncertainty. The volume reduction of the unit cell of B_4C (18%) obtained

by Dera and co-authors [108] matches very well to what we obtained for $B_{13}C_2$. But the volume reduction of the icosahedron in B_4C in the same pressure interval (between ambient and 60 GPa) in [108] appeared to be different (13%).

For understanding a reason of the apparent difference in the ratio of the rigidity of the unit cell and icosahedra found for $B_{13}C_2$ and B_4C [108], the comparison of the behavior of the icosahedron and the unit cell volume with pressure in the stoichiometric boron carbide $B_{13}C_2$ with boron allotropes α-B [172] and γ-B [79] was performed. In the structures of each of these materials, icosahedra (B_{12}) are built of exclusively boron atoms. In the same pressure range (from ambient up to 60 GPa), the unit cell volume reductions for all these materials are similar (ca. 18% within less than 1% deviation). The B_4C, containing $B_{11}C$ icosahedra, is not an exception (18%) [108]. However, the icosahedra volume reductions are all different and reduce in the raw: $B_{13}C_2$ (18.1%), γ-B (16.9%), α-B (14.5%), and B_4C (13%). This observation is striking enough and desires an explanation through an insight into the compressional behavior of individual bonds in these solids.

To visualize the difference in the rates of changes of the bonds length and compare boron carbide $B_{13}C_2$ with α-B and γ-B, experimentally obtained data for the relative changes of the bond lengths (l_P/l_{P0}) *versus* pressure was linearly fitted for all the bonds (l_P is the length of the bond at pressure P; l_{P0} is the length of this bond at $P_0 = 4.0$ GPa, the first pressure point available in our experiment in the DAC). We plotted calculated "line slopes" against corresponding interatomic distances l_{P0} (Figure III.2-2) at the lowest pressure, similarly to how it was done for characterization of the bond lengths' change under pressure for various boron-rich compounds [173] and α-B [172].
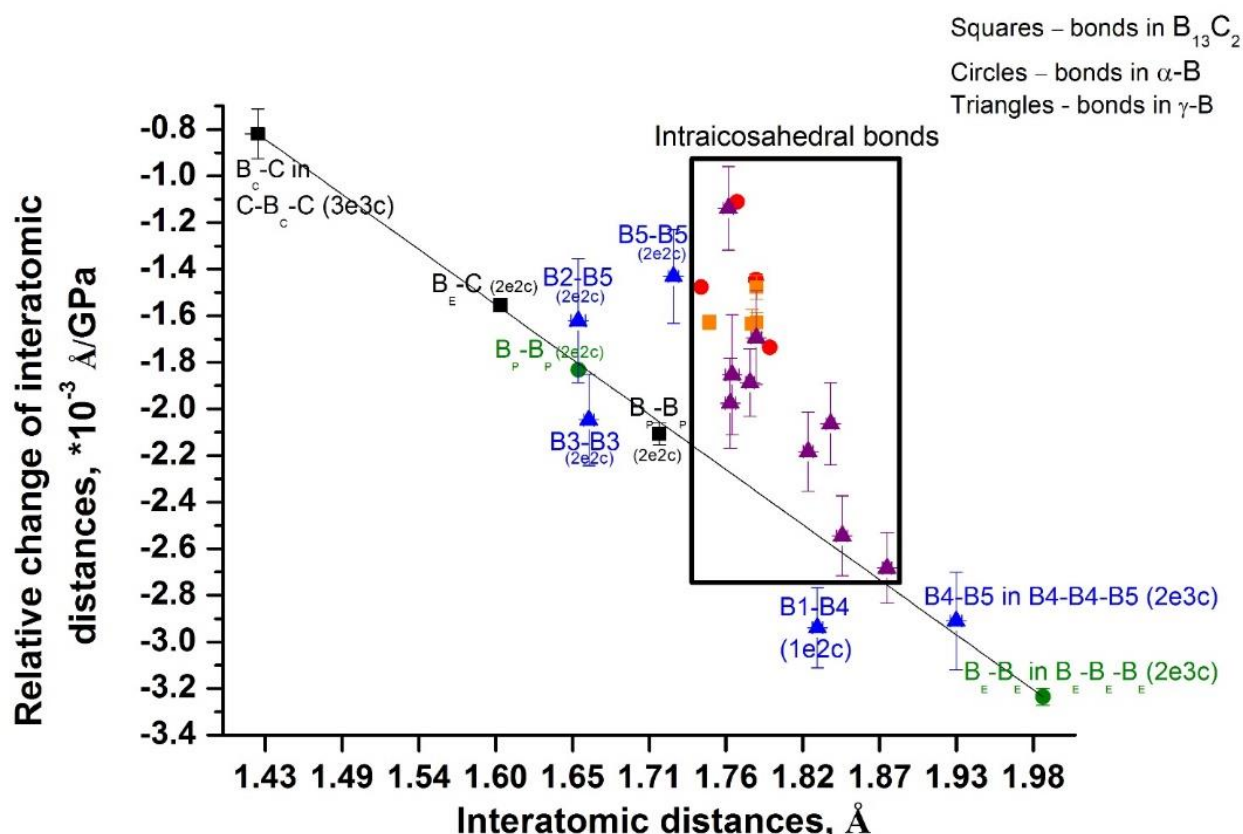
Figure III.2-2. Relative change of interatomic distances for α-B, γ-B and $B_{13}C_2$ single crystal plotted against their length at lowest pressure as revealed by in situ single-crystal X-ray diffraction. Circles stay for bonds in α-B, triangles for γ-B, and squares for $B_{13}C_2$. Intraicosahedral bonds are outlined by the black rectangular; red, purple and orange symbols correspond to α-B, γ-B and $B_{13}C_2$, respectively. Intericosahedral bonds and those involving B-B dumbbells and C-B-C chains are shown in green, blue, and black colors for α-B, γ-B and $B_{13}C_2$, respectively. The bonds in γ-B are shown in triangle: intraicosahedral ones (within black rectangular) are designated in purple, between icosahedra are in blue.

Concerning intraicosahedral bonds, they are very close to each other in α–B and $B_{13}C_2$. In γ–B the lengths of intra-icosahedral contacts at ambient pressure are quite similar to those of α–B and $B_{13}C_2$, whereas rates of their contraction under pressure vary considerably. The inter-cluster bonds are found to be very different in α–B [12], γ–B [13], and $B_{13}C_2$ [11] and all of them fit to the imaginable line from the strongest to the weakest bonds (Figure III.2-2). In boron carbide, the C–B–C chains (3e3c) are rigid and strengthen the structure, while in α–B the B-B-B contacts (2e3c) between icosahedra make it much weaker. This observation gives evidence that the stoichiometric boron carbide $B_{13}C_2$ is a compound with true covalent bonding: B_{12} icosahedra do not play a role of "molecules", their conventional separation is surely convenient for geometric presentation of the structure, but the compressional behavior of the stoichiometric boron carbide is governed by a complex interplay of both intra-cluster and inter-cluster bonds, as well as those involving C-B-C chains.

To sum up, unlike the previous experimental observations, our single-crystal synchrotron X-ray diffraction investigations revealed structural stability of the boron carbide in the studied pressure range. A comparison of the unit cell volume reduction with the reduction of the volume of the B_{12} icosahedron upon compression of $B_{13}C_2$ from ambient pressure to 60 GPa revealed their similarity. This confirms that the stoichiometric boron carbide $B_{13}C_2$ is a true covalent compound and does not show either 'molecular-like' or 'inversed molecular-like' solid behavior upon compression, as previously disputed. Our analysis has shown that, in agreement with the modern understanding of bonding in α–B, γ–B, and $B_{13}C_2$ based on the experimental electron-density studies [11-13], the compressional behavior of these boron allotropes and boron carbide depends on the types of bonding involved in the course of compression, so that the 'effective compressibility' of B_{12} icosahedra may vary in a broad range, from ca. 14% in α–B to ca. 18% in $B_{13}C_2$, as compared to ca. 18% of compression of the corresponding crystals.

III.3. Investigation of single crystals of β-B at high pressure

Single crystals of β-B were studied in the present work at high pressures in three runs of experiments. Single crystals were synthesized using the high-pressure high-temperature technique described in detail in [16] and at ~3 GPa and ~1900 K in the large-volume-press with toroidal anvils (toroidal press). Samples taken from the same batch as described in [16] have black color, while the color of the samples synthesized in the toroidal press varied from light red to deep red depending on the size. To assure the reliability of the obtained experimental results, the structure and purity were carefully characterized by scanning electron microscopy with EDX and X-ray diffraction. The presence of impurities could be excluded.

The unit cell parameters of β-B (space group $R\bar{3}m$) determined in the present study at ambient conditions are $a = 11.0304(30)$ Å, $c = 23.829(2)$ Å (in hexagonal settings). Single crystals of β-B were placed in a DAC and compressed up to 102 GPa. The accurate equation of state was determined in three different experiments and up to the highest pressure reached all observed reflections perfectly match the β-B structure. Figure III.3-1 represents the dependence of the relative unit cell parameters (a/a_0 and c/c_0) and the relative unit cell (V/V_0) volume on pressure. The structure of β-B is as compressible along the c direction as along the a direction. And there are no phase transitions observed unlike previous experimental observations [68,69].
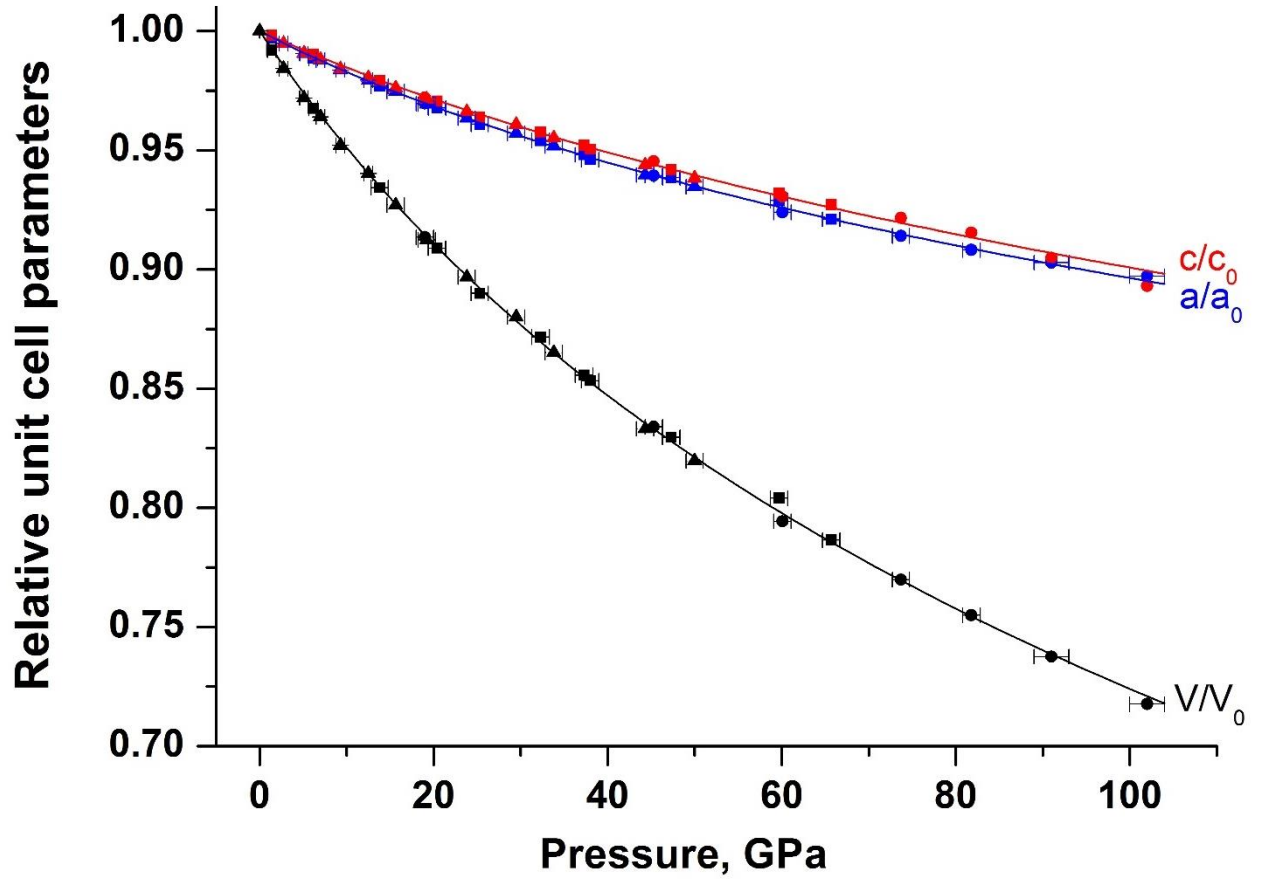
Figure III.3-1. Pressure-dependent evolution of unit cell volume and lattice parameters of β-B single crystals based on high-pressure single-crystal XRD data. Continuous lines show the fit of the pressure-volume data with the third-order Birch-Murnaghan equation of state. Squares, circles and triangles represent the data obtained in three different experiments.

Despite the difference in the values of unit cell volume between all previous experimental studies and reported in present work (~5%), the compressibility of the structure is very similar to the one obtained on single crystals in the same pressure range by [69] (Figure III.3-2).
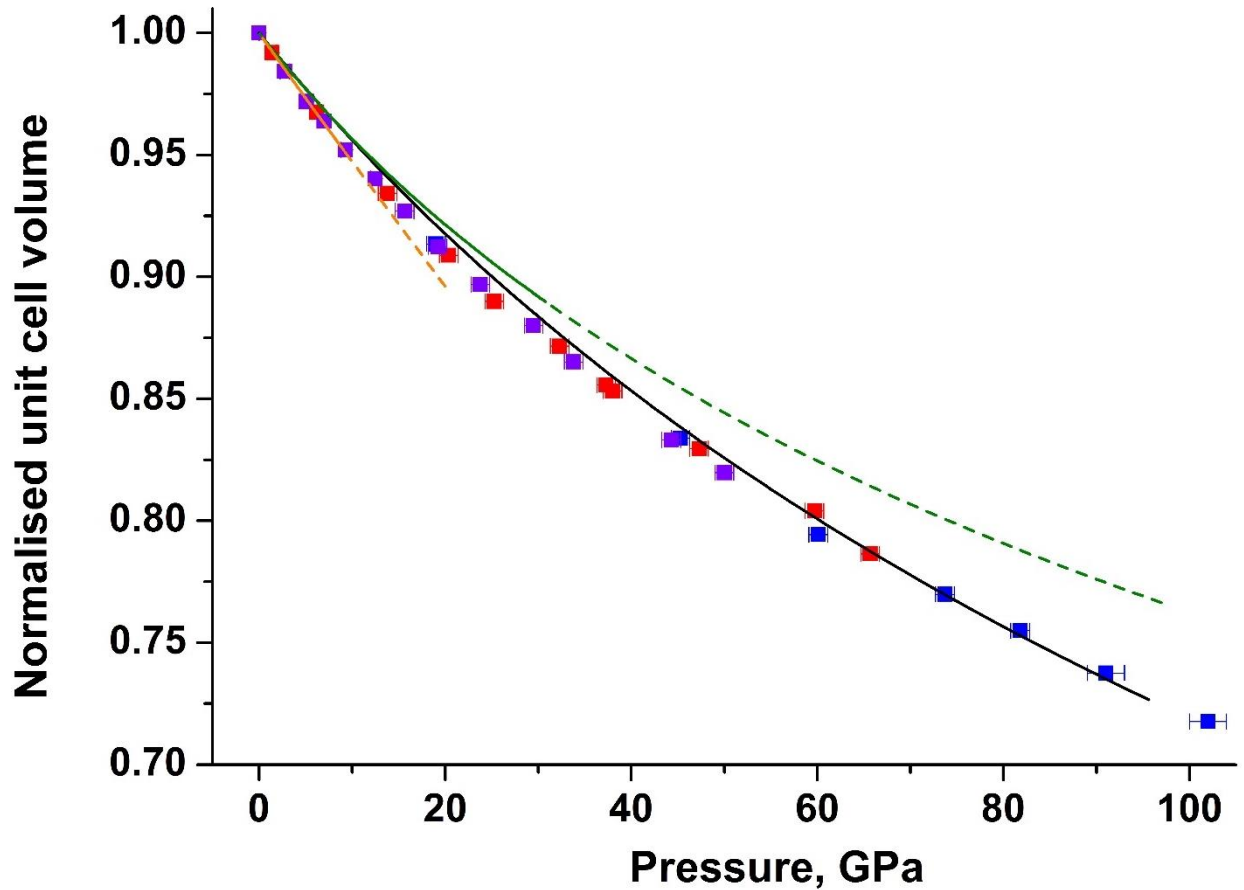
Figure III.3-2. Pressure-dependent evolution of normalised unit cell volume of β-B single crystals based on high-pressure single-crystal XRD data from three different runs (violet, blue and red squares). Continuous lines are attributed to the literature data. Black curve shows the fit of the pressure-volume data with the Vinet equation of state by Sanz, 2002 [69]. Green line represents the fit of the data with the third-order Birch-Murnaghan equation of state by Ma, 2003 [68]. Dashed green curve is its extrapolation to 100 GPa. The orange curve corresponds to the linear fit of pressure-volume data by Nelmes, 1993 [67]. Its extrapolation to 120 GPa is shown by a dashed curve.

Therefore, the structure of β-B synthesized from melt is stable up to 102 GPa and no pressure-induced amorphization was observed, unlike previous experimental observations [69].

.

III.4. Synthesis and investigation of new phase ζ-B

In every experiment on compression of single crystals of β-B DAC at the highest pressure (38(1) GPa, 50(1) GPa and 102(2) GPa) were double-side laser heated to about 2000 K. After the heating the pressure in the DACs (determined using the equation of state of neon) increased up to 42(1) GPa, 58(1) GPa and 115(2) GPa, respectively. At low pressures (42(1) GPa, 58(1) GPa) a transition of β-B to γ-B took place, and diffraction spots of γ-B were clearly observed in the diffraction pattern taken at room temperature (RT), what agrees well with theoretical predictions [73,76,77].

At 115(2) GPa the picture changed dramatically: sample color became black (not reflecting) and the X-ray diffraction pattern had to be treated as of a powder sample. Apart from reflections of Re (gasket material) and Ne (used as PTM), several new relatively weak but clearly detectable reflections were observed. Overcoming difficulties (see chapter IV.4.), crystal structure was solved. It matches perfectly those expected for α-Ga-type structured boron, as predicted by Häusserman et al. [97], and has the *Cmce* space group and 8 atoms per unit cell. The following orthorhombic lattice parameters were obtained at 115 GPa: $a = 2.7039(10)$ Å, $b = 4.8703(32)$ Å, $c = 2.9697(6)$ Å. This new high-pressure boron allotrope was denoted as ζ-B, sequentially after the fifth hitherto established boron allotrope, ε-B [29].

The structure of ζ-B at 115(2) GPa is presented in Figure III.4-1. It may be described as a stacking along the (010) direction of distorted and corrugated hexagonal nets with the 3^6 topology. Within each net each B atom connects to six neighbors and between the nets there is one much shorter bond. Measured precisely interatomic distances do not allow interpreting the structure as layered, as earlier proposed [99].
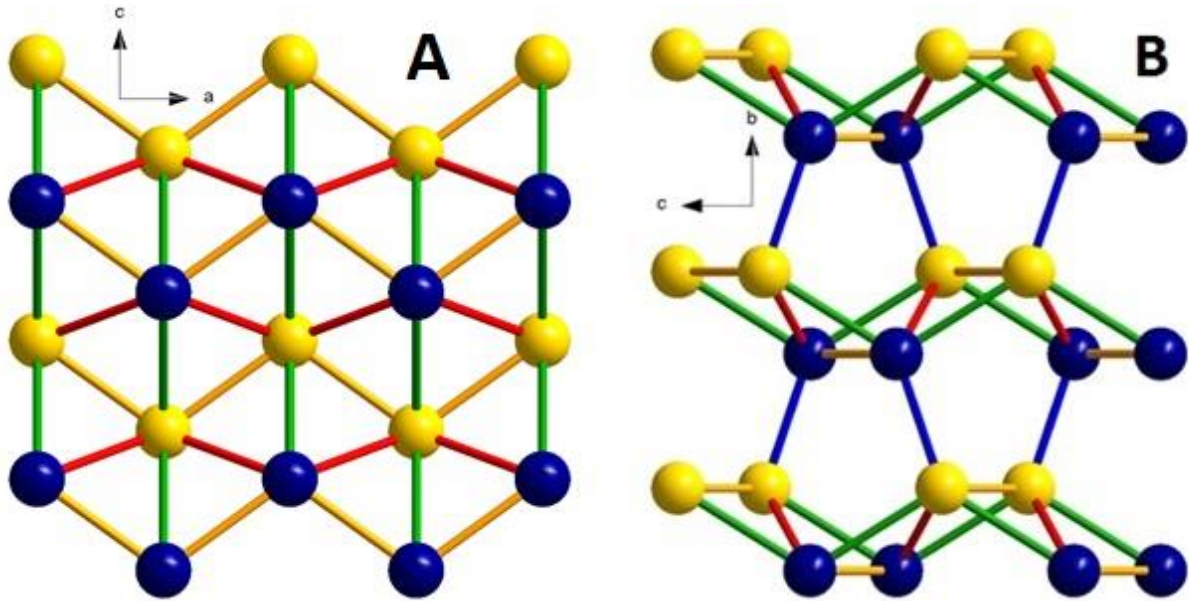
Figure III.4-1. The structure of ζ –B. A. The projection of a fragment of one distorted and corrugated hexagonal net on the *ac* plane. Such nets are stacked along the (010) direction. Blue and yellow atoms do not lie in the same plain (blue atoms are lower and yellow ones are upper if seen along the (010) direction). Bonds with different lengths are shown in different colors: 1.66(1) Å (orange), 1.72(1) Å (red), and 1.75(1) Å (green). **B.** The projection of three nets on the *bc* plain. The lengths of bonds connecting the layers (blue) all are 1.59(1) Å.

Further compression of the material synthesized at 115(2) GPa leads to decrease of the quality of single-crystal reflections. For this reason, the X-ray diffraction data of ζ-B obtained up to 135 GPa were integrated to 1D ´2-theta´ scans. The PV data set of ζ-B in the pressure range of 115 to 135 GPa was fitted using the second-order Birch-Murnaghan (2BM) equation of state (EoS) and gave the following EoS parameters: V_{115} = 39.20(8) Å^3, K_{115} = 575(65) GPa; K´= 4 (fixed); V_{115} is the unit cell volume and K_{115} is the bulk modulus at 115 GPa and room temperature). Therefore, in the studied pressure range (from 115 to 135 GPa) ζ-B is less compressible than any other boron allotropes known so far.

The results of double-side laser heating experiments at high pressure are presented in Figure III.4-2. Based on these results, a new version of the boron phase diagram can be designed.
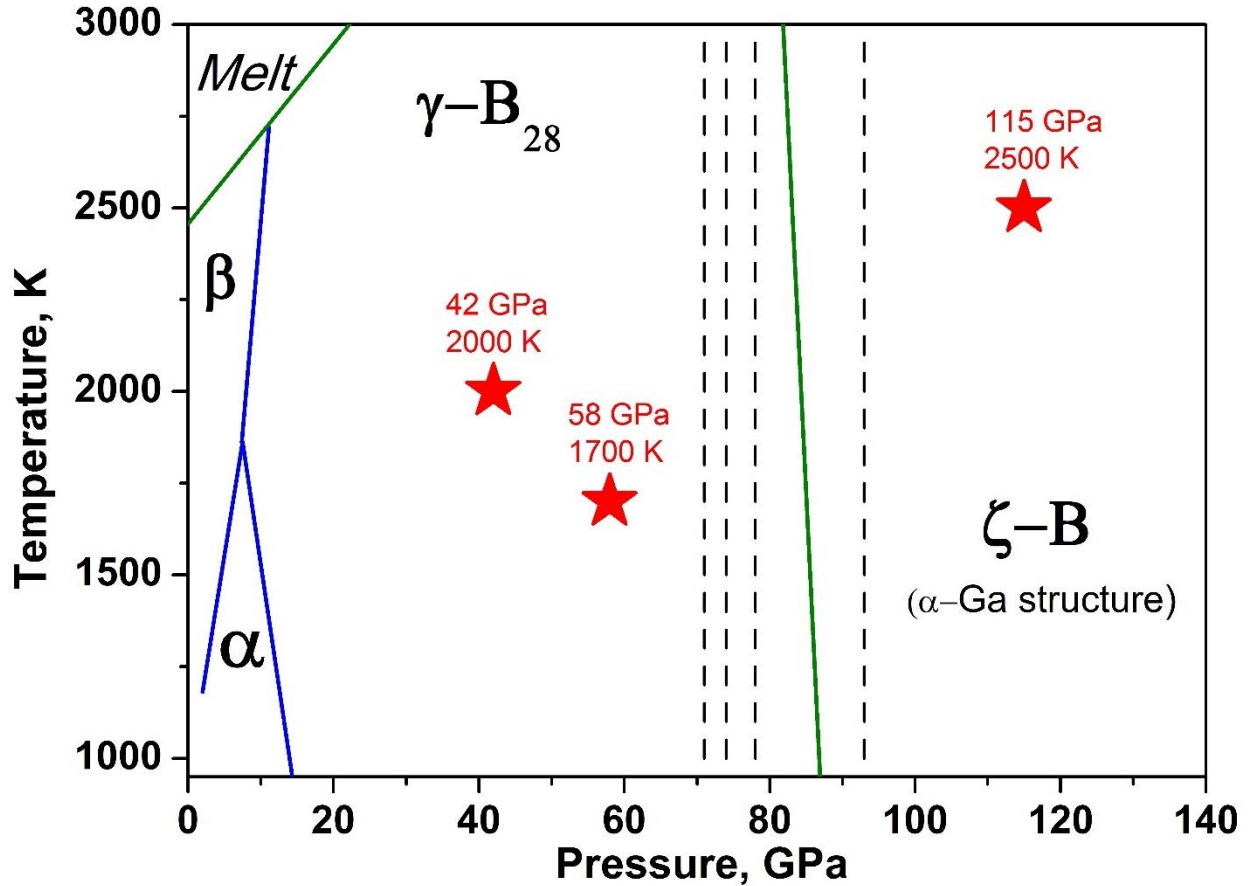
Figure III.4-2. Phase diagram of boron. Red stars show the experiments performed in the present work. Blue solid lines are the phase boundaries between α-/β-phases, α-/γ- phases and β-/γ-B as detected experimentally in [16]. Green solid lines are attributed to the phase boundaries between γ-B and α-Ga structure type B and between melt and β-/γ-B theoretically calculated by [73]. Black dashed lines show theoretical predictions between γ-B and α-Ga structure type B at 74 GPa by [97], at 71 GPa [98], at 78 GPa[76], at 89 GPa [73], and 93 GPa [77].

However, there were very few experiments performed to provide enough information about the phase boundaries of high pressure boron phases. Therefore, further investigations are required.

III.5. List of manuscripts and statement of author's contribution

[1] Chuvashova I., Bykova E., Bykov M., Svitlyk V., Gasharova B., Mathis Y.-L., Caracas R., Dubrovinsky L., Dubrovinskaia N. High-pressure behavior of α-boron studied on single crystals by X-ray diffraction, Raman and IR spectroscopy. *J. Solid State Chem.* **245,** 50–60 (2017).

I. Chuvashova (ICh) selected single crystals, maintained synchrotron single-crystal XRD experiment (with V. Svitlyk (VS), E. Bykova (EB) and M. Bykov (MB)) and analyzed the XRD data (with the help of EB). High pressure Raman spectroscopy was conducted by ICh. Synchrotron infra-red experiment was performed by ICh (with B. Gasharova (BG), Y.-L. Mathis (YLM)). R. Caracas (RC) made theoretical calculations of Raman spectra. ICh, N. Dubrovinskaia (ND) and L. Dubrovinsky (LD) interpreted the results and wrote the manuscript with contributions of all authors. ICh made 80% contribution in the paper.

[2] Chuvashova I., Bykova E., Bykov M., Svitlyk V., Gasharova B., Mathis Y.-L., Dubrovinsky L., Dubrovinskaia N. Structural stability and mechanism of compression of stoichiometric $B_{13}C_2$ up to 68 GPa. *Submitted to Nature Communications.*

ND and LD designed research. EB selected single crystals. ICh collected and analyzed synchrotron single-crystal XRD data (with VS, EB and MB). ICh, ND, and LD interpreted the results. ICh and ND wrote the paper with contributions of all authors. ICh made 70% contribution in the paper.

[3] Chuvashova I., Bykova E., Bykov M., Mezouar M., Dubrovinsky L., Dubrovinskaia N. Equation of state of β-B single crystals up to 102 GPa. *In preparation.*

ICh selected single crystals. Synchrotron single-crystal XRD experiments were conducted (with Mezouar M. (MM), EB and MB) and analysed by ICh. ICh, ND and LD interpreted the results and wrote the manuscript with contributions of all authors. ICh made 90% contribution in the paper.

[4] Chuvashova I., Bykova E., Bykov M., Prakapenka V., Glazyrin K., Mezouar M., Dubrovinsky L., Dubrovinskaia N. First non-icosahedral boron allotrope synthesized at high pressure and high temperature. *Submitted to PRB, Rapid Communications.*

EB selected single crystals. ICh collected and analyzed synchrotron single-crystal XRD data (with, EB, MB, V. Prakapenka (VP), K. Glazyrin (KG) and MM). Structure was solved and refined by EB. ICh, ND and LD interpreted the results and wrote the manuscript with contributions of all authors. ICh made 80% contribution in the paper.

IV. RESULTS

IV.1. High-pressure behavior of α-boron studied on single crystals by X-ray diffraction, Raman and IR spectroscopy

Irina Chuvashova[a,b*], Elena Bykova[b], Maxim Bykov[b], Volodymyr Svitlyk[c], Biliana Gasharova[d,1], Yves-Laurent Mathis[e,1], Razvan Caracas[f], Leonid Dubrovinsky[b], Natalia Dubrovinskaia[a]

[a] *Material Physics and Technology at Extreme Conditions, Laboratory of Crystallography, University of Bayreuth, D-95440 Bayreuth, Germany*
[b] *Bayerisches Geoinstitut, University of Bayreuth, D-95440 Bayreuth, Germany*
[c] *European Synchrotron Radiation Facility, BP 220 F-38043 Grenoble Cedex, France*
[d] *Institute for Photon Science and Synchrotron Radiation, Karlsruhe Institute of Technology, P.O. Box 3640, 76021 Karlsruhe, Germany*
[e] *ANKA Synchrotron Radiation Facility, Karlsruhe Institute of Technology, P.O. Box 3640, 76021 Karlsruhe, Germany*
[f] *CNRS, Laboratoire de Géologie de Lyon, ENS de Lyon, UCBL Lyon 1, Université de Lyon, France*

*Correspondence to: irina.chuvashova@gmail.com
[1]Present affiliation: IBPT, Karlsruhe Institute of Technology, P.O. Box 3640, 76021 Karlsruhe, Germany

IV.1.1. Abstract

In the present study, single crystals of rhombohedral α-B were investigated under pressure to 60 GPa by means of single-crystal X-ray diffraction. The bulk modulus of α-B was found to be $K = 224(7)$ GPa ($K' = 3.0(3)$). Measurements of interatomic distances as a function of pressure revealed that the intericosahedral two-electron two-center (2e2c) bonds are almost as stiff as some of intraicosahedral ones. The two-electron three-center (2e3c) intericosahedral bonds show much higher compliance compared to other bonds in α-B. The vibrational properties of α-B under pressure were investigated by Raman spectroscopy at pressures up to 160 GPa and IR spectroscopy at pressures up to 53 GPa.

IV.1.2. Introduction

Boron has five currently established allotropes (α-B, β-B, γ-B, δ-B (T-50), and ε-B [15,16,29]), and all of them have a common structural feature, B_{12} icosahedron as major building block. Each allotrope possesses a unique Raman spectrum [15,16,29]. Rhombohedral α-B (space group $R\bar{3}m$) has the simplest structure [36] among all of boron phases: it consists of B_{12} icosahedra

71

located at the corners of its rhombohedral unit cell. Under heating up to 1473 K at ambient pressure, α-B transforms into β-B (space group $R\overline{3}m$) [36]. Arrangement of B_{12} icosahedra in β-B is complex, some of B sites are partially occupied [45]. The β-B is more compressible (bulk modulus K = 185–210 GPa [67-69]) in comparison with α-B (K = 213–224 GPa [48,67]). At pressures above 8.5 GPa and temperatures higher than 1773 K, boron crystallizes as a γ-B (B_{28}) phase (space group Pnnm). The structure of γ-B consists of B_{12} icosahedra and B_2 dumbbells covalently bonded with each other ([13,72-74]). The γ-B phase was demonstrated to be stable up to at least 30 GPa and 2000 K [72]. At pressures above 9 GPa, in a broad field of stability of γ-B, another boron phase, δ-B (space group P$4_2/nnm$), was obtained. The unit cell of δ-B consists of 50 boron atoms. They form four icosahedra, and two atoms localize in the intericosahedral space [29]. In a relatively narrow pressure-temperature field, at pressures of 8–9 GPa and temperatures of 1873 – 2073 K, ε-B (space group $R\overline{3}m$) was found in the co-existence with γ-B [29]. This phase is isostructural to $B_{13}C_2$, and the arrangement of B_{12} icosahedra is similar to that in the α-B structure. Instead of C-B-C linear groups in stoichiometric $B_{13}C_2$ [11], the rhombohedral unit cell of ε-B contains three-atomic linear B-B-B groups [29] oriented along the main body-diagonal of the unit cell.

Knowledge about high-pressure high-temperature behavior of elemental materials is important for fundamental understanding of bonding evolution, phase transformations, and establishing of P,T-phase diagrams, which are of high significance for materials' synthesis and applications. The subject of high-pressure investigations in the present work is α-B. Although its structure was established long ago (Fig. IV.1-1), the bonding situation in *α*-B at ambient pressure was clarified only recently [12] due to the analysis of the electron-density in *α*-B based on experimental single-crystal X-ray diffraction data. It was found that between icosahedra of adjacent "close-packed" layers there are 2e2c (two-electron two-center) B1-B1 intercluster bonds of the similar nature as the 2e2c bonds in *γ*-B [13] (Fig. IV.1-1A), while within the same close-packed layer (Fig. IV.1-1B) icosahedra are held together by electron deficient 2e3c (two-electron three-center) B2-B2-B2 bonds [12], which are different from the 2e3c bond in *γ*-B (for details see [12,13]).
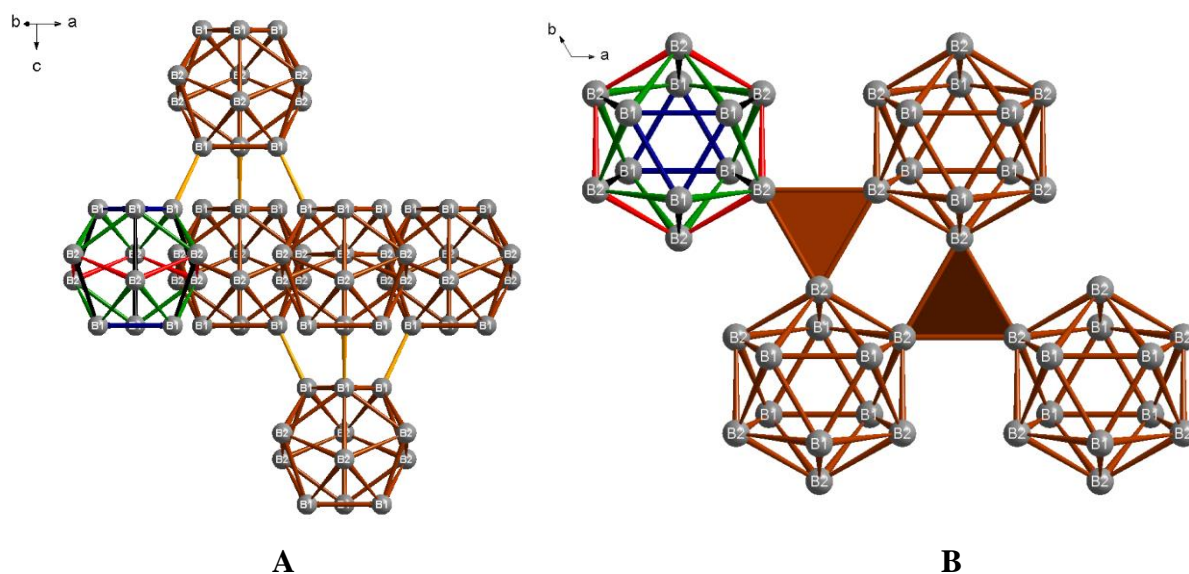
Figure IV.1-1. Perspective view of the α-B structure showing the packing of the icosahedral building blocks. The crystallographically independent atoms B1 and B2 are indicated. Intraicosahedral distances between B2-B2 atoms (multiplicity 6) are shown in red, between B1-B1 (multiplicity 6) are shown in blue, between B1-B2 (multiplicity 12) are shown in green, and between B2-B1 (multiplicity 6) are shown in black. **A)** View of the crystal structure of α-B along the **b** direction. The six intercluster 2e2c bonds for the central B_{12} cluster are highlighted in yellow color. **B)** View of the crystal structure of α-B along the **c** axis. The inter-icosahedral 2e3c bonds of α-B are highlighted in brown triangles.

According to group theory, 10 Raman-active modes (4 A_{1g} singlets and 6 E_g doublets) are expected for α-B [46]. Raman spectroscopy investigations of α-B were started by Richter and Ploog [43] in 1964. Since that time, alongside with theoretical calculations and assignment of the Raman modes [44-47] at ambient conditions, a number of high-pressure experiments have been performed [36,44,48,49], as Raman spectroscopy is a powerful technique for characterization of the behavior of boron allotropes under pressure (see for example [79]). Most of the high-pressure results have been obtained on polycrystalline (powder) samples. Raman spectroscopy measurements at room temperature to 80 GPa [49] did not show any phase transitions in α-B. Powder X-ray diffraction up to 106 GPa [49] and 200 GPa [50] did not show them either, in agreement with theoretical simulations [50,66] which predict structural stability of α-B up to 270 GPa [50].

Raman spectra from single crystals of α-B were measured to 30 GPa in [36] and 71 GPa in [48]. The dependence of the frequency of Raman modes on pressure and temperature was determined at pressures from ambient to 36 GPa in the temperature range of 293–473 K [36].

Group theory determines eight infrared (IR) active modes (3 A_{2u} and 5 E_u) in α-B [53]. The theoretical analysis of the phonon spectra of α-B was conducted in numerous works [46,47,51,54-56]. IR spectroscopy measurements at ambient conditions [51-53] led to identification of the following bands in the transmission spectrum in the range from 400 to 1300 cm^{-1}: 1200, 1080, 920, 806, 705, and 548 cm^{-1}. Only three of them were rather strong (at 920, 806, and 705 cm^{-1}); Beckel

et al. [174] treated the weak lines at 1080 and 1200 cm^{-1} as not being α-B IR absorption lines. All IR measurements were made on polycrystalline samples with a random distribution of very small crystals [51-53] .

Theoretical calculations suggest the onset of the metallization of α-B at about 50 GPa [174], which could be potentially recognized by the high-pressure IR spectroscopy. We could not find any references to IR spectroscopy studies of α-B under pressure. Electrical resistivity measurements conducted up to 112 GPa on powder samples of α-B [49] did not detect the predicted metallization.

Powder X-ray diffraction gives valuable structural information and is often sufficient for acquiring accurate compressibility data, when the unit cell parameters are measured precisely upon pressurizing a sample [175]. The bulk modulus of α-boron was reported to be 224 GPa [175] as measured on a powder sample, and 213(15) GPa [67] and 207(13) GPa [48] on single crystals. Previous high-pressure single-crystal X-ray diffraction studies of α-B [48] aimed at obtaining the unit cell parameters, but atomic coordinates and thermal parameters were not determined.

In this work we used all the research advantages provided by single-crystal high-pressure crystallography [176,177], which allowed us crystal structure determination and refinement for α-B at pressures as high as 60 GPa. Here we present these results along with the data on the high-pressure behavior of α-B studied by Raman spectroscopy up to 160 GPa, and IR spectroscopy up to 53 GPa.

IV.1.3. Experimental

Single crystals of α-B were synthesized using the high-pressure high-temperature technique described in detail in [35]. Their structure and purity were carefully characterized [16] to assure the reliability of the obtained experimental results.

IV.1.3.A. Diamond-anvil cell experiments

The BX90-type diamond anvil cells (DAC) [145] made at Bayerisches Geoinstitut (Bayreuth, Germany) and diamonds with the culet diameters of 120 and 250 μm were used in high pressure experiments. Rhenium gaskets were squeezed between the diamonds to make an indentation with the thickness of 30 μm for 250-μm diamonds and of 20 μm for 120-μm diamonds. Then in the center of the indentations, round holes of 120 μm or 60 μm in diameter, respectively, were drilled. The α-B crystals were placed into these chambers. Sizes of the crystals were about $10 \times 10 \times 25$ μm^3 and $15 \times 10 \times 25$ μm^3, orientation of these two crystals was not specified. Neon was used as a pressure transmitting medium. Ruby served as a pressure marker, and ruby balls were placed into the pressure chamber.

IV.1.3.B. Raman spectroscopy

Raman spectroscopy studies were done on single crystals of α-B with characteristic dimensions of about $7 \times 7 \times 20$ μm^3. The Raman spectra were collected using DilorXY and LabRam systems equipped with the He–Ne (the excitation wavelength 632.8 nm) laser source. The laser power in the range of 15–50 mW was applied. Raman spectra were collected in the region 200 – 1800 cm^{-1} by means of 10 accumulations for 300 seconds each on the Raman system with the red laser. The frequency resolution was 2 cm^{-1}. The positions of Raman peaks and their maxima were determined by processing experimental data using PEAKFIT© v4.12 and Origin software.

There were two experiments performed at room temperature. In the first one, pressure in the cell was increased up to 160 GPa with a step of about 6 GPa. And in the second one, the cell was pressurized up to 31 GPa with a step of 2-3 GPa. At each step a Raman spectrum was measured. The pressure dependence of the Raman shift was subsequently analyzed.

IV.1.3.C. Infrared spectroscopy

Infrared spectroscopy studies were done on single crystals of α-B with characteristic dimensions of ~$10 \times 10 \times 25$ μm^3 at ANKA Synchrotron Facility, Karlsruhe, Germany. Crystals were

loaded into a DAC with type IIA diamond anvils along with Ne used as a pressure transmitting medium. The IR spectra were collected using a Vertex80v FTIR spectrometer coupled to an IRscopeII microscope (Bruker Optics, Ettlingen, Germany): 32 accumulations for 300 seconds for each spectrum, spectral resolution was 2 cm^{-1}. The positions of IR peaks were determined by processing experimental data using OPUS v7.2.139.1294 software.

Pressure in the cell was increased up to 53 GPa with a step of about 6 GPa at room temperature. At each step the IR spectrum was measured. The pressure dependence of the IR frequencies was subsequently analyzed.

IV.1.3.D. Single-crystal X-ray diffraction

Crystals with the size of about $15 \times 10 \times 25$ μm^3 were selected for measurements in a DAC at ID27 at the European Synchrotron Radiation Facility (ESRF). The DAC's pressure chamber was filled by Ne used as a pressure transmitting medium. Diffraction data were collected at 293 K using the Perkin Elmer XRD1621 flat panel detector. The monochromatic radiation had the wavelength of 0.37380 Å and the crystal-to-detector distance was 383 mm. Pressure in the cells was increased up to 60 GPa with a step of about 8 GPa. 160 frames in the omega scanning range of −40° to +40° were collected (0.5° scanning step size) with an exposure time of 1 s. Integration of the reflection intensities and absorption corrections were performed using CrysAlisPro software [164,165]. The structure was refined in the isotropic approximation for all atoms by full matrix least-squares using SHELXL software [166] in the WinGX software package [165]. The crystallographic data of α-B studied at high pressure have been deposited in the Inorganic Crystal Structure Database [178]. The data may be obtained free of charge from Fachinformationszentrum Karlsruhe, 76344 Eggenstein-Leopoldshafen, Germany (Fax: +49 7247 808 666; e-mail: crysdata@fiz-karlsruhe.de, http://www.fiz-karlsruhe.de/request_for_deposited_data.html) on quoting following CSD deposition numbers: 431636-431447(compression from 5.7 to 59 GPa).

IV.1.4. Theoretical

We computed the Raman spectra of α-B from the density-functional perturbation theory. We employed the ABINIT implementation [179-181] with planewaves and norm-conserving pseudopotentials [182]. We used the local-density approximation to describe the exchange-correlation energy, a regular grid of 8 8 8 special k-points [183] and a kinetic energy cut-off of 30 Hartrees (1 Hartree 1⁄4 27.2116 eV) for the wave-functions.

IV.1.5. Results and discussion

IV.1.5.1. Single crystal X-ray diffraction measurements at elevated pressures

The X-ray diffraction data for α-B obtained at variable pressure and some experimental details are presented in Table IV.1-1. The quality of the data was sufficient to refine both the lattice parameters and atomic coordinates. Remarkably, the high-pressure data allowed the same quality of the structural refinement as those obtained at ambient conditions that gives evidence that the crystals were in quasihydrostatic environment up to the highest pressures achieved. The unit cell parameters of α-B in hexagonal settings are a = 4.9065(4) Å, c = 12.5658(5) Å, as determined in [16] (the crystals used in the present study are from the same synthesis batch as in [16]). The structure is shown in Figure IV.1-1. Boron atoms in the crystal structure occupy two crystallographically independent positions and are labeled as B1 and B2; boron-boron distances vary between 1.654(2) and 1.987(2) Å at ambient pressure.

Up to the highest pressure reached in this study, all observed reflections perfectly match the α-B (space group $R\bar{3}m$) structure. Table IV.1-1 presents high-pressure crystallographic data. As seen from the table, R-factors R_{int} and R_1 vary irregularly between ~5 % and ~ 13% that is likely due to problems with sample centering in the tightly focused X-ray beam. Although at all pressures the exposure time was 1 s, there is a difference in the number of observed peaks at different pressures that might be related to some slight changes during the experiment (for example, the X-ray beam intensity varies before and after a refill). We would like to notice that, although we refined the thermal parameters (Table IV.1-1), they cannot be used for any conclusions regarding possible physical phenomena. The observed slight anomalies in the behavior of atomic displacement parameters and a large difference between the U_{eq} values for crystals cr1 and cr2 at the highest pressure are likely attributed to the limited number of peaks in the XRD datasets obtained from crystals in a DAC.

The dependences of the relative unit cell volume (V/V_0) and the relative lattice parameters (a/a_0 and c/c_0) of α-B on pressure up to ca. 60 GPa are shown in Figure IV.1-2. While these characteristics show a smooth decrease with pressure, the ratio of the unit cell parameters c/a non-monotonously increases (Figure IV.1-3) with a bend in the (c/a vs P) line at about 30 GPa.

Table IV.1-1. **Crystallographic details of α-B at variable pressure.** Formula: B; Crystal System: Trigonal; Z=12; Space group: $R\bar{3}m$, crystal size $10 \times 10 \times 15 \mu m^3$ (crystal 1) and $15 \times 10 \times 25\ \mu m^3$ (crystal 2, designated as "cr2").

P, GPa	a, Å	c, Å	V, Å³	R_{int}**	$R_1[I >2\sigma(I)]$**	N_m***	N_i***	Atom*	x	z	U_{eq}, Å²
5.7(5)	4.8646(5)	12.473(1)	255.63(4)	0.08	0.0821	268	109	B1	0.4527(2)	0.0581(1)	0.00333(97)
								B2	0.5305(2)	0.1909(1)	0.00374(96)
10.8(5)	4.8305(5)	12.397(1)	250.51(4)	0.112	0.1091	270	118	B1	0.4525(4)	0.0576(1)	0.0086(15)
								B2	0.5316(3)	0.1915(2)	0.0093(14)
16(1)	4.788(6)	12.312(2)	244.42(5)	0.054	0.0624	233	112	B1	0.4528(2)	0.0582(1)	0.00526(89)
								B2	0.5320(2)	0.1914(1)	0.00565(87)
21(1)	4.762(1)	12.242(2)	240.38(9)	0.045	0.0527	173	102	B1	0.4533(2)	0.0583(1)	0.00526(75)
								B2	0.5326(2)	0.1916(1)	0.00555(74)
28(1)	4.735(1)	12.183(2)	236.55(8)	0.063	0.0573	172	101	B1	0.4535(2)	0.0582(1)	0.00608(76)
								B2	0.5328(2)	0.1918(1)	0.00568(75)
34(1)	4.6965(8)	12.09(2)	230.97(7)	0.065	0.0926	185	103	B1	0.4537(3)	0.0584(2)	0.0084(12)
								B2	0.5331(3)	0.1918(2)	0.0088(12)
43(1) cr2	4.6516(6)	11.971(2)	224.32(5)	0.052	0.0478	185	94	B1	0.45395(14)	0.05845(7)	0.00236(57)
								B2	0.53376(13)	0.19209(8)	0.00304(58)
43(1)	4.6476(12)	11.961(4)	223.8(1)	0.077	0.1054	158	100	B1	0.45395(33)	0.05797(18)	0.0106(14)
								B2	0.53367(33)	0.19217(18)	0.0110(14)
51(1) cr2	4.6141(9)	11.880(2)	219.05(8)	0.044	0.0611	168	90	B1	0.4542(2)	0.05845(8)	0.00293(72)
								B2	0.53430(16)	0.19234(8)	0.00300(72)
51(1)	4.6174(13)	11.895(4)	219.63(11)	0.067	0.1019	144	99	B1	0.4543(4)	0.05815(18)	0.0109(14)
								B2	0.5342(4)	0.19215(18)	0.0114(14)
59(1)	4.5888(13)	11.819(3)	215.5(1)	0.131	0.1317	185	94	B1	0.4550(5)	0.0584(3)	0.0107(17)
								B2	0.5339(5)	0.1924(3)	0.0119(17)
59(1) cr2	4.5799(7)	11.797(3)	214.30(7)	0.042	0.0741	154	92	B1	0.4544(2)	0.05840(9)	0.00351(79)
								B2	0.5346(2)	0.1924(1)	0.00362(78)

*Wyckoff positions are 18h (x, $\bar{x}$, z) for both B1 and B2 atoms. **R_{int} and $R_1[I > 2\sigma(I)]$ relate to data collection and structure refinement, respectively. ***N_m is the number of measured unique reflections; N_i- the number of unique reflections with I>2σ(I)
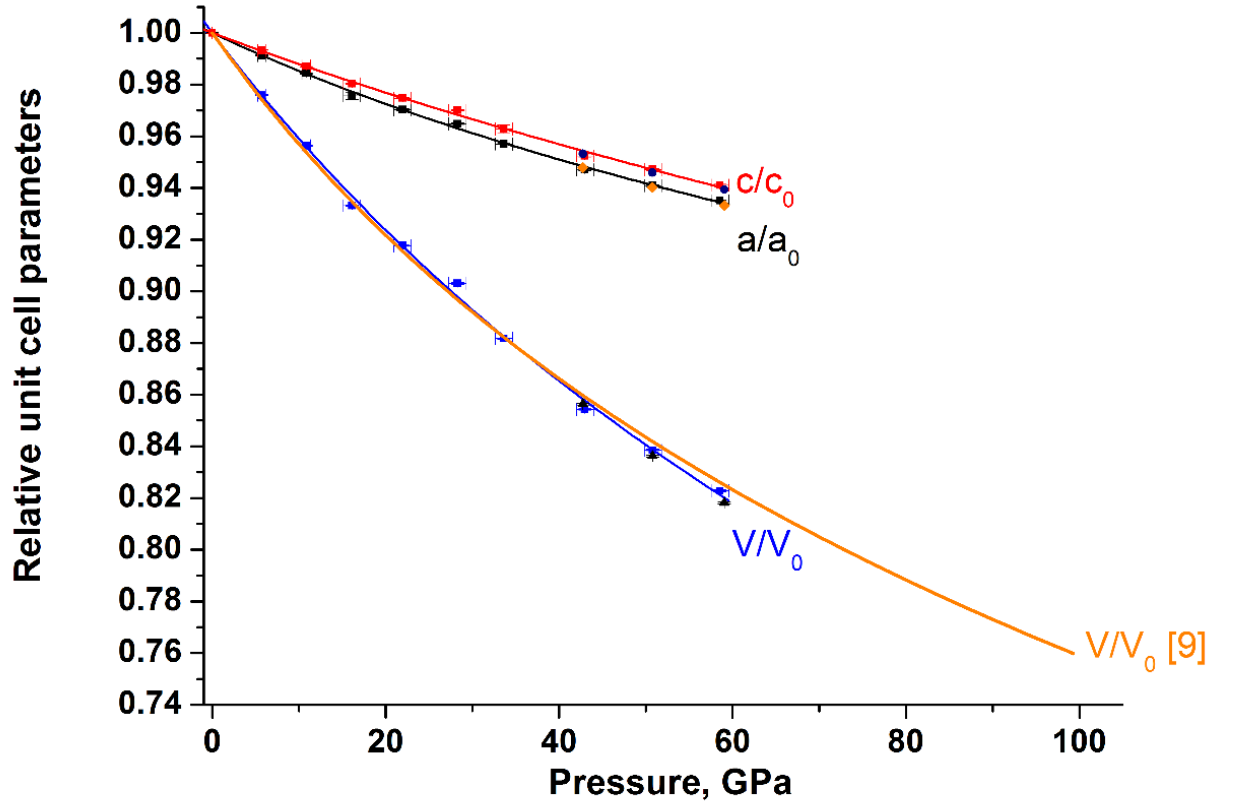
Figure IV.1-2. Pressure-dependent volume and lattice parameter evolution of α-B based on high-pressure single-crystal XRD data. Experimental data are dots with error bars. The margins of errors for the unit cell parameters are within the dots. Above about 40 GPa additional three pressure points correspond to the data obtained from the second crystal. Solid lines show the fit of the pressure-volume data for both crystals with the third-order Birch-Murnaghan equation of state. The compressibility of the structure is almost the same along the *a*- and *c*-directions. Orange line is attributed to ref. [48].
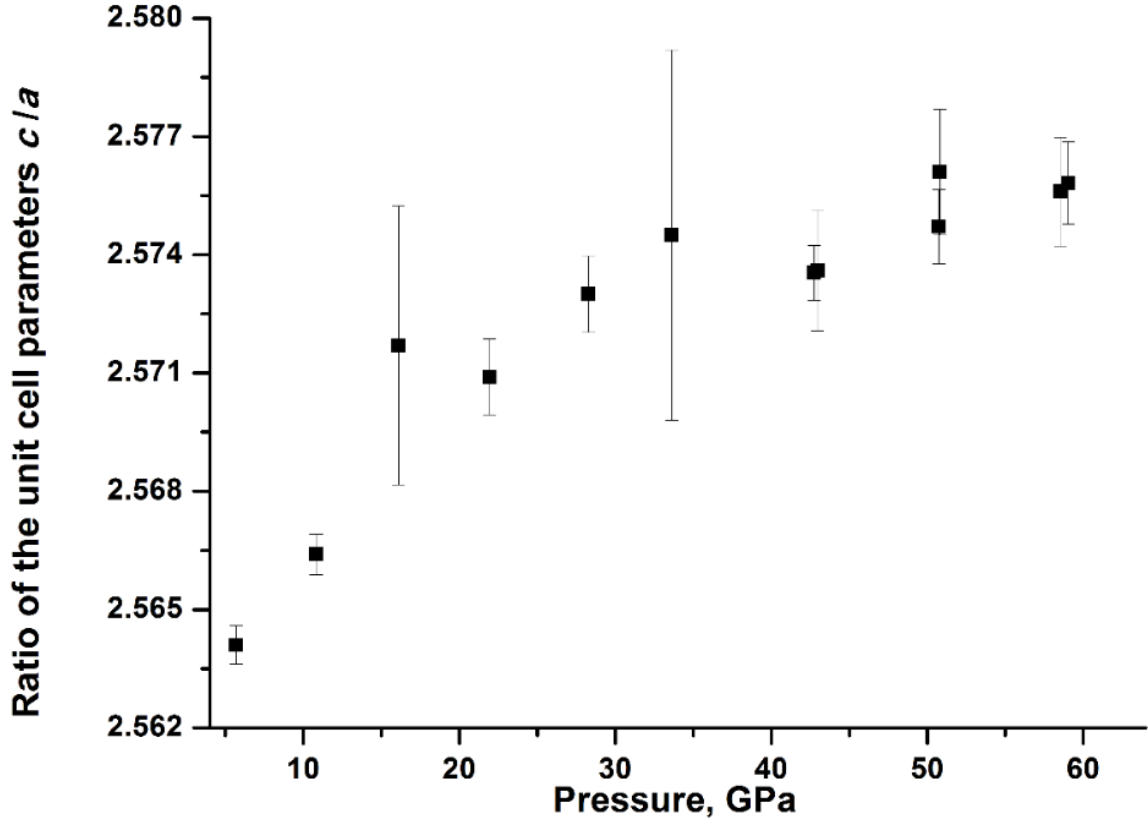
Figure IV.1-3. The ratio of the unit cell parameters of α-B based on high-pressure single-crystal XRD data.

The whole pressure-volume (P-V) data set was used to fit the experimental data with the third-order Birch-Murnaghan (3BM) equation of state that gave the following results: $V_0 = 261.94(3)$ Å^3, $K_{300} = 224(7)$ GPa and $K' = 3.0(3)$ (V_0 is the zero pressure unit cell volume, K_{300} is the bulk modulus, and K' is its first derivative) (Table IV.1-2). The fit with fixed $K' = 4$ resulted in the bulk modulus $K_{300} = 205(3)$ GPa, being lower than that with the free K'. The bulk moduli of α-B were reported in literature based on experimental measurements [48,67,175] and theoretical calculations [17,50,66,128,184] (Table IV.1-3). Nelmes et al. [67] made measurements of the bulk modulus of α-B on single crystals. Although they covered extremely small pressure interval (only up to 4 GPa), a simple linear fit of their three experimental points resulted in the value of the bulk modulus ($K_{300} = 224(15)$ GPa) numerically equal to the one we obtained with the P-V data up to 60 GPa and free K'. Powder XRD data of Fujii et al. [175] gave also the same value ($K_{300} = 224$ GPa, fixed $K' = 4$).

Table IV.1-2. Parameters of the equation of state of α-B at variable K´. A third-order Birch-Murnaghan (3BM) equation of state was fitted to the volume data for the unit cell and the B_{12} icosahedron up to 60 GPa, which gave different sets of the EOS parameters.

Parameters	Bulk α-B		Icosahedron	
V_0, Å^3	261.94(3)	261.94(4)	12.47(5)	12.43(4)
K_{300}, GPa	224(7)	205(3)	273(12)	303(12)
K´	3.0(3)	4 (fixed)	4 (fixed)	3 (fixed)

Polian and co-authors [48] obtained the P-V data from single-crystal XRD up to 100 GPa [48], their fit with the Vinet EOS gave K_{300} = 207(13) GPa and K´ = 4.2(3) that is, within the uncertainties, very close to our result (K = 205(3) GPa with the fixed K´ = 4).

In comparison with other boron allotropes (Table IV.1-3), the bulk modulus of α-B appears to be equal to that of γ-B determined from single-crystal XRD (K = 227(3) GPa, K´ = 2.5(2)) up to 40 GPa, before the isostructural phase transition [79]. The bulk modulus of γ-B measured on a powder sample [185] is higher (K = 237(5) GPa, K´ = 2.7(3)), because in [185] the phase transition was not recognized and the whole data set (below and above 40 GPa) was fitted. Within experimental uncertainties the bulk modulus of α-B is very close to that of β-B, measured by powder [68] and single-crystal X-ray diffraction [69], which gave consistent results (see Table 3). The bulk modulus of β-B obtained from powder neutron diffraction [67] is slightly lower, but it might be related to the use of a solid pressure transmitting medium in [67]. Bulk moduli of boron carbide [108,121,123] are higher than that of α-B, while $B_{13}N_2$, B_6O and Fe_xB_{50} have the bulk moduli smaller than those of boron allotropes [173,186,187] (see Table 3).

Table IV.1-3. Parameters of the equation of state of α-B in comparison with those of other boron allotropes and boron-rich binary compounds. The EOSes are designated as follows: M (Murnaghan), 2BM and 3BM (Birch-Murnaghan of the 2nd and 3rd order), and V (Vinet).

Material	V_0	Single crystal data		Powder data		Ref.	EOS
		K_{300}	K′	K_{300}	K′		
α-B	*261.94(3)*	*224(7)*	*3.0(3)*			*Present study*	*3BM*
		225(8)	*2.9(5)*				*V*
	264.1	213(15)	4 (fixed)			[67]	M
		224(15)					linear
	262(1)	207(13)	4.2(3)			[48]	V
	261.9			224	4 (fixed)	[175]	
β-B	2450(11)			205(16)	4.3 (1.6)	[68]	BM
				208(3)	4 (fixed)		
	2460			210(6)	2.23	[69]	V
	2463(5)			185(7)		[67]	linear
γ-B	197.6(1)			237(5)	2.7(3)	[185]	V
	198.1(3)	227(3)	2.5(2)			[79], p<40 GPa	3BM
	192.6(3)	281(6)	2.8(9)			[79], p>45 GPa	3BM
boron carbide	328.5			199(7)	1(2)	[121]	M
				305.8		[123]	2BM
	330.59(5)	243(3)	3.6(2)			[108]	3BM
		236(8)	4 (fixed)				
$B_{13}N_2$				200(15)	4 (fixed)	[186]	BM
B_6O	314.5			181(5)	6	[187]	V
$Fe_{1,32(1)}B_{50}$	406.6(1.4)	187(9)	4 (fixed)			[173]	2BM
$Fe_{1,01(1)}B_{50}$	407.30(7)	171.6(1.5)	4.1(2)				3BM

The theoretically calculated values of the bulk modulus of α-B vary from 200 to 250 GPa [17,50,66,128,184]. The difference between experimental and theoretically calculated values could be partly due to different equations of state (EoS) used.

Single-crystal X-ray diffraction allowed us to follow changes in the length of each of the six distinct B-B bonds of α-B (four intraicosahedral and two intericosahedral, see Figure IV.1-1) up to ca. 60 GPa. All of them shorten under pressure, but with different rates. To visualize this difference, we first performed linear fits of the experimentally obtained data for the relative changes of the bond lengths (l_P/l_{P0}) *versus* pressure for all the bonds (l_P is the length of the bond at pressure P; l_{P0} is the length of this bond at $P_0 = 5.7$ GPa, the first pressure point available in our experiment in the DAC). The slopes of the lines, characterizing the rate of the bond length's change, were plotted *versus* corresponding interatomic distances l_{P0} (Figure IV.1-4), similarly to how it was done for characterization of the bond lengths' change under pressure for various boron-

rich compounds [173]. Previous experimental observations [128] showed that bonds between icosahedra are softer than the ones within icosahedra. Figure 4 demonstrates that stiffness of the shortest B1-B1 intericosahedral (intercluster) 2e2c bonds is close to that of intraicosahedral bonds, and the B2-B2 intericosahedral 2e3c bonds show much higher compliance compared to other bonds in α-B. This is in qualitative accordance with the previous experimental data [12]. From the topological analysis of the electron density of α-B [12], it was found that the intercluster 2e2c B1–B1 bond is the strongest bond since it has the highest magnitudes of electron density and Laplacian at its bond critical point among all bonds. The pressure dependence of the B1-B1 and B2-B2 intericosahedral distances is shown in Figure IV.1-5 and Table IV.1-4.
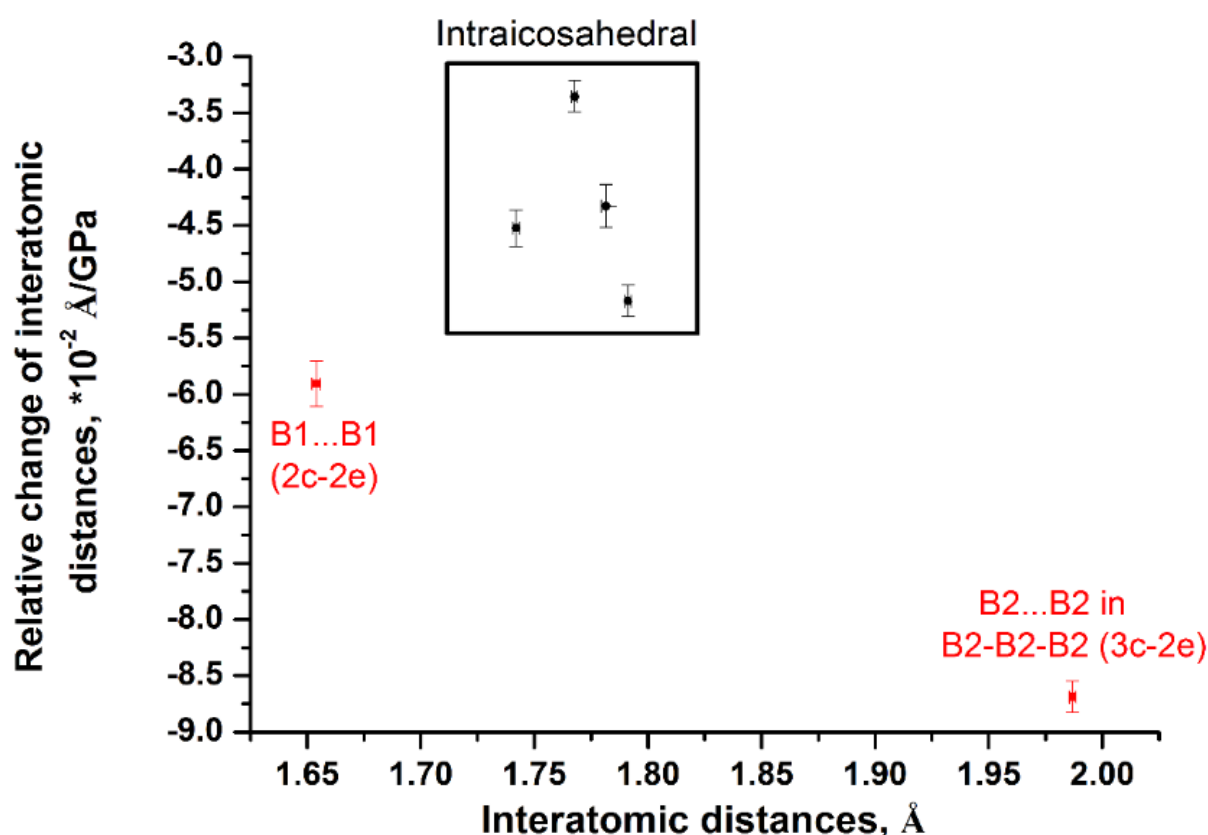
Figure IV.1-4. The relative change of interatomic distances in α-B plotted against their length at 5.7 GPa, as revealed by single-crystal X-ray diffraction. Intericosahedral bonds are designated in red, intraicosahedral bonds - in black. Intraicosahedral B-B bonds (embraced by the black rectangle) are less compressible than intericosahedral ones. Intericosahedral B2-B2 (3c-2e) bonds are much more compressible than the intericosahedral B1-B1 (2c-2e) bonds.
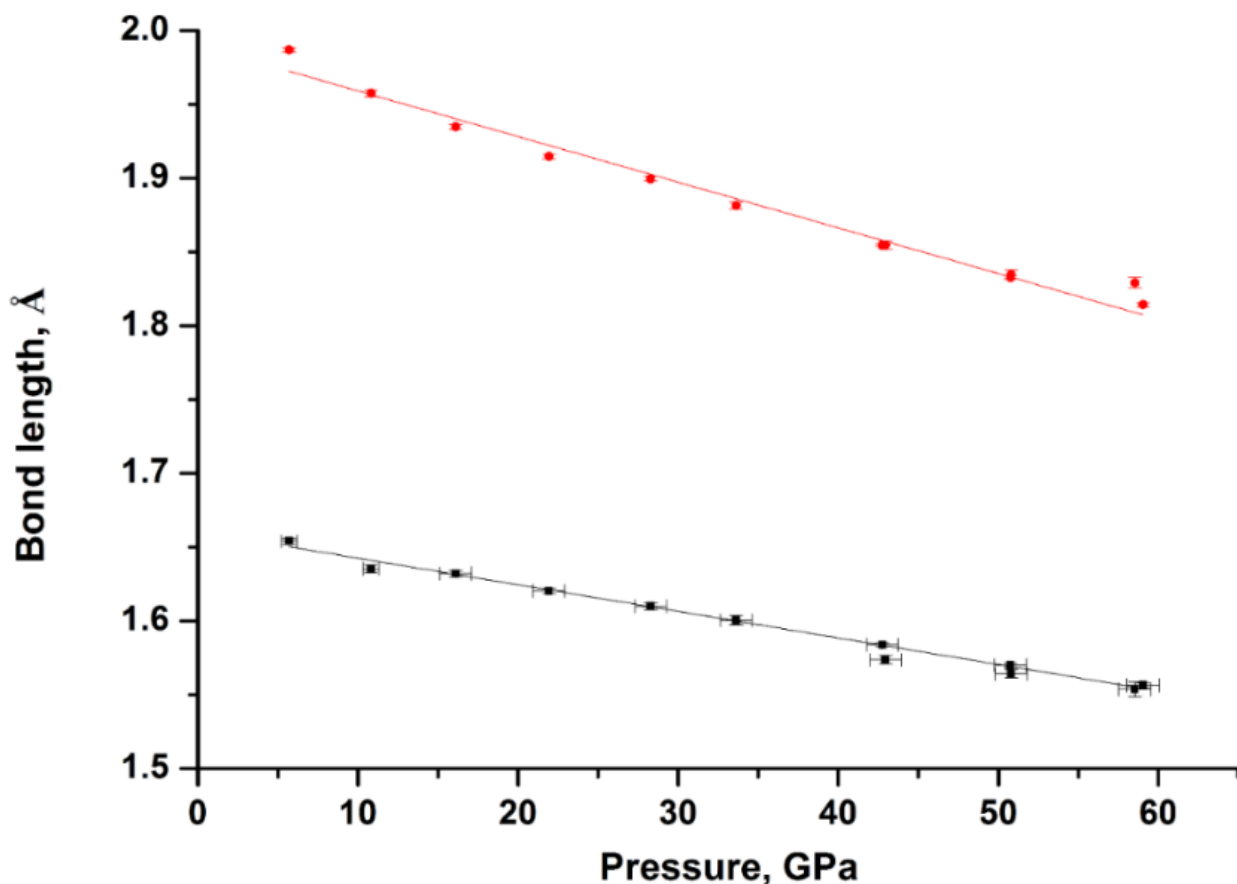
Figure IV.1-5. Pressure-dependent intericosahedral bond length evolution in α-B. B1-B1 bond is black, B2-B2 is red. All the distances gradually decrease. B2-B2 length decreases more rapidly than the B1-B1 one.

Table IV.1-4. Characteristics of B_{12} icosahedra and intericosahedral distances in α-B at variable pressure. Distortion index of the icosahedra was calculated as described in the text. "cr2" designates crystal 2.

P, GPa	V_{ico}, Å³	Distortion index	Intericosahedral distances, Å	
			B1-B1	B2-B2
5.7(5)	12.1928	0.00047	1.6541(19)	1.9869(15)
10.8(5)	12.1062	0.00216	1.6354(27)	1.9577(23)
16(1)	11.7976	0.00382	1.632(2)	1.9347(15)
21(1)	11.6565	0.00508	1.6203(17)	1.9147(15)
28(1)	11.5153	0.00518	1.6099(21)	1.8996(15)
34(1)	11.2567	0.00563	1.6004(30)	1.8814(22)
43(1) cr2	11.0065	0.00728	1.5838(12)	1.8545(10)
43(1)	11.0383	0.0058	1.5737(29)	1.8547(30)
51(1) cr2	10.8155	0.00838	1.5700(14)	1.8328(12)
51(1)	10.8558	0.00676	1.5642(29)	1.8348(29)
59(1)	10.645	0.00556	1.5537(48)	1.8291(37)
59(1) cr2	10.6161	0.00855	1.5564(15)	1.8143(14)

The compressional behavior of B_{12} icosahedra is shown in Figure IV.1-6. The P-V_{ico} (V_{ico} is the volume of a B_{12} icosahedron) data fit using the third-order Birch-Murnaghan equation of state resulted in the bulk modulus of K_{ico} = 273(12) GPa with K_{ico}' = 4 (fixed), and V_{ico0} = 12.47(5) Å^3 (Table IV.1-2). The K_{ico}' = 3 leads to the increase of K_{ico} to 303(12) GPa. Thus, the bulk modulus of the icosahedron is considerably higher than the bulk modulus of bulk α-B (224(7) GPa) what agrees well with the data for compressibility of the B_{12} icosahedron in γ-B (K_{ico} = 285 GPa and K_{300} = 227(3) GPa for the bulk material) [79].
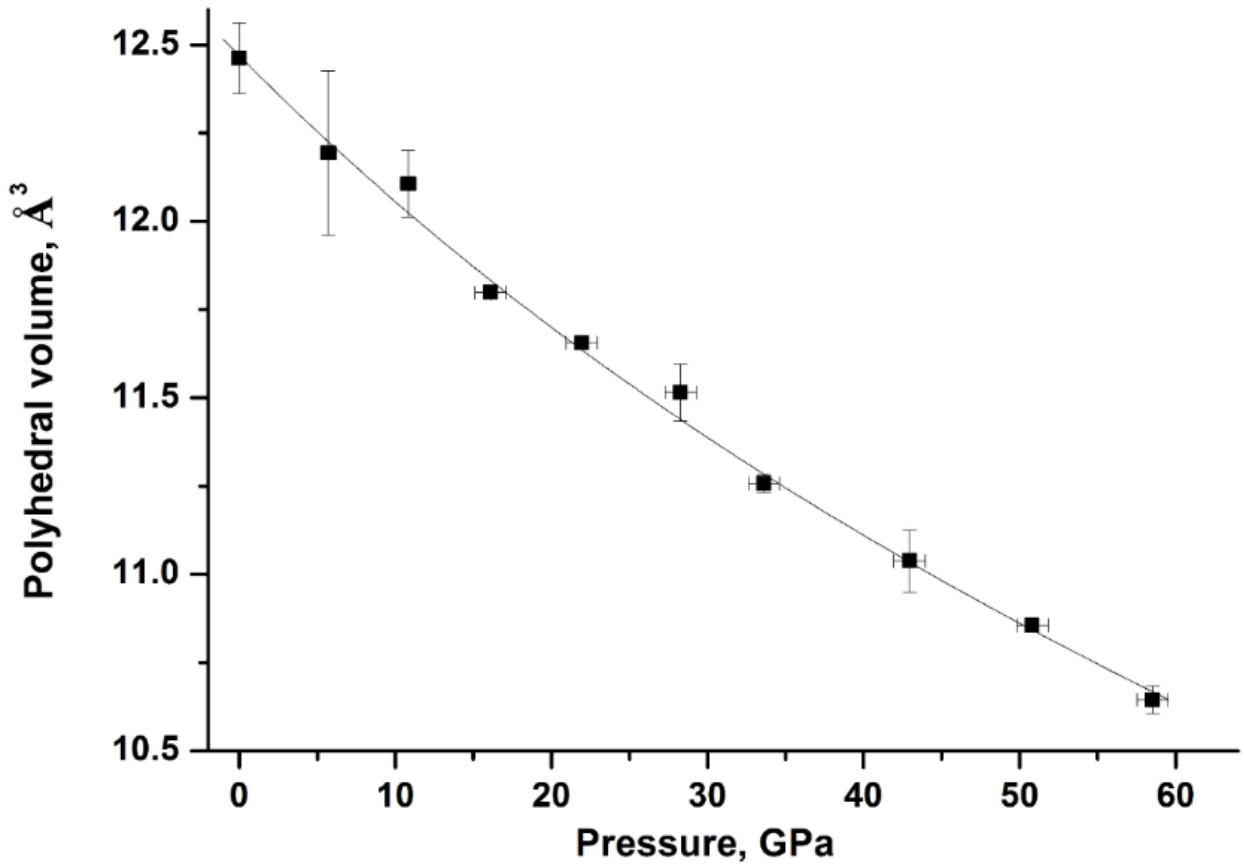
Figure IV.1-6. The volume of B_{12} icosahedra as a function of pressure. Solid line shows the fit of the pressure-volume data with the third-order Birch-Murnaghan equation of state.

Not only the volume of the icosahedra changes upon compression, but they undergo a distortion, which can be characterized by a distortion index, *DI*, defined as follows:

$$DI = \frac{1}{n} \sum_{i=1}^{n} \frac{|l_i - l_{av}|}{l_{av}},$$

where n = 12 for an icosahedron, l_i is the distance from the center of the icosahedron to the *i*th coordinating atom, and l_{av} is the average distance [188]. The distortion index as a function of pressure for B_{12} icosahedra is presented in Figure IV.1-7. It linearly raises five-fold under compression to about 20 GPa. In the pressure interval from about 30 to 60 GPa its magnitude

increases very moderately, within only $1.5*10^{-3}$ unit of the distortion index. It correlates with the change in the behavior of the *c/a* ration at pressures above 30 GPa (see Figure IV.1-3).
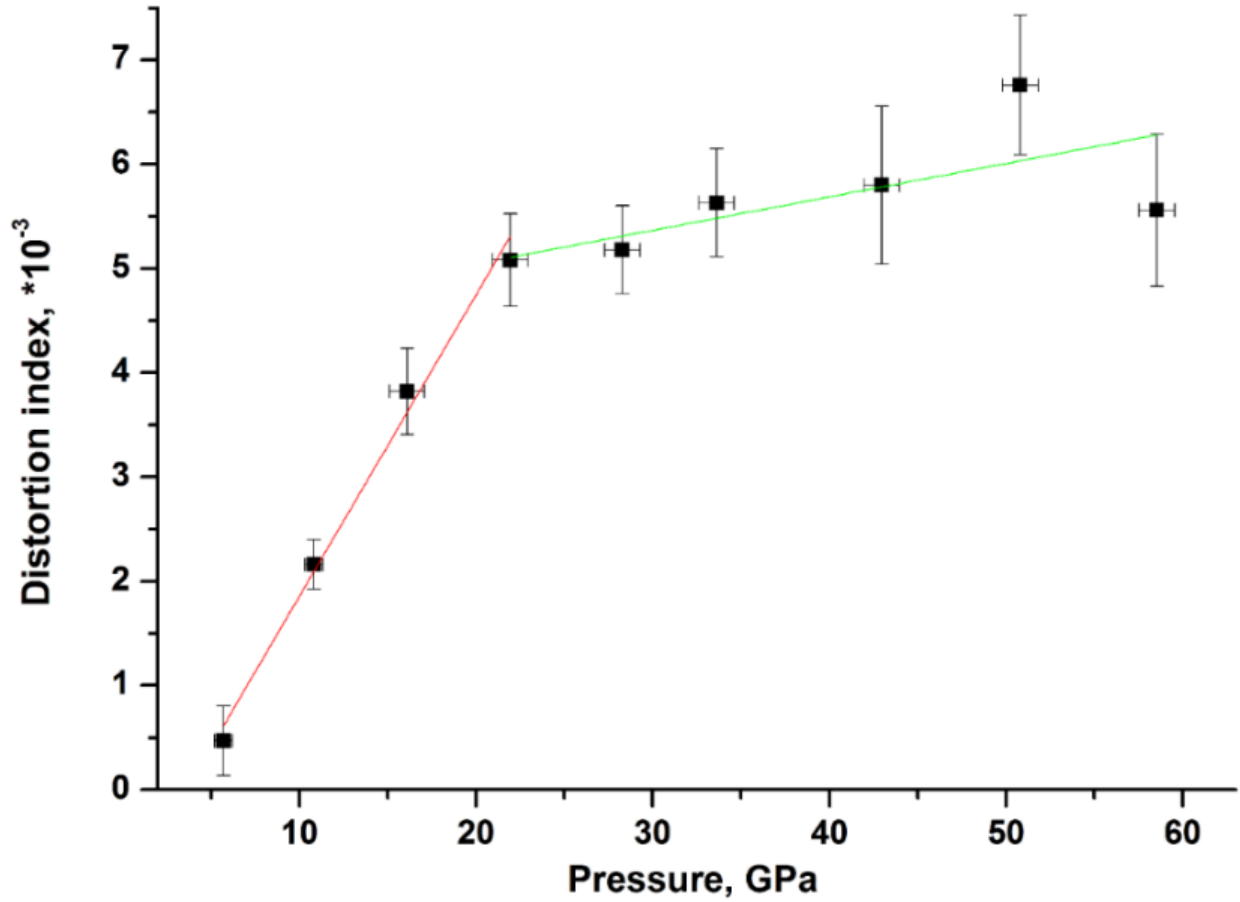
Figure IV.1-7. Distortion index of B_{12} icosahedra as a function of pressure. The distortion of the icosahedra increases rapidly linearly up to ~20 GPa. Above 20 GPa the rate of the distortion change is different.

IV.1.5.2. Spectroscopy investigations

IV.1.5.2.A. Raman spectroscopy

Experimental results were obtained by Raman spectroscopy of α-boron at ambient conditions and compared with the literature data. They are in agreement with those previously reported in [36,43-47]. The systematic shift in the wavenumbers for about 5-10 cm^{-1} compared to [36], is likely attributed to the spectrometer calibration. Like in [36], neither of the surface modes reported in [45] were detected in our study (see discussion in [36]).

Lattice vibrations of α-B were theoretically calculated in [46]. The assignment of Raman modes (see [36] and references therein) is shown in Figure IV.1-8A. Although group theory predicts 10 Raman-active modes [46], the spectrum contains 12 modes. The two additional modes were observed not only in our work, but in previous reports [36,44,48,49] as well. We have no other explanation except that they are probably the hyper-Raman modes [189]. Figure IV.1-8B

demonstrates the Raman spectra of α-B we obtained for selected pressures. Despite the quality of spectra deteriorates with pressure (in particular, because of the broadening of the Raman modes), the most intense modes could be traced up to 160 GPa (Figures IV.1-8B and IV.1-9). As seen, during an isothermal compression to 160 GPa at room temperature (298 K), a monotonous shift of the Raman peaks positions towards higher wavenumbers is observed (Figures IV.1-8B and IV.1-9). The rates of the shift of the frequencies are different for different modes and vary between ~2.2 cm^{-1}/GPa for the 693 cm^{-1} mode and ~5.5 cm^{-1}/GPa for the 1184 cm^{-1} mode (Figure IV.1-9). The behavior of the only mode at 524 cm^{-1} (E_g) is an exception: first, this Raman line does not considerably broaden with a pressure increase, while other modes undergo monotonous pressure-induced broadening. Second, the position of its maximum shifts slowly to higher wavenumbers till about 40 GPa and then starts moving to lower wavenumbers, i.e. it exhibits a clear softening under pressure (Figure IV.1-10). While such a behavior was suggested to be the sign of instability [66], we observed the structure to be stable under compression up to 160 GPa in our X-ray diffraction experiments. The exceptional behavior of the E_g (524 cm^{-1}) mode was recently discussed in the literature [48] and it was suggested that this mode corresponds to the icosahedron librational vibration that is highly harmonic.
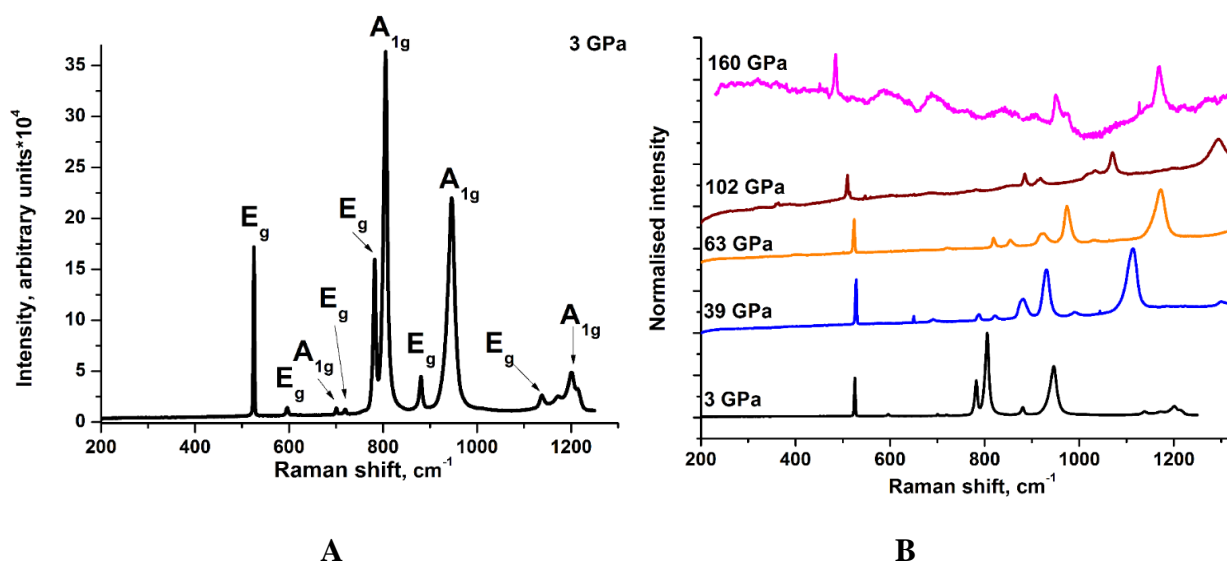
Figure IV.1-8. Raman spectra of α-B. **A.** Raman spectrum of α-B collected at 3 GPa with assignment of Raman modes. **B.** Selected Raman spectra collected in the pressure range from 3 to 160 GPa.
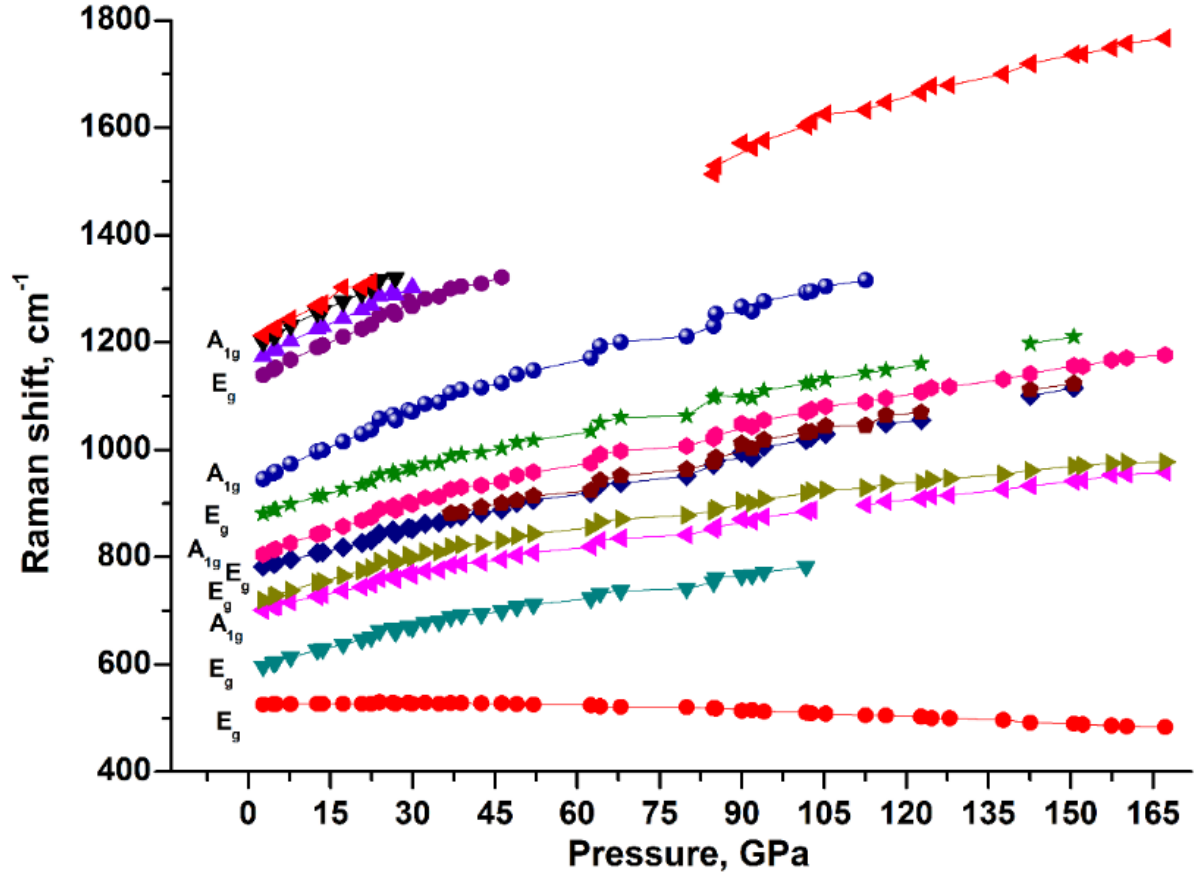
Figure IV.1-9. The pressure-dependent evolution of the Raman modes of α-B measured in the pressure range from 3 to 167 GPa.
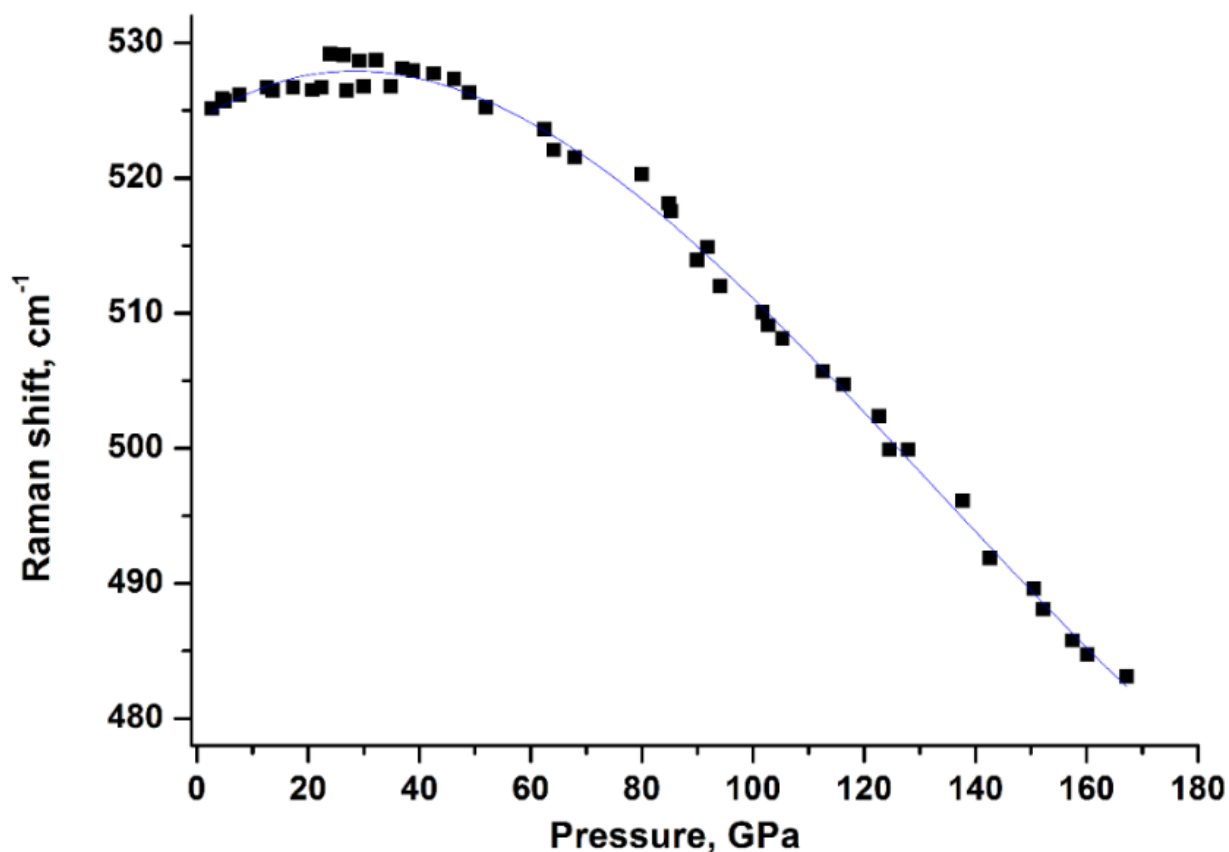
Figure IV.1-10. The behavior of the librational mode E_g of α-B as a function of pressure measured in the pressure range from 3 to 160 GPa. Solid curve is a guide for eyes.

Between ~30 and 40 GPa a new mode at ca. 883 cm^{-1} (pointed out with a red arrow in Figure IV.1-11A, B) appears: it is first clearly observed at ca. 37 GPa on the higher frequency shoulder of the E_g mode at ~ 865 cm^{-1} (pointed out with a blue arrow in Figure IV.1-11B; it has the wavenumber of 774 cm^{-1} at ambient conditions — the breathing mode of the B_{12} icosahedra [46]) as a result of splitting of the latter. The splitting of modes may be an evidence of not only structural changes, but can result from a crystal strain under compression. To clarify the origin of the observed splitting of the E_g mode at ~865 cm^{-1} (774 cm^{-1} at ambient conditions), we specially designed an experiment described below.
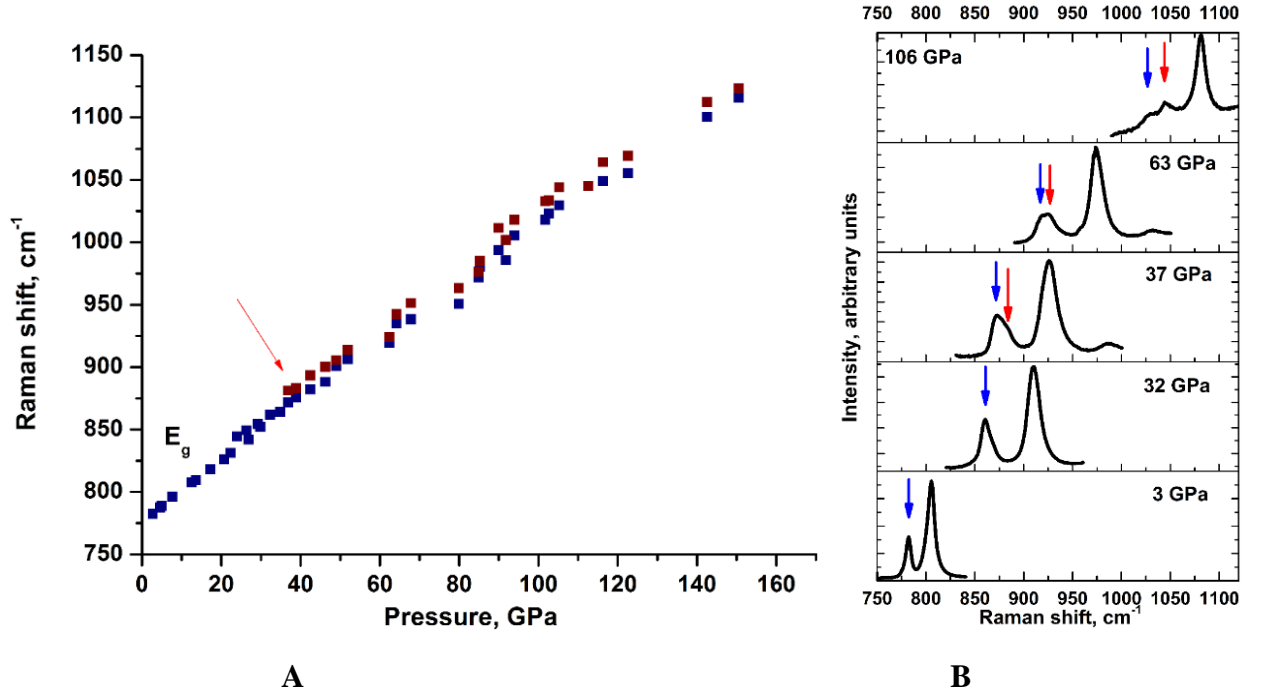
Figure IV.1-11. Pressure-dependent evolution of the E_g mode (at 774 cm^{-1} at ambient conditions) of α-B in the pressure range from 3 to 160 GPa. The splitting of the mode is clearly observed first at ca. 37 GPa on the higher frequency shoulder of the E_g mode at ~ 865 cm^{-1} (pointed out with a red arrow). **A.** The behavior of the mode shown in the full pressure interval. **B.** This mode in the selected Raman spectra at various pressures. At ~37 GPa a new mode at ca. 883 cm^{-1} (pointed out with a red arrow) appears.

Three single crystals of different thickness (~5, 17, and 20 µm) were selected and put into the same DAC (Figure IV.1-12) loaded with neon used as a pressure transmitting medium. The height of the pressure chamber of the DAC was of about 25 µm, so that upon pressurizing the thickest crystal (crystal 3) had to be bridged between the diamond anvils of the DAC first. The crystals were pressurized up to 31 GPa. Upon pressurizing, Raman spectra were collected from each of the three crystals. Figure IV.1-13 shows the pressure-dependent evolution of the same E_g mode (774 cm^{-1} at ambient conditions) for crystals 1, 2 and 3 from their Raman spectra measured at 2, 26, and 31 GPa. It is clearly seen that at 31 GPa the peak of crystal 3 is considerably broader than others at the same pressure and resembles two merged Raman lines, while the same peak of crystal 2 only starts splitting, and that of crystal 1 (the thinnest one) has not split yet. We explain this observation as a result of the consequent bridging of the crystals between the anvils due to their different sizes, and the splitting of the Raman E_g mode as a result of stress imposed upon crystals due to the bridging. Indeed, while the biggest crystal 3 is already stressed at 31 GPa, the crystal 2 just starts touching the anvils, and the crystal 1 is still in quasihydrostatic conditions. If the splitting of the E_g line under consideration would have been the result of a structural transformation, it had to be observed on each crystal at the same pressure.
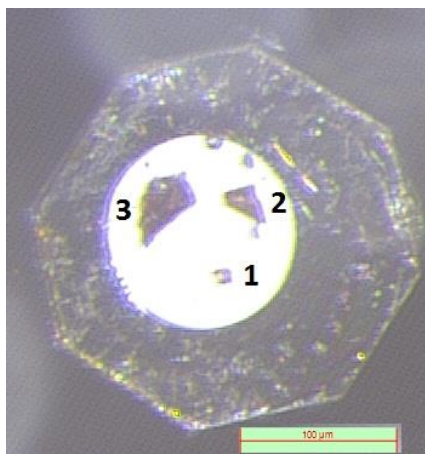
Figure IV.1-12. An image of the sample chamber of a diamond anvil cell. This experiment was designed to clarify the influence of stress on the Raman spectra of α-B. The α-B crystals are placed into a 250-µm hole drilled in the rhenium gasket. Neon was used as the pressure transmitting medium. The numbers 1, 2, 3 notate the crystals of different thickness (ca. 5, 17 and 20 µm, respectively). A ruby ball for pressure monitoring is seen in the top of the image of the pressure chamber.
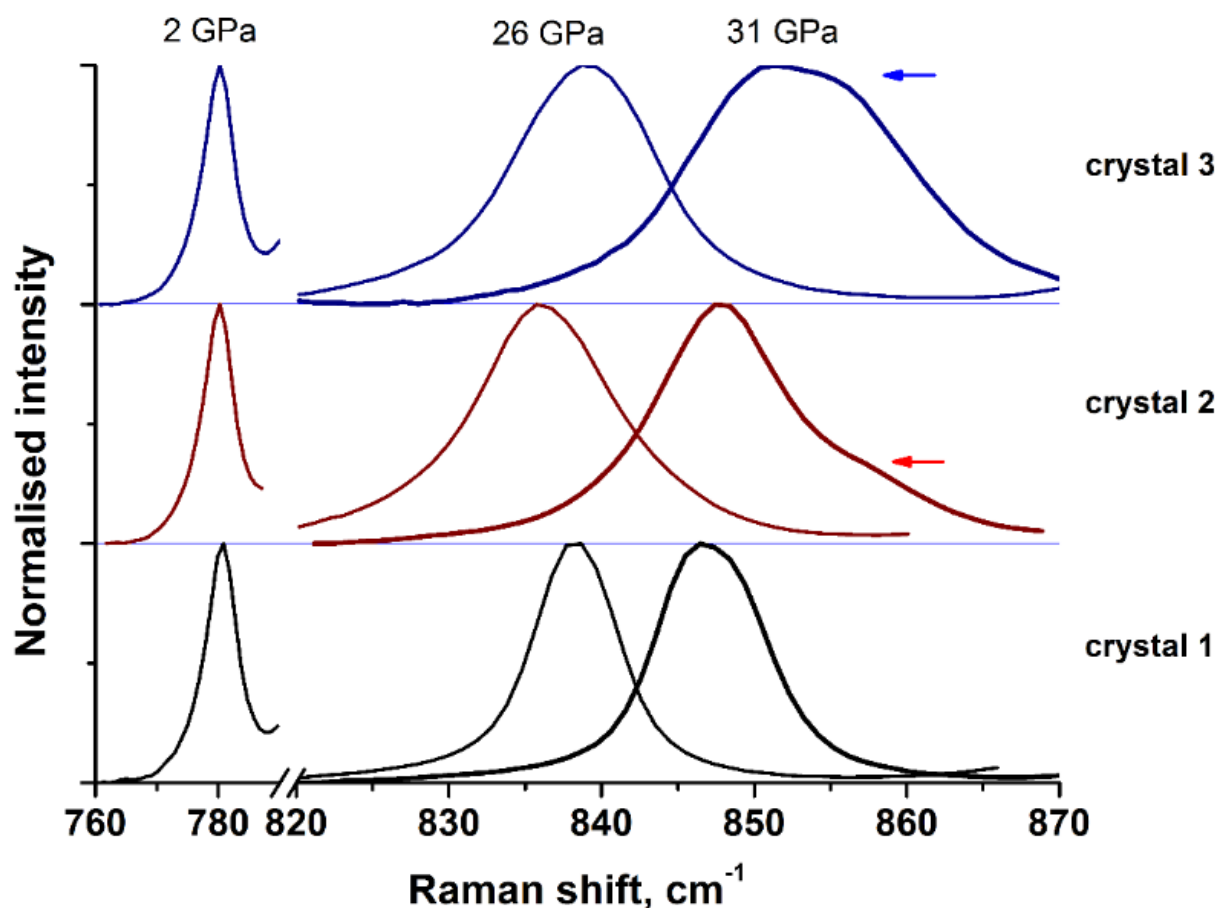
Figure IV.1-13. The pressure-dependent evolution of the same E_g mode (774 cm^{-1} at ambient conditions) for crystals 1 (5 µm thick), 2 (17 µm), and 3 (20 µm) from their Raman spectra collected at 2, 26, and 31 GPa. Broadening and finally splitting of this mode is a result of stress imposed on the crystals upon bridging between the diamond anvils. Blue arrow points out these features in the spectrum of crystal 3; red arrow- in that of crystal 2.

Our conclusion is supported by theoretical calculations of the influence of strain on the behavior of Raman modes of α-B. First, we computed the Raman spectrum at 40 GPa on a fully relaxed theoretical structure, i.e. under pure hydrostatic stresses and null residual forces on the atoms. Then we applied a series of uniaxial and of pure shear deformations. For each deformed strained structure we relaxed the position of the atoms and computed again the Raman spectrum. This allowed us to follow the changes in the Raman spectrum in terms of peak position and symmetry as a function of system and amount of deformation.

We focused on five main Raman peaks (2 E_g and 3 A_{1g}), which were clearly observed experimentally up to the highest pressures achieved. Figure IV.1-14 shows the strain-dependent evolution of these five modes under uniaxial compression applied in various directions. Because the symmetry is preserved during the compression along the z axis (Figure IV.1-14A), the degeneracy of the peaks is not modified; only their frequency is shifted to higher wavenumbers. All the other systems of deformation (Figures IV.1-14B, C, and D) involving at least one component along the x axis, or any shear, will break the symmetry and raise degeneracy. The result is that the E_g peaks will be split into two. The largest splitting is observed in the E_g mode at computed 898 cm^{-1} (at 40 GPa) for the uniaxial compression along the x axis (Figure IV.1-14B), pure shear along the xy plane (Figure IV.1-14C), and pure shear along the xz plane (Figure IV.1-14B). This mode corresponds to a complex asymmetric stretching mode within the B_{12} cages. According to our calculations, theoretical splitting of up to 25 cm^{-1} can occur under 2.5% non-hydrostatic stress. The intensity of the two resulting peaks is not similar. However, it is extremely difficult at this point to assess theoretically beyond doubt the effect of the deformation on the intensity of the individual peaks. The E_g mode at 520 cm^{-1} shows a small theoretical splitting; it corresponds to tilts of the B_{12} cages around the x and y Cartesian axis. The third E_g mode, at 1017 cm^{-1} is the breathing mode of the cages. Its splitting is also limited.
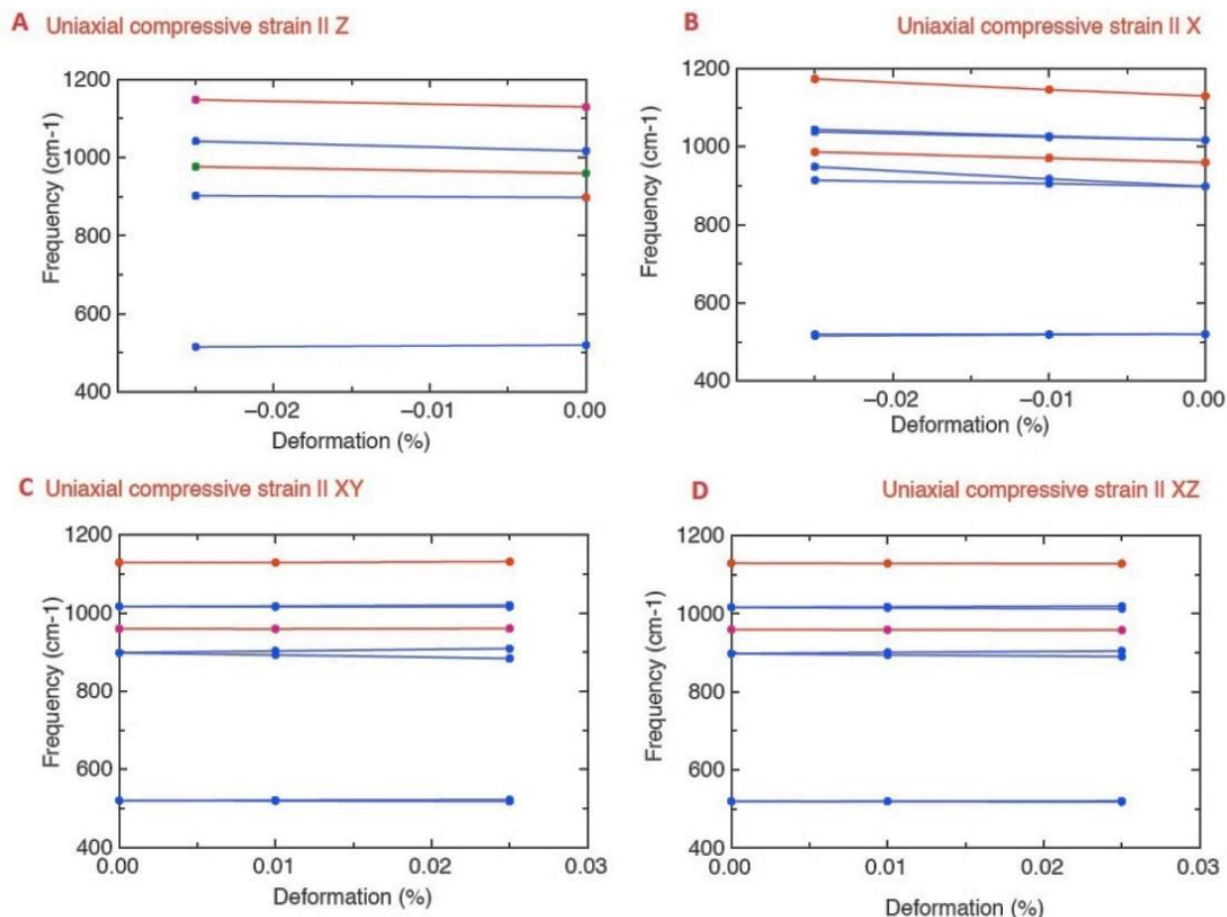
Figure IV.1-14. The results of theoretical calculations of the influence of strain on the behavior of Raman modes of α-B. Five main Raman modes (2 E_g and 3 A_{1g}), which were clearly observed experimentally up to the highest pressures achieved were considered. The strain-dependent evolution of these five modes under uniaxial compression applied in various directions is shown in panels **A, B, C** and **D**. For the interpretation and explanations see the text.

In our Raman spectroscopy experiments we indeed observed the splitting of the E_g mode (see above) in agreement with our theoretical calculations.

IV.1.5.2.B. IR spectroscopy

All IR spectroscopy measurements were made in a DAC with a Ne pressure medium. As synthesized, single crystals of α-B had the thickness of about 10 μm and were not suitable for IR measurements in transmission, because the crystals showed too strong absorption, so that very thin plates of them were needed. The plates with the thickness of about 3-4 μm were prepared using the focused ion beam (FIB) milling. Figure IV.1-15 shows an image of the pressure chamber of a DAC with two plates of FIB-milled α-B crystals. The initial diameter of the pressure chamber was 120 μm. The minimum pressure after loading of neon was 3 GPa. The IR spectrum of α-B obtained in the range from 600 to 1100 cm^{-1} at 3 GPa is shown in Figure IV.1-16A. Two very strong bands at 725 and 827 cm^{-1} correspond well to the bands at 705 and 806 cm^{-1} reported in [51,52] at ambient

pressure. The shift to the higher wavenumber in our spectrum is due to the difference in pressure. A very weak but noticeable absorption centered at about 940 cm⁻¹ well correlates with the one at 920 cm⁻¹ of intermediate strength reported in [51,52]. A dip in transmission centered at about 1060 cm⁻¹ is very broad. We do not have any interpretation to the rather sharp band at 711 cm⁻¹, which was not mentioned in previous experimental studies, although in the spectrum shown in [51] there is a noticeable dip on a lower frequency shoulder of the 705 cm⁻¹ band.

We traced the behavior of all the observed IR bands up to ca. 53 GPa (Figure IV.1-16B). All of them monotonously move with pressure to the higher wavenumbers (Figure IV.1-16). At pressure about 20 GPa a dip centered at about 1010 cm⁻¹ appears, but we consider it as an experimental artefact because it appears in both the background and sample spectra and does not change its position with pressure. The rate of the shifts of the frequencies varies for different modes between 2.0 cm⁻¹/GPa for the 725 cm⁻¹ line and 3.4 cm⁻¹/GPa for the 827 cm⁻¹ line (Figure IV.1-17). High-pressure IR spectroscopy data did not reveal metallization of α-B up to 53 GPa.
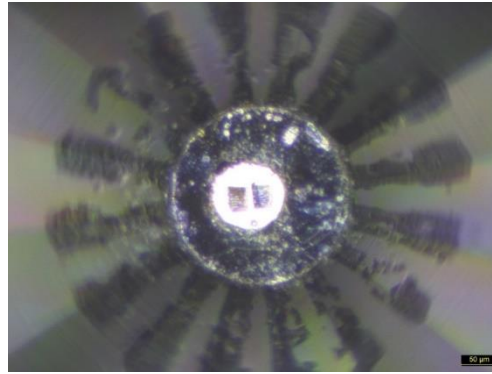
Figure IV.1-15. An image of the pressure chamber of a DAC with two plates of FIB-milled α-B crystals. The thickness of the plates was about 3-4 µm. The starting diameter of the hall was 120 µm.

A **B**
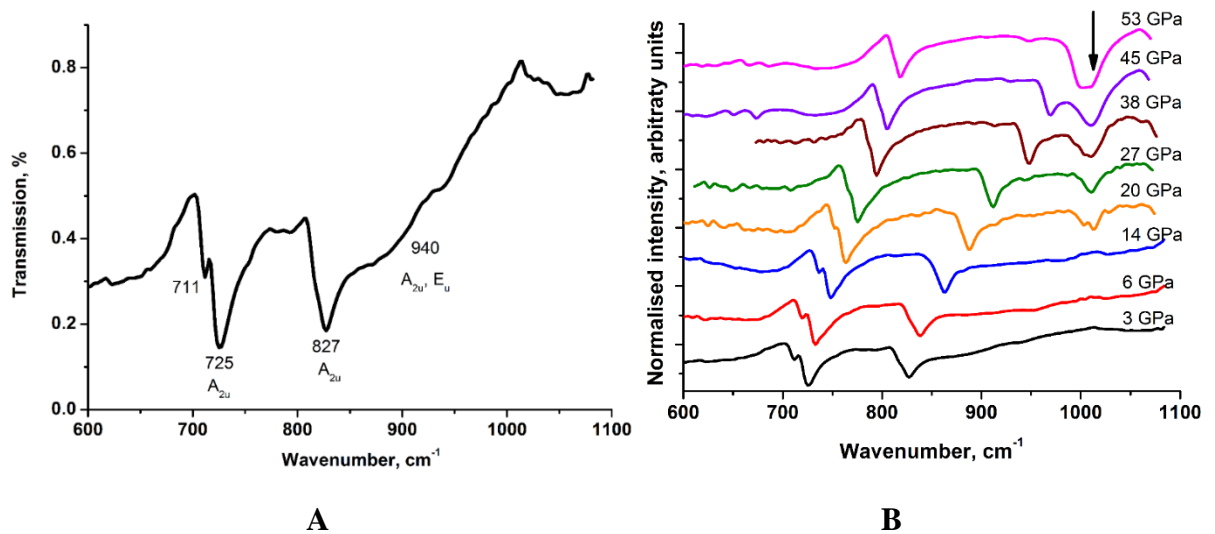
Figure IV.1-16. Infrared transmission spectra of α-B. **A)** IR spectrum measured at 3 GPa. Mode assignment is given according to [46]. **B)** The pressure-dependent evolution of the IR modes in the pressure range from 3 to 53 GPa. The arrow marks the experimental artefact at 1010 cm⁻¹.
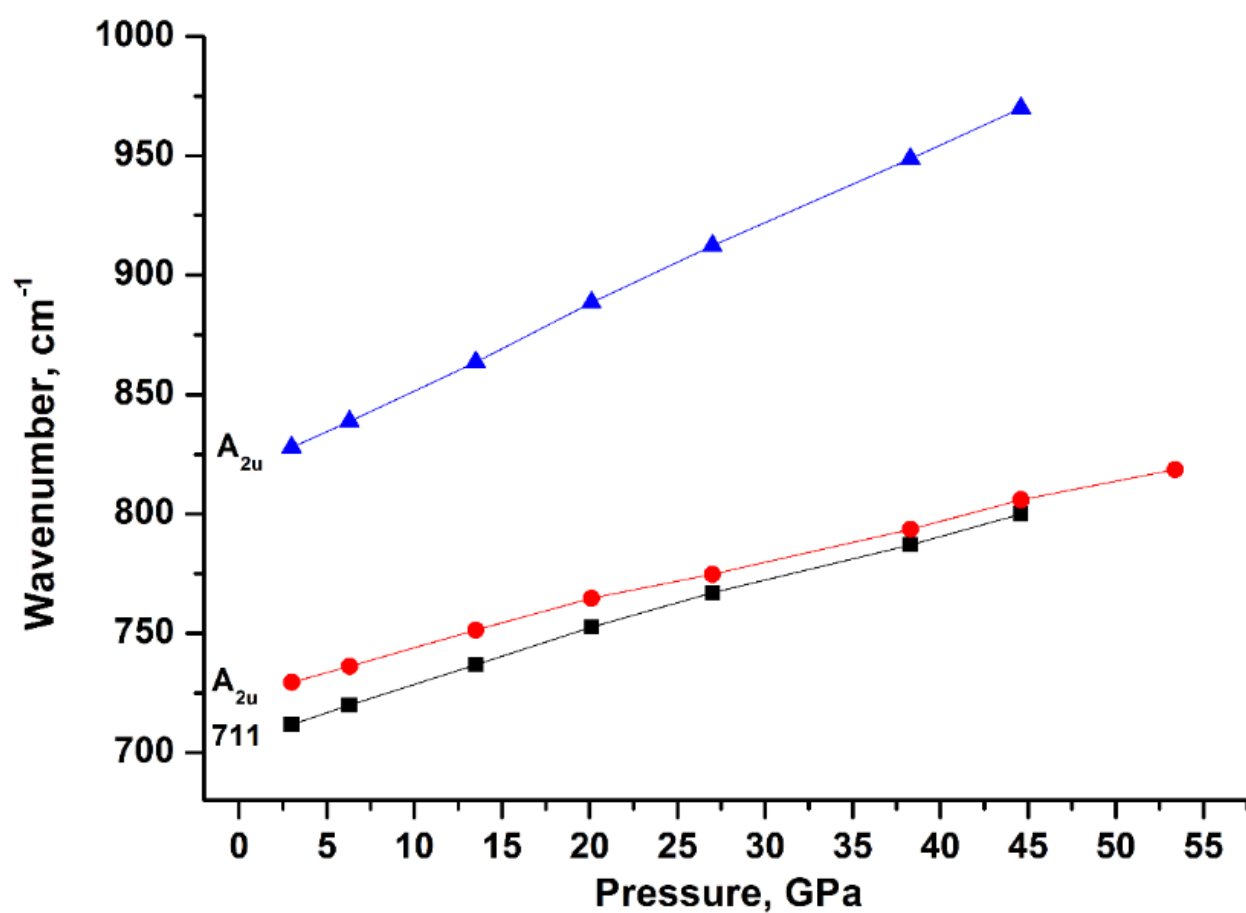
Figure IV.1-17. The pressure-dependent evolution of the IR modes of α-B measured in the pressure range from 3 to 53 GPa.

IV.1.6. Conclusions

In the present work, we have investigated the behavior of α-B under pressure using high-purity single crystals synthesized by the high-pressure high-temperature large volume press technique. The structure of α-B was studied at pressures up to 60 GPa by single-crystal X-ray diffraction in a diamond anvil cell. The bulk modulus of α-B was found to be $K_{300} = 224(7)$ GPa, while the bulk modulus of individual B_{12} icosahedra K_{ico} appeared to be as high as 303(12) GPa. Thus, the compressibility of icosahedra is considerably lower than that of the bulk material. Measurements of interatomic distances as a function of pressure revealed that the intericosahedral B1-B1 2e2c bonds are almost as stiff as intraicosahedral ones. This is in accordance with the previous experimental data [12], which showed that the B1–B1 bond is the strongest one among all bonds in α-B. The B2-B2 2e3c intericosahedral bond shows much higher compliance compared to other bonds in α-B. The vibrational properties of α-B under pressure were investigated by Raman spectroscopy up to 160 GPa and synchrotron IR spectroscopy up to 53 GPa, which gave evidence of structural stability of this boron allotrope in the broad pressure interval, in agreement with X-ray diffraction data. Raman spectra of a satisfactory quality were observed up to the highest pressure reached that gives evidence that metallization of α-B does not occur up to 160 GPa. A comparison of theoretical calculations of the behavior of Raman modes of α-B under stress conditions with experimental data led to conclusion that stress in certain directions results in the splitting of some of the Raman modes.

IV.1.7. Acknowledgements

IV.2. Structural stability and mechanism of compression of stoichiometric B$_{13}$C$_2$ up to 68 GPa.

Irina Chuvashova[a,b*], Elena Bykova[b], Maxim Bykov[b], Volodymyr Svitlyk[c], Leonid Dubrovinsky[b], Natalia Dubrovinskaia[a]

[a]*Material Physics and Technology at Extreme Conditions, Laboratory of Crystallography, University of Bayreuth, D-95440 Bayreuth, Germany*
[b]*Bayerisches Geoinstitut, University of Bayreuth, D-95440 Bayreuth, Germany*
[c]*European Synchrotron Radiation Facility, BP 220 F-38043 Grenoble Cedex, France*

*Correspondence to: irina.chuvashova@gmail.com

Submitted to Nature Communications.

IV.2.1. Abstract

Boron carbide is a ceramic material with unique properties widely used in numerous, including armor, applications. Its mechanical properties, mechanism of compression, and limits of stability are of both scientific and practical value. Here, we report the behavior of the stoichiometric boron carbide B$_{13}$C$_2$ studied on single crystals up to 68 GPa. As revealed by synchrotron X-ray diffraction, B$_{13}$C$_2$ maintains its crystal structure and does not undergo phase transitions. Accurate measurements of the unit cell and B$_{12}$ icosahedra volumes as a function of pressure led to conclusion that they reduce similarly upon compression that is typical for covalently bonded solids. A comparison of the compressional behavior of B$_{13}$C$_2$ with that of α–B, γ–B, and B$_4$C showed that it is determined by the types of bonding involved in the course of compression. Neither 'molecular-like' nor 'inversed molecular-like' solid behavior upon compression was detected that closes a long-standing scientific dispute.

IV.2.2. Introduction

Boron carbide B$_4$C was discovered [100] in 1858, and its crystal structure was first established [101] in 1934. It belongs to icosahedral boron compounds, a family of crystalline solids with crystal structures based on various arrangements of B$_{12}$ icosahedra, which are considered to be some kind of B$_{12}$ "molecules". In such solids chemical bonding has been rationalized in terms of polycenter bonds on the B$_{12}$ *closo*-cluster (boron icosahedron) and two-electron-two-center (2e2c) and two-electron-three-center (2e3c) bonds between the clusters [15]. According to the Wade-Jemmis rule [190-192] 26 out of 36 valence electrons of a B$_{12}$ cluster are accommodated in 13 molecular-orbital-like bonding orbitals to form the cluster. This leaves 10 electrons for external

bonding using 12 equivalent external bonding orbitals, thus creating an electron deficiency in the B_{12} cluster. For a long time, this 'electron deficiency' of the intraicosahedral bonding relative to the intericosahedral one was expected to make the icosahedra more compressible compared to the unit cell, contrary to what is known for typical molecular solids. For this reason the icosahedral boron-rich solids were understood as "inverted-molecular" solids [193]. This gave the origin to the problem of the ratio of the rigidity of the B_{12} *closo*-cluster and the unit cell and the mechanism of compression in icosahedral boron-rich solids that had to be proven experimentally.

The first work, which aimed to shed light into the mechanism of compression of icosahedral boron-rich solids in general and boron carbide in particular, was a high-pressure powder neutron diffraction study of boron carbide (B_4C) to 11 GPa conducted by Nelmes and co-authors [121]. By the linear fit of the experimental 'pressure *versus* volume' (P-V) data obtained for both the icosahedron and the unit cell of B_4C, the bulk moduli of the icosahedron and the entire structure were determined to be 169(6) GPa and 199(7) GPa, respectively. This led to conclusion that the icosahedron is 23(4) % more compressive than the unit cell of boron carbide, which thus behaved as an "inverted-molecular" solid [121].

An experimental evidence that icosahedral boron materials on compression may not behave as "inverted-molecular" solids came from the single-crystal X-ray diffraction data to 65 GPa obtained for the high-pressure boron allotrope, γ-B [79]. The bulk modulus of the B_{12} icosahedron was determined to be 285(6) GPa, whereas the bulk modulus of the entire γ-B structure was found to be 227(3) GPa [79].

A new insight into the situation in boron carbide, compared to the very first measurements [121], was given due to a compressibility study of 'nearly stoichiometric boron carbide B_4C' [108]. Single crystals of B_4C were investigated using synchrotron X-ray diffraction in a diamond anvil cell to 74 GPa. The structure of B_4C was understood as consisting of $B_{11}C$ icosahedra interconnected by the C-B-C chains. The parameters of the equation of state (EoS) of boron carbide were K_{300}=243(6) GPa (K´=3.6(2)) or 236(8) at fixed K´=4 (K_{300} is the bulk modulus, and $K´$ is its pressure derivative; the zero pressure unit cell volume was fixed on the ambient pressure experimental value). Dera et al. [108] pointed out that the "icosahedron volume compression did not follow a typical EoS functional behavior" and they did not calculate the bulk modulus of the $B_{11}C$ icosahedron. Nevertheless, they reported that the $B_{11}C$ icosahedron showed a 13% volume reduction, which was smaller than that of the unit cell volume (18 %). The general conclusion was that B_4C behaves as a molecular solid [108] that is in accordance with the results obtained for γ-B [79].

Optical properties and evolution of Raman modes of the same B_4C samples, which were characterized and studied using single-crystal X-ray diffraction in [108], were also investigated up to 70 GPa by the same research group [116]. Based on their spectroscopy data, the authors [116] reported high-pressure phase transition in boron carbide at 40 GPa, although, according to [108], no signatures of structural phase transitions were observed in B_4C by high-pressure XRD studies up to 70 GPa [108]. Verifying these mutually contradictive reports on boron carbide is not only scientifically important on itself, but it is additionally justified in connection to the commercial value of this unique material. Boron carbide is a very hard and, at the same time, lightweight material for applications in personal security (bullet-proof vests) [15]. It possesses the highest Hugoniot elastic limit of ceramic materials (ca. 17–20 GPa), i.e. the maximum uniaxial dynamic stress that the material can withstand elastically, surpassing all its denser competitors such as silicon carbide and alumina by a factor of 2 [28]. However, it fails just above the Hugoniot elastic limit and the possible source of failure could be clarified through high-pressure experiments. Thus, establishing the mechanism of compression of boron carbide, clarifying its mechanical properties and limits of its stability under loading, are of both scientific and practical interest.

Here we report high-pressure investigations of stoichiometric boron carbide $B_{13}C_2$ using high-pressure single-crystal X-ray diffraction up to 68 GPa. Single crystals of $B_{13}C_2$, which we study here, were characterized in detail in previous work of our group [11]. As it was established that $B_{13}C_2$ is fully ordered and stoichiometric, and carbon atoms occupy a single position (at the ends of the C-B-C chains) [11], in the present work we could track all changes of the crystal structure, atomic positions, and bond lengths with the high accuracy up to 68 GPa. This enabled us to establish the equations of state of both the $B_{13}C_2$ crystal and the B_{12} icosahedron. As the B_{12} icosahedra in the stoichiometric boron carbide $B_{13}C_2$ do not contain any carbon atoms, contrary to all previously investigated boron carbides [102,103,105,107-115,121], we could compare the compressional behavior of B_{12} *closo*-clusters in $B_{13}C_2$ and boron allotropes α-B and γ-B and conclude not only regarding the ratio of the rigidity of the B_{12} *closo*-cluster and the unit cell in these materials, but also concerning the mechanism of compression of boron-rich icosahedral solids.

IV.2.3. Methods summary

IV.2.3.A. Synthesis of crystals

Single crystals of $B_{13}C_2$ were synthesized at high pressures (8.5–9 GPa) and high temperatures (1873–2073 K) using the large-volume-press technique. The stoichiometric composition $B_{13}C_2$ was determined by single-crystal X-ray diffraction in agreement with energy-dispersive X-ray (EDX) analysis ($B_{6.51(12)}C$) [11]. The presence of impurities could be excluded.

IV.2.3.B. Diamond-anvil cell experiments

The BX90-type diamond anvil cells (DAC) [145] made at Bayerisches Geoinstitut (Bayreuth, Germany) and diamonds with the culet diameters of 250 μm were used in high pressure experiments. Rhenium gaskets were squeezed between the diamonds to make an indentation with the thickness of 30 μm. Then in the center of indentations, round holes of 120 μm in diameter were drilled. The $B_{13}C_2$ crystals were placed into these chambers. Sizes of the crystals were about $10 \times 10 \times 15$ μm^3 and $20 \times 15 \times 10$ μm^3. Neon was used as a pressure transmitting medium. Ruby served as a pressure calibrant, and ruby balls were placed into the pressure chamber.

IV.2.3.C. Single-crystal X-ray diffraction

Crystals with size of about $10 \times 10 \times 15$ μm^3 were selected for measurements in a DAC at ID27 at the European Synchrotron Radiation Facility (ESRF). Diffraction data were collected at 293 K using the Perkin Elmer XRD1621 flat panel detector. The monochromatic radiation had the wavelength of 0.37380 Å and the crystal-to-detector distance was 383 mm. Pressure in the cell was increased up to 68 GPa with a step of about 6 GPa. 160 frames in the omega scanning range of −40° to +40° were collected (0.5° scanning step size) with an exposure time of 1 s. Integration of the reflection intensities and absorption corrections were performed using CrysAlisPro software [164,165]. The structure was refined in the anisotropic approximation for all atoms by full matrix least-squares using Jana software [194]. The crystallographic data of $B_{13}C_2$ studied at high pressure have been deposited in the Inorganic Crystal Structure Database [178]. The data may be obtained free of charge from Fachinformationszentrum Karlsruhe, 76344 Eggenstein-Leopoldshafen, Germany (Fax: +49 7247 808 666; e-mail: crysdata@fiz-karlsruhe.de, http://www.fiz-karlsruhe.de/request_for_deposited_data.html) on quoting the following CSD deposition numbers: 432649-432659 (compression from 4 to 68 GPa).

IV.2.4. Results

IV.2.4.1. The equations of state of $B_{13}C_2$ and B_{12} icosahedra

The single-crystal X-ray diffraction data for $B_{13}C_2$ obtained at variable pressure and some experimental details are presented in Table IV.2.4-1. The quality of the data allowed the refinement of both the lattice parameters and atomic coordinates (Supplementary Table IV.2.4-S1). The quality of the structural refinement was good up to the highest pressures achieved that gives evidence that in the course of compression the crystals were maintained in quasihydrostatic environment.

Table IV.2-1. Crystallographic details of $B_{13}C_2$ at variable pressure. Formula: $B_{13}C_2$; Crystal System: Trigonal; Z=3; Space group: R$\overline{3}$m, crystal size $10 \times 10 \times 15\mu m^3$ (crystal 1) and $20 \times 15 \times 10$ μm^3 (crystal 2, designated as "cr2").

P, GPa	a, Å	c, Å	V, Å^3	R$_{int}$*	R$_1$[I>3σ(I)]*	N$_m$**	N$_i$**
0.00010(1)[11]	5.5962(3)	12.0661(7)	327.25(3)	0.0197	0.0227	505	440
4.0(5)	5.5653(6)	11.9811(11)	321.37(6)	0.093	0.0755	272	155
10.0(5)	5.5321(9)	11.898(2)	315.33(9)	0.024	0.0762	221	150
20(1)	5.4708(5)	11.7296(9)	304.03(4)	0.025	0.0577	362	149
23(1)	5.4597(12)	11.6932(19)	301.86(11)	0.024	0.1096	202	148
30(1) cr2	5.4134(8)	11.5589(18)	293.35(8)	0.023	0.0659	291	123
35(1) cr2	5.383(4)	11.472(8)	287.9(3)	0.030	0.0595	316	122
43(1) cr2	5.353(4)	11.413(8)	283.2(4)	0.028	0.0617	268	117
49(1) cr2	5.335(4)	11.334(8)	279.3(3)	0.024	0.0584	247	119
56(1) cr2	5.3007(9)	11.257(2)	273.91(9)	0.024	0.0617	236	121
65(1)	5.2683(10)	11.1812(16)	268.75(8)	0.055	0.0816	184	100
68(1) cr2	5.2529(50)	11.1267(10)	265.88(4)	0.024	0.0645	200	109

*R$_{int}$ and R$_1$[I > 3 σ(I)] relate to data collection and structure refinement, respectively.
**N$_m$ is the number of measured unique reflections; N$_i$ - the number of unique reflections with I>3σ(I)

In the structure of boron carbide B_{12} icosahedra are located in the corners of the rhombohedral cell, and intericosahedral three-atom C-B-C linear chains are oriented along its body diagonal (Fig. IV.2-1A, right). As seen in Figure IV.2-1, the structure of $B_{13}C_2$ is very similar to those of α-B and γ-B, which can be described in terms of a cubic closest packing (*ccp*) of spheres, where B_{12} icosahedra play the role of "spheres" (Figure IV.2-1A,B). The unit cell parameters of $B_{13}C_2$ in hexagonal setting are a = 5.5962(3) Å, c = 12.0661(7) Å, (space group R$\overline{3}$m), as determined in [11]. Boron atoms in the crystal structure of $B_{13}C_2$ (Figure IV.2-1) occupy three

crystallographically independent positions (B_P, B_E, and B_C) and the forth position is occupied by carbon atoms in the C-B-C chains [11]. In the present paper we adopt the nomenclature introduced by [11]: boron atoms forming the boron icosahedra are labeled as B_P (polar positions) and B_E (equatorial positions), B_C designates the boron atom in the center of the C-B-C chain (Figure IV.2-1).
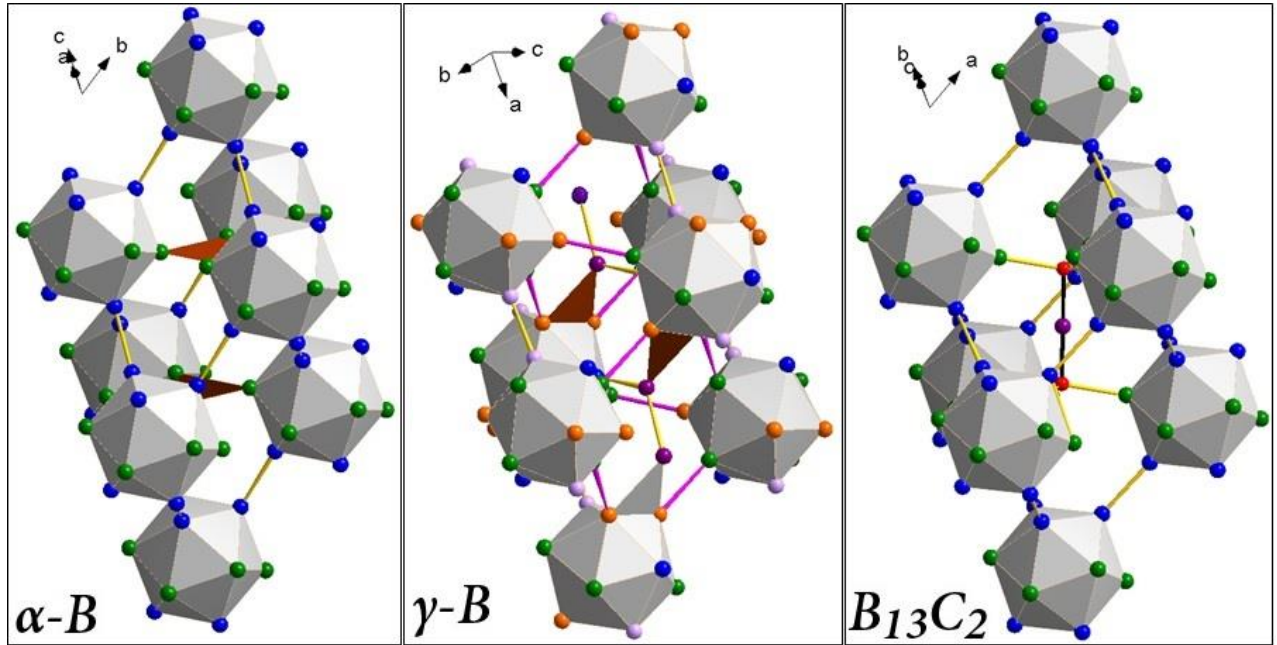
A.
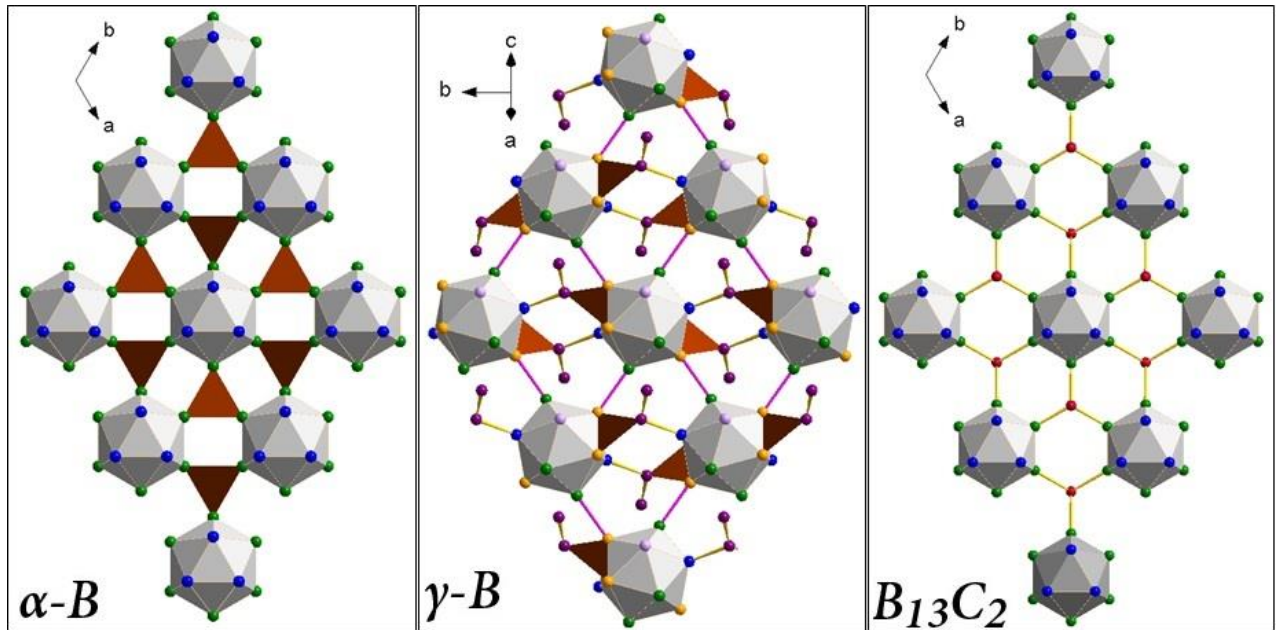
B.
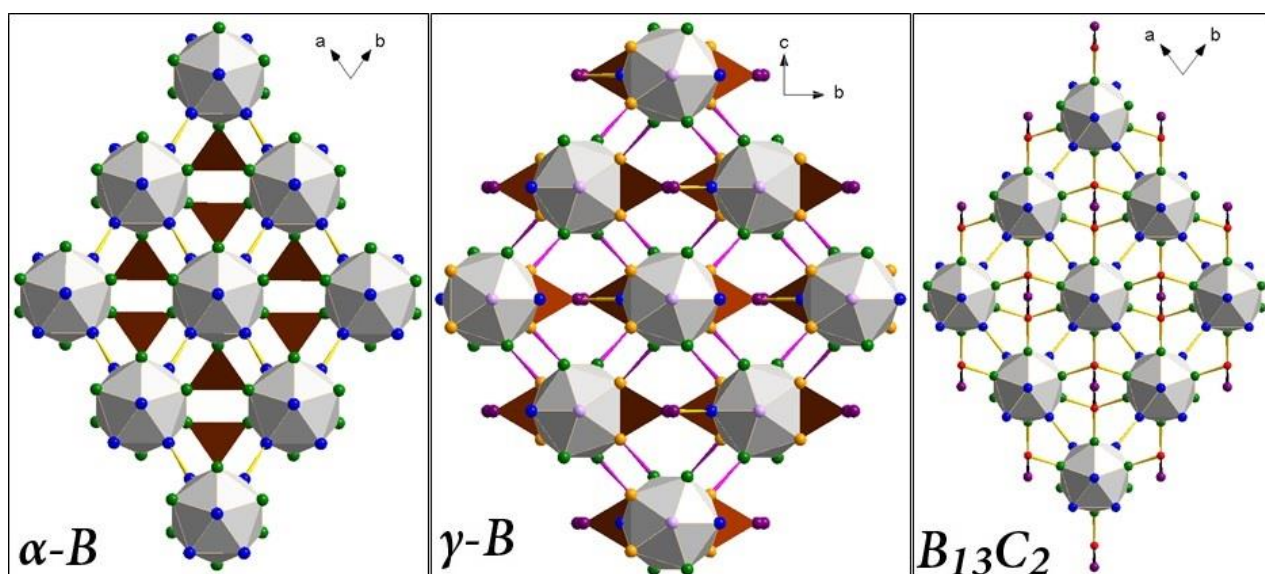
c.
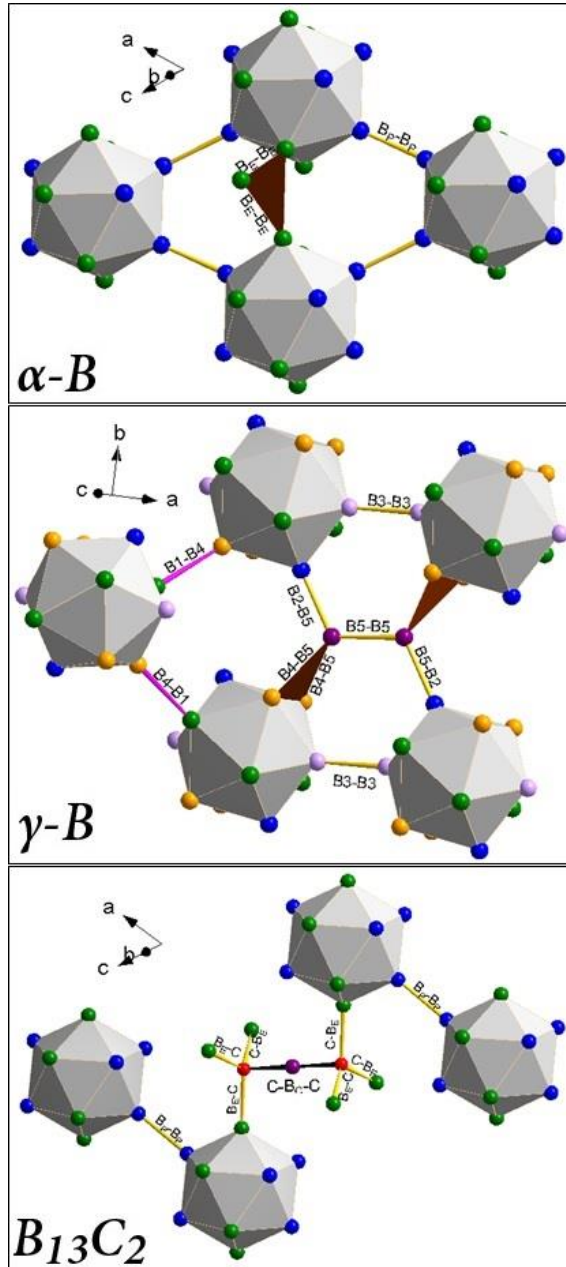
D.

Figure IV.2-1. Crystal structures of α-B, γ-B and B₁₃C₂. A. Rhombohedral cells of α-B and B$_{13}$C$_2$ compared to the elemental rhombohedron which can be selected in the structure of γ-B. **B.** Single layers of the cubic closest packing (*ccp*) of icosahedra in the structures of α-B, γ-B and B$_{13}$C$_2$. The view is perpendicular to the layers: for α-B and B$_{13}$C$_2$ the direction of the view coincides with the *c*-axis of the trigonal unit cell (hexagonal settings), for γ-B it coincides with the *c′* direction (see text). **C.** The packing of icosahedra shown in projection along the axes of the rhombohedral cells for α-B and B$_{13}$C$_2$ and along the *a*-axis for γ-B. **D.** Fragments of the structures of α-B, γ-B and B$_{13}$C$_2$ showing different types of bonds in the corresponding structures (see text for details). In all structure drawings, atoms in crystallographically independent positions are marked in different colors: for α-B and B$_{13}$C$_2$ B$_P$ are blue, B$_E$ are green; for B$_{13}$C$_2$ carbon and boron atoms of the C-B-C chains are B$_C$ (violet) and C (red). For γ-B B1 are blue, B2 are green, B3 are purple, B4 are orange, B5 are violet. Different types of bonds are shown in different colors: 2e2c bonds are yellow, 1e2c bonds are magenta, 2e3c bonds are brown triangles, 3e3c bonds are black.

In this study, all observed reflections perfectly match the $B_{13}C_2$ structure up to the highest pressure reached. Our X-ray diffraction data did not reveal any indication of a phase transition. All the unit cell parameters smoothly decrease on compression (Table IV.2-1). Figure IV.2-2 presents the dependence of the relative unit cell parameters (a/a_0 and c/c_0) and the relative unit cell (V/V_0) volume of $B_{13}C_2$ on pressure up to 68 GPa. As seen (Figure IV.2-2), the structure of $B_{13}C_2$ is slightly more compressible along the c direction.
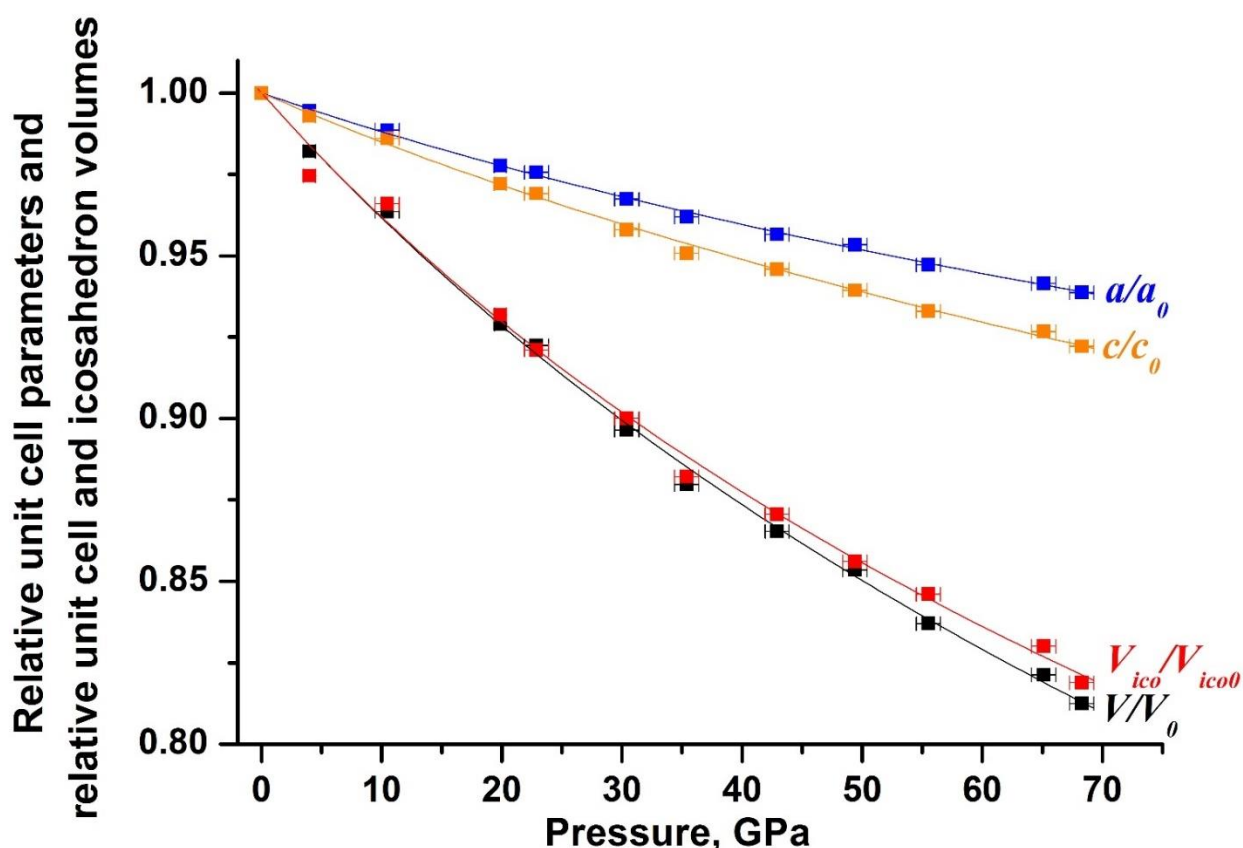
Figure IV.2-2. Pressure-dependent evolution of the relative unit cell volume, lattice parameters and the volume of the B_{12} icosahedron of $B_{13}C_2$. Continuous lines show the fit of the pressure-volume data with the third-order Birch-Murnaghan equation of state.

The whole experimental volume-pressure data set was fitted using the third-order Birch-Murnaghan (3BM) equation of state that gave the following EoS parameters: $V_0 = 327.25(4)$ Å^3, $K_{300} = 239(7)$ GPa and $K' = 3.2(3)$ (V_0 is the zero pressure unit cell volume, K_{300} is the bulk modulus, and K' is its pressure derivative) (Table IV.2-2). The fit with the fixed $K' = 4$ resulted in the bulk modulus of $K_{300} = 222(2)$ GPa, being lower than that with the free K'.

Table IV.2-2. Parameters of the equations of state of $B_{13}C_2$, B_4C, α-B, and γ-B obtained on the basis of single-crystal XRD in comparison with those of icosahedra. Volume reduction of the unit cells and icosahedra on compression was calculated for the pressure range from ambient to 60 GPa.

Material		Ref.	K_{300}, GPa	K'	K_{ico}, GPa	K'_{ico}	Volume reduction	
							Unit cell	Icosahedron
boron carbide	$B_{13}C_2$	*Present study*	*239(7)*	*3.2(3)*	*239(23)*	*3.8(8)*	*18.7*	*18.1*
	B_4C	Dera et al., 2014 [108]	243(3)	3.6(2)			18	13
α-B		Chuvashova et al., 2017 [172]	224(7)	3.0(3)	273(12)	4(fixed)	18.0	14.5
γ-B		Zarechnaya et al., 2010 [79], p<40 GPa	227(3)	2.5(2)	285(6)	1.8(3)	18.9	16.9

The evolution of the relative volume of the B_{12} icosahedron (V_{ico}/V_{ico0}) with pressure is presented in Figure IV.2-2. It is very similar to that of the unit cell volume. The whole experimental data set of the icosahedra volumes *versus* pressure (Table IV.2-3) was fitted using the 3BM EoS. The EoS parameters were obtained as follows: V_{0ico} = 12.50(3) Å^3, K_{ico} = 239(23) GPa, and K_{ico}' = 3.8(8) (V_{0ico} is the zero pressure icosahedron volume, K_{ico} is the bulk modulus of icosahedra, and K_{ico}' is its pressure derivative). The fit with the K_{ico}' = 4 (fixed) results in a very close value of K_{ico} = 234(7) GPa. A comparison of the bulk moduli found for the $B_{13}C_2$ crystal and the B_{12} icosahedron (Table IV.2-2) shows that the bulk $B_{13}C_2$ and the icosahedron have the similar rigidity.

Table IV.2-3. The B_{12} icosahedron volume and bond lengths in boron carbide at variable pressure. "cr2" designates crystal 2. B_P, B_E and B_C are designations from Mondal et al. [11]; b1 through b7 are designations from Dera et al. [108].

P, GPa	V_{ico}, Å^3	Bonds involving CBC		Inter-cluster bonds	Intra-cluster bonds			
		B_E-C (b7)	B_C -C (b1)	B_P-B_P (b2)	B_P–B_P (b6)	^1B_P–B_E (b4)	^2B_P–B_E (b5)	B_E–B_E (b3)
0.00010(1)[11]	12.501	1.6037(2)	1.4324(5)	1.7131(4)	1.8053(4)	1.7997(4)	1.7848(5)	1.7590(3)
4.0(5)	12.1908	1.5980(17)	1.4246(48)	1.7112(32)	1.7825(26)	1.7826(28)	1.7786(33)	1.7480(23)
10.0(5)	12.0831	1.5828(16)	1.4194(36)	1.6874(31)	1.7769(26)	1.7817(28)	1.7686(33)	1.7394(22)
20(1)	11.6379	1.5653(21)	1.4098(35)	1.6649(30)	1.7523(26)	1.7605(27)	1.7474(30)	1.7177(21)
23(1)	11.5144	1.5627(41)	1.4102(70)	1.668(62)	1.7406(52)	1.7525(53)	1.7469(58)	1.7147(41)
30(1) cr2	11.2751	1.5476(15)	1.3963(35)	1.6346(26)	1.7420(17)	1.7412(21)	1.7232(31)	1.6989(17)
35(1) cr2	11.0331	1.5418(11)	1.3904(34)	1.6234(26)	1.7274(17)	1.7292(22)	1.7130(28)	1.6855(16)
43(1) cr2	10.8796	1.5321(11)	1.3890(34)	1.6113(26)	1.7146(17)	1.7207(22)	1.7109(28)	1.6778(16)
49(1) cr2	10.7212	1.5222(11)	1.3871(34)	1.5915(24)	1.7057(17)	1.7160(21)	1.6990(28)	1.6667(16)
56(1) cr2	10.5721	1.5159(11)	1.3790(34)	1.5821(24)	1.6994(17)	1.7064(22)	1.6921(28)	1.6594(16)
65(1)	10.4294	1.5016(15)	1.3775(45)	1.5689(34)	1.6890(33)	1.6974(35)	1.6867(40)	1.6545(29)
68(1) cr2	10.2436	1.498(2)	1.3719(33)	1.5757(30)	1.6778(25)	1.6876(27)	1.6735(31)	1.6477(21)

IV.2.4.2. Evolution of the bonds lengths on compression of $B_{13}C_2$

Recent experimental electron-density study using low-temperature high-resolution single-crystal synchrotron X-ray diffraction data [11] clarified the bonding situation in the stoichiometric boron carbide $B_{13}C_2$. In the present work, we investigated single crystals from the same batch. For consistency, we adopt here the notations of bonds introduced in [11].

There are seven distinct bonds in the structure of boron carbide (Table IV.2-3), which get into three groups [11] (see Figure IV.2-1D, bottom, for bonds notations): intra-cluster polycentral bonds (B_P–B_P, B_E–B_E, ^1B_P–B_E and ^2B_P–B_E); inter-cluster bonds (B_P–B_P), which connect atoms in the polar sites (B_P) of the neighboring icosahedra; and bonds involving C-B-C chains (C–B_E–and C–B_C).

Single-crystal X-ray diffraction data, collected at eleven pressure points in the interval from 4 GPa to 68 GPa, allowed us to follow changes in the length of each of the seven bonds in the structure of boron carbide $B_{13}C_2$ (Table IV.2-3). All bonds gradually shorten under compression (Figure IV.2-3); their pressure-dependent evolution does not show any anomalies (Figure IV.2-3).
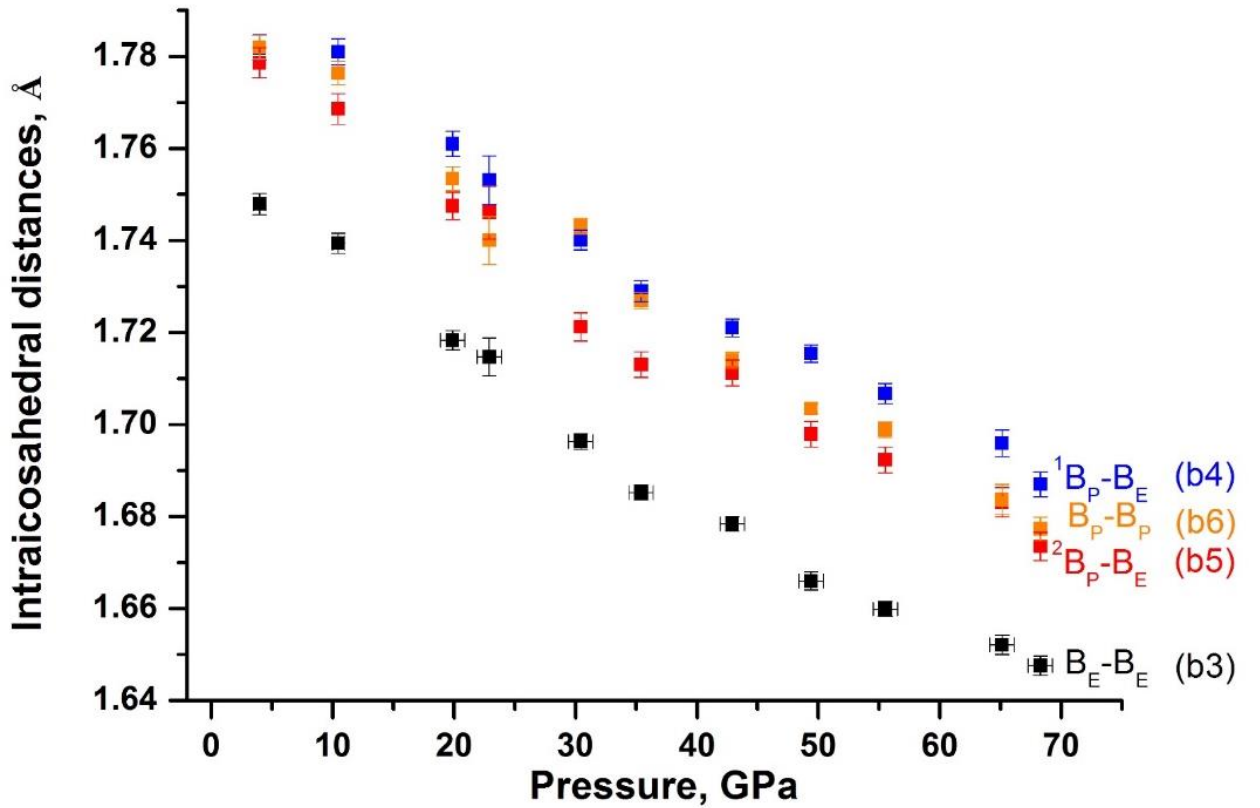
A.
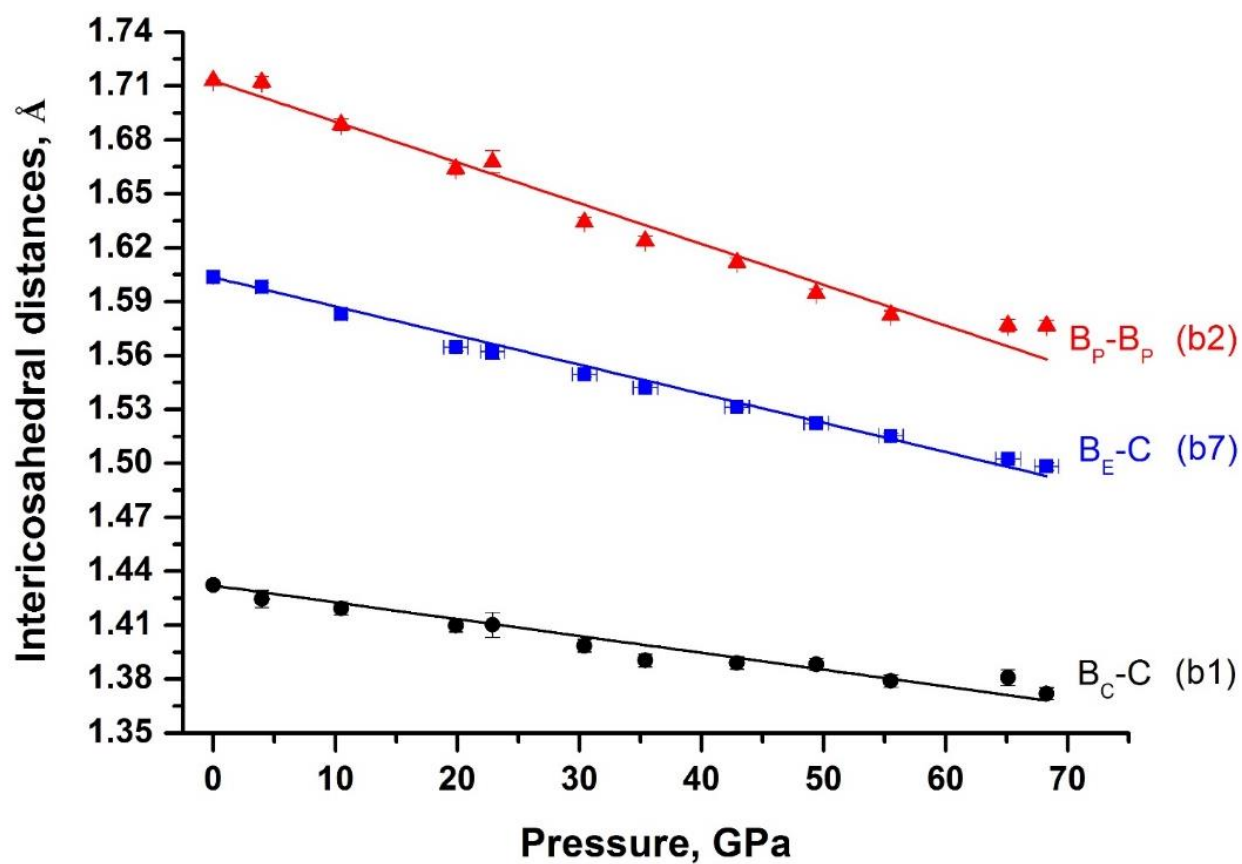
B.

Figure IV.2-3. Pressure-dependent evolution of bonds of $B_{13}C_2$. **A.** Intraicosahedral bonds; **B.** Intericosahedral bonds. Bonds designations are according to Mondal et al. [11], corresponding notations from Dera et al. [108] (b1 through b7) are given in brackets to make it easier to compare.

IV.2.5. Discussion

As mentioned in the introduction, bulk compressibility of boron carbide compared to compressibility of icosahedra has been a matter of debate. Nelmes et al. [121] reported the crystal structure to be more rigid than the icosahedron cluster, whereas Dera et al. [108] observed an opposite relation.

Our results have shown that the rigidity of the crystal structure of stoichiometric boron carbide $B_{13}C_2$ is similar to that of the B_{12} icosahedron. Within the standard uncertainty, the bulk moduli of the bulk material and the icosahedra we found to be similar: $K_{300} = 239(7)$ GPa ($K' = 3.2(3)$) *versus* $K_{ico} = 239(23)$ ($K_{ico}' = 3.8(8)$) (with the fixed $K' = 4$, $K_{300} = 222(2)$ GPa *versus* $K_{ico} = 234(7)$ GPa). The volume reduction of the unit cell of $B_{13}C_2$ and the volume reduction of the icosahedron in the pressure interval between ambient and 60 GPa were calculated to be also similar (18.7% *versus* 18%, respectively); the difference is less than 1% and within the uncertainty. The bulk modulus obtained by Dera and co-authors [108] for the crystals of B_4C is in a very good agreement with our result: their 3BM EoS parameters are $K_{300} = 243(3)$ GPa, $K' = 3.6(6)$, and $V_0 = 330.59(5)$ Å^3 (V_0 was fixed at experimental value obtained at ambient conditions); with the fixed $K' = 4$, they got $K = 236(8)$ GPa [108]. The volume reduction of the unit cell of B_4C (18%) [108] matches very well to what we obtained for $B_{13}C_2$. But interestingly, the volume reduction of the icosahedron in B_4C in the same pressure interval (between ambient and 60 GPa) in [108] appeared to be different (13%) (see Table IV.2-2).

To clarify a reason of the apparent difference in the ratio of the rigidity of the unit cell and icosahedra found for $B_{13}C_2$ and B_4C [108], we first compared the icosahedron and the unit cell volume evolution with pressure in the stoichiometric boron carbide $B_{13}C_2$ and boron allotropes α-B [172] and γ-B [79]. In the structures of each of these materials, icosahedra (B_{12}) are built of exclusively boron atoms. Table IV.2-2 demonstrates a remarkable observation: in the same pressure range (from ambient up to 60 GPa), the unit cell volume reductions for all these materials are similar (ca. 18% within less than 1% deviation). The B_4C, containing $B_{11}C$ icosahedra, is not an exception (18%) [108]. However, the icosahedra volume reductions are all different and reduce in the raw $B_{13}C_2$ (18.1%), γ-B (16.9%), α-B (14.5%), and B_4C (13%). This observation is striking enough and desires an explanation through an insight into the compressional behavior of individual bonds in these solids.

To visualize the difference in the rates of changes of the bonds length and compare boron carbide $B_{13}C_2$ with α-B and γ-B, experimentally obtained data for the relative changes of the bond lengths (l_P/l_{P0}) *versus* pressure was linearly fitted for all the bonds (l_P is the length of the bond at pressure P; l_{P0} is the length of this bond at $P_0 = 4.0$ GPa, the first pressure point available in our

experiment in the DAC). We plotted calculated "line slopes" against corresponding interatomic distances l_{P0} (Figure IV.2-4) at the lowest pressure, similarly to how it was done for characterization of the bond lengths' change under pressure for various boron-rich compounds [173] and α-B [172].
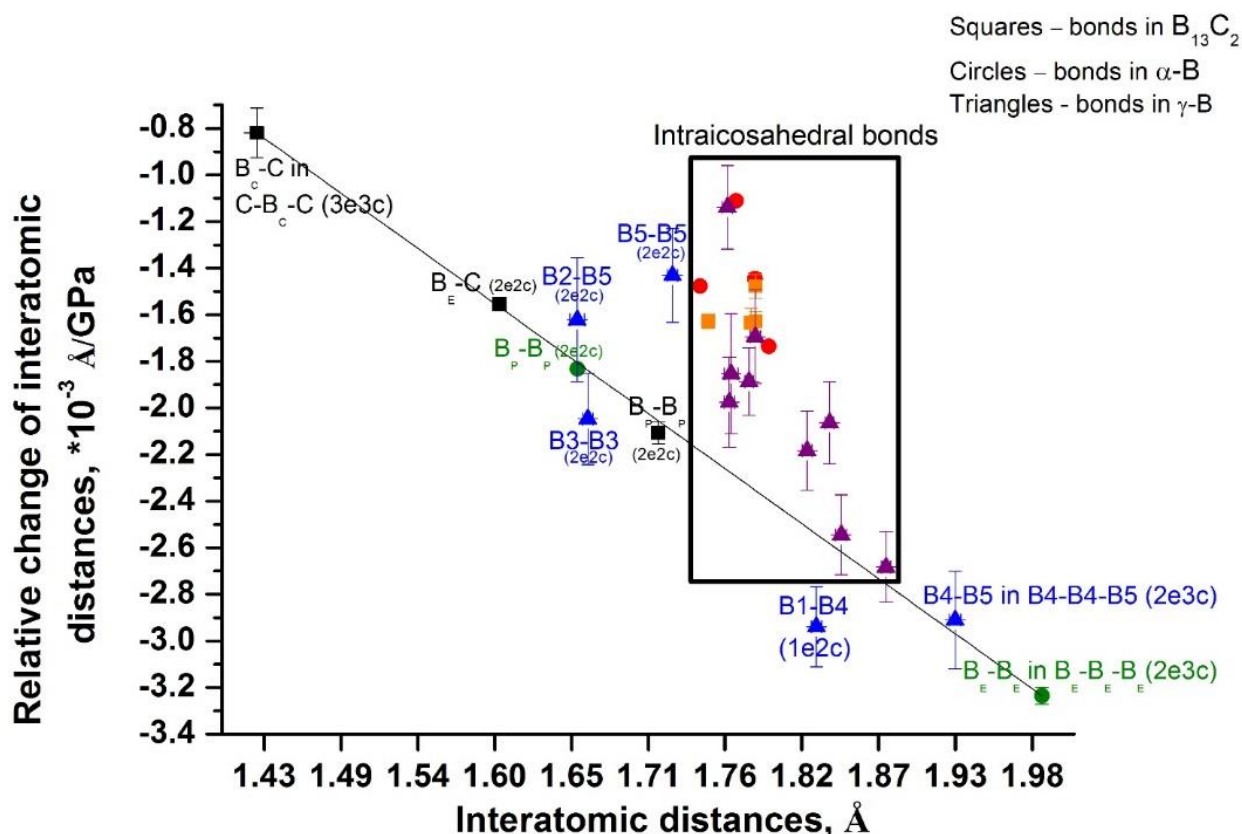
Figure IV.2-4. Relative change of interatomic distances for α-B, γ-B and B$_{13}$C$_2$ single crystal plotted against their length at lowest pressure as revealed by in situ single-crystal X-ray diffraction. Circles stay for bonds in α-B, triangles for γ-B, and squares for B$_{13}$C$_2$. Intraicosahedral bonds are outlined by the black rectangular; red, purple and orange symbols correspond to α-B, γ-B and B$_{13}$C$_2$, respectively. Intericosahedral bonds and those involving B-B dumbbells and C-B-C chains are shown in green, blue, and black colors for α-B, γ-B and B$_{13}$C$_2$, respectively. The bonds in γ-B are shown in triangle: intraicosahedral ones (within black rectangular) are designated in purple, between icosahedra are in blue.

As seen in Figure IV.2-4, all the points corresponding to the inter-cluster bonds (C–B$_C$, C–B$_E$, and B$_P$–B$_P$) in B$_{13}$C$_2$ (black squares) lie on one line, and the rate of their compression depends on the initial length of the bonds (the C–B$_C$ bond between carbon and boron atoms of the C–B$_C$–C chain is the shortest one, see Figure IV.2-1A, right panel; Figure IV.2-1D, bottom panel; Figure IV.2-1B, right panel). Points corresponding to inter-icosahedral bonds in α-B (green circles in

Figure 4) drop on the same line: initially shorter B_P–B_P bonds contract slower than the initially longer B_E–B_E contacts. All points corresponding to the intra-cluster B-B contacts, i.e. those involved in formation of the polycentral bonds of the B_{12} *closo*-cluster, for both $B_{13}C_2$ and α-B (orange squares and red circles, correspondingly, in Figure IV.2-4) appear in a very compact area in Figure IV.2-4, indicating similar rates of contraction and their similar lengths at ambient conditions. Why then the B_{12} icosahedra in $B_{13}C_2$ and α-B undergo such a dramatically different volume reduction (18.1 *vs* 14.5%) when their crystals are compressed to 60 GPa? Purely geometrical consideration is simply not appropriate. One must take into account types of bonding in each of the solids.

As already mentioned, due to recent experimental electron-density studies of boron allotropes and boron carbide [11-13], the validity of the Wade-Jemmis model (see introduction) was demonstrated for α–B [12], γ–B [13], and $B_{13}C_2$ [11]. In all these solids, the molecular-orbital-type bonding on the icosahedral clusters leaves for *exo*-cluster bonding twelve *sp* hybrid orbitals perpendicular to the surface of the clusters. Thus, in terms of bonding, we can consider B_{12} *closo*-clusters to be similar in these three substances. Concerning the inter-cluster bonds, they were found to be very different in α–B [12], γ–B [13], and $B_{13}C_2$ [11]. In α–B and $B_{13}C_2$ the B_P–B_P bonds connecting polar B_P atoms (those between neighboring close-packed layers of B_{12} icosahedra) are strong covalent 2e2c bonds (see Figure IV.2-1A-C, left and right panels; Figure IV.2-1D, top and bottom panels). The B_E–B_E contacts in α–B [12] are very flexible, because they are a part of relatively weak 2e3c B_E–B_E–B_E bonds (shown by brown triangles in Figure IV.2-1). Instead of these weak bonds, in the same positions (octahedral voids of the *ccp*) $B_{13}C_2$ possesses three strong 2e2c C–B_E bonds, which are additionally strengthened by the 3e3c bonds of the C–B_C–C chains, which impose supplementary negative pressure upon the surroundings, as described in [11]. Now it is clear that the similar contraction of the crystals of α–B and $B_{13}C_2$ (ca. 18%) happens in $B_{13}C_2$ on the expense of the icosahedra, which are set into the very rigid surrounding of strong 2e2c and even stronger 3e3c bonds, but in α–B on the expense of weak 2e3c bonds. This conclusion is justified by the behavior of the unit cell parameters ratio c/a in α–B and $B_{13}C_2$ upon compression: in α–B the c/a ratio increases with pressure, but it decreases in $B_{13}C_2$ (Figure IV.2-5). In the both cases, above ca. 40 GPa a clear tendency to the leveling is observed that reflects the more homogeneous compression in the both directions at further pressure increase.

In the light of the consideration made for α–B and $B_{13}C_2$ above, it is not a surprise now that the volume reduction of B_{12} icosahedra in γ–B (16.9%) is intermediate between those in α–B and $B_{13}C_2$ in the same pressure range. As shown in [13], in γ–B there is a broad diversity of inter-icosahedral bonds and those involving the boron dumbbell (Figure IV.2-1A-D, middle panels):

three different kinds of strong 2e2c bonds (B3-B3, B2-B5, and B5-B5); for consistency, we follow here the atoms and bonds notations introduced for γ–B in [79] and [13]. Although initially B5-B5 is slightly longer than B3-B3 and B2-B5, it contracts slightly slower than the latter two. The presence of two types (2e3c and 1e2c) of polar-covalent bonds (2e3c B4-B4-B5, involving two boron atoms of one icosahedron and one atom of a dumbbell, and 1e2c B1-B4, involving atoms of neighboring icosahedra at a distance slightly shorter than that between the B_E atoms in α–B) makes the rigidity of the inter-icosahedral space in γ–B to be intermediate between those in α–B and $B_{13}C_2$ (see Figure IV.2-1). To compare the pressure evolution of the c/a ratio in α–B and $B_{13}C_2$ with the evolution of the corresponding c´/a´ ratio in the structure of γ–B (c´ is in the direction perpendicular to the close-packed layers and a´ - within the layer), we expressed the c´ and a´ through the a, b and c parameters of the orthorhombic unit cell of γ–B and plotted the c´/a´ ratio *vs* P in Figure IV.2-5. As seen, the c´/a´ ratio in γ–B, similarly to what is observed in α–B, first slightly increases, then saturates. Supplementary Figure IV.2-S1, shows the pressure evolution of the normalized c/a ratios for all of these three solids: the c´/a´(P) curve of γ–B indeed takes an intermediate position between the c/a(P) curves of α–B and $B_{13}C_2$. Thus, the compressional behavior of γ–B is likely controlled by the balance between the contraction of icosahedra and the inter-icosahedral bonds. Figure IV.2-4 confirms this interpretation: the lengths of intra-icosahedral contacts in γ–B at ambient pressure are quite similar to those of α–B and $B_{13}C_2$ (see positions of purple triangles in Figure IV.2-4), whereas rates of their contraction under pressure vary considerably (see their scatter within the black rectangular outlining the intra-icosahedral bonds in Figure IV.2-4). Some of them are as compliant as inter-icosahedral contacts (B1-B4 and B5-B5), whereas others are almost as stiff as 2e2c bonds inter-icosahedral and dumbbell bonds of γ–B itself and 2e2c bonds of boron carbide.
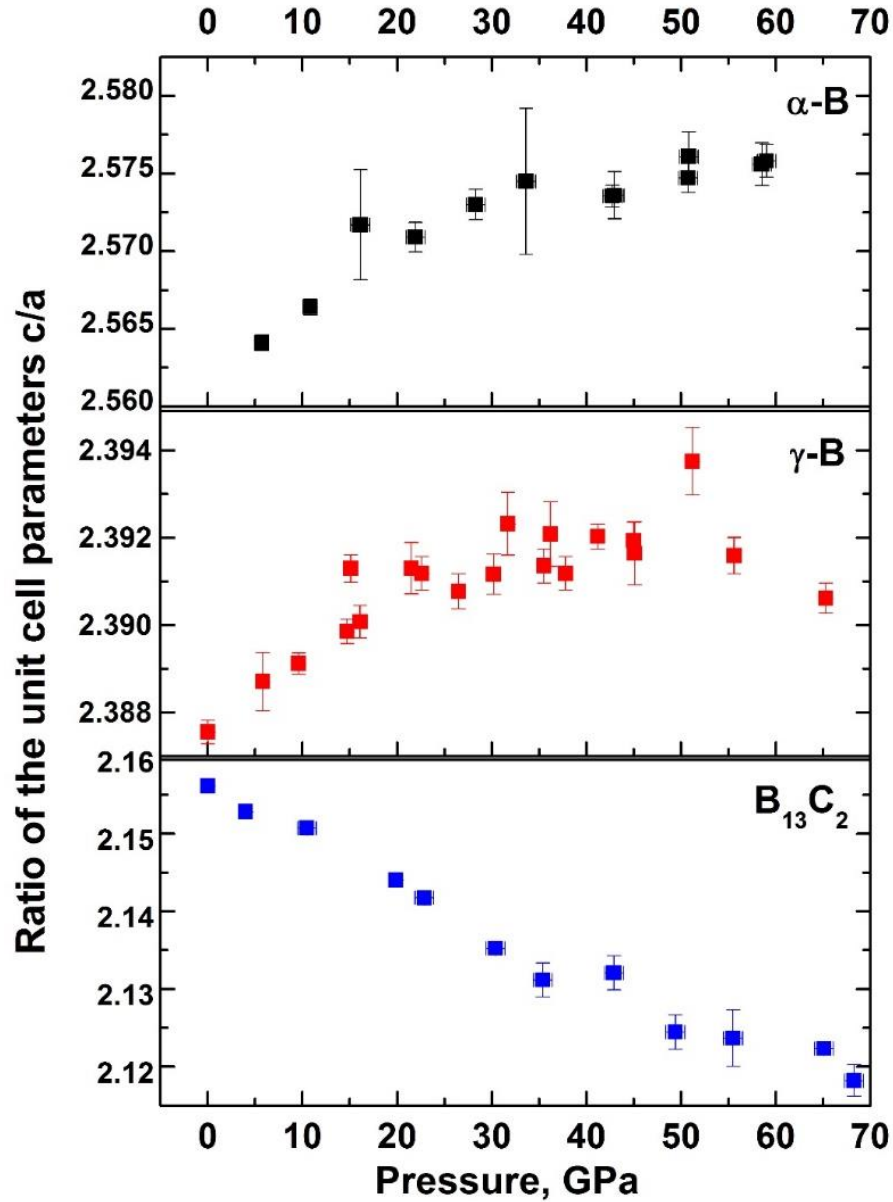
Figure IV.2-5. Evolution of the ratios of the unit cell parameters *c/a* of α-B and $B_{13}C_2$ compared to that of c´/a´ of γ-B. For α-B the data are taken from Chuvashova et al. [172] for γ-B from Zarechnaya et al. [79]

Coming back to the difference in the compressibility of icosahedra in B_4C [108] and stoichiometric boron carbide $B_{13}C_2$, one should take into account different chemical composition, i.e. the boron to carbon ratio, of these two carbides. It is established that boron carbide exists as a single-phase material with a wide homogeneity range of carbon content, from ~7 at. % ($B_{14}C$) to ~20 at. % ($B_{4.3}C$), realized by the substitution of boron and carbon atoms for one another within both the icosahedra and intericosahedral chains [105]. Proposed stoichiometries are based on two extreme models, $B_{12}(CBB)$ on the boron-rich and $B_{11}C(CCC)$ on carbon-rich ends. The location of C atoms in the crystal structure, which is a long-standing debate [102,103,105,107-115], is

difficult to clarify even on single-crystal diffraction data because of the similarity in both electronic and nuclear scattering cross-sections for boron and carbon.

For their "nearly stioichiometric boron carbide B_4C" Dera et al. [108] suggested the presence of 85 atomic % boron and 15 atomic % carbon in the B_P positions in $B_{11}C$ icosahedra. The presence of carbon likely has to lead to an increase of the rigidity of the icosahedron *closo*-cluster of B_4C due to the higher electronegativity of carbon compared to boron. Indeed, the volume reduction of the $B_{11}C$ icosahedron (13%) [108] appears to be smallest compared to B_{12} icosahedra in boron allotropes α–B (14.5%) and γ–B (16.9%) (see Table IV.2-2). The stoichiometric boron carbide $B_{13}C_2$ studied in the present work has been proven to contain carbon only in the C-B-C chains [11], so that its B_{12} icosahedra are much more compliant than $B_{11}C$ (Table IV.2-2), moreover their compliance is similar to that of the whole structure. This observation gives additional evidence that the stoichiometric boron carbide $B_{13}C_2$ is a compound with true covalent bonding: B_{12} icosahedra do not play a role of "molecules", their conventional separation is surely convenient for geometric presentation of the structure, but the compressional behavior of the stoichiometric boron carbide is governed by a complex interplay of both intra-cluster and inter-cluster bonds, as well as those involving C-B-C chains.

To conclude, in the present work we have studied the compressional behavior of the stoichiometric boron carbide $B_{13}C_2$ in the pressure interval up to 68 GPa. Our single-crystal synchrotron X-ray diffraction investigations revealed structural stability of the boron carbide in the studied pressure range. A comparison of the unit cell volume reduction with the reduction of the volume of the B_{12} icosahedron upon compression of $B_{13}C_2$ from ambient pressure to 60 GPa revealed their similarity. This confirms that the stoichiometric boron carbide $B_{13}C_2$ is a true covalent compound and does show neither 'molecular-like' nor 'inversed molecular-like' solid behavior upon compression, as previously disputed. Our analysis has shown that, in agreement with the modern understanding of bonding in α–B, γ–B, and $B_{13}C_2$ based on the experimental electron-density studies [11-13], the compressional behavior of these boron allotropes and boron carbide depends on the types of bonding involved in the course of compression, so that the 'effective compressibility' of B_{12} icosahedra may vary in a broad range, from ca. 14% in α–B to ca. 18% in $B_{13}C_2$, as compared to ca. 18% of compression of the corresponding crystals.

IV.2.6. Acknowledgements

IV.2.7. Supplementary Materials.

Supplementary Table IV.2-S1. Fractional atomic coordinates for $B_{13}C_2$ at variable pressure. (Crystal 2 is designated as "cr2"). *Wyckoff positions are 18h (x, $\bar{x}$, z) for both B_P and B_E atoms, 3a (0,0, 0) for B_C atom and 6c (0, 0, z) for C atom.

P, GPa	Atom*	x	z	U_{eq}, Å^2
4.0(5)	B_P	0.4401(3)	0.0527(2)	0.0028(10)
	B_E	0.5032(3)	0.1922(2)	0.0033(10)
	B_C	0	0	0.0091(19)
	C	0	0.1189(4)	0.0036(11)
10.0(5)	B_P	0.4404(3)	0.0522(2)	0.0101(10)
	B_E	0.5038(3)	0.1918(2)	0.0102(10)
	B_C	0	0	0.0123(17)
	C	0	0.1193(3)	0.0097(11)
20(1)	B_P	0.4401(3)	0.05192(19)	0.0070(7)
	B_E	0.5036(3)	0.19179(18)	0.0075(8)
	B_C	0	0	0.0120(15)
	C	0	0.1202(3)	0.0074(9)
23(1)	B_P	0.4396(6)	0.0519(4)	0.0156(15)
	B_E	0.5034(6)	0.1921(3)	0.0156(15)
	B_C	0	0	0.020(3)
	C	0	0.1206(6)	0.0162(18)
30(1) cr2	B_P	0.4406(2)	0.05175(19)	0.0029(9)
	B_E	0.5036(2)	0.1918(2)	0.0032(9)
	B_C	0	0	0.0071(15)
	C	0	0.1208(3)	0.0036(9)
35(1) cr2	B_P	0.4403(2)	0.05150(19)	0.0076(8)
	B_E	0.5032(2)	0.19180(17)	0.0075(8)
	B_C	0	0	0.0144(15)
	C	0	0.1212(3)	0.0088(9)
43(1) cr2	B_P	0.4401(2)	0.05114(19)	0.0074(8)
	B_E	0.5032(2)	0.19201(17)	0.0072(8)
	B_C	0	0	0.0147(15)
	C	0	0.1217(3)	0.0079(9)
49(1) cr2	B_P	0.4401(2)	0.05062(18)	0.0055(8)
	B_E	0.5033(2)	0.19167(18)	0.0061(8)
	B_C	0	0	0.0153(15)
	C	0	0.1226(3)	0.0075(9)
56(1) cr2	B_P	0.4402(2)	0.05059(18)	0.0041(8)
	B_E	0.5032(2)	0.19185(19)	0.0050(8)
	B_C	0	0	0.0151(16)
	C	0	0.1225(3)	0.0060(9)
65(1)	B_P	0.4402(4)	0.0504(2)	0.0044(11)
	B_E	0.5036(4)	0.1921(3)	0.0057(12)
	B_C	0	0	0.016(2)
	C	0	0.1232(4)	0.0069(12)
68(1) cr2	B_P	0.4398(3)	0.0509(2)	0.0026(9)
	B_E	0.5035(3)	0.1920(2)	0.0024(9)
	B_C	0	0	0.0153(18)
	C	0	0.1233(3)	0.0036(10)
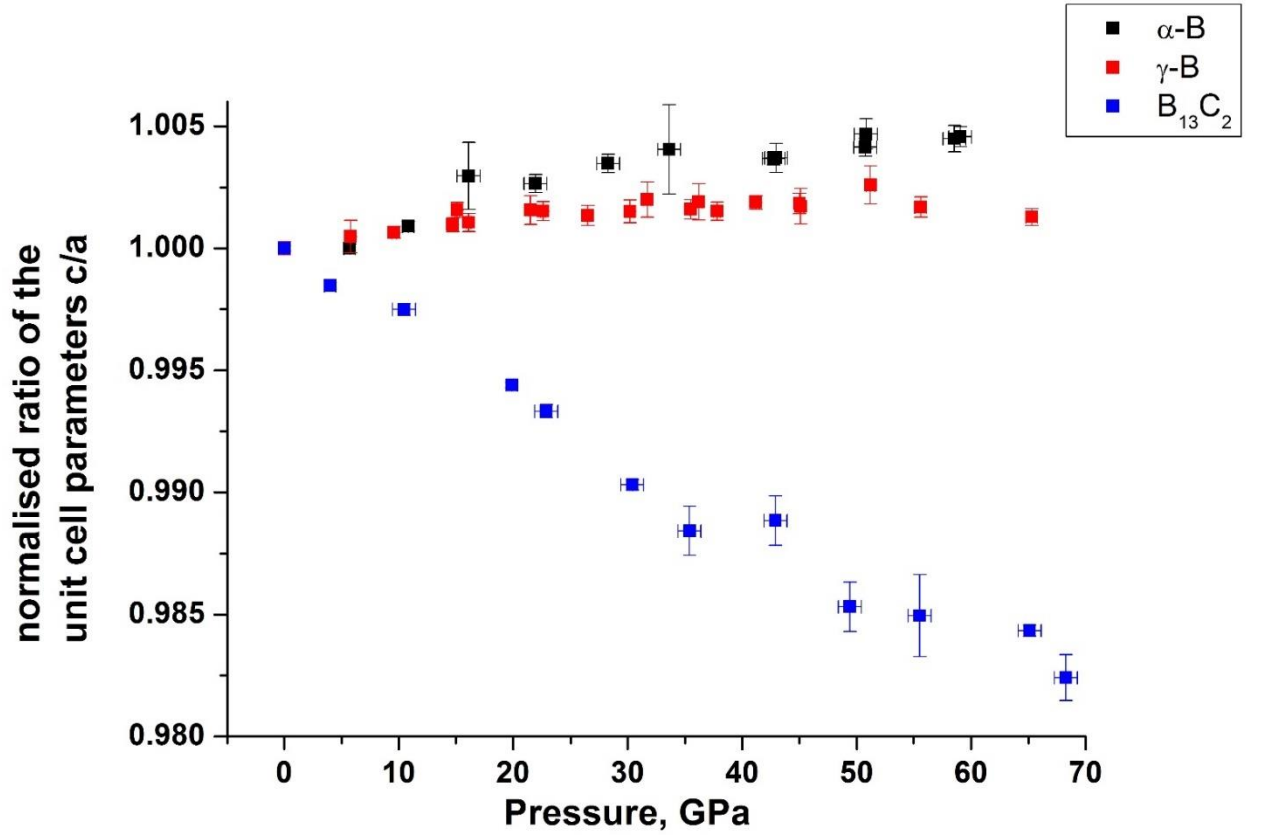
Supplementary Figure S1. Evolution of the normalized ratios of the unit cell parameters *c/a* of α-B and B$_{13}$C$_2$ compared to that of *c´/a´* of γ-B. For α-B the data are taken from Chuvashova et al. [172] for γ-B from Zarechnaya et al. [79].

IV.3. Equation of state of β-B single crystals up to 102 GPa.

Irina Chuvashova[a,b*], Elena Bykova[b], Maxim Bykov[b], Mohamed Mezouar[c], Leonid Dubrovinsky[b], Natalia Dubrovinskaia[a]

[a] *Material Physics and Technology at Extreme Conditions, Laboratory of Crystallography, University of Bayreuth, D-95440 Bayreuth, Germany*
[b] *Bayerisches Geoinstitut, University of Bayreuth, D-95440 Bayreuth, Germany*
[c] *European Synchrotron Radiation Facility, BP 220 F-38043 Grenoble Cedex, France*

*Correspondence to: irina.chuvashova@gmail.com

In preparation.

IV.3.1. Abstract

In the present work we have studied the behavior of β-B under pressure using single crystals synthesized by different high-pressure high-temperature large-volume-press techniques: multi-anvil apparatus and toroidal press. Single crystals were investigated up to 102 GPa using single-crystal X-ray diffraction, which didn't reveal any phase transitions. The bulk modulus of β-B was found to be K=183(3) GPa (K′=3.4(1)).

IV.3.2. Introduction

Boron is a material with remarkable properties (extreme hardness, exceptional chemical stability in crystalline form [11-13], pressure-induced metallization, superconductivity [14]) due to its unusual chemical bonding. Being an object of researchers' interest for a long time (see the review article [15] and references therein), currently it has five experimentally established allotropes of boron: α-B, β-B, γ-B, δ-B ("T-50"), and ε-B [15,16,29,35,67,72]. Structures of all these allotropes have a common structural feature B_{12} icosahedron connected to each other in a variety of ways. Each allotrope possesses a unique Raman spectrum [15,16,29].

Commercial availability of β-boron leads to a lot of studies on optical [63], electrical [64] and mechanical [65] properties. In a conductivity measurement a transformation of β-B from a wide band gap semiconductor to a superconductor at 160 GPa was found [14] what is in agreement with previous theoretical predictions [66].

Mechanical properties are important characteristics of a material. Compressional behavior of β-B and its equation of state (EoS) was measured in the ranges of 0-10 GPa [67] by means of neutron powder diffraction and obtained EoS parameters in comparison with ones of α-B proved

that the structural differences between the two forms have a significant effect on the compressibility. Investigations in the ranges of 0-30 GPa [68] were performed at room temperature as well as under double-sided laser heating to temperatures of 3500 K by powder X-ray diffraction. In [68] the *a* direction in the structure is less compressible than c direction, what indicates the smaller rigidness of B_{28}–B–B_{28} compared to B_{12} icosahedron. The only high-pressure single crystal study of β-B was performed by [69] in the ranges of 2-97 GPa using angle-dispersive powder and energy-dispersive single-crystal X-ray diffraction. Their fit of the P-V data [69] with the Vinet EoS gave $K_{300} = 210(6)$ GPa and $K' = 2.23$. However, they used very limited datasets (with only seven diffraction peaks) to extract the unit cell parameters. Even in case of combination with angle-dispersive SC XRD the number of diffraction peaks was very small and sometimes the indexing was ambiguous. At about 100 GPa the pressure-induced amorphization was observed.

In comparison with boron allotropes (Table IV.3-1) in all experimental studies the β-B is found to be more compressible: bulk modulus $K = 185–210$ GPa [67-69], for α-B $K = 213–224$ GPa [48,67,172], for γ-B before the isostructural transition $K_{300} = 227(3)$ GPa, $K' = 2.5(3)$ [79] determined on the base of powder [68] and single-crystal X-ray diffraction [69], which gave consistent results. Apparently, it may be related to the presence of voids and partially occupied sites as well as complex organization of B_{12} icosahedra in the structure, which makes it softer and therefore more compressible; whereas the structure of α-B consists of boron icosahedra only, and γ-B has the B-B dumbbells in the intericosahedral space.

Table IV.3-1. Parameters of the equation of state of β-B in comparison with those of other boron allotropes. The EOSes are designated as follows: M (Murnaghan), 2BM and 3BM (Birch-Murnaghan of the 2nd and 3rd order), and V (Vinet).

Material	V_0, Å³	Single crystal data		Powder data		Ref./EOS		
		K_{300}, GPa	K´	K_{300}, GPa	K´			
β-B	2511.1(5)	183(3)	3.4(1)			*Present study*	3BM	
		169(1)	4 (fixed)					
		183(3)	3.4(1)				V	
	2450(11)			205(16)	4.3 (1.6)	[68]	3BM	
				208(3)	4 (fixed)			
	2460	210(6)	2.23			[69]	V	
	2463(5)			185(7)		[67]	linear	
		203.5	4.5			[17]	β-105	theory
		220	2.60			[87]	β-105	
		216	2.45				β-106	
		199				[86]	β-106	
α-B	261.94(3)	224(7)	3.0(3)			[172]	3BM	
	264.1	213(15)	4 (fixed)			[67]	M	
		224(15)					linear	
	262(1)	207(13)	4.2(3)			[48]	V	
	261.9			224	4 (fixed)	[175]		
γ-B	197.6(1)			237(5)	2.7(3)	[185]	V	
	198.1(3)	227(3)	2.5(2)			[79]	p<40 GPa	3BM
	192.6(3)	281(6)	2.8(9)				p>45 GPa	

Due to a lack of experimental data and complexity of the structure and theoretical predictions, further investigations of β-B at high pressures are required.

Here we report the results of experimental study of single crystals of β-B by means of single-crystal X-ray diffraction, at pressures as high as 102 GPa.

IV.3.3. Experimental

IV.3.3.A. Large-volume press synthesis

Single crystals of β-B studied in run 1 and 2 of the present work at high pressures were synthesized using the multi-anvil high-pressure high-temperature technique described in detail in [16].

For run 3 single crystals of β-B were synthesized at ~3 GPa and ~1900 K in the large-volume-press with toroidal anvils (toroidal press). The toroidal press installed in the Laboratory of Crystallography in the University of Bayreuth in 2014 (called Orange Mammoth, Figure IV.3-1) is the 12MN Laboratory press of frame construction *MavoPress LPRU 1200 – 555/50*, manufactured by the Max Voggenreiter GmbH.
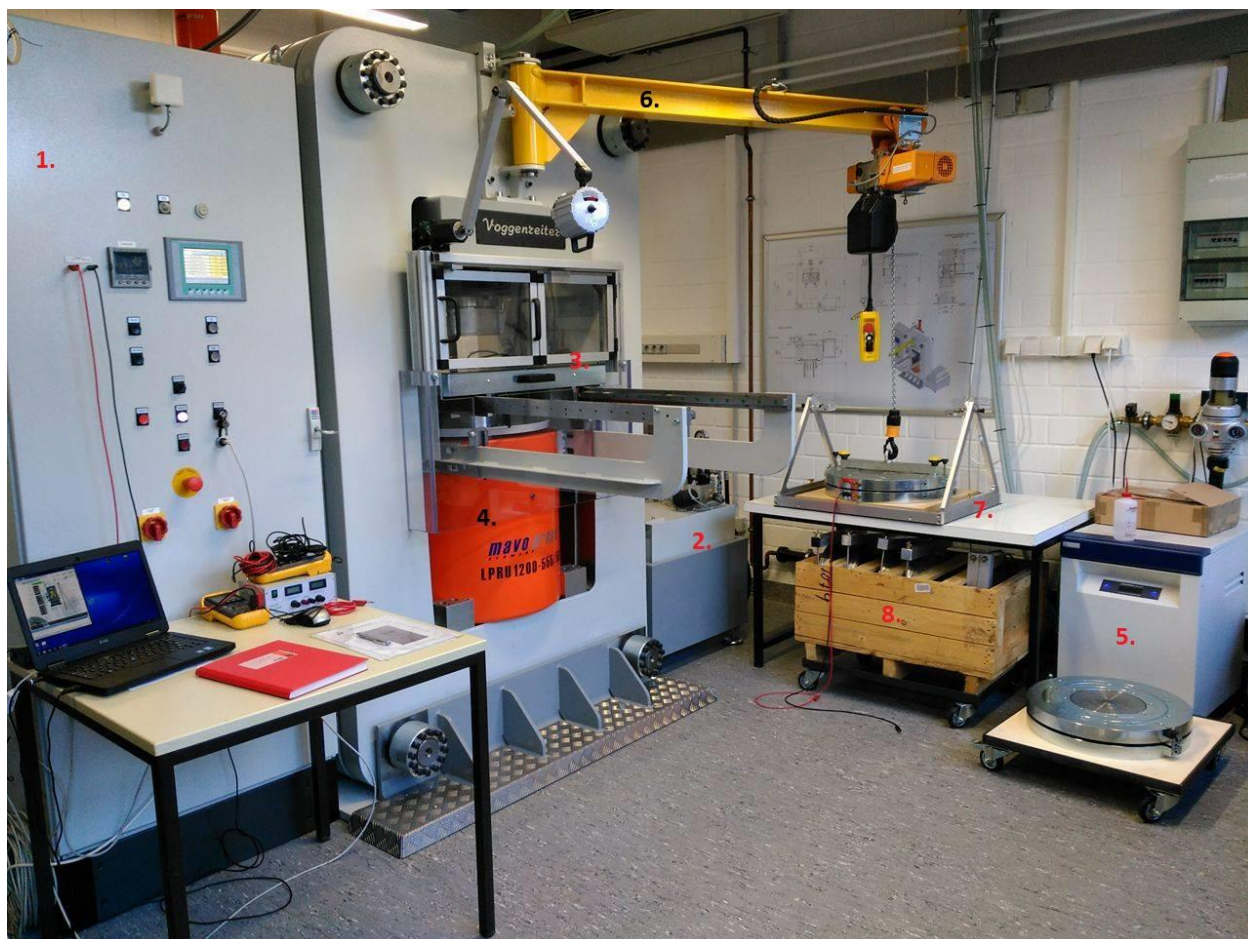
Figure IV.3-1. 12MN Laboratory press of frame construction MavoPress LPRU 1200 – 555/50. It is equipped with toroidal anvils. The system consists of the control box (1), the hydraulic aggregates (2), the working space with protecting windows (3), the hydraulic cylinder (4), the water cooling system (5), the tilt crane (6). Cleaning holder (7), holder for spare sets of anvils (8) are also shown.

A toroidal press is a hydraulic press equipped with toroidal anvils, which comprise the HP device that is a descendant of Bridgman anvils apparatus. It consists of two identical coaxial dies.

Each die has a central section and a circular groove located concentrically [132]. When dies are forced together, the grooves form a central chamber and a secondary cavity of a toroidal shape, which enclose a gasket of a corresponding form. The gasket contains a sample and its material serves as a pressure transmitting medium. The presence of a toroidal recess around the central part on the working surfaces of the anvils reduces the extrusion of the central portion of a gasket and decreases the magnitude of shear stress in anvils.

The toroid press Orange Mammoth consists of the control block (1), the hydraulic aggregate (2), the working space with protecting windows (3), the hydraulic cylinder (4), the water cooling system (5), the tilt crane (6), cleaning holder (7), holder for spare sets of anvils (8) Figure IV.3-1. The press can be operated both manually and automatically, through the control system from the controlling laptop using the software installed. A program is written setting the desirable parameters of an experiment, such as attained pressure, speed of compression and decompression as well as duration of the experiment. If necessary, cycling experiments can also be programmed. For the current work, the compression and decompression rates were 10 bar/minute and the duration of the experiment was 7 hours.

The table of the holder for cleaning is the place where the anvils are stored between the experiments. Under the table there is a container with sets of changeable toroidal anvils with different sizes. For the current work, Toroid-14/6 were used (14 mm and 6 mm are the central recess diameter and the height of the gasket, respectively).

Between the anvils the sample assembly is placed. For the current experiments, the assembly consisted of (Figure IV.3-2): a gasket made of sintered chromium doped magnesium oxide Cr:MgO produced by Ceramic Substrates & Components Ltd using 95% high purity MgO (1); ZrO_2 insulator (2); graphite heater (3); h-BN capsule with sample volume of ~6.5 mm^3.
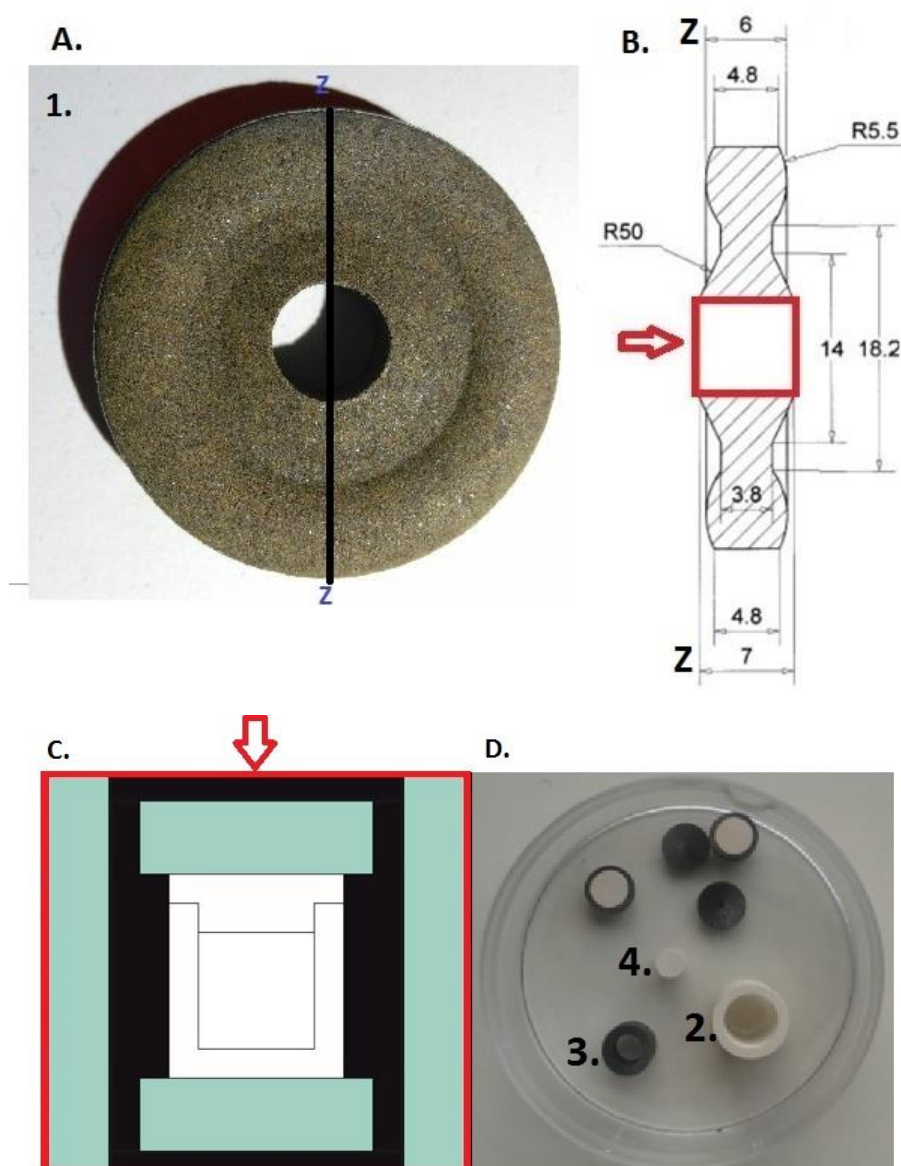
Figure IV.3-2. The sample assembly for the laboratory toroidal LVP Orange Mammoth. **A.** Photo of a gasket (1) made of sintered chromium doped magnesium oxide Cr:MgO produced by Ceramic Substrates & Components Ltd using 95% high purity MgO. **B.** Schematic representation of cross-section of gasket. **C.** Schematic representation of sample chamber. **D.** Photo of parts of assembly (2. ZrO_2 insulator; 3. graphite heater; 4. h-BN capsule).

Pressure calibrations of the toroidal press was performed using pressure-induced fixed-point phase transitions of Bi and Yb at room temperature. Electrical resistance of the assembly was measured depending on the oil pressure during both compression and decompression. The maximum pressure achieved with Toroid-14/6 anvils is 10 GPa. The pressure uncertainty is about 0.5 GPa.

For temperature calibration of the toroidal press, the melting points of a number of metals (silver, aluminum, gold, platinum, and iron) were used. After carrying out several experiments for

each metal, the dependence of temperature on applied power, i.e. temperature calibration curve was plotted. The temperature uncertainty did not exceed ±90 K.

The structure and purity of single crystals were carefully characterized to assure the reliability of the obtained experimental results. The presence of impurities could be excluded. Experimental details are presented in Table 2.

Table IV.3-2. Parameters of three different experiments performed in the present study.

Parameters	Run 1	Run 2	Run 3
Conditions of synthesis of b-B crystals studied here	[16] 5 GPa, ~1700 K	[16] 5 GPa, ~1700 K	Toroidal press 3 GPa, ~1900 K
Diamond culet diameters in the DAC, μm	250	120	250
Thickness of indentation, μm	30	20	30
Diameter of the pressure chamber, μm	120	60	120
PTM	Ne	Ne	Ne
Pressure calibrant	Ruby	Ne	Ruby
Pressure range, GPa	0-66	0-102	0-50
Omega scanning range, degrees	−40 to +40	−35 to + 35	−40 to +40
Exposure time, s	1	2	2

IV.3.3.B. Diamond-anvil cell experiments

The BX90-type diamond anvil cells (DAC) [145] made at Bayerisches Geoinstitut (Bayreuth, Germany) and Boehler-Almax type [146] beveled diamonds were used in high pressure experiments. Rhenium gaskets were squeezed between the anvils to make an indentation with different thickness (for details see in Table IV.3-2). Then in the center of the indentations, round holes were drilled. Two β-B crystals were placed into these chambers in every run. Sizes of the crystals were about $10 \times 10 \times 15$ μm^3 and orientation of the crystals was not specified. Neon was used as a pressure transmitting medium (PTM) and as pressure standard [195] in run 2. In run 1 and 3 ruby was served as a pressure calibrant, and ruby balls were placed into the pressure chamber.

IV.3.3.B. Single-crystal X-ray diffraction

Single crystals of β-B in a DAC were studied on ID27 at the European Synchrotron Radiation Facility (ESRF). Diffraction data were collected at 293 K using the Perkin Elmer

XRD1621 flat panel detector. The monochromatic radiation had the wavelength of 0.37380 Å and the crystal-to-detector distance was 383 mm. Pressure in the cells was increased stepwise, and single-crystal diffraction data for β-B were collected at each pressure point. 160 frames in the omega scanning range of −35° to +35° (in 0.5° steps) were recorded. Integration of the reflection intensities and absorption corrections were performed using CrysAlisPro software [164,165]. The structure was refined in the anisotropic approximation for all atoms by full matrix least-squares using SHELXL software [166] in the WinGX software package [165].

IV.3.4. Results and discussion

The unit cell parameters of β-B (space group $R\bar{3}m$) determined in the present study at ambient conditions are $a = 11.0304(30)$ Å, $c = 23.829(2)$ Å (in hexagonal settings). In Table IV.3-3 they are compared with available literature data. The unit cell parameters as a function of pressure were extracted from single-crystal diffraction dataset obtained at each pressure point. In this study, all observed reflections perfectly match the β-B structure up to the highest pressure reached. Figure IV.3-3 represents the dependence of the relative unit cell parameters (a/a_0 and c/c_0) and the relative unit cell (V/V_0) volume on pressure up to 102 GPa. As seen from Figure IV.3-3, the structure of β-B is as compressible along the c direction as along the a direction. While these characteristics show a smooth decrease with pressure, the ratio of the unit cell parameters c/a non-monotonously increases (Figure IV.3-4) with a bend in the (c/a vs P) line at about 80 GPa.

Table IV.3-3. Unit cell parameters of β-B single crystals obtained at ambient pressure in comparison with literature data. EDX is designated as energy-dispersive X-ray diffraction, ADX stays for angle-dispersive X-ray diffraction.

Source	a, Å	c, Å	V, Å^3	Method
Present study	*11.0304(30)*	*23.829(2)*	*2511.1(5)*	*Monochromatic single-crystal X-ray diffraction*
[69],[61]	10.92	23.81	2460	ADX on powders and EDX on single crystals
[68]	10.91(3)	23.8(1)	2450(11)	Powder XRD
[67]	10.934(11)	23.79(3)	2463(5)	Neutron diffraction

Figure IV.3-3. Pressure-dependent evolution of unit cell volume and lattice parameters of β-B single crystals based on high-pressure single-crystal XRD data. Continuous lines show the fit of the pressure-volume data with the third-order Birch-Murnaghan equation of state. Squares, circles and triangles represent the data obtained in three different experiments.
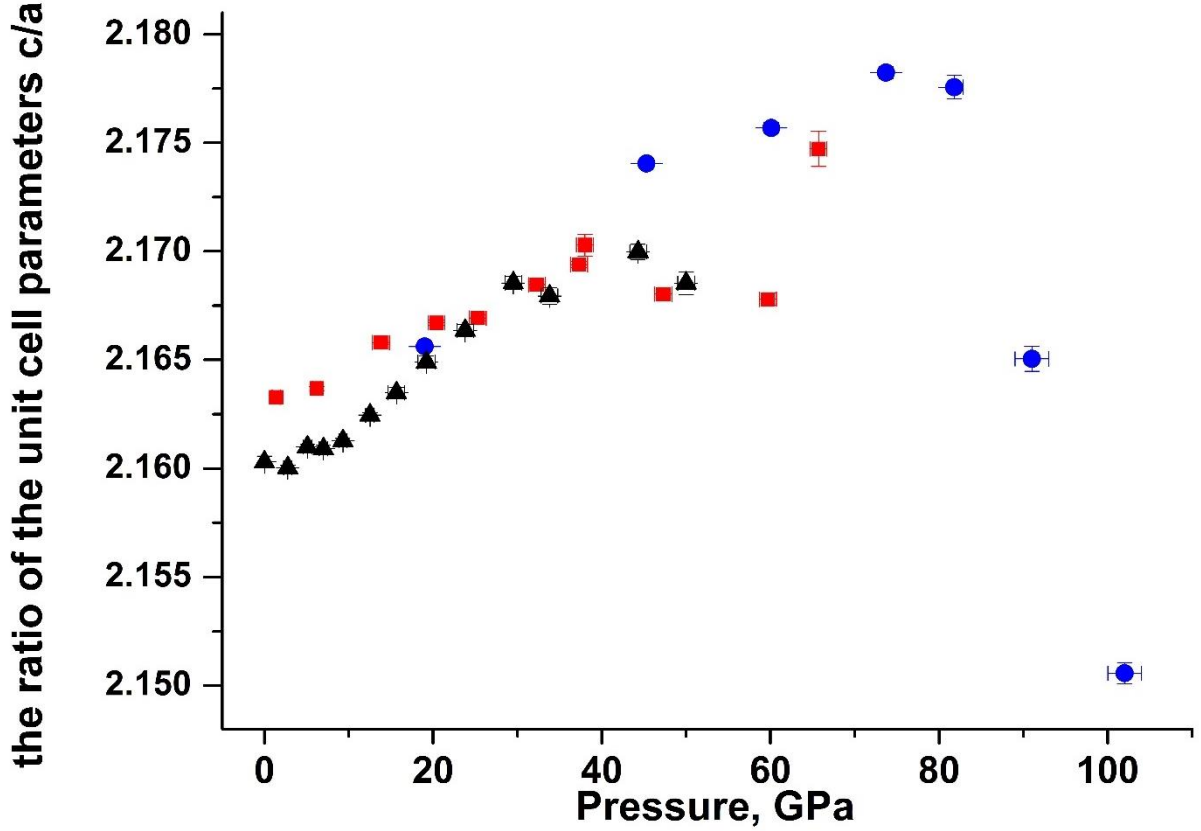
Figure IV.3-4. The ratio of unit cell parameters of β-B single crystal based on high-pressure single-crystal XRD data. Red squares are attributed to the data from run 1, blue circles represent the data from run 2, black triangles show the data from run 3.

The whole pressure-volume (P-V) dataset was used to fit the experimental data with the third-order Birch-Murnaghan (3BM) equation of state that gave the following results: $V_0 = 2511.1(5)$ Å^3, $K_{300} = 183(3)$ GPa and K´ = 3.4(1) (V_0 is the zero pressure unit cell volume, K_{300} is the bulk modulus, and K´ is its first derivative) (Table IV.3-1). The fit with fixed K´ = 4 resulted in the bulk modulus $K_{300} = 169(1)$ GPa, being lower than that with the free K´. The compressibility of β-B was reported in literature based on experimental measurements [67-69] and theoretical calculations [17,86,87] (Table IV.3-1). In all previous experimental studies unit cell volume was reported significantly lower in value (~5%) than found in our study as seen from Figure IV.3-5. Sanz and co-authors [69] obtained the P-V data from single-crystal XRD up to 100 GPa [69], their fit with the Vinet EoS gave $K_{300} = 210(6)$ GPa and K´ = 2.23 that is, within the uncertainties, very close to our result (K = 206(2) GPa with the K´ = 2.23). However, it might happen by chance: limited datasets and use of EDX SC XRD may lead to systematic errors in refinement of the lattice parameters and with the pressure increase the behavior of the EoS becomes non-physical. Despite all these experimental differences, the dependence of the normalized unit cell volume on pressure in our study is very close to [69] (Figure IV.3-6). However, we haven't observed the reported amorphization at 100 GPa [69].
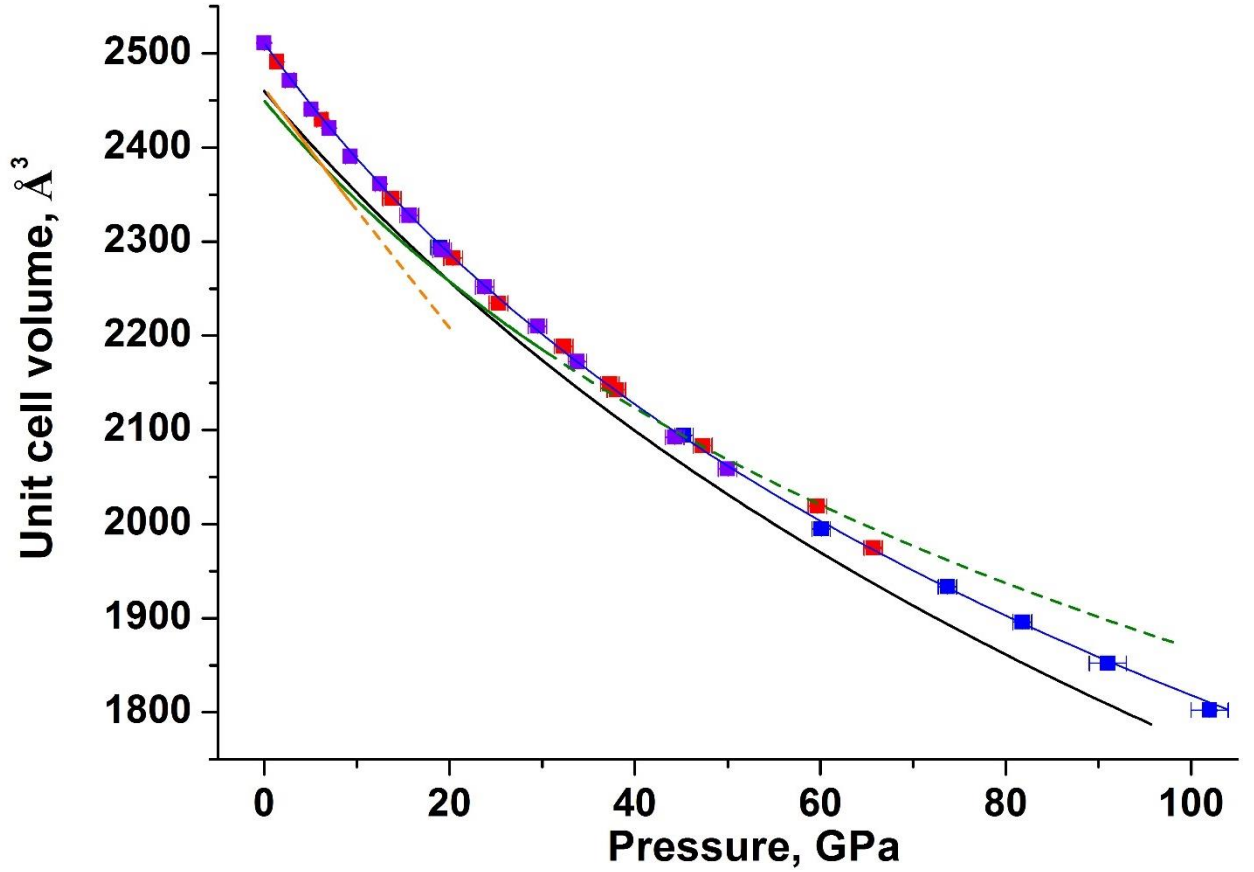
Figure IV.3-5. The pressure dependence of the unit cell volumes of β-B single crystals based on high-pressure single-crystal XRD data from three different runs (violet, blue and red squares). The connecting solid blue curve corresponds to the third-order Birch-Murnaghan equation of state of β-B up to 100 GPa ($V_0 = 2511.1(5)$ Å^3, $K_{300} = 183(3)$ GPa, $K' = 3.4(1)$). Continuous lines are attributed to the literature data. Black curve shows the fit of the pressure-volume data with the Vinet equation of state by [69]. Green line represents the fit of the data with the third-order Birch-Murnaghan equation of state by [68]. Dashed green curve is its extrapolation to 100 GPa. The orange curve corresponds to the linear fit of pressure-volume data by [67]. Its extrapolation to 100 GPa is shown by a dashed curve.

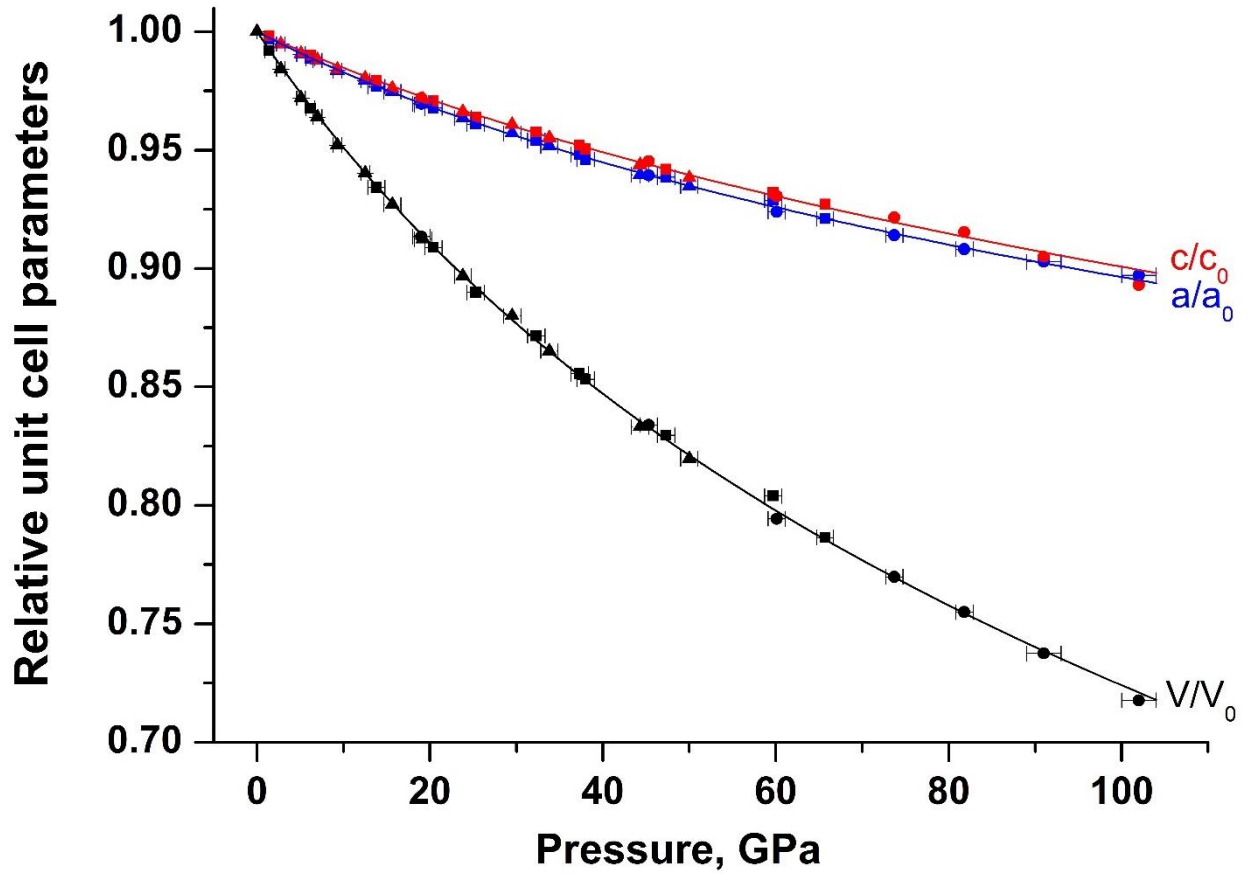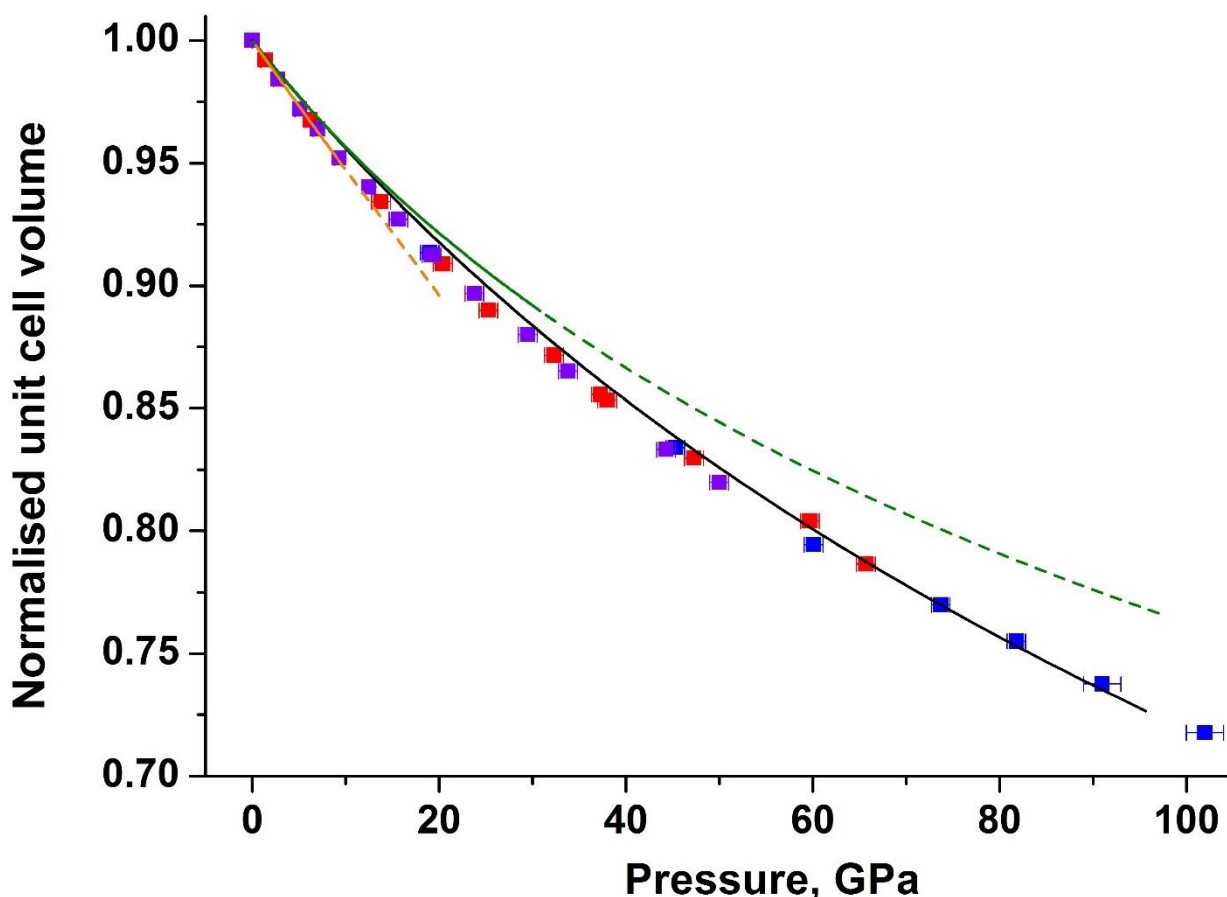**Figure IV.3-6.** Pressure-dependent evolution of normalised unit cell volume of β-B single crystals based on high-pressure single-crystal XRD data from three different runs (violet, blue and red squares). Continuous lines are attributed to the literature data. Black curve shows the fit of the pressure-volume data with the Vinet equation of state by [69]. Green line represents the fit of the data with the third-order Birch-Murnaghan equation of state by [68]. Dashed green curve is its extrapolation to 100 GPa. The orange curve corresponds to the linear fit of pressure-volume data by [67]. Its extrapolation to 100 GPa is shown by a dashed curve.

Nelmes et al. [67] made measurements of the bulk modulus of β-B on powder samples using neutron powder diffraction and NaCl as a PTM. Although they covered extremely small pressure interval (only up to 10 GPa), a simple linear fit of their five experimental points resulted in the value of the bulk modulus ($K_{300} = 185(7)$ GPa) numerically equal to the one we obtained with the P-V data up to 102 GPa and free K´. However, extrapolation of their fit to higher pressure (20 GPa) show that their structure was too soft compared to later experimental studies (Figures IV.3-5 and IV.3-6).

Powder XRD data of Ma et al. [68] was performed on polycrystalline β-B sample with 4:1 methanol-ethanol mixture as a PTM up to 31 GPa. The fitted value of bulk modulus is in good agreement within the uncertainties ($K_{300} = 205(16)$ GPa, K´ =4.3) with present study. The obtained values of EoS parameters make a too stiff structure in the 100 GPa range (Figures IV.3-5 and IV.3-6).

Theoretical calculations are mostly performed for α-B owing to its simplicity. Most of ab initio calculations on β-B assume perfect symmetry of $R\bar{3}m$ [17] and fully occupied structure [86,87]. The simplification leads to slightly higher values of the compressibility of the structure (K_{300} = 200-220 GPa).

Compressibility of lattice parameter a in our study differs from those previously reported in the literature [67-69] (Figure IV.3-7). The value at ambient conditions found in the present study is significantly higher (~5%) than in all previous experimental studies. In [68] in the range of 0 to 30 GPa a is less compressible than in the present work. At the same time, despite the small pressure range, in [67] the compressibility is similar to the one reported in [69]. The behavior of lattice parameter a upon compression up to 100 GPa [69] is similar to the one found in present study with 5 % difference in values.
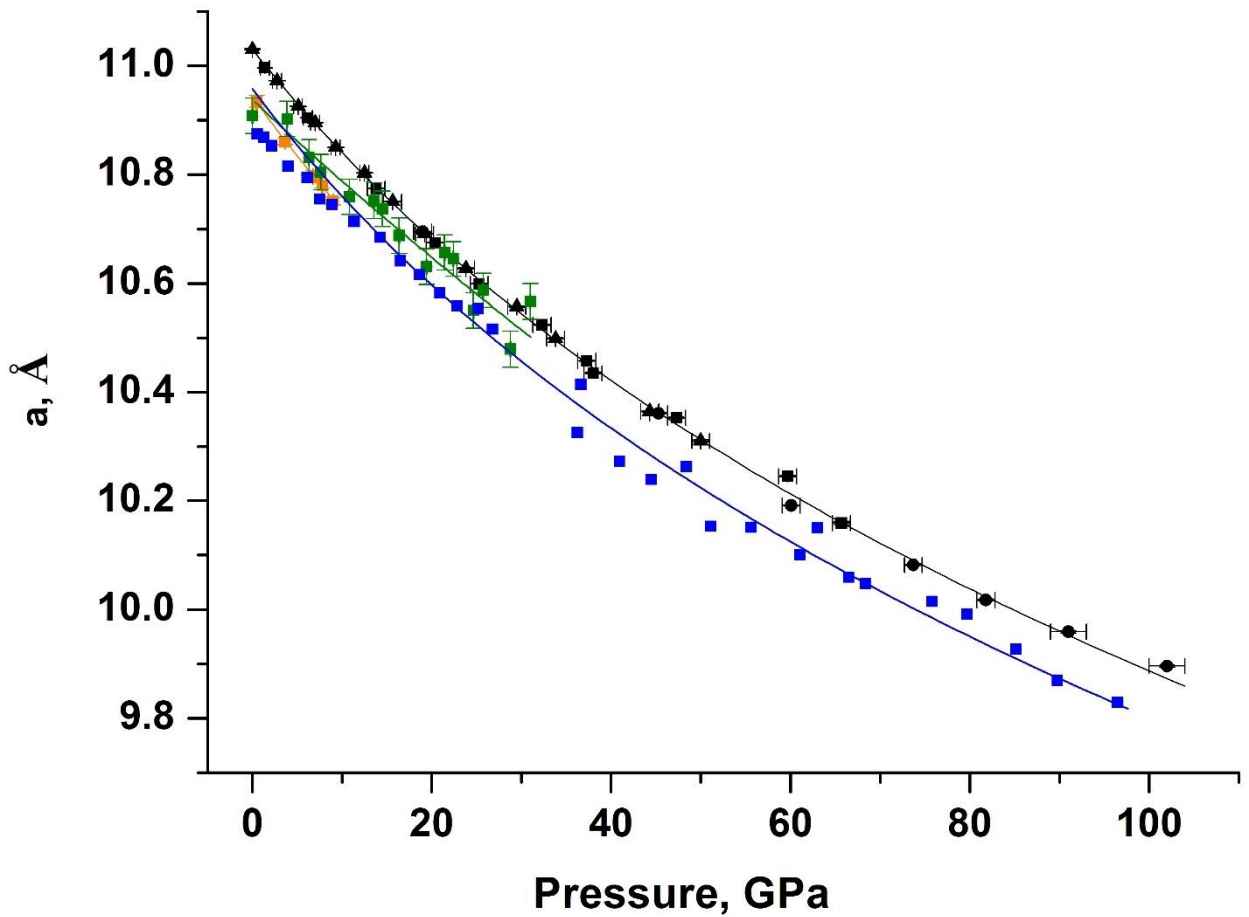
Figure IV.3-7. Pressure-dependent evolution of the lattice parameter a of β-B single crystals based on high-pressure single-crystal XRD data (black squares, circles and triangles represent different runs) and compared with data by [67] (orange), by [69] (blue) and by [68] (green). Continuous lines show fit of the pressure-lattice parameter data with equations of state: for present work (black), for [68] (green) the third-order Birch-Murnaghan was used. In [69] (blue) the used fit was Murnaghan, and in [67] (orange) linear.

Lattice parameter c in all reported data is very close to the one obtained in our study at ambient pressure and smoothly decrease upon compression (Figure IV.3-8). In the range of 0 to

30 GPa [68] observed nonlinear behavior of *c* maybe due to significant reported values of error margins. In the range of 0 to 10 GPa the behavior of *c* reported by [67] is similar to the one obtained in present study. Study of 100 GPa pressure range by [69] showed good agreement between the results. However, the *c* parameter is slightly stiffer in our study.
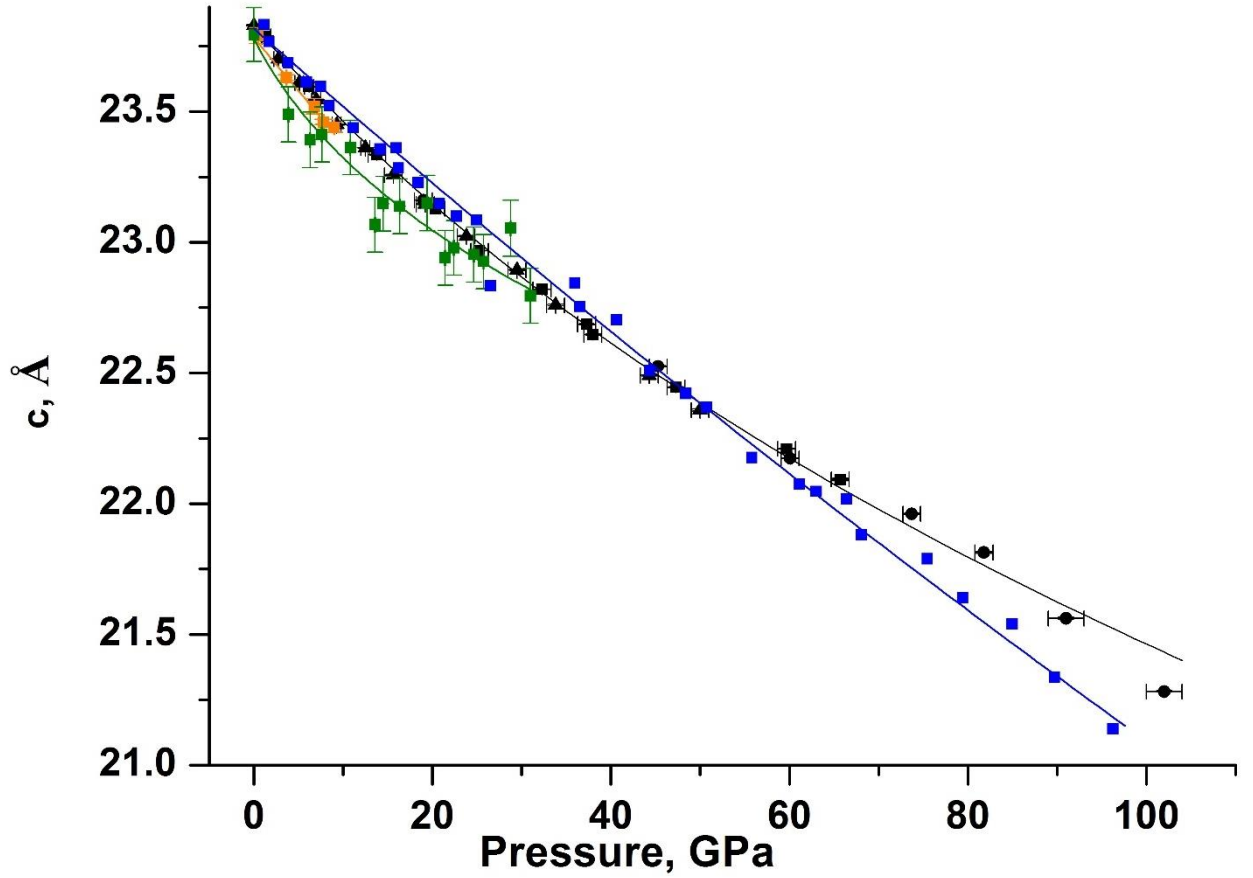
Figure IV.3-8. Pressure-dependent evolution of the lattice parameter *c* of β-B single crystals based on high-pressure single-crystal XRD data (black squares, circles and triangles represent different runs) and compared with data by [67] (orange), by [69] (blue) and by [68] (green). Continuous lines show fit of the pressure-lattice parameter data with equations of state: for present work (black), for [68] (green) the third-order Birch-Murnaghan was used. In [69] (blue) the used fit was Murnaghan, and in [67] (orange) linear.

The comparison of the ratio of lattice parameters *c/a* with literature data is shown in Figure IV.3-9. In [67] reported five pressure points show linear behavior of *c/a* upon compression. The values obtained by [68] show significant nonlinearity and are not consistent with our study, for which *c/a* increases linearly upon compression up to ~80 GPa. The difference might be due to the fact that the random error is higher than the real integration error so reliability of the data might be questionable. In the only single crystal study [69] the values of lattice parameters were reported without any error bars. Up to 40 GPa the ratio of the lattice parameters *c/a* doesn't change however, after 40 GPa a clear bend appears in the (*c/a vs* P) line. However, they don't report any phase transitions up to 97 GPa.
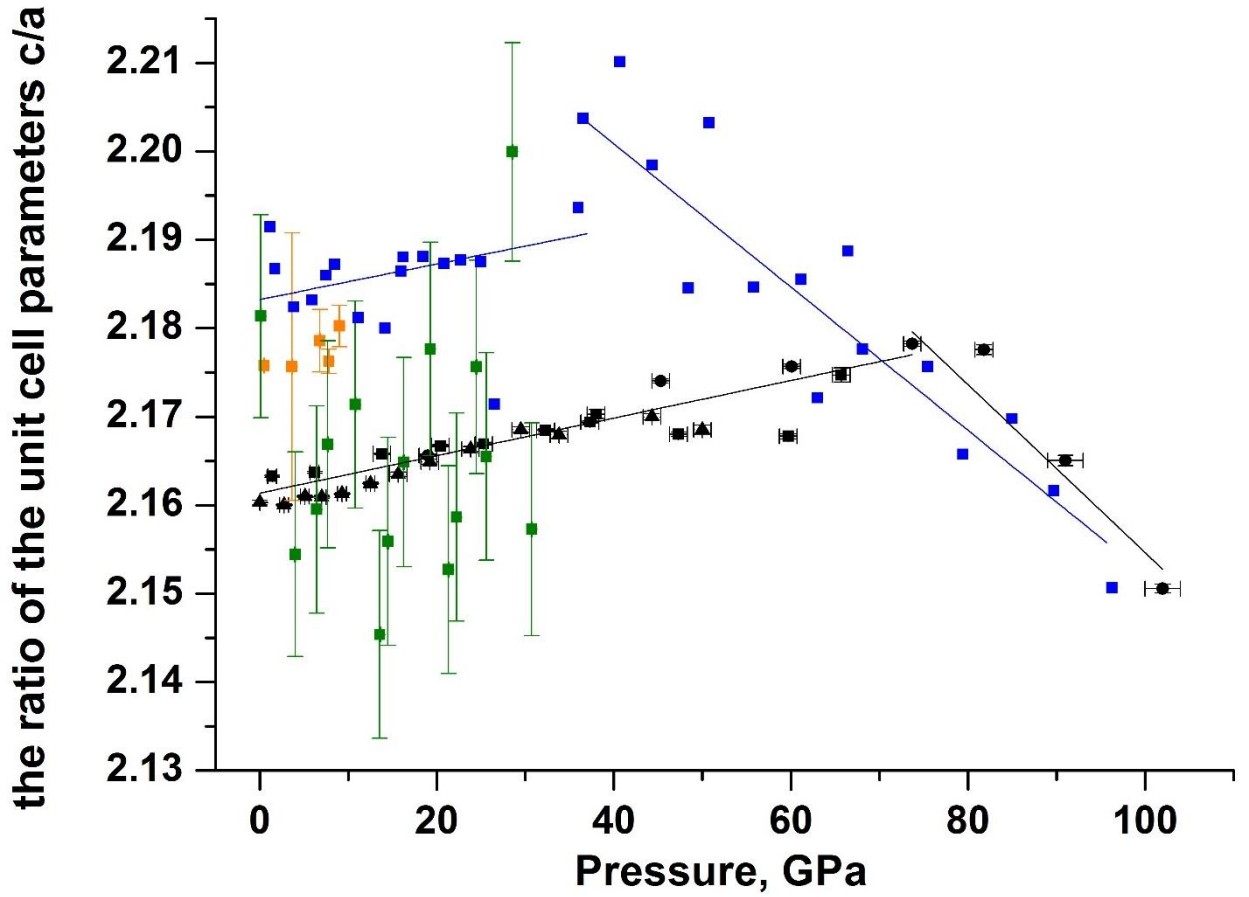
Figure IV.3-9. The ratio of unit cell parameters of β-B single crystal based on high-pressure single-crystal XRD data. Black squares, circles and triangles represent different runs of the present work. Black solid lines are a guide for eyes. Orange scatters represent data by [67]. Green scatters show the data from [68]. Blue scatters are from [69].

IV.3.5. Conclusions

In the present work, we have investigated the behavior of β-B under pressure using high-purity single crystals synthesized by the high-pressure high-temperature multi-anvil and toroidal press techniques. The unit cell parameters of β-B were extracted from the single-crystal XRD datasets at each pressure point in a diamond anvil cell. The accurate equation of state was determined in three different experiments up to 102 GPa. The bulk modulus of β-B was found to be $K_{300} = 183(3)$ GPa. Unlike the previous experimental observations, our single-crystal X-ray diffraction data for β-B give no evidence of phase transitions or amorphization up to 102 GPa.

IV.3.6. Acknowledgements

V.4. First non-icosahedral boron allotrope synthesized at high pressure and high temperature

Irina Chuvashova[a,b*], Elena Bykova[b], Maxim Bykov[b], Vitali Prakapenka[c], Konstantin Glazyrin[d], Mohamed Mezouar[e], Leonid Dubrovinsky[b], Natalia Dubrovinskaia[a]

[a] *Material Physics and Technology at Extreme Conditions, Laboratory of Crystallography, University of Bayreuth, D-95440 Bayreuth, Germany*
[b] *Bayerisches Geoinstitut, University of Bayreuth, D-95440 Bayreuth, Germany*
[c] *Center for Advanced Radiation Sources, University of Chicago, 9700 South Cass Avenue, Argonne, IL 60437, USA*
[d] *Photon Science, Deutsches Elektronen-Synchrotron, Notkestrasse 85, D-22607 Hamburg, Germany*
[e] *European Synchrotron Radiation Facility, BP 220 F-38043 Grenoble Cedex, France*

Correspondence to: irina.chuvashova@gmail.com

IV.4.1. Abstract

Theoretical predictions of pressure-induced phase transformations often become long-standing enigmas because of limitations of contemporary available experimental possibilities. Hitherto the existence of a non-icosahedral boron allotrope has been one of them. Here we report on the first non-icosahedral boron allotrope, which we denoted as ζ-B, with the orthorhombic α-Ga-type structure (space group *Cmce*) synthesized in a diamond anvil cell at extreme high-pressure high-temperature conditions (115 GPa and 2100 K). The structure of ζ-B was solved using single-crystal synchrotron X-ray diffraction and its compressional behavior was studied in the range of very high pressures (115 GPa to 135 GPa). Experimental validation of theoretical predictions reveals the degree of our up-to-date comprehension of condensed matter and promotes further development of the solid state physics and chemistry.

IV.4.2. Introduction

Boron has been widely studied due to its complex polymorphism (see the review article [15] and references therein). All five of the hitherto experimentally established boron allotropes (α-B, β-B, γ-B, δ-B, and ε-B) [15,16,29,35,67,72] belong to the family of icosahedral solids: there structures are based on various arrangements of B_{12} icosahedra, since three valence electrons of boron atoms are insufficient to form a simple covalent structure. However, van Schnering and

Nesper [96] suggested the α-Ga structure to be an alternative to the boron structure. According to these authors, the α-Ga structure built up from open polyhedral fragments is strongly related to the closed polyhedral boron clusters B_n. Their extended Hückel calculations supported the α-Ga model and showed that the α-Ga structure is an appropriate covalent three-electron arrangement and is not electron-deficient [96].

The pressure-temperature (PT) experimental phase diagram of boron is currently limited to 20 GPa and 3500 K [14,16,49,68-70,84], but there are a number of theoretical predictions concerning the behavior of boron at higher pressures and temperatures [73,76,77,92-95,97]. Häusserman et al. (2003) [97] predicted the phase transition from α-B to α-Ga-structured phase, accompanied by a nonmetal-metal transition at 74 GPa. The authors [97] used *ab initio* calculations employing pseudopotentials and a plane wave basis set in the framework of the density functional theory (DFT). The α-Ga-structured boron phase was suggested to be stable up to 790 GPa; beyond this pressure a transition to the *fcc* structure had to take place according to [97]. In parallel, Segal and Arias (2003) [98] performed calculations using a method based on perturbation theory and all-electron calculations with plane-wave-basis in DFT. The α-Ga-structured boron was shown to be favorable in energy among other boron phases in the interval between 71 GPa and 500 GPa. Note that at that time γ-B was not discovered yet. Later, a comparison of the stability of γ-B with respect to the α-Ga-type boron phase led to consequent shift of their phase boundary from 78 GPa, as calculated in [76], to 89 GPa [73], and 93 GPa [77]. Calculations predict α-Ga-structured boron to be an incompressible (K_{300} = 263 GPa) [94], superconducting material with strong anisotropy [99] due to its layered crystal structure [98,99]. Electric resistivity measurements [14] showed that compression of β-B leads to metallization of the material under investigation at pressures above 160 GPa and ambient temperature, and to formation of a superconducting phase above 175 GPa and 6 K [14]. The structure of metallic superconducting boron is unknown.

Although the idea of possible existence of boron with the α-Ga structure is already more than 25 years old [96], it has remained difficult to prove. First, very high pressures are required for its synthesis, as predicted by [97]; second, boron is a weak X-ray scatterer that means that HPHT experiments are not straight forward and have to be done on a synchrotron; and third, a precursor material has to be of a very high purity, what is not always easy to reach with the highly reactive boron.

The logic of our experimental approach, aimed at overcoming the challenges listed above, is as follows. As a precursor material, we used single crystals of β-B from the same synthesis batch as those which were fully characterized in our previous work [16]. The crystals were proven to be

of high quality and high purity. To assure that we can follow the known β-B to γ-B transition at moderate pressures [72], we conducted first a few synchrotron XRD experiments below one Mbar to see if our results are in accordance with our own previous observations and available literature data. Further experiments at higher pressures, up to above one Mbar, aimed at investigating the HP behavior of β-B to track possible phase transitions at room temperature (Eremets et al. [14] reported a visible step in the resistance of β-B at 110 GPa) and upon heating.

Here, we report a new boron allotrope (ζ-B) with the α-Ga-type structure synthesized from β-B at pressures over 115 GPa and temperatures over 2100 K using a laser heated diamond anvil cell (DAC). Its crystal structure was determined based on single-crystal synchrotron X-ray diffraction (XRD) data. The behavior of ζ-B under compression from 115 GPa to 135 GPa was characterized using powder synchrotron XRD.

IV.4.3. Experimental

IV.4.3.A. Synthesis of a precursor material.

Single crystals of β-B studied in the present work at high pressures and high temperatures were synthesized using the high-pressure high-temperature technique described in detail in [16]. Their structure and purity were carefully characterized to assure the reliability of the obtained experimental results. The presence of impurities could be excluded.

IV.4.3.B. Diamond-anvil cell experiments.

The BX90-type diamond anvil cells (DAC) [145] made at Bayerisches Geoinstitut (Bayreuth, Germany) and Boehler-Almax type [146] beveled diamonds with the culet diameters of 120 μm were used in high pressure experiments. Rhenium gaskets were squeezed between the anvils to make an indentation with the thickness of about 20 μm. Then in the center of the indentations, round holes of about 60 μm in diameter were drilled. Two β-B crystals were placed into these chambers. Sizes of the crystals were about $10 \times 10 \times 15$ μm^3 and orientation of the crystals was not specified. Neon was used as a pressure transmitting medium (PTM) and as pressure standard [195].

IV.4.3.C. Single crystal synchrotron X-ray diffraction.

Single crystals of β-B in a DAC were studied on ID27 at the European Synchrotron Radiation Facility (ESRF) and on P02.2 at PETRA III, DESY [196].

At ID27 diffraction data were collected at 293 K using the Perkin Elmer XRD1621 flat panel detector. The monochromatic radiation had the wavelength of 0.37380 Å and the crystal-to-detector distance was 383 mm. Pressure in the cells was increased stepwise up to about 115 GPa, and single-crystal diffraction data for β-B were collected at each pressure point. 160 frames in the omega scanning range of −40° to +40° (in 0.5° steps) were recorded with an exposure time of 2 s. A portable double-sided laser heating system [154] was used to heat β-B crystals under pressure in experiments at ID27 (ESRF). Upon heating entire crystals were located in the laser beam and there were no measurable temperature gradients within the samples. The temperature variation during heating did not exceed ±100 K.

At P02.2 diffraction data were collected at 293 K using the Perkin Elmer XRD1621 detector. The monochromatic radiation had the wavelength of 0.29464 Å and the crystal-to-detector distance was 439 mm. Data were collected at one pressure point at about 115 GPa on the sample

laser heated at ID27. 152 frames in the omega scanning range of $-38°$ to $+38°$ were collected (in 0.5° steps) with an exposure time of 10 s per frame.

Integration of the reflection intensities and absorption corrections were performed using CrysAlisPro software [164,165]. The structure of γ-B was refined in the anisotropic approximation for all atoms by full matrix least-squares Due to small amount of the observed data the structure of ζ-B was refined in isotropic approximation. Refinements of the crystal structures were performed using SHELXL software [166] implemented in the WinGX software package [165]. The crystallographic data of ζ-B studied at 115 GPa have been deposited in the Inorganic Crystal Structure Database [39]. The data may be obtained free of charge from Fachinformationszentrum Karlsruhe, 76344 Eggenstein-Leopoldshafen, Germany (Fax: +49 7247 808 666; e-mail: crysdata@fiz-karlsruhe.de, http://www.fiz-karlsruhe.de/request_for_deposited_data.html) on quoting following CSD deposition number: 432572.

IV.4.3.D. Powder XRD measurements.

Samples of ζ-B were studied at room temperature in angle-dispersive mode with a wavelength of 0.2952 Å at the 13-IDD beamline at APS, Argonne. Pressure in the cells was increased from 115 to 135 GPa with a step of about 2 GPa. Diffraction images were collected at each pressure using a MAR CCD detector in the omega scanning range of $-20°$ to $+20°$ with an exposure time of 40 s. The images were integrated using the DIOPTAS software [161] and the resulting diffraction patterns were processed using biased model in the EXPGUI software [162] in the GSAS Software package [163].

IV.4.4. Results and discussion

In two independent DAC experiments at ID27 at ESRF single crystals of β-B were compressed up to 38(1) and 50(1) GPa, respectively. At these pressures the observed diffraction patterns perfectly match that of β-B (details of the HP structural studies of β-B will be published elsewhere). The lattice parameters and the molar volume of β-B corresponding to these two pressures are in agreement with the literature data of Sanz et al. [69], who measured the lattice parameters of β-B up to 100 GPa. Figure IV.4-1 shows the pressure dependence of the relative unit cell volume of β-B, as experimentally determined in [69] (black curve), and our two experimental points (black squares), which appear very close to the curve. After compression and the XRD measurements, the both crystals of β-B were double-side laser heated to about 2000 K. After the heating the pressure in the both DACs (determined using the equation of state of neon) increased and became 42(1) GPa in the first DAC and 58(1) GPa in the second one. In accordance with the experimental PT phase diagram of boron [16], a transition of β-B to γ-B took place, and diffraction spots of γ-B were clearly observed in the diffraction pattern taken at room temperature (RT) after heating at 42 and 58 GPa. The quality of the HP single-crystal X-ray diffraction data was sufficient to refine both the lattice parameters and atomic coordinates of γ-B (details of the refinement of the structure of γ-B at 58(1) GPa are presented in Supplementary Table IV.4-S1). The structure of γ-B is orthorhombic (space group *Pnnm*) and built of covalently bonded B_{12} icosahedra and B_2 dumbbells [71].

To compare the compressional behavior of various boron allotropes and to plot the P-V data on the same graph (Figure IV.4-1), the relative unit cell volumes for all considered allotropes were normalized to the unit cell volume of β-B per atom (320 atoms in β-B were accepted following [69]). The blue curve in Figure 1 corresponds to the experimental data for γ-B from [72].Two experimental points obtained in the present study are shown by blue diamonds and lie on this curve.
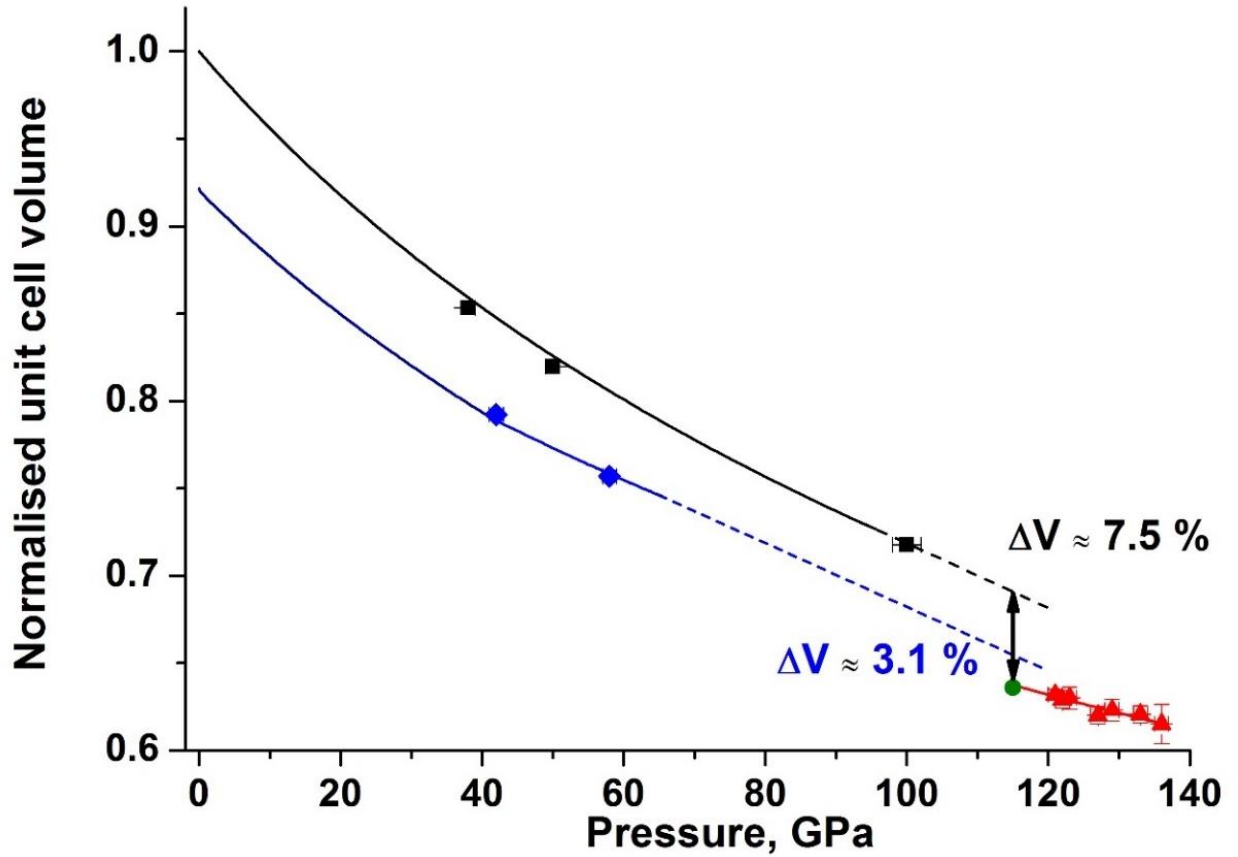
Figure IV.4-1. The pressure dependence of the normalized relative unit cell volumes of three boron allotropes, β-B, γ-B and ζ-B. The volumes were normalized on the volume of β-B per atom calculated from the experimental data of Sanz et al. [69]. The solid black curve corresponds to the Vinet equation of state of β-B up to 100 GPa from [69] (V_0 = 2460 Å^3, K_{300} = 210(6) GPa, K´ = 2.23). Dashed black curve is its extrapolation to 120 GPa. Black squares represent our experimental data points for β-B (see text). The green circle represents the volume data for ζ-B obtained from our single-crystal XRD at 115 GPa (after laser heating of β-B at this pressure a phase transition occurred, accompanied with the volume reduction by ca.7.5 %). The red triangles correspond to the PV data of ζ-B obtained from powder XRD. Their fit with the 2BM EoS is shown by the red solid curve. The blue curve corresponds to the 3BM EoS of γ-B according to [79] (below 40 GPa: V_0=198.1(3) Å^3, K_{300}=227(3) GPa, K'=2.5(2)); above 45 GPa: V_0=192.6(3) Å^3, K_{300}=281(6) GPa, K'=2.8(9)). Its extrapolation to 120 GPa is shown by a dashed blue curve. Blue diamonds show our two experimental points (see text). The volume difference between γ-B and ζ-B at 115 GPa is ca. 3.1 %.

In order to study the behavior of boron in a megabar pressure range, on ID27 at ESRF single crystals of β-B were first compressed up to 100(2) GPa. At this pressure at room temperature, all observed reflections were attributed to β-B. This point (the black square in Figure IV.4-1 corresponding to 100 GPa) fits well to the curve of Sanz et al. [69] extrapolated to 115 GPa (dashed black curve). After double-sided laser-heating up to 2100(100) K using portable laser heating set up, pressure increased to 115(2) GPa. The material in the heated spot changed its color from dark-reddish to black (not reflecting). The X-ray diffraction pattern changed dramatically and had to be treated as of a powder sample. Apart from reflections of Re (gasket material) and Ne (used as PTM), several new relatively weak but clearly detectable reflections were observed.

Their d-spacings perfectly matched those expected for α-Ga-type structured boron, as predicted by Häusserman et al. [97]. The following orthorhombic lattice parameters were obtained at 115 GPa: $a = 2.7159(11)$ Å, $b = 4.8399(2)$ Å, $c = 2.9565(6)$ Å.

The DAC with the sample described above was transported to the P02.2 beamline at PETRA III, where combination of a small size of the X-ray beam and its short wavelength increases chances for accumulating diffraction data suitable for single-crystal structural analysis. Detailed inspection of the diffraction pattern obtained on this beamline from the heated spot at 115 GPa (Supplementary Figure IV.4-S1) revealed individual single crystal reflections related to the high-pressure high-temperature boron phase. Its structure was solved; some experimental details and crystallographic data are given in Supplementary Table IV.4-S1. The structure belongs to the α-Ga structure type; it has the *Cmce* space group and 8 atoms per unit cell. The unit cell parameters determined from the single-crystal data ($a = 2.7039(10)$ Å, $b = 4.8703(32)$ Å, $c = 2.9697(6)$ Å) are slightly different from those obtained from powder XRD at ID27, as they were determined using different sets of reflections, as well as different procedures of finding peaks positions, weight schemes in least square optimizations, etc. The new high-pressure boron allotrope with the α-Ga-type structure was denoted as ζ-B, sequentially after the fifth hitherto established boron allotrope, ε-B [29].

The structure of ζ-B at 115(2) GPa is presented in Figure IV.4-2. It may be described as a stacking along the (010) direction of distorted and corrugated hexagonal nets (Figure IV.4-2A) with the 3^6 topology, in accordance with the descriptions of van Schnering et al. [96,197] and Häusserman et al. [96,197]. Within each net each B atom connects to six neighbors, and the B-B bond lengths are 1.66(1) Å, 1.72(1) Å, and 1.75(1) Å (notated in Figures IV.4-2). The bonds between the nets bring the seventh neighbor to the coordination sphere of each boron atom (Figure IV.4-2B). These B-B bonds appear to be the shortest (1.59(1) Å) in the structure of ζ-B. Thus, despite seemingly 'layered' appearance, the ζ-B structure is in fact a 3D network. Puckered fragments of the nets can be considered as open polyhedral fragments related to the closed icosahedral boron clusters.
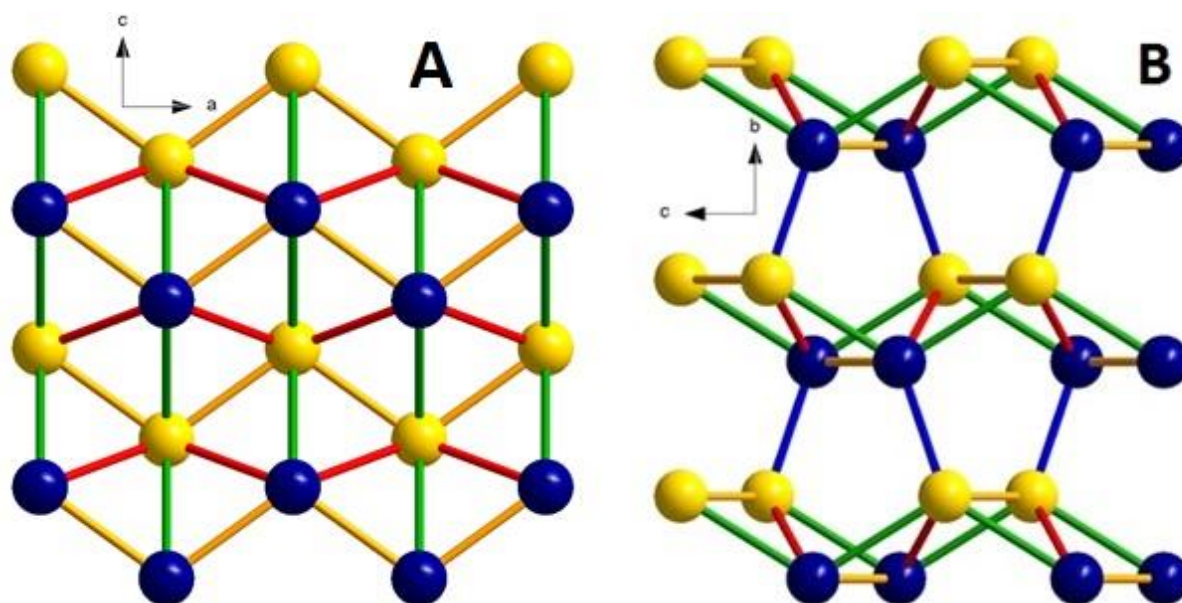
Figure IV.4-2. The structure of ζ –B. **A.** The projection of a fragment of one distorted and corrugated hexagonal net on the *ac* plane. Such nets are stacked along the (010) direction. Blue and yellow atoms do not lie in the same plain (blue atoms are lower and yellow ones are upper if seen along the (010) direction). Bonds with different lengths are shown in different colors: 1.66(1) Å (orange), 1.72(1) Å (red), and 1.75(1) Å (green). **B.** The projection of three nets on the *bc* plain. The lengths of bonds connecting the layers (blue) all are 1.59(1) Å.

As mentioned above, in ζ-B each boron atom has a coordination number (CN) equal to 7. In α-B a half of boron atoms have CN=6, and a half CN=7 [172], and in γ-B out of 28 atoms in the unit cell eight atoms have CN=6, and other twenty atoms have CN=7 [79]. For a complex and still controversial structure of β-B a simple count is not possible, but anyhow most of the boron atoms in this phase have CN=6. Thus, comparing the structures of the boron allotropes, we observe a tendency to a rise of the CN of boron for high-pressure polymorphs. This agrees with the empiric rule that upon pressure-induced phase transition coordination number increases [198]. As expected [199], an average interatomic distance in the first coordination sphere is the longest for ζ-B (1.68 Å) in comparison with corresponding values for α-B (1.59 Å) [172], and γ-B (1.66 Å) [79] at 115 GPa.

A phase transition of β-B to ζ-B manifested in a drastic reduction of the molar volume: at 115 GPa the molar volume of ζ-B is by ~7.5 % less than that of β-B. According to theoretical calculations [73,76,94] and our previous [16] and current experimental observations (up to about 60 GPa), γ-B is more stable at high pressures than β-B. If we compare the difference in the molar volume between γ-B and ζ-B at 115 GPa, it is only about 3.1% (see Figure IV.4-1, where the pressure dependence of the normalized volume of γ-B taken from [72] was plotted for the comparison).

It is worth mentioning here that we pressurized single crystals of β-B beyond the pressure (110 GPa), at which Eremets et al. [14] observed a kink in the room-temperature *R(P)* (resistance *vs* pressure) curve. The authors [14] suggested the possibility that the transition of β-B to the metallic state occurs at 130 GPa. Häusserman et al. [97] proposed the α-Ga structure as a structural model for a metallic high-pressure modification of B after a phase transition of either semiconducting icosahedral α-B or β-B. We did not observe any transformations in β-B up to 115 GPa, and the transition to the α-Ga-structured phase required heating to very high temperatures. Thus, it is very improbable that ζ-B with the α-Ga structure may be associated with the metallic high-pressure modification of boron discussed in [14,97].

Further compression of the material synthesized at 115(2) GPa leads to decrease of the quality of single-crystal reflections. For this reason, the diffraction data of ζ-B obtained up to 135 GPa on 13-IDD at the APS were integrated to 1D ´2-theta´ scans. An example of a diffraction pattern at 121(2) GPa is presented in Figure 3. The unit cell parameters decreased with pressure. The linear compressibility along the *a* and *c* axes was found to be ~$7(3)*10^{-4}$GPa^{-1}, and along the *b* axis - a bit lower, ~$4(3)*10^{-4}$ GPa^{-1} that can be explained by the shortest B-B bonds in the (010) direction. The PV data set of ζ-B in the pressure range of 115 to 135 GPa was fitted using the second-order Birch-Murnaghan (2BM) equation of state (EoS) and gave the following EoS parameters: $V_{115} = 39.20(8)$ Å^3 and $K_{115} = 575(65)$ GPa; K´= 4 (fixed); V_{115} is the unit cell volume and K_{115} is the bulk modulus at 115 GPa and room temperature; K´ is the pressure derivative of the bulk modulus) (Table IV.4-1). Use of the Vinet EoS led to the following parameters: $V_{115} = 39.19(8)$ Å^3 and $K_{115} = 577(65)$ GPa; K´= 4 (fixed).
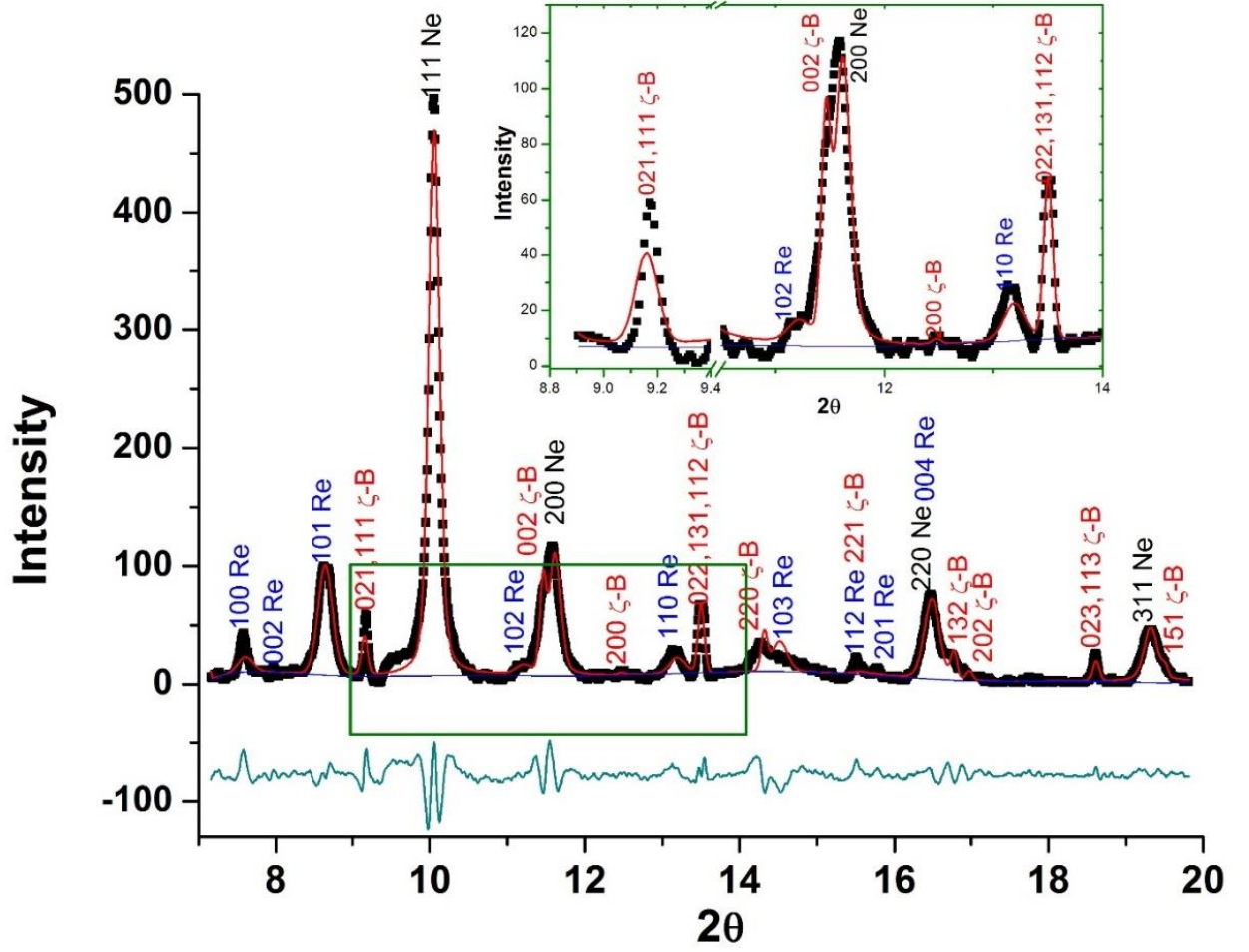
Figure IV.4-3. X-ray diffraction pattern of ζ-B obtained at 121(2) GPa. Black dots represent experimental data. Red solid line derives the refinement using biased model, blue solid line states for calculations of background). Green curve is the intensity difference ($I_{obs} - I_{calc}$) between experimental data and calculations. Reduced $\chi^2 = 1.953$. The reflections are assigned to Re, Ne, and ζ-B; their *hkl* are designated in different colors for clarity.

Table IV.4-1. Parameters of the equations of state of ζ-B compared to theoretical predictions. The EoSes are designated as follows: BM stays for the Birch-Murnaghan (3BM for the 3rd order, 2BM for the 2nd order), M for Murnaghan and V for Vinet.

ζ-B	EoS	V_{115}, Å³	K_{115}, GPa	K´	Ref.
Experiment	V	39.19(8)	577(65)	4	*present study*
	2BM	39.20(8)	575(66)	4	
ab initio calculations	3BM	38.99(4)	626	3.6	[77]
	2BM	39.11(4)	674	4	[94]
	M	38.09(3)	640	3.26	[99]

The bulk moduli of α-Ga-structured boron at ambient conditions were calculated in [77,94,99]. To compare these predictions with our experimental results, we computed the theoretical values of the bulk moduli to be at 115 GPa according to these three papers (Table IV.4-1). The EoSFit-7c software [200] was used. As seen, experimental values of the bulk modulus are lower than the theoretically predicted ones. Supplementary Figure IV.4-S2 shows the pressure dependence of the unit cell volume of ζ-B, as experimentally determined in the present work and theoretically predicted [77,94,99]. There is a significant difference (about 4%) between the earlier [99] and recent [77,94] theoretical predictions. Our experimental results are in reasonable agreement with data of [77,94] (Supplementary Figure IV.4-S2).

IV.4.5. Conclusions

To verify theoretical predictions regarding the existence of α-Ga-structured boron and its behavior at high pressures [73,76,77,96,97], we have conducted a series of high-pressure high-temperature experiments. We demonstrated that the predicted boron allotrope [96,97] can be obtained by laser-heating of single crystals of β-B to over 2100 K at pressures above 115 GPa. This phase, which we call ζ-B, has the α-Ga-type orthorhombic structure as revealed by single-crystal X-ray diffraction. Measured precisely interatomic distances and linear compressibilities along the major crystallographic directions do not allow interpreting the structure as layered, as earlier proposed [99]. In the studied pressure range (from 115 to 132 GPa) ζ-B is less compressible than any other boron allotropes known so far. Based on our experimental data we do not see a relation between ζ-B and the metallic high-pressure modification of B discussed by [14,97].

IV.4.6. Acknowledgements

IV.4.7. Supplementary Materials

Supplementary Table IV.4-S1. Some experimental details and single crystal X-ray diffraction and structural refinement data of γ-B and ζ-B determined in the present work.

Parameter	γ-B	ζ-B
Pressure (GPa)	58(1)	115(2)
Empirical formula	B_{28}	B_8
Formula weight (g/mol)	302.7	86.48
Wavelength (Å)	0.3738	0.29464
Crystal system	Orthorhombic	Orthorhombic
Space group	*Pnnm*	*Cmce*
a (Å)	4.7521(16)	2.7039(10)
b (Å)	5.295(2)	4.8703(32)
c (Å)	6.4742(11)	2.9697(6)
V (Å^3)	162.92(9)	39.11(3)
Z	1	1
Calculated density (g/cm^3)	3.08546	3.6715
Crystal size (μm^3)	5 × 6 × 8	8 × 7 × 10
Theta range for data collection (deg)	1.6543 to 17.0036	4.57 to 15.73
Index range	-5 < h < 5 -5 < k < 6 -7 < l < 7	-3 < h < 4 -6 < k < 5 -4 < l < 4
Reflections collected	388	88
Independent reflections/R_{int}	177 / 0.0496	35 / 0.1499
Refinement method	Least squares on F^2	Least squares on F^2
Data / restraints / parameters	131 / 0 / 37	35 / 0 / 4
Goodness of fit on F^2	1.056	1.293
Final R indices [I>2σ(I)]	$R_1 = 0.0676$	$R_1 = 0.1368$
R indices (all data)	$R_1 = 0.0854$; $wR_2 = 0.1645$	$R_1 = 0.1783$; $wR_2 = 0.3106$
Largest diff. peak and hole (e/Å^3)	-0.52 and 0.43	-0.50 and 0.55
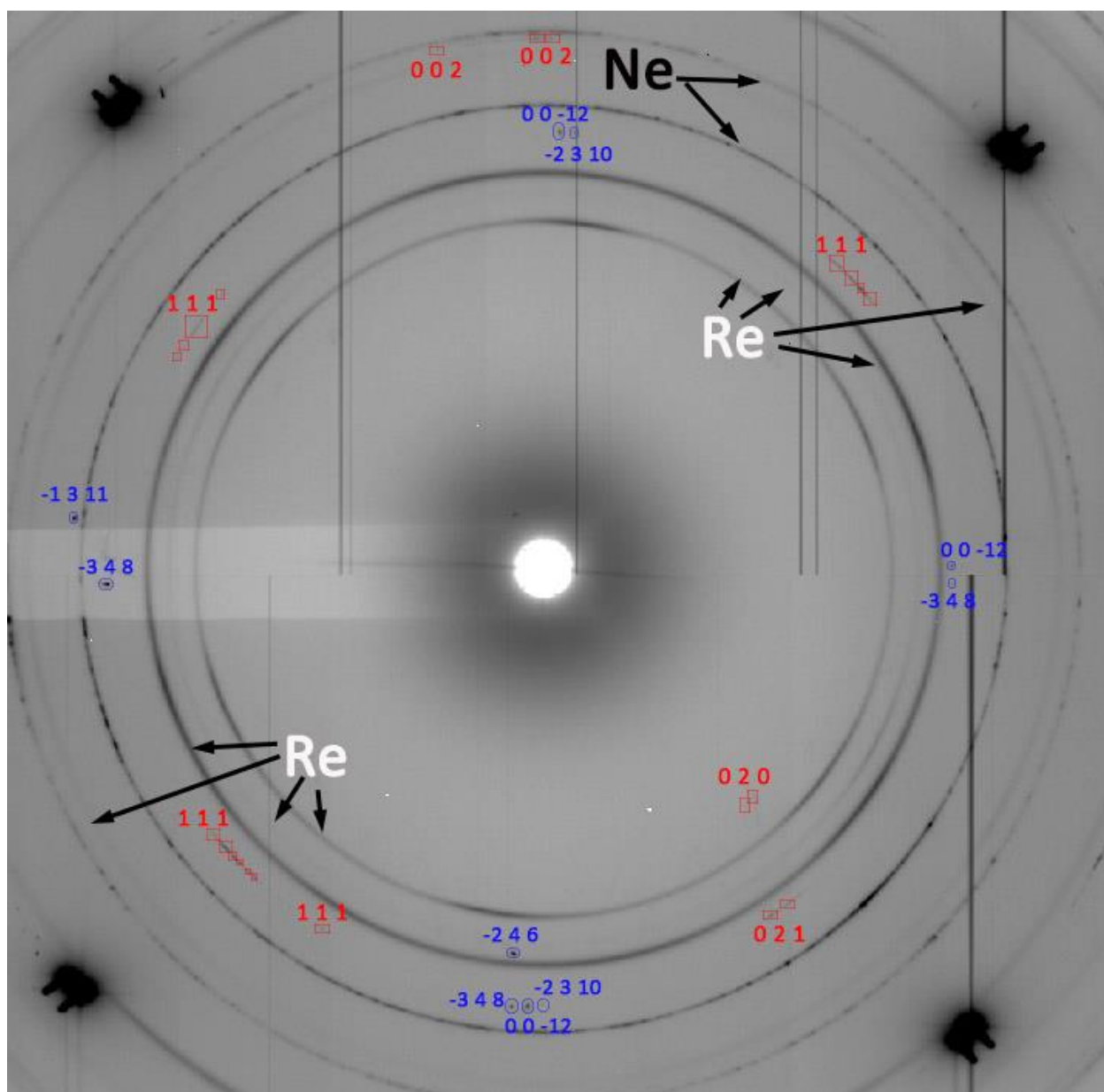
Supplementary Figure IV.4-S1. The 2D wide-scan X-ray diffraction image of ζ-B obtained at 115(2) GPa collected at P02.2 DESY and given as an example. Diffraction lines assigned to Re and Ne are pointed out by arrows. Blue circles mark the reflections related to untransformed β-B, red squares mark the reflections related to ζ-B. Black oversaturated reflections in the corners of the image are from the diamond anvils.
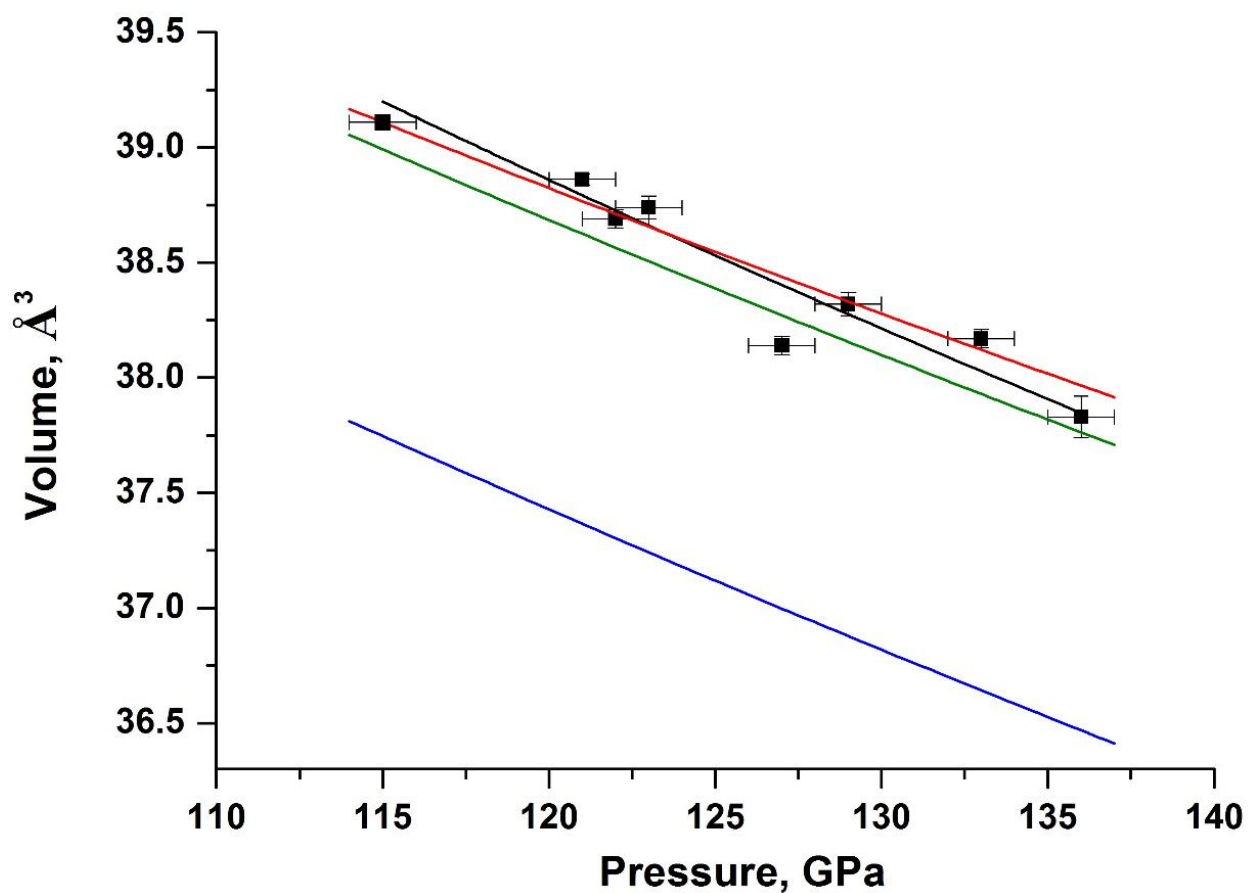
Supplementary Figure IV.4-S2. The dependence of the unit cell volume of ζ-B on pressure. Black squares are our experimental points obtained from powder and single-crystal XRD data. Black line is the fit of our PV data with the 2BM EoS. Theoretically calculated EoSes are from the literature data [77] (green line, 3BM), [94] (red line, 3BM), and [99] (blue line, M).

V. BIBLIOGRAPHY

1. Golikova, O.A., Zaitsev, V.K., Orlov, V.M., Petrov, A.V., Stilbans, L.S., and Tkalenko, E.N., Thermal conductivity of boron and of its crystal structure analoges, *Physica Status Solidi (A)* **21**, 405-12 (1974).

2. *Boron isotopes*, Https://En.Wikipedia.Org/Wiki/Boron.

3. Samsonov, G.V., Hagenmuller, P., Lundstrom, T., and Matkovich, V.I., *Boron and refractory borides* (Springer-Verlag Berlin Heidelberg, 1977).

4. R, A.I., (Google Patents, 1960).

5. Takeshima, E., Takatsu, K., Asano, N., and Hozumi, M., (Google Patents, 1991).

6. Coderre, J.A. and Morris, G.M., The radiation biology of boron neutron capture therapy, *Radiation Research* **151**, 1-18 (1999).

7. Barth, R.F., A critical assessment of boron neutron capture therapy: An overview, *Journal of Neuro-Oncology* **62**, 1-5 (2003).

8. Barth, R.F., Soloway, A.H., and Fairchild, R.G., Boron neutron capture therapy of cancer, *Cancer Research* **50**, 1061-70 (1990).

9. Tilekar, K.V., Gajbhiye, V.P., Prasanth, H., and Soman, T., Preparation of high purity amorphous boron powder, *2005* **55**, 5 (2005).

10. Lin, J.-F., Shu, J., Mao, H.-K., Hemley, R.J., and Shen, G., Amorphous boron gasket in diamond anvil cell research, *Review of Scientific Instruments* **74**, 4732-6 (2003).

11. Mondal, S., Bykova, E., Dey, S., Ali, S.I., Dubrovinskaia, N., Dubrovinsky, L., Parakhonskiy, G., and Van Smaalen, S., Disorder and defects are not intrinsic to boron carbide, *Scientific Reports* **6**, 19330, 19330 (2016).

12. Mondal, S., Van Smaalen, S., Parakhonskiy, G., Prathapa, S.J., Noohinejad, L., Bykova, E., Dubrovinskaia, N., Chernyshov, D., and Dubrovinsky, L., Experimental evidence of orbital order in α-B_{12} and γ-B_{28} polymorphs of elemental boron, *Physical Review B* **88**, 024118, 024118 (2013).

13.   Mondal, S., Van Smaalen, S., Schonleber, A., Filinchuk, Y., Chernyshov, D., Simak, S.I., Mikhaylushkin, A.S., Abrikosov, I.A., Zarechnaya, E., Dubrovinsky, L., and Dubrovinskaia, N., Electron-deficient and polycenter bonds in the high-pressure γ-B$_{28}$ phase of boron, *Physical Review Letters* **106**, 215502, 215502 (2011).

14.   Eremets, M.I., Struzhkin, V.V., Mao, H.-K., and Hemley, R.J., Superconductivity in boron, *Science* **293**, 272 (2001).

15.   Albert, B. and Hillebrecht, H., Boron: Elementary challenge for experimenters and theoreticians, *Angewandte Chemie-International Edition* **48**, 8640-68 (2009).

16.   Parakhonskiy, G., Dubrovinskaia, N., Bykova, E., Wirth, R., and Dubrovinsky, L., Experimental pressure-temperature phase diagram of boron: resolving the long-standing enigma, *Scientific Reports* **1**, 96, 96 (2011).

17.   Masago, A., Shirai, K., and Katayama-Yoshida, H., Crystal stability of α- and β-boron, *Physical Review B* **73**, 104102, 104102 (2006).

18.   Garrett, D.E., in *Borates* (Academic Press, San Diego, 1998), pp. 1-50.

19.   Hayun, S., Dilman, H., Dariel, M.P., and Frage, N., The effect of aluminum on the microstructure and phase composition of boron carbide infiltrated with silicon, *Materials Chemistry and Physics* **118**, 490-5 (2009).

20.   Telle, R., Borides - a new generation of highly resistant materials?, *Chemie in Unserer Zeit* **22**, 93-9 (1988).

21.   Riedel, R., Novel ultrahard materials, *Advanced Materials* **6**, 549-60 (1994).

22.   Chopra, N.G., Luyken, R.J., Cherrey, K., Crespi, V.H., Cohen, M.L., Louie, S.G., and Zettl, A., Boron nitride nanotubes, *Science* **269**, 966 (1995).

23.   Amendola, S., (Google Patents, 1999).

24.   Schell, G., Winter, H., Rietschel, H., and Gompf, F., Electronic structure and superconductivity in metal hexaborides, *Physical Review B* **25**, 1589-99 (1982).

25.   Werheit, H., Boron-rich solids: A chance for high-efficiency high-temperature thermoelectric energy conversion, *Materials Science and Engineering: B* **29**, 228-32 (1995).

26.   Imai, Y., Mukaida, M., Ueda, M., and Watanabe, A., Screening of the possible boron-based n-type thermoelectric conversion materials on the basis of the calculated densities of states of metal borides and doped β-boron, *Intermetallics* **9**, 721-34 (2001).

27.   Kitamura, J., Usuba, S., Kakudate, Y., Yokoi, H., Yamamoto, K., Tanaka, A., and Fujiwara, S., Formation of boron carbide coating by electromagnetically accelerated plasma spraying, *Surface and Coatings Technology* **169–170**, 324-7 (2003).

28.   Fanchini, G., Mccauley, J.W., and Chhowalla, M., Behavior of disordered boron carbide under stress, *Physical Review Letters* **97**, 035502 (2006).

29.   Parakhonskiy, G., Dubrovinskaia, N., Bykova, E., Wirth, R., and Dubrovinsky, L., High pressure synthesis and investigation of single crystals of metastable boron phases, *High Pressure Research* **33**, 673-83 (2013).

30.   Weintraub, E., Preparation and properties of pure boron., *Transactions of The American Electrochemical Society* **16**, 165-84 (1909).

31.   Mccarty, L.V., Kasper, J.S., Horn, F.H., Decker, B.F., and Newkirk, A.E., A new crystalline modification of boron, *Journal of the American Chemical Society* **80**, 2592- (1958).

32.   Horn, F.H., On the crystallization of simple rhombohedral boron from platinum, *Journal of The Electrochemical Society* **106**, 905-6 (1959).

33.   Amberger, E. and Dietze, W., Zur Bildung von α-rhomboedrischem, rotem Bor, *Zeitschrift für anorganische und allgemeine Chemie* **332**, 131-9 (1964).

34.   Wald, F., Stability of the red α-rhombohedral B modification, *Electron Technol* **3**, 103-8 (1970).

35.   Parakhonskiy, G., Dubrovinskaia, N., Dubrovinsky, L., Mondal, S., and Van Smaalen, S., High pressure synthesis of single crystals of α-boron, *Journal of Crystal Growth* **321**, 162-6 (2011).

36.   Parakhonskiy, G., Vtech, V., Dubrovinskaia, N., Caracas, R., and Dubrovinsky, L., Raman spectroscopy investigation of α-boron at elevated pressures and temperatures, *Solid State Communications* **154**, 34-9 (2013).

37.   Will, G. and Kiefer, B., Electron deformation density in rhombohedral α-boron, *Zeitschrift für anorganische und allgemeine Chemie* **627**, 2100-4 (2001).

38.   Decker, B.F. and Kasper, J.S., The crystal structure of a simple rhombohedral form of boron, *Acta Crystallographica* **12**, 503-6 (1959).

39.   Morosin, B., Mullendore, A.W., Emin, D., and Slack, G.A., Rhombohedral crystal structure of compounds containing boron-rich icosahedra, *AIP Conference Proceedings* **140**, 70-86 (1986).

40.   Switendick, A.C. and Morosin, B., Electronic charge density and bonding in α-boron: An experimental-theoretical comparison, *AIP Conference Proceedings* **231**, 205-11 (1991).

41.   Parakhonskiy, G., Synthesis and investigation of boron phases at high pressures and temperatures (PhD thesis), University of Bayreuth, 2012, 117 p., Bayreuther Graduiertenschule für Mathematik und Naturwissenschaften (BayNAT).

42.   Terauchi, M., Kawamata, Y., Tanaka, M., Takeda, M., and Kimura, K., Electron Energy-Loss Spectroscopy study of the electronic structure of α-rhombohedral boron, *Journal of Solid State Chemistry* **133**, 156-9 (1997).

43.   Richter, W. and Ploog, K., Raman-active phonons in α-boron, *Physica Status Solidi B-Basic Research* **68**, 201-5 (1975).

44.   Vast, N., Baroni, S., Zerah, G., Besson, J.M., Polian, A., Grimsditch, M., and Chervin, J.C., Lattice dynamics of icosahedral α-boron under pressure, *Physical Review Letters* **78**, 693-6 (1997).

45.   Werheit, H., Filipov, V., Kuhlmann, U., Schwarz, U., Armbruster, M., Leithe-Jasper, A., Tanaka, T., Higashi, I., Lundstrom, T., Gurin, V.N., and Korsukova, M.M., Raman effect in icosahedral boron-rich solids, *Science and Technology of Advanced Materials* **11**, 023001, 023001 (2010).

46.   Beckel, C.L., Yousaf, M., Fuka, M.Z., Raja, S.Y., and Lu, N., Lattice-vibrations of the icosahedral solid α-boron, *Physical Review B* **44**, 2535-53 (1991).

47.   Shirai, K. and Katayama-Yoshida, H., The narrow Raman linewidth of a librational mode of α-rhombohedral boron and its anharmonic effects, *Journal of the Physical Society of Japan* **67**, 3801-8 (1998).

48.   Polian, A., Chervin, J.C., Munsch, P., and Gauthier, M., in *Joint 21st AIRAPT and 45th EHPRG International Conference on High Pressure Science and Technology* (Journal of Physics: Conference Series, 2008), p. 042017.

49.   Kaneshige, M., Hirayama, S., Yabuuchi, T., Matsuoka, T., Shimizu, K., Mita, Y., Hyoudo, H., and Kimura, K., Measurement of electrical resistance and Raman spectrum of α-boron under high pressure, *Journal of the Physical Society of Japan* **76**, 19-20 (2007).

50.   Shirai, K., Dekura, H., Mori, Y., Fujii, Y., Hyodo, H., and Kimura, K., Structural study of α-rhombohedral boron at high pressures, *Journal of the Physical Society of Japan* **80**, 084601, 084601 (2011).

51.   Werheit, H., Kuhlmann, U., Solov'ev, N.E., Tsiskarishvili, G., and Tsagareishvili, G., in *AIP Conference Proceedings*, edited by Emin, D., Aselage, T.L., Switendick, A.C., Morosin, B., and Beckel, C.L. (New York, 1990), pp. 350-4.

52.   Golikova, O.A., Drabkin, J.A., Zaitsev, V.K., Kazanin, M.M., Mirlin, D.N., Nelvson, J.V., Tkalenko, E., and Chomidov, T., in *The international Symposium on Boron* (Mecniereba, U.S.S.R., 1974, Tbilisi, 1972), pp. 44-58.

53.   Werheit, H. and Haupt, H., Lattice-vibrations, MIR and fir optical-properties of boron and icosahedral boron-rich borides .1. α-rhombohedral structure-group, *Zeitschrift Fur Naturforschung Section a-a Journal of Physical Sciences* **42**, 925-34 (1987).

54.   Shirai, K. and Gonda, S., Polar vibrations and the effective charges of the icosahedral boron solid, *Journal of Physics and Chemistry of Solids* **57**, 109-23 (1996).

55.   Werheit, H. and Kuhlmann, U., Is the established structure of α-rhombohedral boron correct? Comparative study of IR-active phonons with B_6O, $B_{4.3}C$ and β-rhombohedral boron, *Journal of Physics-Condensed Matter* **24**, 305401, 305401 (2012).

56.   Weber, W. and Thorpe, M.F., Vibrations in icosahedral boron molecules and in elemental boron solids, *Journal of Physics and Chemistry of Solids* **36**, 967-74 (1975).

57.   Cueilleron, J. and Viala, J.C., The chemical and pyrometallurgical purification of β-rhombohedral boron, *Journal of the Less Common Metals* **67**, 333-7 (1979).

58.   Sands, D.E. and Hoard, J.L., Rhombohedral elemental boron, *Journal of the American Chemical Society* **79**, 5582-3 (1957).

59.   Hughes, R.E., Kennard, C.H.L., Sullenger, D.B., Weakliem, H.A., Sands, D.E., and Hoard, J.L., The structure of β-rhombohedral boron, *Journal of the American Chemical Society* **85**, 361-2 (1963).

60.   Hoard, J.L., Sullenger, D.B., Kennard, C.H.L., and Hughes, R.E., The structure analysis of β-rhombohedral boron, *Journal of Solid State Chemistry* **1**, 268-77 (1970).

61.   Callmer, B., An accurate refinement of the β-rhombohedral boron structure, *Acta Crystallographica Section B* **33**, 1951-4 (1977).

62.   Slack, G.A., Hejna, C.I., Garbauskas, M.F., and Kasper, J.S., The crystal structure and density of β-rhombohedral boron, *Journal of Solid State Chemistry* **76**, 52-63 (1988).

63.   Spitzer, W.G. and Kaiser, W., Optical properties of crystalline boron, *Physical Review Letters* **1**, 230-2 (1958).

64.   Greiner, E.S. and Gutowski, J.A., Electrical resistivity of boron, *Journal of Applied Physics* **28**, 1364-5 (1957).

65.   Tsagareishvili, G.V., Tsagareishvili, D.S., and Khvedelidze, A.G., Estimation of some thermoelastic properties of β-rhombohedral boron in wide ranges of temperature and pressure, *Journal of the Less Common Metals* **75**, 141-5 (1980).

66.   Mailhiot, C., Grant, J.B., and Mcmahan, A.K., High-pressure metallic phases of boron, *Physical Review B* **42**, 9033-9 (1990).

67.   Nelmes, R.J., Loveday, J.S., Allan, D.R., Besson, J.M., Hamel, G., Grima, P., and Hull, S., Neutron-diffraction and X-ray-diffraction measurements of the bulk modulus of boron, *Physical Review B* **47**, 7668-73 (1993).

68.   Ma, Y.Z., Prewitt, C.T., Zou, G.T., Mao, H.K., and Hemley, R.J., High-pressure high-temperature X-ray diffraction of β-boron to 30 GPa, *Physical Review B* **67**, 174116, 174116 (2003).

69.   Sanz, D.N., Loubeyre, P., and Mezouar, M., Equation of state and pressure induced amorphization of β-boron from X-ray measurements up to 100 GPa, *Physical Review Letters* **89**, 245501, 245501 (2002).

70.   Wentorf, R.H., in *Boron: Volume 2: Preparation, properties, and applications*, edited by Gaulé, G.K. (Springer US, Boston, MA, 1965), pp. 97-100.

71.   Zarechnaya, E.Y., Dubrovinsky, L., Dubrovinskaia, N., Miyajima, N., Filinchuk, Y., Chernyshov, D., and Dmitriev, V., Synthesis of an orthorhombic high pressure boron phase, *Science and Technology of Advanced Materials* **9**, 4, 044209 (2008).

72.   Zarechnaya, E.Y., Dubrovinsky, L., Dubrovinskaia, N., Filinchuk, Y., Chernyshov, D., Dmitriev, V., Miyajima, N., El Goresy, A., Braun, H.F., Van Smaalen, S., Kantor, I., Kantor, A., Prakapenka, V., Hanfland, M., Mikhaylushkin, A.S., Abrikosov, I.A., and Simak, S.I., Superhard semiconducting optically transparent high pressure phase of boron, *Physical Review Letters* **102**, 185501, 185501 (2009).

73.   Oganov, A.R., Chen, J., Gatti, C., Ma, Y., Ma, Y., Glass, C.W., Liu, Z., Yu, T., Kurakevych, O.O., and Solozhenko, V.L., Ionic high-pressure form of elemental boron, *Nature* **457**, 863-7 (2009).

74.   Oganov, A.R., Chen, J.H., Gatti, C., Ma, Y.Z., Ma, Y.M., Glass, C.W., Liu, Z.X., Yu, T., Kurakevych, O.O., and Solozhenko, V.L., Ionic high-pressure form of elemental boron, *Addendum. Nature* **460**, 292 (2009).

75.   Zarechnaya, E.Y., Dubrovinskaia, N., and Dubrovinsky, L., Polarized Raman spectroscopy of high-pressure orthorhombic boron phase, *High Pressure Research* **29**, 530-5 (2009).

76.   Aydin, S. and Simsek, M., First-principles calculations of elemental crystalline boron phases under high pressure: Orthorhombic B_{28} and tetragonal B_{48}, *Journal of Alloys and Compounds* **509**, 5219-29 (2011).

77.   Fan, C., Li, J., and Wang, L., Phase transitions, mechanical properties and electronic structures of novel boron phases under high-pressure: A first-principles study, *Scientific Reports* **4**, 6786 (2014).

78.   Solozhenko, V.L., Kurakevych, O.O., and Oganov, A.R., On the hardness of a new boron phase, orthorhombic γ-B28, *Journal of Superhard Materials* **30**, 428-9 (2008).

79.   Zarechnaya, E., Dubrovinskaia, N., Caracas, R., Merlini, M., Hanfland, M., Filinchuk, Y., Chernyshov, D., Dmitriev, V., and Dubrovinsky, L., Pressure-induced isostructural phase transformation in γ-B_{28}, *Physical Review B* **82**, 184111, 184111 (2010).

80.   Laubengayer, A.W., Hurd, D.T., Newkirk, A.E., and Hoard, J.L., Boron. I. Preparation and properties of pure crystalline boron, *Journal of the American Chemical Society* **65**, 1924-31 (1943).

81.   Will, G. and Ploog, K., Crystal structure of I-tetragonal boron, *Nature* **251**, 406-8 (1974).

82.   Longuet-Higgins, H.C. and De V. Roberts, M., The electronic structure of the borides MB_6, *Proceedings of the Royal Society of London. Series A. Mathematical and Physical Sciences* **224**, 336-47 (1954).

83.   Zarechnaya, E.Y., Dubrovinskaia, N., Dubrovinsky, L., Filinchuk, Y., Chernyshov, D., and Dmitriev, V., Growth of single crystals of B_{28} at high pressures and high temperatures, *Journal of Crystal Growth* **312**, 3388-94 (2010).

84.   Qin, J., Irifune, T., Dekura, H., Ohfuji, H., Nishiyama, N., Lei, L., and Shinmei, T., Phase relations in boron at pressures up to 18 GPa and temperatures up to 2200 C, *Physical Review B* **85**, 014107 (2012).

85.   Oganov, A.R., in *Boron Rich Solids: Sensors, Ultra High Temperature Ceramics, Thermoelectrics, Armor*, edited by Orlovskaya, N., and Lugovy, M. (Springer Netherlands, Dordrecht, 2011), pp. 207-25.

86.   Van Setten, M.J., Uijttewaal, M.A., De Wijs, G.A., and De Groot, R.A., Thermodynamic stability of boron: The role of defects and zero point motion, *Journal of the American Chemical Society* **129**, 2458-65 (2007).

87.   Siberchicot, B., Ab initio equation of state of alpha- and beta-boron: Possible amorphization of beta-boron under high pressure, *Physical Review B* **79**, 224101 (2009).

88.   Prasad, D.L.V.K., Balakrishnarajan, M.M., and Jemmis, E.D., Electronic structure and bonding of β-rhombohedral boron using cluster fragment approach, *Physical Review B* **72**, 195102 (2005).

89.   Shirai, K., Electronic Structures and Mechanical Properties of Boron and Boron-Rich Crystals (Part 2), *Journal of Superhard Materials* **32**, 336-45 (2010).

90.   Ogitsu, T., Gygi, F., Reed, J., Motome, Y., Schwegler, E., and Galli, G., Imperfect Crystal and Unusual Semiconductor: Boron, a Frustrated Element, *Journal of the American Chemical Society* **131**, 1903-9 (2009).

91.   Widom, M. and Mihalkovič, M., Symmetry-broken crystal structure of elemental boron at low temperature, *Physical Review B* **77**, 064113 (2008).

92.   Zhao, Y., Xu, Q., Simpson, L.J., and Dillon, A.C., Prediction of diamond-like, metallic boron structures, *Chemical Physics Letters* **496**, 280-3 (2010).

93.   Oganov, A.R. and Solozhenko, V.L., Boron: a hunt for superhard polymorphs, *Journal of Superhard Materials* **31**, 285 (2009).

94.   Xu, Y.-H., Liu, H.-Y., Hao, X.-F., Chen, R.-N., and Gao, F.-M., First principles study on mechanical properties of superhard α-Ga boron, *Chinese Physics Letters* **32**, 026101 (2015).

95.   Li, D., Bao, K., Tian, F., Jin, X., Duan, D., He, Z., Liu, B., and Cui, T., High-pressure close-packed structure of boron, *RSC Advances* **4**, 203-7 (2014).

96.   Von Schnering, H.G. and Nesper, R., α-Gallium - an alternative to the boron structure, *Acta Chemica Scandinavica* **45**, 870-2 (1991).

97.   Haussermann, U., Simak, S.I., Ahuja, R., and Johansson, B., Metal-nonmetal transition in the boron group elements, *Physical Review Letters* **90**, 4, 065701 (2003).

98.   Segall, D.E. and Arias, T.A., Ab initio approach for high-pressure systems with application to high-pressure phases of boron: Perturbative momentum-space potentials, *Physical Review B* **67**, 064105 (2003).

99.   Ma, Y., Tse, J.S., Klug, D.D., and Ahuja, R., Electron-phonon coupling of α-Ga boron, *Physical Review B* **70**, 214107 (2004).

100.   Thévenot, F., Boron carbide — A comprehensive review, *Journal of the European Ceramic Society* **6**, 205-25 (1990).

101.   Ridgway, R.R., Boron carbide: A new crystalline abrasive and wear-resisting product, *Transactions of The Electrochemical Society* **66**, 117-33 (1934).

102.   Kirfel, A., Gupta, A., and Will, G., The nature of the chemical bonding in boron carbide, $B_{13}C_2$. I. Structure refinement, *Acta Crystallographica Section B* **35**, 1052-9 (1979).

103.   Bouchacourt, M. and Thevenot, F., Analytical investigations in the B-C system, *Journal of the Less Common Metals* **82**, 219-26 (1981).

104.   Wood, C. and Emin, D., Conduction mechanism in boron carbide, *Physical Review B* **29**, 4582-7 (1984).

105.   Emin, D., Structure and single-phase regime of boron carbides, *Physical Review B* **38**, 6041-55 (1988).

106.   Tallant, D.R., Aselage, T.L., and Emin, D., in *AIP Conference Proceedings*, edited by Emin, D., Aselage, T.L., Switendick, A.C., Morosin, B., and Beckel, C.L. (New York, 1990), pp. 301-11.

107.   Domnich, V., Reynaud, S., Haber, R.A., and Chhowalla, M., Boron carbide: Structure, properties, and stability under stress, *Journal of the American Ceramic Society* **94**, 3605-28 (2011).

108.   Dera, P., Manghnani, M.H., Hushur, A., Hu, Y., and Tkachev, S., New insights into the enigma of boron carbide inverse molecular behavior, *Journal of Solid State Chemistry* **215**, 85-93 (2014).

109.   Morosin, B., Kwei, G.H., Lawson, A.C., Aselage, T.L., and Emin, D., Neutron powder diffraction refinement of boron carbides - nature of intericosahedral chains, *Journal of Alloys and Compounds* **226**, 121-5 (1995).

110.   Kwei, G.H. and Morosin, B., Structures of the boron-rich boron carbides from neutron powder diffraction: Implications for the nature of the inter-icosahedral chains, *Journal of Physical Chemistry* **100**, 8031-9 (1996).

111.   Lazzari, R., Vast, N., Besson, J.M., Baroni, S., and Dal Corso, A., Atomic structure and vibrational properties of icosahedral B$_4$C boron carbide, *Physical Review Letters* **83**, 3230-3 (1999).

112.   Tallant, D.R., Aselage, T.L., Campbell, A.N., and Emin, D., Boron-carbide structure by Raman spectroscopy, *Physical Review B* **40**, 5649-56 (1989).

113.   Saal, J.E., Shang, S., and Liu, Z.-K., The structural evolution of boron carbide via ab initio calculations, *Applied Physics Letters* **91**, 231915 (2007).

114.   Stein, H., Aselage, T.L., and Emin, D., in *AIP Conference Proceedings*, edited by Emin, D., Aselage, T.L., Switendick, A.C., Morosin, B., and Beckel, C.L. (New York, 1990), pp. 322-5.

115.   Morosin, B., Aselage, T.L., and Emin, D., in *AIP Conference Proceedings*, edited by Emin, D., Aselage, T.L., Switendick, A.C., Morosin, B., and Beckel, C.L. (New York, 1990), pp. 193-6.

116.   Hushur, A., Manghnani, M.H., Werheit, H., Dera, P., and Williams, Q., High-pressure phase transition makes B$_{4.3}$C boron carbide a wide-gap semiconductor, *Journal of Physics-Condensed Matter* **28**, 12, 045403 (2016).

117.   Taylor, D.E., Mccauley, J.W., and Wright, T.W., The effects of stoichiometry on the mechanical properties of icosahedral boron carbide under loading, *Journal of Physics: Condensed Matter* **24**, 505402 (2012).

118.   Vogler, T.J., Reinhart, W.D., and Chhabildas, L.C., Dynamic behavior of boron carbide, *Journal of Applied Physics* **95**, 4173-83 (2004).

119.   Zhang, Y., Mashimo, T., Uemura, Y., Uchino, M., Kodama, M., Shibata, K., Fukuoka, K., Kikuchi, M., Kobayashi, T., and Sekine, T., Shock compression behaviors of boron carbide (B$_4$C), *Journal of Applied Physics* **100**, 113536-700 (2006).

120.   Somayazulu, M., Akella, J., Weir, S., Hauserman, D., and Shen, G., X-ray diffraction measurements on B$_4$C boron carbide at high pressures and high temperatures, *Advanced Photon Source Activity Reports* (2001).

121.   Nelmes, R.J., Loveday, J.S., Wilson, R.M., Marshall, W.G., Besson, J.M., Klotz, S., Hamel, G., Aselage, T.L., and Hull, S., Observation of inverted-molecular compression in boron-carbide, *Physical Review Letters* **74**, 2268-71 (1995).

122.   Dandekar, D.P., Ciezak, J.A., and Somayazulu, M., in *26th Army Science Conference*Orlando, Florida, 2008), pp. GP-05.

123.   Fujii, Y., Mori, Y., Hyodo, H., and Kimura, K., in *Joint 22nd AIRAPT and HPCJ-50 International Conference on High Pressure Science and Technology* (Journal of Physics: Conference Series, 2010), p. 012011.

124.   Werheit, H. and Shalamberidze, S., Advanced microstructure of boron carbide, *Journal of Physics-Condensed Matter* **24**, 12, 385406 (2012).

125.   Werheit, H. and Haupt, H., in *AIP Conference Proceedings*, edited by Emin, D., Aselage, T.L., Switendick, A.C., Morosin, B., and Beckel, C.L. (New York, 1990), pp. 355-9.

126.   Shirai, K. and Emura, S., Lattice vibrations of boron carbide, *Journal of Solid State Chemistry* **133**, 93-6 (1997).

127.   Guo, J., Zhang, L., Fujita, T., Goto, T., and Chen, M., Pressure-induced depolarization and resonance in Raman scattering of single-crystalline boron carbide, *Physical Review B* **81**, 060102 (2010).

128.   Vast, N., Besson, J.M., Baroni, S., and Dal Corso, A., Atomic structure and vibrational properties of icosahedral α-boron and B_4C boron carbide, *Computational Materials Science* **17**, 127-32 (2000).

129.   Shirai, K. and Emura, S., Lattice vibrations and the bonding nature of boron carbide, *Journal of Physics: Condensed Matter* **8**, 10919 (1996).

130.   Shirai, K., Sakuma, K., and Uemura, N., Theoretical study of the structure of boron carbide $B_{13}C_2$, *Physical Review B* **90**, 064109 (2014).

131.   Khvostantsev, L.G., Slesarev, V.N., and Brazhkin, V.V., Toroid type high-pressure device: history and prospects, *High Pressure Research* **24**, 371-83 (2004).

132.   Khvostantsev, L.G., Sidorov, V.A., and Tsiok, O.B., in *Properties of Earth and planetary materials at high pressure and temperature* (American Geophysical Union, 1998), pp. 89-96.

133.   *The bronze statue picture*, Https://En.Wikipedia.Org/Wiki/Eyrarland_Statue.

134.   Fang, J., Bull, C.L., Loveday, J.S., Nelmes, R.J., and Kamenev, K.V., Strength analysis and optimisation of double-toroidal anvils for high-pressure research, *Review of Scientific Instruments* **83**, 10, 093902 (2012).

135.   Ivanov, A.N., Nikolaev, N.A., Pashkin, N.V., Savenko, B.N., Smirnov, L.S., and Taran, Y.V., Ceramic high pressure cell with profiled anvils for neutron diffraction investigations (up to 7 GPa), *High Pressure Research* **14**, 203-8 (1995).

136.   Ivanov, A.N., Nikolaev, N.A., Pashkin, N.V., Savenko, B.N., Smimov, L.S., and Taran, Y.V., *Trudy ITEF* **76** (1991).

137.   Tsiok, O.B. and Khvostantsev, L.G., Phase transitions of Zr at high pressures up to 15 GPa and high temperatures, *ZhETF* **120**, 1438 (2001).

138.   Sidorov, V.A., Nicklas, M., Pagliuso, P.G., Sarrao, J.L., Bang, Y., Balatsky, A.V., and Thompson, J.D., Superconductivity and quantum criticality in $CeCoIn_5$, *Physical Review Letters* **89**, 157004 (2002).

139.   Sidorov, V.A., Bauer, E.D., Frederick, N.A., Jeffries, J.R., Nakatsuji, S., Moreno, N.O., Thompson, J.D., Maple, M.B., and Fisk, Z., Magnetic phase diagram of the ferromagnetic Kondo-lattice compound $CeAgSb_2$ up to 80 kbar, *Physical Review B* **67**, 224419 (2003).

140.   Decker, D.L., Bassett, W.A., Merrill, L., Hall, H.T., and Barnett, J.D., High-pressure calibration: A critical review, *Journal of Physical and Chemical Reference Data* **1**, 773-836 (1972).

141.   Bean, V.E., Akimoto, S., Bell, P.M., Block, S., Holzapfel, W.B., Manghnani, M.H., Nicol, M.F., and Stishov, S.M., Another step toward an international practical pressure scale, *Physica B & C* **139**, 52-4 (1986).

142.   Fuse, A., Nakamoto, G., Kurisu, M., Ishimatsu, N., and Tanida, H., The valence state of Yb metal under high pressure determined by XANES measurement up to 34.6 GPa, *Journal of Alloys and Compounds* **376**, 34-7 (2004).

143.   Bedford, R.E., Bonnier, G., Maas, H., and Pavese, F., Recommended values of temperature on the International Temperature Scale of 1990 for a selected set of secondary reference points, *Metrologia* **33**, 133 (1996).

144.   Dubrovinskaia, N., Dubrovinsky, L., Solopova, N.A., Abakumov, A., Turner, S., Hanfland, M., Bykova, E., Bykov, M., Prescher, C., Prakapenka, V.B., Petitgirard, S., Chuvashova, I., Gasharova, B., Mathis, Y.-L., Ershov, P., Snigireva, I., and Snigirev, A., Terapascal static pressure generation with ultrahigh yield strength nanodiamond, *Science Advances* **2** (2016).

145.   Kantor, I., Prakapenka, V., Kantor, A., Dera, P., Kurnosov, A., Sinogeikin, S., Dubrovinskaia, N., and Dubrovinsky, L., BX90: A new diamond anvil cell design for X-ray diffraction and optical measurements, *Review of Scientific Instruments* **83**, 6, 125102 (2012).

146.   Boehler, R. and De Hantsetters, K., New anvil designs in diamond-cells, *High Pressure Research* **24**, 391-6 (2004).

147.   Mao, H.K., Xu, J., and Bell, P.M., Calibration of the ruby pressure gauge to 800 kbar under quasi-hydrostatic conditions, *Journal of Geophysical Research: Solid Earth* **91**, 4673-6 (1986).

148.   Dewaele, A., Torrent, M., Loubeyre, P., and Mezouar, M., Compression curves of transition metals in the Mbar range: Experiments and projector augmented-wave calculations, *Physical Review B* **78**, 104102 (2008).

149.   Fei, Y., Ricolleau, A., Frank, M., Mibe, K., Shen, G., and Prakapenka, V., Toward an internally consistent pressure scale, *Proceedings of the National Academy of Sciences* **104**, 9182-6 (2007).

150.   Dorogokupets, P.I. and Dewaele, A., Equations of state of MgO, Au, Pt, NaCl-B1, and NaCl-B2: Internally consistent high-temperature pressure scales, *High Pressure Research* **27**, 431-46 (2007).

151.   Dubrovinsky, L., Dubrovinskaia, N., Bykova, E., Bykov, M., Prakapenka, V., Prescher, C., Glazyrin, K., Liermann, H.P., Hanfland, M., Ekholm, M., Feng, Q., Pourovskii, L.V., Katsnelson, M.I., Wills, J.M., and Abrikosov, I.A., The most incompressible metal osmium at static pressures above 750 gigapascals, *Nature* **525**, 226-9 (2015).

152. Dubrovinskaia, N. and Dubrovinsky, L., Whole-cell heater for the diamond anvil cell, *Review of Scientific Instruments* **74**, 3433-7 (2003).

153. Dubrovinsky, L., Glazyrin, K., Mccammon, C., Narygina, O., Greenberg, E., Ubelhack, S., Chumakov, A.I., Pascarelli, S., Prakapenka, V., Bock, J., and Dubrovinskaia, N., Portable laser-heating system for diamond anvil cells, *Journal of Synchrotron Radiation* **16**, 737-41 (2009).

154. Kupenko, I., Dubrovinsky, L., Dubrovinskaia, N., Mccammon, C., Glazyrin, K., Bykova, E., Ballaran, T.B., Sinmyo, R., Chumakov, A.I., Potapkin, V., Kantor, A., Rüffer, R., Hanfland, M., Crichton, W., and Merlini, M., Portable double-sided laser-heating system for Mössbauer spectroscopy and X-ray diffraction experiments at synchrotron facilities with diamond anvil cells, *Review of Scientific Instruments* **83**, 124501 (2012).

155. Blake, A.J., Clegg, W., Cole, J.M., Evans, J.S.O., Main, P., Parsons, S., and Watkin, D.J., *Crystal structure analysis. Principles and practice* (Oxford University Press, Great Britain, 2009), 2nd edn.

156. Ladd, M. and Palmer, R., *Structure determination by X-ray crystallography. Analysis by X-rays and neutrons.* (Springer US, 2013), 5 edn.

157. Giacovazzo, C., *Fundamentals of crystallography* (Oxford University Press, 2002).

158. *Illustration of Bragg's law*, Https://En.Wikipedia.Org/Wiki/Bragg's_Law.

159. Fei, Y. and Wang, Y., High-pressure and high-temperature powder diffraction, *Reviews in Mineralogy and Geochemistry* **41**, 521-57 (2000).

160. Mcmahon, M.I., in *High-Pressure Crystallography*, edited by Katrusiak, A., and Mcmillan, P. (Springer Netherlands, Dordrecht, 2004), pp. 1-20.

161. Prescher, C. and Prakapenka, V.B., DIOPTAS: a program for reduction of two-dimensional X-ray diffraction data and data exploration, *High Pressure Research* **35**, 223-30 (2015).

162. Toby, B., EXPGUI, a graphical user interface for GSAS, *Journal of Applied Crystallography* **34**, 210-3 (2001).

163.   Larson, A.C. and Von Dreele, R.B., General Structure Analysis System (GSAS), *Los Alamos National Laboratory Report No. LAUR 86-748* (2000).

164.   Technologies, A., Technologies, A., and Uk Ltd., O., Uk, Crysalispro Software System, CrysAlisPro Software system, 2013.

165.   Farrugia, L.J., WinGX and ORTEP for Windows: An update, *Journal of Applied Crystallography* **45**, 849-54 (2012).

166.   Sheldrick, G.M., A short history of SHELX, *Acta Crystallographica Section A* **64**, 112-22 (2008).

167.   Nakamoto, K., in *Handbook of Vibrational Spectroscopy* (John Wiley & Sons, Ltd, 2006).

168.   Brisdon, A.K., *Inorganic spectroscopic methods* (OUP Oxford, 1998).

169.   *Diagram of photon transitions in molecules under laser excitation*, Http://Oce.Oceanoptics.Com/Measurementtechnique/Raman/.

170.   *Scheme of vibrational spectrum*, Http://131.104.156.23/Lectures/Chem_207%20copy/Vibrational_Spectroscopy.

171.   Goldstein, J., Newbury, D.E., Joy, D.C., Lyman, C.E., Echlin, P., Lifshin, E., Sawyer, L., and Michael, J.R., *Scanning Electron Microscopy and X-ray microanalysis* (Springer US, 2012), 3rd edn.

172.   Chuvashova, I., Bykova, E., Bykov, M., Svitlyk, V., Gasharova, B., Mathis, Y.-L., Caracas, R., Dubrovinsky, L., and Dubrovinskaia, N., High-pressure behavior of α-boron studied on single crystals by X-ray diffraction, Raman and IR spectroscopy, *Journal of Solid State Chemistry* **245**, 50-60 (2017).

173.   Bykova, E., Gou, H., Bykov, M., Hanfland, M., Dubrovinsky, L., and Dubrovinskaia, N., Crystal structures and compressibility of novel iron borides Fe_2B_7 and Fe_xB_{50} synthesized at high pressure and high temperature, *Journal of Solid State Chemistry* **230**, 102-9 (2015).

174.   Shirai, K., Dekura, H., and Yanase, A., Electronic structure and electrical resistivity of α-boron under high pressure, *Journal of the Physical Society of Japan* **78**, 084714, 084714 (2009).

175.   Fujii, Y., Mori, Y., Nishii, T., Fujii, A., Hyodo, H., Takarabe, K., and Kimura, K., in *Joint 21st AIRAPT and 45th EHPRG International Conference on High Pressure Science and Technology* (Journal of Physics: Conference Series, 2008), p. poster 0311.

176.   Zarechnaya, E., The 5-th element. A new high pressure high temperature allotrope (PhD thesis), University of Bayreuth, 2010, 147 p., Fakultät für Chemie und Geowissenschaften der Universität Bayreuth.

177.   Bykova, E., Dubrovinsky, L., Dubrovinskaia, N., Bykov, M., Mccammon, C., Ovsyannikov, S.V., Liermann, H.P., Kupenko, I., Chumakov, A.I., Rüffer, R., Hanfland, M., and Prakapenka, V., Structural complexity of simple Fe_2O_3 at high pressures and temperatures, *Nature Communications* **7**, 10661 (2016).

178.   Belsky, A., Hellenbrandt, M., Karen, V.L., and Luksch, P., New developments in the Inorganic Crystal Structure Database (ICSD): Accessibility in support of materials research and design, *Acta Crystallographica Section B* **58**, 364-9 (2002).

179.   Gonze, X., Rignanese, G.M., and Caracas, R., First-principle studies of the lattice dynamics of crystals, and related properties, *Zeitschrift Fur Kristallographie* **220**, 458-72 (2005).

180.   Veithen, M., Gonze, X., and Ghosez, P., Nonlinear optical susceptibilities, Raman efficiencies, and electro-optic tensors from first-principles density functional perturbation theory, *Physical Review B* **71**, 14, 125107 (2005).

181.   Gonze, X., Amadon, B., Anglade, P.M., Beuken, J.M., Bottin, F., Boulanger, P., Bruneval, F., Caliste, D., Caracas, R., Cote, M., Deutsch, T., Genovese, L., Ghosez, P., Giantomassi, M., Goedecker, S., Hamann, D.R., Hermet, P., Jollet, F., Jomard, G., Leroux, S., Mancini, M., Mazevet, S., Oliveira, M.J.T., Onida, G., Pouillon, Y., Rangel, T., Rignanese, G.M., Sangalli, D., Shaltaf, R., Torrent, M., Verstraete, M.J., Zerah, G., and Zwanziger, J.W., ABINIT: First-principles approach to material and nanosystem properties, *Computer Physics Communications* **180**, 2582-615 (2009).

182.   Payne, M.C., Teter, M.P., Allan, D.C., Arias, T.A., and Joannopoulos, J.D., Iterative minimization techniques for abinitio total-energy calculations - molecular-dynamics and conjugate gradients, *Reviews of Modern Physics* **64**, 1045-97 (1992).

183.   Monkhorst, H.J. and Pack, J.D., Special points for brillouin-zone integrations, *Physical Review B* **13**, 5188-92 (1976).

184.   Lee, S., Bylander, D.M., and Kleinman, L., Elastic-moduli of B_{12} and its compounds, *Physical Review B* **45**, 3245-7 (1992).

185.   Le Godec, Y., Kurakevych, O.O., Munsch, P., Garbarino, G., and Solozhenko, V.L., Equation of state of orthorhombic boron, γ-B_{28}, *Solid State Communications* **149**, 1356-8 (2009).

186.   Kurakevych, O.O. and Solozhenko, V.L., 300-K equation of state of rhombohedral boron subnitride, $B_{13}N_2$, *Solid State Communications* **149**, 2169-71 (2009).

187.   Nieto-Sanz, D., Loubeyre, P., Crichton, W., and Mezouar, M., X-ray study of the synthesis of boron oxides at high pressure: Phase diagram and equation of state, *Physical Review B* **70**, 214108, 214108 (2004).

188.   Momma, K. and Izumi, F., VESTA 3 for three-dimensional visualization of crystal, volumetric and morphology data, *Journal of Applied Crystallography* **44**, 1272-6 (2011).

189.   Kroumova, E., Aroyo, M.I., Perez-Mato, J.M., Kirov, A., Capillas, C., Ivantchev, S., and Wondratschek, H., Bilbao Crystallographic Server : Useful databases and tools for phase-transition studies, *Phase Transitions* **76**, 155-70 (2003).

190.   Jemmis, E.D., Balakrishnarajan, M.M., and Pancharatna, P.D., A Unifying electron-counting rule for macropolyhedral boranes, metallaboranes, and metallocenes, *Journal of the American Chemical Society* **123**, 4313-23 (2001).

191.   Wade, K., The structural significance of the number of skeletal bonding electron-pairs in carboranes, the higher boranes and borane anions, and various transition-metal carbonyl cluster compounds, *Journal of the Chemical Society D: Chemical Communications*, 792-3 (1971).

192.   Wade, K., in *Advances in Inorganic Chemistry and Radiochemistry*, edited by Eméleus, H.J., and Sharpe, A.G. (Academic Press, 1976), pp. 1-66.

193.   Emin, D., Icosahedral boron-rich solids, *Physics Today* **40**, 55-62 (1987).

194.   Petricek, V., Dusek, M., and Palatinus, L., Crystallographic Computing System JANA2006: General features, *Zeitschrift Fur Kristallographie* **229**, 345-52 (2014).

195.   *Pressure scale from EOS*, Http://Kantor.50webs.Com/Diffraction.Htm.

196.   Liermann, H.-P., Konopkova, Z., Morgenroth, W., Glazyrin, K., Bednarcik, J., Mcbride, E.E., Petitgirard, S., Delitz, J.T., Wendt, M., Bican, Y., Ehnes, A., Schwark, I., Rothkirch, A., Tischer, M., Heuer, J., Schulte-Schrepping, H., Kracht, T., and Franz, H., The Extreme Conditions Beamline P02.2 and the Extreme Conditions Science Infrastructure at PETRA III, *Journal of Synchrotron Radiation* **22**, 908-24 (2015).

197.   Häussermann, U., Lidin, S., Simak, S.I., and Abrikosov, I.A., The Structure of α-Gallium and Its Relationship to Deltahedral Clusters, *Chemistry – A European Journal* **3**, 904-11 (1997).

198.   Neuhaus, A., Synthese strukturverhalten valenzzustande der anorganischen materie im bereich hoher-hochster drucke, *Chimia* **18**, 93 (1964).

199.   Kleber, W., Das „Druck-Abstands-Paradoxon", *Kristall und Technik* **2**, 13-4 (1967).

200.   Angel Ross, J., Alvaro, M., and Gonzalez-Platas, J., EosFit7c and a Fortran module (library) for equation of state calculations, *Zeitschrift für Kristallographie - Crystalline Materials* **229**, 405 (2014).

(Eidesstattliche) Versicherungen und Erklärungen

(§ 8 S. 2 Nr. 6 PromO)

Hiermit erkläre ich mich damit einverstanden, dass die elektronische Fassung meiner Dissertation unter Wahrung meiner Urheberrechte und des Datenschutzes einer gesonderten Überprüfung hinsichtlich der eigenständigen Anfertigung der Dissertation unterzogen werden kann.

(§ 8 S. 2 Nr. 8 PromO)

Hiermit erkläre ich eidesstattlich, dass ich die Dissertation selbständig verfasst und keine anderen als die von mir angegebenen Quellen und Hilfsmittel benutzt habe.

(§ 8 S. 2 Nr. 9 PromO)

Ich habe die Dissertation nicht bereits zur Erlangung eines akademischen Grades anderweitig eingereicht und habe auch nicht bereits diese oder eine gleichartige Doktorprüfung endgültig nicht bestanden.

(§ 8 S. 2 Nr. 10 PromO)

Hiermit erkläre ich, dass ich keine Hilfe von gewerbliche Promotionsberatern bzw. -vermittlern in Anspruch genommen habe und auch künftig nicht nehmen werde.

…………………………………………………………………………
Ort, Datum, Unterschrift